A study on the recent climate variability and climate change in Northeast India, and its influence on vegetation pattern

A Thesis submitted to the University of Hyderabad

by

Soraisam Bidyabati

In partial fulfillment of the requirements

for the Degree of

DOCTOR OF PHILOSOPHY

Centre for Earth, Ocean, and Atmospheric Sciences
School of Physics
University of Hyderabad
Hyderabad – 500046, India

December, 2020

Declaration

Centre for Earth, Ocean and Atmospheric Sciences

School of Physics,

University of Hyderabad

Hyderabad - 500046

I hereby declare that, this thesis entitled **"A study on the recent climate variability and climate change in Northeast India, and its influence on vegetation pattern"** is the result of investigation carried out by me in the Centre for Earth, Ocean and Atmospheric Sciences (School of Physics), University of Hyderabad, India under the guidance and supervision of Professor Karumuri Ashok and Co-guide, Professor P. S. Roy, is a bonafide research work and free from plagiarism. I also declare that it has not been submitted previously, in part or in full to this University or any other University or Institute, for the award of any degree or diploma.

A report on the Plagiarism statistics from the University of Hyderabad Librarian is enclosed.

Place: Hyderabad

Date: 28th December, 2020

Name: Soraisam Bidyabati

Regd. No. 14ESPE01

University of Hyderabad

Notification of Results

Course: Ph.D. 1541

Month & Year: April, 2015
Semester: II

Subject: Earth and Space Sciences

Sl. No	Registration No.	Name of the Student	ES-801	ES-805	ES-806	ES-807	AP-811-830
01	13ESPE02	Madri Pramod Kumar	Pass	Pass	Pass	Pass	Pass
02	14ESPE01	Soraisam Bidyabati	Pass	Pass	Pass	Pass	Pass
03	14ESPE02	Bhavani Yadav	Pass	Pass	Pass	Pass	Pass
04	14ESPE03	Shiva Prasad Sharma	Pass	Pass	Pass	Exempted	Pass
05	14ESPE04	Karnati Shankaraiah	Pass	Pass	Pass	Exempted	Pass
06	14ESPE05	Niranjan Mohanty	Pass	Pass	Pass	Exempted	Pass
07	14ESPE06	Pottapinjara Vijay	Pass	Pass	Pass	Pass	Pass

Course No.	Course Title	Credits
ES -801	Earth System Sciences	4
ES-805	Research Methodology	3
ES-806	Mathematics for Earth Sciences	4
ES-807	Interdisciplinary course	3
AP-811-830	Special Paper on Specifiled Research Topic	2

Notice Board 27/10/15

Dated: 16.10.2015

Controller of Examinations 16-10-15

Copy to:

Dean, School of Physics
Head, Centre for Earth & Space Sciences

27/10

Acknowledgements

I wish to express my gratitude to my supervisor, Professor Karumuri Ashok for his support and valuable guidance throughout my PhD. I am extremely grateful to him for offering me deep insight into the study and encouraging me to carry out my research work throughout my journey.

I am extremely thankful to my co-guide Professor P. S. Roy for his kind support, suggestions and helping me throughtout my research.

I am thankful to the Head, CEOAS for his support and provding me the necessary facilities to carry out my thesis at the Centre.

I am grateful to Dr. Vijay Kanawade for his kind support and suggestions.

I am thankful to Dr. Sayed Maqbool Ahmed for supporting my research for his valuable suggestions.

I am also thankful to Dr. S. Sri Lakshmi for her useful suggestions during my research work.

I am grateful to Professor Ulrich Cubash of Institute of Meteorology under Freie Universitat, Berlin for helping me in my research work.

I am thankful to Dr. Malay Ganai, IITM Pune for his guidance during my research work.

I am thankful to Indian Space Research Organization (ISRO) for providing us the LULC data for the periods of 1985, 1995 and 2005. I also acknowledge NASA EOSDIS for making the MODIS data available to us for carrying out my research.

I am also thankful to Uwe Schulzweida from the Max Planck Institute for Meteorology for developing Climate Data Operator and made it available for research purposes. I also acknowledge the Center for Ocean-Land-Atmosphere Studies (COLA), located at George Mason University in Fairfax, Virginia for developing GrADS by making it freely available to us.

I acknowledge India Meteorology Department for provding data to my research work. I also acknowledge Centre for Climate Change Research, Indian Institute of Meteorology, Pune, India for providing the climate model data for my research work.

I am thankful to Feba Francis, Govardhan Dandu, Charan Tejavath, Boyaj Alugula, Vikas Kumar, Reshma Ramachandran and Bhavani Pinjarla for their help in carrying out my research work.

I am thankful to Manoj Khakhlary for his constant moral support and encouraging me to carry out my research work.

A very special gratitude goes out to Jawaharlal Nehru Memorial Fund, Delhi and Erasmus Plus for helping and providing the funding for the work.

Lastly, I would like to thank my parents and family for their love, strength and moral support to carry out my research work.

ABSTRACT

In the last few decades, the Northeast-India one of the rich biodiversity hotspot, has encountered various changes in terms of climatic-vegetation related issues due to anthropogenic activities and other various possible reasons. Annual cycle, seasonal climatology and trends, and extreme month for summer monsoon season and winter monsoon season during the historical period (1970 to 2005) have been studied. For this, precipitation, maximum and minimum temperature data sets collected from the observed climate data from the India Meteorological Department (1° × 1°), Aphrodite and CRU-reanalysis (both 0.5° × 0.5°), and five regional-climate-model simulations (LMDZ, MPI, GFDL, CNRM and ACCESS) data from AR5/CORDEX-South-Asia (0.5° × 0.5°) are used. The models are able to capture the annual cycle and seasonal area-averaged trends qualitatively though a large spread and differences in the locations are found across the models in spatial distribution of various climatologies of all the climatic variables used. No significant trend in precipitation over the region is found while significant trends are observed in the area-averaged minimum temperature during winter season. The heaviest extreme seasonal rainfall captured by models is underestimated as compared to observation data. The ENSO does not have any signficant impact or association with the climate over the region during the two seasons.

The Last Millennium (LM) particularly, Medieval Climate Anomaly period (MCA): 935 CE to 1034 CE & Little Ice Age (LIA): 1735 CE to 1834 CE collected from the PMIP3/CMIP5 models CCSM4, MRI-CGCM3, MPI-ESM-P, available at 288 x 192 x L26 1, 320 x 160 x L48, and 196 x 98 x L47 discretization have been studied. In addition to this, a higher resolution outputs from the ECHAM5, an atmospheric general circulation model (AGCM) at T106 (~1.125° x 1.125°) horizontal resolution from the Max Planck Institute for Meteorology, Germany for the period of 30 years (MCA: 935 CE to 965 CE and LIA: 1735 CE to 1765 CE) are also used. The simulations from the models do

not show any changes over the region during these two periods. The ENSO indices show weak and statistically insignificant during these two periods

In the future projections (2011 to 2060) study from the CORDEX-South-Asia model, a decreasing insignificant trend is projected in seasonal precipitation while an increasing trend is observed for both seasonal maximum and mimum temperature during the future projections over the region. The change in extreme rainfall is not clear in the future projections while the frequency of extreme monthly maximum and minimum temperature are projected to increase. The results show the uncertainty exists in the CORDEX-South-Asia model projections over the region in spite of the relatively high resolution.

To understand whether vegetation changes are associated with climate change, three seasons, namely the wet season (June–October), winter (November–February) and dry season (March–May) are evaluated using the vegetation patterns (Deciduous Broad Leaf forest, Evergreen Broad Leaf forest, Evergreen Needle Leaf forest, Mixed Forest, Shrubland, and Grassland) to the current day climate observations over the region. For this study, I use the Normalized Difference Vegetation Index (NDVI) datasets (500 m resolution), for the 2000-2017 period, from the Moderate Resolution Imaging Spectroradiometer on board the MODIS-Terra satellite against rainfall (0.25° x 0.25°) maximum and minimum temperature datasets (1° x 1°) from the India Meteorological Department, Normalized Difference Wetness Index (NDWI) (500 m resolution) from MODIS and aridity data (5 km x 5 km) from TerraClimate. The field-sample data on vegetation types collected from land use land cover map of 2005 are also used.

Interannual and inter-seasonal variations in the anomalies of the area-averaged NDVI for all the vegetation are seen in all the seasons which can be attributed to variation in rainfall distribution.

Two/three years lagged dependency, or even a one year lag of the NDVI anomaly to the rainfall anomaly within each season are found but insiginificantly. Evergreen Broad Leaf forest and Deciduous Broad Leaf forests are particularly seen to be affected drastically while the Evergreen Needle Leaf forest, which does not get affected much is also found to be fluctuated, by making this study a first of its kind in delivering the message of the prevailing situation in the region. The NDVI anomalies of winter season show a greater magnitude in declining towards negative anomalies than the other two seasons (wet and dry season) indicating the impact of sharp decline of summer monsoon rainfall on winter season NDVI. The NDVI anomaly responses are seen to be more strongly associated with rainfall in all seasons indicating the limiting factor for the growth of the vegetation types. However, during the summer monsoon and pre-monsoon season, the moisture availability from the NDWI, aridity due to the fluctuations of maximum and minimum temperature are also seen indicating a combine effect of temperature and rainfall. Negative anomailes in NDVI during drought years are more prominently seen. The correlation, lag correlation, and regression analyses calculated between NDVI and the rest of the parameters are statistically weak and insignificant for all the vegetation studied. The maximum NDVI values, both area-averaged and spatially, show that the winter season has the highest NDVI values due to cumulative contribution of summer monsoon rainfall and winter monsoon rainfall while dry season being the lowest due to moisture deficit. Thus, the study provides the first report of evident stress in the different vegetation types associated with climate change, though the magnitude varies with the season.

Table of Contents

List of References

Research Publications

Conference certificates

Plagiarism reports

List of Figures

List of Tables

List of Abbreviations

AGCM	Atmospheric General Circulation Model
APHRODITE	Asian Precipitation Highly Resolved Observational Data Integration Towards Evaluation of water resource
AVHRR	Advanced Very High-Resolution Radiometer
BoB	Bay of Bengal
BUFR	Binary Universal Form for the Representation of meteorological data
CCSM4	Community Climate System Model 4
CDO	Climate Data Operator
CORDEX-SA	Coordinated Regional Downscaling Experiment-South Asia
CMIP3	Coupled model intercomparison project phase 3
CMIP5	Coupled model intercomparison project phase 5
CMR	Core Monsoon Region
CNRM	Centre National de Recherches Météorologique
CRU	Climatic Research Unit
DBF	Deciduous Broad Leaf Forest
DJF	December to February
FSI	Forest Survey of India
EBF	Evergreen Broad Leaf Forest
ENF	Evergreen Needle Leaf Forest
ENSO	El Niño–Southern Oscillation
ERDAS	Earth Resources Data Analysis System
ESDS	Earth Science Data Systems
GCM	General Circulation Model
GFDL	Geophysical Fluid Dynamics Laboratory
GIMMS	Global Inventory Modeling and Mapping Studies
GIS	Geographical Information System
GL	Grassland
GrADS	Grid Analysis and Display System
HadRM3	Regional Climate Model of the Hadley Centre

HadISST	Hadley Centre Global Sea Ice and Sea Surface Temperature
HDF	Hierarchical Data Format
HEG	HDF-EOS to GeoTIFF
IGBP	International Geosphere and Biosphere Programme
IMD	India Meteorological Department
IPCC	Intergovernmental Panel on Climate Change
ISMR	Indian summer monsoon rainfall
ISRO	Indian Space Research Organization
JJAS	June to September
LIA	Little Ice Age
LM	Last Millennium
LMDZ	Laboratoire de Météorologie Dynamique
LULC	Land Use and Land Cover
MCA	Medieval Climate Anomaly
MPIM	Max Planck Institute for Meteorology
MRI	Meteorological Research Institute
NASA	National Aeronautics and Space Administration
NCAR	National Center for Atmospheric Research
NetCDF	Network Common Data Form
NDVI	Normalized Difference Vegetation Index
NDWI	Normalized Difference Water Index
NER	Northeast India
NEISMR	Northeast India summer monsoon rainfall
NIR	Near-Infrared
MF	Mixed Forest
M-K	Mann Kendall
MODIS	Moderate Resolution Imaging Spectroradiometer
NOAA	National Oceanic and Atmospheric Administration
PMIP3	Paleoclimate Modelling Intercomparison Project
RCP4.5	Representative Concentration Pathway
SL	Shrub Land
SST	Sea Surface Temperature
SWIR	Shortwave Infrared

TEJ	Tropical Easterly Jet Stream
WG	Working Group
WGS	World Geodetic System
WRCP	World Climate Research Programme

CHAPTER-1

INTRODUCTION

The chapter briefly explains and discusses the general findings on the climate change signatures in the Indian summer monsoon rainfall and its variability, with a focus on those in north-eastern India (NER), the study area. It also briefly provides a review of the importance of climate to the vegetation in the NER region and the consequences due to its variation in the climate. At the end of the chapter, based on the research gaps elucidated, I introduce the objectives of this thesis.

1.1 General Introduction on monsoon and its variability and change

Impacts of warming due to anthropogenic emissions from the pre-industrial period (from 1870s) to the present period, which exacerbated in the last 4-5 decades are stated to persist for centuries to millennia thereby causing a long-term change in the climate system as reported by the Intergovernmental Panel on Climate Change (IPCC, 2013 and Working Group III, 2018). Human influence has been detected in the warming of the atmosphere and oceans according to the WG1 report of the IPCC 2013. Rainfall and temperature are the two key elements of climate that are commonly used as indicators of global climate (Pai et al., 2014). The anthropogenic climate change manifested as changing temperatures and rainfall, is likely to pose a serious risk to ecosystems, economy, water shortages, increased in heat-induced mortality to extreme events, and widespread health impacts to human society according to the WG3 (Working Group III) report of the IPCC, 2019. Both rainfall and temperature are major components of

the terrestrial hydrological cycle (Pai et al., 2014) and changes in its pattern would directly influence the water resources of the concerned region (Jain et al., 2013).

The climate of the Indian subcontinent is dominated by the monsoons which are pronounced seasonal reversals of winds and transitions from drier to wetter regimes (Rao, 1976; Pant and Rupa Kumar 1997). The southwesterly winds, during the summer, pick up moisture from the northern Indian Ocean and drop on the landmass providing the summer monsoon rainfall. The Indian sub-continent, home to more than 1.3 billion people, receives about 70%-75% of its annual rainfall (Figure 1) during June-September months (henceforth JJAS) and is known as the Indian summer monsoon season (Pant and Kumar, 1997).

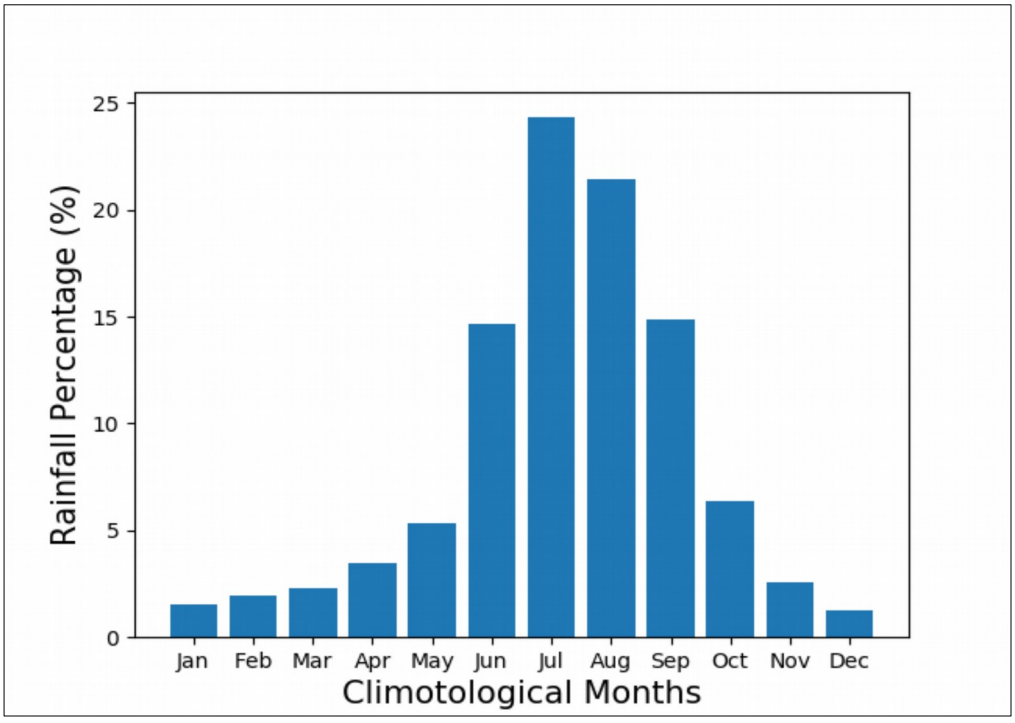

Figure 1. The area-averaged climatological monthly rainfall over the Indian region as a percentage of annual rainfall (Source data: C. T. Tejavath).

The mean area-averaged Indian summer monsoon rainfall (ISMR) over the last 100 years is about 890 mm (Pattanaik, Chapter 2, Meteorological Monographs, 2012). During the Northeast winter monsoon season, the winds blow from the northeast regions of the Asian continent and travel towards the Indian Ocean (Singhvi and Krishnan, 2014). The monsoon system operates via connections between atmosphere, land, and ocean systems, through fluxes of heat, moisture, and momentum between them (Pant, 2003). The El Niño–Southern Oscillation (ENSO), among others, is the most prominent of the drivers of Indian climate variability (Sikka, 1980; Keshavamurty, 1982; Mohanty et al., 2020). A recent review provides details of this association and earlier references (Ashok et al., 2019).

As per the Fifth Assessment Reports of the (IPCC 2013), an increase in global mean surface temperature over a range from 1.1 °C to 2.6 °C is projected in response to increasing emissions, as simulated by the Coupled model intercomparison project phase 5 (CMIP5). As per the report, the Indian subcontinent will be adversely affected by rising temperature and substantial changes in summer rainfall. Indeed, the Indian landmass has been warming up for the last 4-5 decades (Revadekar et al., 2012 and Kothawale et al., 2012). The Indian summer monsoon is also seeing signatures of a weakening trend in central states such as Chhattisgarh (e.g. Krishnan et al., 2016). General circulation models of the CMIP5 vintage fail to simulate the mild weakening trend in the observed rainfall (Jourdain et al., 2013). Fortunately, several downscaled regional climate model simulations, which downscaled the CMIP5 seem to capture the weakening trend in the Indian summer monsoon rainfall (ISMR). An example is the Laboratoire de Météorologie Dynamique (LMDZ) model simulations, under the aegis of The Coordinated Regional Downscaling Experiment (CORDEX) South Asia at high resolution (Krishnan et al., 2016). The regional climate models, by virtue of their higher resolution compared to the General Circulation Model (GCM) outputs under the CMIP5, have been increasingly used to examine patterns of climatic variables. These can be expected to represent the climate as

realistic as possible building the confidence to address the future projections under different climate scenarios (Pattnayak et al., 2017).

Precipitation and temperature over the Indian landmass exhibit a considerable variation both spatially as well as temporally (Pattnayak et al., 2017). The spatial variability of rainfall in Northeast India (NER), our study area, during the monsoon season is highly complex and could be due to the larger influence of the monsoon trough, westerly systems, and significant interaction between convection and basic flow due to varied physiography of the region (Mohapatra et al., 2011). The main sources of moisture for the summer monsoon rains over the NER are claimed to be from the Indian Ocean and the northern Bay of Bengal (Breitenbach et al., 2010). The summer monsoon rainfall in the NER shows a weak association with the area-averaged Indian summer monsoon, and even shows a weak negative correlation with summer monsoon over the central and north-western parts of India (Parthasarathy et al., 1984). Sparse observations, and rapid changes in the topography that affect the weather and climate substantially, pose a potential challenge in documenting the mean climate, let alone the climate variability and change over NER.

1.2 Northeast India, and its climate

Northeast India (NER ≈ 89.5^{o} E to 98.5^{o} E and 21.5^{o} N to 29.5^{o} N; Figure 2), a prominent region of India, covers a geographical area of 262,230 km², and home to a population of about 45 million (Ministry of Home Affairs, Government of India). Out of this total geographical area, 28.3% has an elevation of more than 1200 m, 17.9% between 600 m and 1200 m and about 10.8% between 300 m and 600 m above mean sea level (Laskar et al., 2014). Around 82% of the total population is characterized by a largely rural population with low population density, a large percentage of indigenous tribal communities (34-91%), and a large area under forests (60%) (Ravindranath et al.,

2011). The entire region is a part of Indo-Burma and Himalayan hotspots, 2 of 25 such hotspots in the world (Jain et al., 2013). The region is located at the confluence of the Indo-Malayan, Indo-Chinese, and biogeographical realms (Tripathi et al., 2016). It shares international borders with Myanmar, China, Bhutan, and Bangladesh (Chakravarty et al., 2012). The region comprises seven states, popularly known as seven sisters, namely, Arunachal Pradesh, Assam, Meghalaya, Mizoram, Manipur, Nagaland, and Tripura (Sikkim is not included in the study area). The region has complex terrain, excessive sloping land with rolling topography, different altitudinal patterns, unique ethnicity (Laskar et al., 2014).

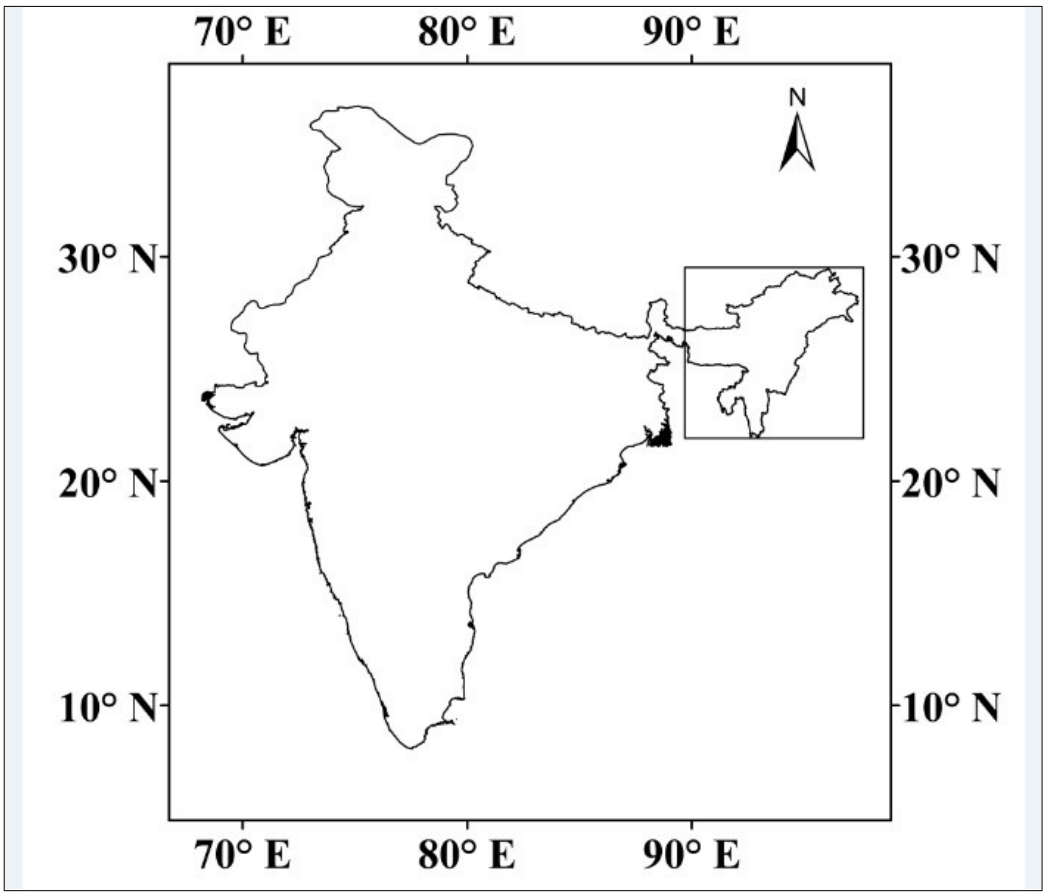

Figure 2: Study area (Northeast India, bounded by black box)

As the region have varied physiological features and altitudinal differences (Laskar et al., 2014), it is characterized by diverse climate regimes (Ravindranath et al., 2011) with predominantly humid subtropical with hot, humid summers, severe monsoons, and mild winters (Laskar et al., 2014). It has an area-averaged seasonal rainfall of 152 cm (Parthasarathy et al., 1995). The orographic dominance leads to enhanced convection making rainfall distribution more complex over the region (Mohapatra et al., 2011). Cherrapunji, a town in the NER, with the highest rainfall of ~12,000 mm in the world has been recently overtaken by a neighboring town, Mawsynram which is 80 km away (Jain et al., 2013). The Northeast India summer monsoon rainfall (NERSMR) simulations indicate a decreasing summer monsoon rainfall unlike rainfall received in mainland India (Dash et al., 2012 and Krishnan et al., 2016). The region is highly dependent on the summer monsoon rainfall and over 60% of the crop area is under rainfed agriculture, and so is in areas highly vulnerable to climate variability and climate change (Ravindranath et al., 2011). The mean temperature varies from 5° C to 30° C and the mean relative humidity remains between 70% and 85% for the most part of the year (Jain et al., 2013).

The NER is also endemic to many flora and fauna making it one of the richest providing habitats with diverse biota and a high level of endemism (Chakraborty et al., 2012 and Tripathi et al., 2016). The region has a great range of ecological habitats due to tremendous climatic, edaphic, and altitudinal variations (Tripathi et al., 2016). The vegetation ranges from alpine to subtropical and tropical wet evergreen, semi-evergreen, and moist deciduous (Saikia, 2009 and Dash, et al., 2015). According to the Forest Survey of India (FSI), 2017 the north-eastern states of India account for one-fourth of the country’s forest cover and there is a net decline of 630 km2 in forest cover compared with the previous assessment. While FSI, 2019 reported a decrease in the forest cover in 2019 in all the Northeastern states, except for Assam and Tripura. They reported that the forest cover in Arunachal Pradesh has decreased by 276.22 sq km, Meghalaya by 27.21 sq km, Nagaland by 2.60 sq km, Manipur by 499.10

sq km, Mizoram by 180.49 sq km while Assam has increased by 221.51 sq km and Tripura by 0.41 sq km. Due to poor infrastructure, lack of provisions supplied and other necessary livelihood requirements, the region has no basic government facilities, as a result of which the resources of the forests are exploited (Tripathi et al., 2016).

Vegetation is a vital component of the terrestrial ecosystem. It forms a green blanket on the earth (Roy et al., 2015b) with great variability over time and space (Sarmah et al., 2018). It characterizes the landscape both functionally as well as structurally (Roy et al., 2015b). It not only plays an important role in regulating biodiversity but also contributes to the variation of terrestrial net carbon uptake on Earth (Li et al., 2016). In addition to this, it is an essential element of the land surface system linking soil, water, air, and other environmental components which provides valuable information about the phenological change, crop status, land degradation, and most importantly global warming (Liu et al., 2015).

Global warming in recent decades has induced shifts in vegetation, causing a potential reduction in biodiversity and eventually alteration of ecosystems (Li et al., 2016). The productivity of vegetation ecosystems around the world has been greatly influenced by climate change. Changes in vegetation patterns in the mountain ecosystems are considered as one of the important and most noticeable forms of biodiversity affected by climate change (Li et al., 2016). Any changes in the vegetation density are associated with the annual and seasonal dynamics of the climatic variables of the respective region (Revadekar, Tiwari, & Kumar, 2012). The climate variability mainly reflected in precipitation and temperature is a major driver of vegetation dynamics. The relative impact of these two climatic variables on vegetation growth varies with time (Liu et al., 2015). Warming reduces the vegetation growth because moisture deficit due to increased evapotranspiration may offset the positive effect of

temperature on vegetation growth (Liu et al., 2015). Any distinct regional and local patterns of climate, say, changing rapidly due to topography, also uniquely influence the growth of the vegetation. Thus, the study of phenology i.e. life cycle of the plant provides an excellent quantity in evaluating the impact of climate change on vegetation. These periodic events (life cycle) of plants are initiated by climatic variations and climate change, in addition to other environmental factors (Chandola et al., 2010). The vegetation plays a vital role in water conservation as trees and other vegetation reduce the runoff and also increase percolation of water into the soil thereby improving the water regime in the area (Forest Survey of India, 2019).

Remote sensing is an important method for gathering information through mapping, measuring, and understanding changes in vegetation over spatial and temporal scales (Bhandari et al., 2012). Remote sensing-based satellite data has been very useful in studying the vegetation dynamics as it helps in identifying direct factors such as climate variability, human land-use management, and indirect factors such as climate change, CO2 fertilization, nitrogen deposition, and recovery from natural disturbances (Chen et al., 2019). The spectral signature of the vegetation of an area differs to changes in growth, phenological stage, and health of the vegetation and this information is useful in the study of the seasonal and inter-year changes associated with the vegetation cover over a given region (Hasan et al., 2011 and Nischitha et al., 2014). The measure of the vegetation cover and biomass could be evaluated by using a vegetation index, an indicator used for primary productivity and crop yield. It has been used for various purposes such as for detecting vegetation dynamics, agricultural production (Milesi et al., 2010), and long-term land use land cover variations (Reed et al., 1994; Revadekar et al., 2012 and Nischitha et al., 2014) for modeling terrestrial ecosystems on the global, continental and regional scales. As the human-induced and climate changes taking place, the study of time series of satellite data

is valuable because they provide a monitoring system with repeatable vegetation index measurements (Jong et al., 2012).

1.3 Literature Review

1.3.1 Recent Climate change over India, with focus on north-eastern India

1.3.1.1 Climate change over India

The daily rainfall data set from 1951 to 2000 (Goswami et al., 2006). They found a rising trend significantly in the frequency and also, the magnitude of extreme rain events. They also found a decreasing trend significantly in the frequency of moderate events over central India. While Goswami et al., (2006) claimed that seasonal mean rainfall over the region does not show a significant trend, subsequent studies show a significant decreasing trend in summer monsoon rainfall over states such as Chattisgarh in central India e.g. (Guhathakurta and Rajeevan, 2008; Rajendran et al., 2013 and Krishnan et al., 2016, etc). The temperature time series over North and South India during dry (November to May) season and wet (June to October) season for the period 1901–2007 (Kothawale et al., 2012). They found that the temperature shows a significant increasing trend over the regions. An increase in surface temperatures across various regions of India during the recent 3–4 decades as compared to the earlier period is also seen (Revadekar et al., 2012). They also found that the temperature during the winter season is expected to be prominent. The number of cold events is found to decrease by more than 75% while hot events increases are seen in around 70% of stations.

As far as climate projections are concerned, the general circulation models under the CMIP have a limited capability. For example, the variability of mean summer monsoon rainfall have been carried out in Indian and Australian monsoon using simulations from multi model mean summer monsoon rainfall

from 59 models using CMIP3 and CMIP5 simulations (Jourdain et al., 2013). The study in Indian and Australian monsoon shows that the observational uncertainty and model spread exists over the Indian region. They have also stated that the CMIP5 model performs better in reproducing the mean ISMR than the CMIP3 models. The CMIP3 and CMIP5 models have shown challenges in simulating the teleconnections and trends of the Indian summer monsoon rainfall owing to poor resolution, inadequate simulation of ENSO annual cycle, and consequent poor replication of monsoon-ENSO association, and importantly, spread in the observation-based gridded rainfall and temperature datasets (Jourdain et al. 2013 and Collins et al., 2013). The problem is more acute in reanalysis (also see Prakash et al., 2014). The decreasing Indian summer monsoon rainfall trend during the past decades (Guhathakurta and Rajeevan, 2008; Rajendran et al., 2013 and Krishnan et al., 2016, etc.) is not reproduced by the CMIP5 models, which is a serious limitation of the GCMs at coarse resolution in capturing the south Asian climate change in the recent decades (Roxy et al., 2015 and Krishnan et al., 2016).

As per a recent report by the Ministry of Earth Sciences (Krishnan et al., 2020), the summer monsoon rainfall has declined by 6% over India during the recent decades. An increase in the variability of summer monsoon rainfall and mean rainfall is projected by the end of the 21st century. It is also reported that the average temperature in India has risen by around 0.7°C during the recent decade. The temperature is projected to be rising by 4.4°C over India under the RCP8.5 scenario. Further details about the trends in the climate of India during the recent 4-5 decades, and the projections, can be availed from a recent report by the Ministry of Earth Sciences (Krishnan et al., 2020).

1.3.1.2 Recent climate variability and change over northeast India

The NER has a much larger seasonal summer monsoon mean rainfall (June to September) of around 152 cm than the rest of all India average which has about 86.5 cm (Parthasarathy et al.,1995). The

region as mentioned above receives the highest seasonal rainfall in India during the summer monsoon season. The temporal trends of precipitation and temperature from 1970 to 2099 over the NER using stations data sets have been studied where they have found out that the precipitation decreases while the temperature (maximum and minimum) increases in some portions of the region (Dash et al., 2015). The climate statistics evaluated by them show that the study varies from place to place due to sparse observational data sets and computational methods applied to the respective area over which the rainfall is averaged. Daily rainfall data from 15 stations for the period 1975 to 2006 in the NER studied by Goswami et al., 2010 found that the extreme rainfall events in NER decrease in the last few decades. This suggests an opposite pattern to the increase in the extreme rainfall events over central India. The difference is the topography of the region and its distance from Central India. The climate change vulnerability profiles of the NER at the district level for water, forest, and agriculture sectors for the current and future projections have been studied (Ravindranath et al., 2011). The study revealed that there is a significant decreasing trend in observed rainfall and increasing temperature in various places in the region. The region is seen affecting by climate change which may lead to droughts in the future due to a decrease in rainfall and an increase in temperature (Mondal et al., 2014).

1.3.2 Climate change studies based on the future projections, and climate during Last Millennium

While future climate projections cannot be verified, the simulations of the past climate, particularly that in the last millennium (LM), may be compared with the available paleo-observations, sparse as they are.

Analysis of Paleoclimate Modelling Intercomparison Project 3 *(*PMIP3) outputs by Tejavath et al., 19 (T19) shows a higher number of El Niños relative to La Niñas during the Medieval Climate Anomaly

(MCA), and vice-versa during the Little Ice Age (LIA). Notwithstanding that, the simulated Indian summer monsoon climate was relatively warm and wet (cold and dry) during the MCA (LIA). According to T19, changes in divergence/convergence patterns in the Indian monsoon region due to multi-centennial east-west shifts in the Walker circulation over the tropical Indo-pacific, result in a reduction of the ENSO impacts on the ISMR. The evolution of climate during the LM in the NER has been subject to local topography, among other factors (Mehrotra et al., 2014). They emphasize the spatial-diversity in the climate evolution in the NER during the MCA and LIA. Even a 1^{o}~2^{o} difference seems to matter owing to the topography. For example, some of these palynological studies suggest warmer and humid conditions during MCA and moderately humid LIA in the field sampled locations of the NER (Chauhan and Mandaokar, 2006; Bhattacharyya et al., 2007; Nautiyal and Chauhan, 2009; Basumatary and Bera, 2010 and Tripathi et al., 2017). In contrast, a weakening of the Southwest Monsoon since 900 BP in lower Assam (Dixit and Bera, 2012), and a generally cold-dry to a cold-moist oscillation of climate in the highland state of Sikkim, concurrent with the global LIA and MCA signals (Sharma and Chauhan, 1999) have been suggested. Further north between 27^{o} N-28^{o} N, warm and moist conditions from 2500 BP till today are indicated (Sharma and Chauhan, 2001; Bhattacharyya et al., 2007). Besides, an analysis of a sedimentary section from Arunachal Pradesh in the northeast Himalaya indicates a stable climatic condition from 1200 BP to the present (Agrawal et al., 2012). A speleothem record from the Wah-Shikar cave record (Gupta et al., 2019) indicates a relatively wet condition during MCA and mixed conditions and even mega-floods during the LIA. These studies suggest that the climate across NER throughout the LM may have been uniform, unlike other Indian regions.

Coming to future projections analysis, multi-model and multi-scenario precipitation and temperature projections for India based on CMIP5 for the period 1860 to 2099 and found that the CMIP5 ensemble

means the climate is closer to observed climate than any other individual model (Chaturvedi et al., 2012). They have also observed that mean warming in India between RCP6 and RCP8.5 is likely to be in the range of 1.7 °C to 2°C by 2030s and 3.3 °C to 4.8 °C by 2080s. They have also projected an increase of all India precipitation from 4 to 5% by 2030s and from 6 to 14% by 2080s. The present-day climatic conditions over the NER using the India Meteorological Department (IMD) and Regional Climate Model version 3 (Dash et al., 2012). They found wet bias over major parts of the region in the model precipitation. Warm nights in the summer months was found to be more frequent than the warm days. They also simulated a rise in the annual mean temperature in the future years. They are the only ones who have studied the climate variability over the region using model data based on downscaling CMIP3 datasets. They have found that the models overestimate rainfall data during the current period. The CMIP3 models projected an increase in the annual mean temperature.

1.3.3 Vegetation change studies based on remote sensing tools

The following is a brief review of the recent research on changes in the vegetation and its dynamics mainly in the NER, based on remote sensing studies. I also briefly discuss such studies for other regions, but relevant for my work reported in the thesis.

The time series of vegetation greenness data from satellites using Normalized Difference Vegetation Index (NDVI) satellite data between 1982 and 2008 have been examined globally (Jong et al., 2012). They have found both abrupt and gradual changes in large parts of the world with net greening detecting in all biomes, most notably in croplands and least notably in needle leaf forests. However, they have reported that 15% of the global land area, trends were found to have changed between browning and greening. They stated that such trends at large temporal extents may not be significant

and are often highly uncertain. Vegetation dynamics over South Asia using Advanced Very High-Resolution Radiometer (AVHRR) Normalized Difference Vegetation Index (NDVI) have been studied (Sarmah et al., 2018). They stated that various vegetation indices show diverse trend patterns over the same area where discrepancies occurred in tropical and subtropical areas during the summer monsoon season. From the recent satellite data for the period 2000 to 2017, China and India show a greening pattern that overlaps with croplands worldwide (Chen et al., 2019). The greening trend in China accounts for 42% from forests, 32% from croplands while in India, 82% from croplands and 4.4% from forests.

The vegetation in India using NDVI data from the Global Inventory Modeling and Mapping Studies (GIMMS) dataset obtained from the Advanced Very High-Resolution Radiometer (AVHRR) instrument onboard the National Oceanic and Atmospheric Administration (NOAA) satellite between 1982 and 2003 have been studied (Jeyaseelan et al., 2007). They found positive anomaly trends in vegetation change in most parts of the Indian region. The Spatio-temporal variability has been examined in some parts of India including Northeast India using data sets from the Advanced Very High-Resolution Radiometer (AVHRR) for the period 1981–2000, and Moderate Resolution Imaging Spectroradiometer (MODIS) Aqua data that was available for the 2000–2010 period (Revadekar et al., 2012). Their analysis shows that precipitation has a positive influence on the variability of vegetation. They have also found year to year variations in NDVI depending on the performance of the monsoon. A new vegetation type map of India has been prepared using satellite remote sensing where shifting cultivation was identified as the primary cause of deforestation in northeast India and seemed to be one of the major causes of forest conversion (Roy et al., 2015a). They have stated that due to practicing shifting cultivation by the people living in or near the forest, it continues to have a constant impact on the neighboring forests.

The fractional vegetation cover analysis in Northeast India using IRS WiFS NDVI has been studied for the period 1998 to 2000 during which they have found a decrease in fractional vegetation cover and increase in some other areas due to abandoned shifting cultivation (Lele et al., 2005). The forest fragmentation in Northeast India has been carried out using landscape matrices where they have found that the forest has been severely fragmented and the loss could be attributed to shifting cultivation, firewood, and fodder collection (Lele et al., 2008). The vegetation cover in NER using NDVI from NOAA/AVHRR and GIMMS data sets against rainfall and temperature from the Climate Research Unit's CR TS 2.1 data sets for 34 study sites for the period 1982 to 2002 where a decrease in the vegetation cover was found stating the causal factors to be climate change, shifting cultivation and rapid deforestation (Saikia, 2009). They have also reported a weak linear relationship between the growing season and, one- and two-month lags respectively, to rainfall and temperature over the region. Seasonal greenness over different forest types of India using MODIS time series NDVI data for the period 2001 to 2014 where 80% of the total negative changes in seasonal greenness are found in the core forest areas (Chakraborty et al., 2018). They also indicated that most of the changes are of high to medium category signifying the vulnerability of the Indian forest. The impact of climate change on Indian forests is based on climate projections of the Regional Climate Model of the Hadley Centre (HadRM3) and the dynamic global vegetation model IBIS for A2 and B2 scenarios (Chaturvedi et al., 2011). They presented a vulnerability index where northern and central parts of Western Ghats, parts of central India, upper Himalayas show most vulnerable to projected climate change while Northeastern forests show more resilient.

1.4 Research Gaps

The study primarily focuses on climate change during historical, future projections, the last millennium, and its impact on the vegetation over the region. The main reasons for conducting this study are as follows:

Firstly, the region, Northeast-India, as mentioned above has been affected drastically due to a decrease in rainfall and temperature. Despite having changes due to climate change, there is a lack of understanding of the interannual climate variability and teleconnections over the region. Only Dash et al 2012 have studied the recent and projected future climate change based on model studies. This indicates a very limited field sample of future projections over the region making it uncertain in terms of climate study. Therefore, there is a need for assessing the recent climate change using modern multiple datasets including many new available projections. Not only this, there is a need to compare the current climate with paleoclimate to generate better future scenarios.

Importantly, availability of multiple observational rainfall datasets such as the gridded IMD rainfall datasets as well as the Asian Precipitation Highly Resolved Observational Data Integration Towards Evaluation of water resource (APHRODITE) rainfall datasets is an opportunity to intercompare the results, have a measure of uncertainty, and also explore whether model projections fall in the uncertainty range from observations (e.g. Jourdain et al., 2013). It is also important to compare the signals from the gridded rainfall datasets vis a vis those from the station observations which is available from 1951 to 2014. Furthermore, the availability of relatively high-resolution CORDEX south Asia projections from multiple models help us to study the NER climate variability and future projections and add to the state of the art knowledge in this regard.

Secondly, the vegetation is associated with the annual and seasonal variations of the climate (Revadekar, Tiwari, & Kumar, 2012). Therefore, any changes in the local climate of the region could be a critical factor to the ecosystem thereby affecting the water balance in the soil moisture. This eventually affects the growth and distribution of vegetation. The response of vegetation to the changing environment or climate change is not yet well established over the region due to sparse datasets available. Therefore, using high-resolution satellite-based datasets, the impact of climate change on the vegetation profile for the region can be understood.

Based on the above, and gaps that exist as seen in this sub-section as well as others that were seen from the literature survey, I have defined the following objectives that I address in this thesis.

1.5 Objectives of the Thesis

The main goal of this work is to examine climate change and its impact in North East India. To attain the goal, the main objectives considered in this study are as follows:

1). To explore the current climate and its variability in Northeast India, using observations and CORDEX-SA historical simulations.

2). To study the past climate and future climate scenarios in light of observation data sets.

3). To examine the vegetation pattern in response to the current climate profile over the region.

1.6 Significance of the Study

Given the uncertainty that arises and with limited sampling available over the region, the study would be an opportunity in addressing the future climate at a higher resolution in light of the observation data available. Not only the current and future climate, but a paleo-research study would also be useful in attributing the studies as climate change is unprecedented. Past climate analysis may provide analogs

that may help us understand the current climate change and future projections better. For example, paleo simulation analysis would help in determining whether the changes between the two climate phenomena i.e. summer monsoon rainfall and ENSO are over long periods(e.g. Tejavath et al., 2019; 2020). As the region has the highest density of biodiversity, analysis of climate variability in the past over the region will be interesting. In this context, a brief analysis during the last millennium (LM) and future projections scenarios have been evaluated over the region to make a qualitative evaluation of whether the NER climate has changed over the last millennium, just as over the rest of India. This has obvious implications for juxtaposing the future changes of NER with that over other regions of India, say, the core monsoon region. Having said that, the region given its importance, studying its climate variability across the past through the future will be interesting.

Any changes in the phenological events of plants indicate variations be it climate or the condition of the plants and their environment (Reed at al., 1994). The spatial pattern of vegetation trends and their drivers vary significantly in different regions and seasons due to interannual variability (Sarmah et al., 2018). Therefore, such a study over the concerned region where the conventional observations are limited could provide linkages between climate cycles and trends in vegetative cover. The interaction between the climate variability and vegetation dynamics needs to be better understood as the monsoon has a great influence on it over the region and the annual trend alone cannot explain in detail the growth patterns. Proper and detailed monitoring is needed to assess whether the changes are taking place or not, and also for the development of the concerned ecosystem and human resource development.

Because of the above reasons, the study focuses on climate change and its responses to the vegetation at periodic level over the NER.

1.7 Outline of the thesis

This thesis is structured into four chapters:

In chapter 1, the general concept of climate change, a brief introduction of ISMR and its variability are discussed. A brief introduction on vegetation profile, its contribution and importance in the concerned region, its responses to changing climate, and the consequences have been discussed. These are followed by the objectives of the study, scope, and literature review. A detailed study area in terms of its topography, climate, and vegetation has also been discussed in this section.

Chapter 2 provides a detailed description of the data sets used, methodology applied and the respective tools used in this work.

Chapter 3 presents the results and discussion of the current climate observations and their variability over the region. The climate variation during the future projection scenarios and for the Last Millennium are also presented here. These are followed by the responses of vegetation patterns to current climate observations over the region.

Finally, chapter 4 summarizes the main conclusions of the study followed by future scopes.

The next chapter presents various data sets used and the methodology applied in the study.

CHAPTER-2

MATERIALS AND METHODOLOGY

This chapter illustrates the datasets used and the methodology applied in the thesis. The detailed description of the datasets and how they are applied in the study are explained here. This is followed by a detailed description of the software and tools used.

2.1 Data sets

In this study, I have used various in situ observations-derived gridded datasets, reanalysis datasets, outputs from various climate change simulations, remote sensing-based datasets, interpolated datasets, and field datasets were used.

2.1.1 Observations (and reanalysis) based datasets

The gridded rainfall and temperature data set, based on the in-situ observations from the IMD has been widely used for the climate change study over India due to its better accuracy in representing the magnitude and spatial variability. This has been demonstrated in an intercomparison of various observation-based gridded rainfall datasets, for example (Prakash et al., 2014). Therefore, this rainfall (Rajeevan et al., 2005), for the period 1970 to 2005 at 1° × 1° resolution, maximum and minimum temperature (Srivastava et al., 2009) datasets have been used as observation data. As can be seen from the relevant references, these gridded rainfall datasets have been generated by interpolating station

measurements from 1803 stations by the interpolation method proposed by Shepard (1968). Before carrying out the interpolation analysis, standard quality controls were also made (Rajeevan et al., 2005). 395 station data which are maintained and under controlled qualitatively by applying the interpolation method of Shepard's angular distance weighing algorithm (Sivastava et al., 2009) was used to develop the gridded maximum and minimum temperature.

Historical observation data sets mentioned above have been collected only till 2005 to match with the CORDEX South Asia historical simulations we have used (discussed in the next section), which are available up to 2005. The span of data helps us to validate the CORDEX- South Asia datasets. However, for some other analysis to document recent variations in the climate and relevance for vegetation in the northeast, as required, I have also utilized, the gridded rainfall dataset of 0.25° × 0.25° resolution collected from the IMD prepared from 6995 rain gauge stations in India for the period from 2000 to 2017 (Pai et al., 2014). The maximum and minimum temperature data mentioned above have also been used for the period 2000 to 2017. All these rainfall, maximum and minimum temperature data sets are available at http://www.imdpune.gov.in/Clim_Pred_LRF_New/Grided_Data_Download.htmlfbclid=IwAR3Z_ZfZkvwjaXAAFPRSDHc4TUywjddFZYMNIJIP78vVjFR-PK1iQDVksn8. As the observations in the NER are very sparse, it could lead to uncertainties. Therefore, in addition to the IMD rainfall datasets, the Asian Precipitation Highly Resolved Observational Data Integration Towards Evaluation of water resource (Aphrodite) precipitation data (Yatagai et al., 2012) for the period 1970 to 2005, available at 0.5° × 0.5° resolution, have been used for comparison of deductions from the IMD rainfall datasets, and also have a qualitative view of uncertainty associated with the gridded observational datasets over north-eastern India. The Aphrodite data are based on a dense network of rain-gauge data from Asia, including the Himalayas, South and Southeast Asia, and mountainous areas in the Middle East (Yatagai

et al., 2012). The Aphrodite data are available at https://climatedataguide.ucar.edu/climate-data/aphrodite-asian-precipitation-highly-resolved-observational-data-integration-towards.

The mean temperature data from Climatic Research Unit (CRU) TS v. 4.00 of 0.5° × 0.5° resolution for the period 1970 to 2005 were used in addition to the IMD temperature observations to account for the uncertainty. Monthly observations of station data sets collected globally were used for developing these datasets (Harris et al., 2014). The monthly datasets were developed by interpolating the land surface global stations (anomalies) datasets (excluding Antarctica) combined with the existing climatology into 0.5° x 0.5° resolutions for the period 1961 to 1990. (Harris et al., 2014). The data product is available at (http://www.cru.uea.ac.uk/ and http://badc.nerc.ac.uk/data/cru/).

The HadISST datasets for the period 1970 to 2005 have been used in teleconnection analysis. As per Rayner et al., 2003, the concentration of sea ice was combined with SST datasets (global monthly data) for the period 1871 till the present to develop these datasets. The dataset is available at https://www.metoffice.gov.uk/hadobs/hadisst/data/download.html.

2.1.2 Model datasets

Climate Model data for the historical period and future projections

The climate model data outputs of rainfall, maximum and minimum temperature from the LMDZ, MPI, ACCESS, GFDL, and CNRM models, available at the horizontal resolution of 0.5° x 0.5° under the aegis of the CORDEX South-Asia (Sabin et al., 2013) were used. These are dynamically-downscaled datasets based on CMIP5 climate projections. I have used these datasets for the ‘historical period’, i.e. from 1970 to 2005. I have analyzed various simulated climate statistics of the NER for the historical

period and compared them with those from the observations to ascertain that the models can simulate the current day climate reasonably. This gives some confidence, and a justifiable rationale, in accepting outcomes from any analysis of the future climate projections.

I have also used the future projections from 2011 to 2060 under the RCP4.5. These datasets are generated by the Centre for Climate Change Research, Indian Institute of Tropical Meteorology, Pune and the details of the above given five models are available at http://cccr.tropmet.res.in/workshop/oct2012/presentations/R%20Krishnan_CCCR_CORDEXSA.pdf, http://cccr.tropmet.res.in/workshop/oct2012/presentations/JSanjay_CORDEX-SAsia_RCM_data.pdf, and http://cordex.dmi.dk/joomla/images/CORDEX/cordex_archive_specifications_120126.pdf. The historical runs of these models are forced by observed natural and anthropogenic composition while the future projections are forced by Representative Concentration Pathways (RCP) 4.5 (Taylor et al., 2012 and Dufresne et al., 2013).

Climate model data for the Last Millennium

The climate model data for the study of the Last Millennium (LM) particularly, Medieval Climate Anomaly period (MCA): 935 CE to 1034 CE & Little Ice Age (LIA): 1735 CE to 1834 CE, were collected from the PMIP3/CMIP5 models CCSM4, MRI-CGCM3, MPI-ESM-P, available at 288 x 192 x L26 1, 320 x 160 x L48, and 196 x 98 x L47 discretization. The PMIP3 is an initiative endorsed by the World Climate Research Programme (WRCP); JSC/CLIVAR working group on coupled models and the International Geosphere and Biosphere Programme (IGBP; PAGES) (Braconnot et al., 2012). These datasets are available at https://cera-www.dkrz.de/WDCC/ui/cerasearch/. The reason why these three models were selected was because of the relatively higher resolution than other PMIP3 models that is potentially important given the complex topography changes and land surface changes across the

NER. The last millennium variations in the summer monsoon climate over the Indian region simulated by these three models also match with a majority of nine models and match with findings from several proxy-observational studies (Tejavath et al., 2017; 2019). In addition to these three models, higher resolution outputs from the ECHAM5, an atmospheric general circulation model (AGCM) at T106 (~1.125° x 1.125°) horizontal resolution for the period of 30 years (MCA: 935 CE to 965 CE and LIA: 1735 CE to 1765 CE) were also used. These simulations were carried out at the Max Planck Institute for Meteorology (MPIM) Germany (Roeckner et al., 2003). The datasets are available at https://refubium.fu-berlin.de/handle/fub188/6348?show=full. This dataset from the AGCM has been analyzed in tandem with the aforementioned outputs from the coupled models to explore the relevance of the tropical coupled oceanic processes, or the lack thereof, for the NER climate during the last millennium.

2.1.3 Remote sensing-based observation data

The satellite remote sensing data have been used in various studies due to its convenience and high efficiency providing a truly synoptic view of the earth (Revadekar, Tiwari, & Kumar, 2012 and Roy et al., 2015b). Therefore, to study the impact of climate change over the NER, in this study, few satellite datasets were used. The datasets are followed as:

NDVI data

The Normalized Difference Vegetation Index (NDVI) (Didan, 2015) data product, MOD13A1 (version 6), of 36 spectral channels collected from MODIS instrument onboard Terra satellite for the period 2000 to 2017 were used. The data product is a 16-day composite of resolution 500 m. The NDVI is computed from the surface reflectance (bidirectional) which has been corrected atmospherically with other masked datasets such as heavy aerosols, water, and cloud shadows. The NDVI data is available at

https://search.earthdata.nasa.gov/. The MODIS-derived NDVI data have been demonstrated to be of high fidelity and are more sensitive to chlorophyll concentration and other variations such as land cover, seasonal vegetation, and biophysical parameters (Huete et al., 2002) and less sensitive to conditions such as atmospheric vapor as the MODIS has narrower bands in the red and NIR wavelengths (Chang et al., 2014). It is the ration of the red and near-infrared (NIR) bands of a sensor (Rouse et., 1973) and is represented as follows:

$$NDVI = NIR – RED/NIR + RED \qquad \text{Equation 1}$$

where, NIR is the near-infrared reflectance at 0.77-0.86 μm and RED is the visible reflectance at 0.62-0.68 μm.

NDWI data

The Normalized Difference Water Index (NDWI), a surface spectral reflectance (product name: MOD09A1, version 6) measured at ground level derived from the MODIS of 8-day composite, L3 at 500 m resolution were used (Vermote, 2015). The data are derived from the MODIS channels of band 2(Near-Infrared) and band 6(Short-wave-infrared). These estimate the leaf water content at the canopy level (Gao, 1996). The variations caused by the leaf's internal structure and its dry matter content are eliminated by the combination of these two bands. By doing so, the accuracy is improved, in retrieving the water content of vegetation (Ceccato et al., 2001). It has been refined for internal snow, cloud, and cloud shadow detection algorithms. The data are available at https://earthdata.nasa.gov/. The calculation of the index is explained below in the methodology section.

2.1.4 Reanalysis Aridity data

Aridity data (5 km x 5 km) derived from TERRAClimate (Abatzoglou, J.T. et al., 2018) collected from the National Center for Atmospheric Research (NCAR) for the period 2000 to 2017 were used. These are monthly surface water balance interpolated datasets. To prepare these datasets, high-resolution spatial data of WorldClim climatological normals are combined. Water balance model incorporating temperature, precipitation, evapotranspiration, and interpolated soil water capacity extracted from the plant was used for the preparation of this data. The spatiotemporal aspects of TerraClimate have been validated using annual precipitation, temperature, evaporation from station data, and annual runoff from streamflow gauges. Important inputs in studying the hydrological and ecological issues at global scales where high spatial resolution climatic water balance data are needed can be achieved by these datasets (Abatzoglou, J.T. et al., 2018). The data is available at https://climatedataguide.ucar.edu/climate-data/terraclimate-global-high-resolution-gridded-temperature-precipitation-and-other-water.

2.1.5 Field sample data (Land-use-and-land-cover map (LULC))

The LULC map for the year 2005 generated during the project of the Development of Decadal (1985–1995–2005) Land Use and Land Cover Database for India using multi-spectral and multi-temporal satellite data of medium resolution (Roy et al., 2015a) was used. The accuracy of the map was determined using pre-determined field sample points collected for the characterization project of the Indian Space Research Organization (ISRO) and the Department of Biotechnology (DBT) (Roy et al., 2015a). Six vegetation classes collected from the LULC map given below were studied for NER.

DBF	Deciduous Broad Leaf Forest
EBF	Evergreen Broad Leaf Forest
ENF	Evergreen Needle Leaf Forest
MF	Mixed Forest
SL	Shrub Land
GL	Grassland

Table 1: Types of vegetation classes used in the study.

2.2 Methodology

2.2.1 Evaluation of the current climate and its variability

In this study, the current climate (1970 to 2005; also referred to as historical period to match with model output terminology), and its variability over the NER were evaluated using the observation data of rainfall, maximum and minimum temperature derived from the IMD, other observation-based data including Aphrodite data, the reanalysis data from the CRU and the CORDEX-SA historical simulations.

Model validation

For better accuracy in statistical analysis, the region bounded by the latitudes from 25.5° N through 28.5° N, and longitudes from 92.5° E through 94.5° E are referred to as the NER in the study. The validation of the downscaled historical simulation outputs is done by comparing the climatology of all the models with observed rainfall, maximum, and minimum temperature patterns. To facilitate the validation, the observed datasets are refield sampled into 0.5° resolutions using a bilinear interpolation method. By doing this, the future climate change in the NER could be assessed taking into account uncertainty associated with intermodel variability.

Then the interannual variability and seasonal variability of rainfall and temperature have been assessed during the summer monsoon season (JJAS) and winter monsoon season (DJF). This is followed by the statistical analysis presented in the later statistical section.

2.2.2 Evaluation of the past climate especially the last millennium period and future projections scenarios

Last Millennium

Given the importance of summer monsoon rainfall in NER, my analysis of this paleoclimate study pertains only to the identical season. Before analyzing the above past climate simulations, the simulations for the current period 1961 to 1990, broadly compatible with the 'historical period' have been validated against the corresponding observed rainfall data from the IMD. This period has been selected as the rainfall data from the ECHAM5 model is available for this period. Then the seasonal climatology of simulated rainfall between the MCA and the LIA period over the NER have been analyzed. The remaining analysis is presented in the statistical section.

Future projections

The future climate change over the region has been evaluated from the simulated CORDEX SA model outputs of rainfall, maximum and minimum temperature data sets over JJAS and DJF seasons for the period 2011 to 2060. Likewise, current climate study, interannual and seasonal variations are analyzed for this period. In addition to this, to have an estimation of the future climate change in NER, the historical climatology of each parameter was subtracted from the corresponding future climatology. For

example, say "C hist" as the historical climatology and "C RCP" as the future climatology, then let ΔC = C RCP − C hist.

2.2.3 Impact of climate change on the vegetation pattern

I have carried out a two pronged-analysis, one, at field sample points in the NER, as elaborated below, and another, considering the whole domain of the NER. In other words, various datasets have been analyzed at field sample points in the NER, identified based on the distribution of six vegetation classes from the LULC map namely, Deciduous Broad Leaf Forest, Evergreen Broad Leaf Forest, Evergreen Needle Leaf Forest, Mixed Forest, Shrub Land, and Grassland, as well as for the entire NER region. The extracted NDVI data collected from the MODIS of all the vegetation classes were analyzed by using the observed data sets of rainfall, maximum and minimum temperature from the IMD, along with NDWI and aridity data sets from 2000 to 2017.

2.2.3.1 Field sample points

Area-averaged anomalies of NDVI

The fortnightly normalized difference vegetation index (NDVI) data (HDF format) were downloaded from the National Aeronautics and Space Administration (NASA)'s Earth Science Data Systems (ESDS) program (https://earthdata.nasa.gov/) from 2000 to 2017. The Hierarchical Data Format (HDF) format was converted into Geotiff using HDF-EOS to GeoTIFF Conversion Tool (HEG) software. The GeoTIFF files were then imported into .img format in Earth Resources Data Analysis System (ERDAS) imagine. All the raster files in .img were layers-stacked in ERDAS. The study area of the NER has been subset from the stacked raster files using a shapefile of NER. The subset raster file was projected to World Geodetic System (WGS) 84 zone 44, a reference coordinate system used to define the exact

positions of the study area. Then the processed datasets were multiplied by a scale factor of 0.0001 to achieve the actual NDVI data value as the raw NDVI data is not in the normal NDVI range. The subset fortnight NDVI data were area-averaged into three seasons namely, wet (June to October), winter (November to February), and dry (March to May). Using field sample point locations based on the land use land cover categories (LULC map of 2005), the NDVI of six vegetation classes (Table 1) were extracted in R software. The anomalies of NDVI for each vegetation class were calculated by subtracting the mean NDVI of each year from the long-term average NDVI for all three seasons respectively.

Area-averaged anomalies of NDWI

The Normalized Difference Water Index (NDWI) data and datasets of surface reflectance 2 and surface reflectance 6 were also downloaded from the same data source (https://earthdata.nasa.gov/). The data followed the same pre-processing methods used for NDVI up to scale factor multiplication. After this, the NDWI was computed using the near-infrared: (NIR – MODIS surface reflectance band 2) and the shortwave infrared: (SWIR – MODIS surface reflectance band 6) (Gao, 1996) in the model maker in ERDAS following the formula (NIR-SWIR/NIR+SWIR). The study area was subset from the NDWI data using the Northeast shapefile. Then the subset NDWI data were averaged into the same three seasons and six vegetation classes were extracted using field sample points from the LULC map. Anomalies of NDWI were calculated following the same methods used in NDVI.

Area-averaged anomalies of aridity

Aridity data derived from monthly TerraClimate was downloaded in NetCDF format from the National Center for Atmospheric Research (NCAR). The data were converted into raster and .img format for further processing in ERDAS. Then subsetting the study area, averaging into three seasons, extraction

of vegetation classes, and finally, anomaly calculation was done following the same methods used above.

Area-averaged anomalies of observed data

The rainfall data of 0.25° × 0.25° resolution (Pai et al., 2014) and, maximum and minimum temperature of 1° × 1° resolution (Srivastava et al., 2009) for the period 2000 to 2017 collected from the IMD were first detrended using Climate Data Operator (CDO) tool to remove the probable distortion caused and to see the local impact more accurately. Then the detrended rainfall, maximum, and minimum temperature datasets were area-averaged into three seasons namely, wet (June to October), winter (November to February), and dry (March to May). Using ArcGIS, the Network Common Data Form (NetCDF) format of these datasets were converted into raster and .img format for further processing of the data. After conversion, the field sample points of the six vegetation classes from these datasets were extracted. Likewise, the NDVI anomalies, the anomalies of rainfall, the maximum and minimum temperature for all three seasons of the six vegetation classes were calculated.

The NDVI anomalies calculated using the field sample points were evaluated against the corresponding rainfall, maximum, minimum temperature, aridity, and NDWI anomalies for the three seasons from 2000 to 2017 to understand the temporal patterns and also the association of the NDVI with the corresponding parameters.

2.2.3.2 Entire Northeast region

The entire grids points of NDVI in raster format for each season were converted into .csv format to acquire the numerical value using ArcGIS and excel sheet. Then all the values were averaged for each season and calculated anomalies (same methods used above were applied) for the entire region of the

three seasons. Similarly, anomalies of rainfall in the NetCDF format of the entire region have been calculated using the Grid Analysis and Display System (Grads) tool. Then the NDVI anomalies were evaluated against the rainfall anomalies for all three seasons from 2000 to 2017.

In addition to the above analysis, for more transparency and also to support the studies carried out, the following analyses have been carried out to find out which season has the highest to lowest NDVI. For this, the maximum value of NDVI for all three seasons from 2001 to 2017 were collected from the raster file of NDVI using ArcGIS. The period (2001 to 2017) was made similar for all three seasons to make it easier in figuring out the season. Then the values were plotted in an excel sheet with the help of a trend line. Furthermore, the values of NDVI in raster format from 2001 to 2017 for all the three seasons were also plotted spatially using ArcGIS. This was done to see the variability taking place on yearly basis.

2.2.4 Statistical analysis

Current climate variability

A linear trend analysis was applied on the area-averaged rainfall and that of the temperature over the NER for the period 1970 to 2005 by using the Least square linear fit (Jhajhariaa and Singh, 2011; Jain and Kumar, 2012 and Dubey and Krishnakumar, 2014) on the observed and simulated rainfall and temperature datasets. Then the significance test of the linear trend has been evaluated by using the Student t-test and Mann Kendall (M-K) trend test at 0.05% significance level. The M-K test is a non-parametric test for identifying the trend in time series data and extensively used in climate studies for verifying spatial variation and temporal deviation of any climatic series (Kumar et al., 2010; Jain and Kumar, 2012; Jain et al., 2013; Laskar et al., 2014 and Chinchorkar et al., 2015). This statistical method

is used to test the null hypothesis that the trend is insignificant, and its significance is evaluated based on the Z value. The null hypothesis is rejected at α level of significance in a two-sided test if the computed value of |Z | > Z α/2. Any increasing trend is denoted by a very high and positive value of S while the decreasing trend is denoted by a low and negative value of S (Laskar et al., 2014).

M-K statistics for a series, say x (x_1, x_2, x_3, x_4, ..., x_n) follows as:

$$S = \sum_{i=1}^{n-1} \sum_{j=i+1}^{n} \operatorname{sgn}(x_i - x_j) \qquad \text{Equation (2)}$$

where the value of sgn ($x_i - x_j$) is computed as follows:

$$\operatorname{sgn}(x_i - x_j) \begin{cases} = 1 & \text{if } x_i - x_j > 0 \\ = 0 & \text{if } x_i - x_j = 0 \\ = -1 & \text{if } x_i - x_j < 0 \end{cases} \qquad \text{Equation (3)}$$

and variance of M-K test statistics is computed

$$Var(S) = \frac{n(n-1)(2n+5) - \sum_{k=1}^{n} t_k \left(t_k - 1\right)\left(2t_k + 1\right)}{18} \qquad \text{Equation (4)}$$

where "*n*" is the number of data points, "*k*" is the number of tied groups and "t_k" is the number of data points in kth tied group. Then the Z statistics test (standard normal deviation) is computed as follows:

$$Z = \begin{cases} = \dfrac{S-1}{\sqrt{Var(S)}} & \text{if S} > 0 \\ = 0 & \text{if S} = 0 \\ = \dfrac{S+1}{\sqrt{Var(S)}} & \text{if S} < 0 \end{cases} \qquad \text{Equation (5)}$$

The observed and simulated rainfall, maximum and minimum temperature datasets, and the HadISST datasets for the historical period (1970 to 2005) have been used to decipher the teleconnections between the summer monsoon climate in the NER and ENSO. The well-known Nino 3.4 index is used to represent the ENSO activity. This index is obtained by area-averaging the SST anomalies over the region (5° N–5° S and 120° W–170° W). Then a linear correlation method known as Pearson correlation was applied to check the association of the ENSO events with the NER climate. This method measures the statistical association or relationship between two variables. The value ranges from -1 to +1, with -1 indicating a negative correlation and +1, a positive correlation between the two variables. A negative correlation indicates that if one variable increases, the other decreases, and vice versa, while a positive correlation indicates that both variables decrease or increase together. Then statistical significance test is computed using a two-tailed Student t-test where the p-value is compared to the significance level of 0.05. If the p-value is less than or equal to the significance level then the test is statistically significant, and if more then it is statistically insignificant.

Extremes of rainfall, maximum and minimum temperature datasets from both the observed and simulated historical datasets have been estimated using the histogram method.

Last Millennium

Teleconnections between the indices (NINO3 and NINO3.4), and the simulated datasets were evaluated by area-averaging the sea surface temperature (SST) anomalies over the 5° S to 5° N and 150° W to 90° W (NINO3) and 5° S to 5° N and 170° W to 120° W (NINO3.4) to represent the ENSO variability. Using two-tailed Student's t-tests, statistical significance tests have been calculated for correlations performed for teleconnection. The Student’s t-tests are also performed on the difference of means calculated between the MCA and the LIA period.

Future projections

The Least square linear fit was also applied on the area-averaged rainfall and temperature for the period 2011 to 20160. The significance test was done using the Student's t-test and M-K test.

Variability of vegetation patterns

Means and standard deviations of field sample points of all the six vegetation classes for all three seasons were calculated for NDVI and rainfall from 2000 to 2017 to find out the variation and also, the association between them over the region. To see the relationship more precisely between the NDVI pattern and the rest of the parameters used, the correlation coefficient, multiple regression, and lag correlation were computed at the 0.05% significance level.

2.3 Software used

In this study, the gridded observation datasets, and climate model datasets have been analyzed using tools such as GrADS (version 2.2.1), Climate Data Operators of version 1.9.6. For the analysis of satellite datasets, software such as ERDAS Imagine (version 9.1), ArcGIS (version 10.2), HEG software (version 2.12), and R software (version 3.1.1) were used for pre-processing, extraction, etc.

GrADS: It is a freely available interactive desktop tool commonly used for easy access, manipulation, and visualization of earth science data. This tool handles both gridded data as well as station data. It supports many data formats such as binary, NetCDF, GRIB, HDF & BUFR for station data.

CDO: It is a freely available software used for fast processing climate and forecast model data. This software operates arithmetic functions, statistical, data selection, subsampling tools, and spatial

interpolation. It supports file formats such as NetCDF, GRIB, SERVICE, EXTRA, and IEG, etc. More than 600 operators are available in CDO.

HEG: It is a tool developed for the conversion of HDF-EOS formatted granules of Geographical Information System (GIS) compatible formats particularly GeoTIFF. This tool reformats HDF-EOS Swath & Grid data to the HDF-EOS grid, GeoTIFF, or a generic format. The tool is available as a down-loadable tar file.

ERDAS Imagine: It is an image processing remote sensing software used to process geospatial, other imagery, raster as well as vector data. It allows us to prepare, display, and enhance digital images. This tool runs on the windows operating system used to study many satellite imageries and other advanced remote sensing data sets.

ArcGIS: It is a geographic information system software used for creating maps, editing datasets, compiling geographic data and information in a database.

R software: It is a free language software used for statistical computing and graphics under the terms of the Free Software Foundation's GNU General Public License in source code form. It runs on Windows, UNIX platforms & MacOS.

Softwares	Links
GrADS	http://cola.gmu.edu/grads/
CDO	https://code.mpimet.mpg.de/projects/cdo/
HEG	https://hdfeos.org/software/heg.php
ERDAS	https://www.hexagongeospatial.com/products/power-portfolio/erdas-imagine/erdas-imagine-remote-sensing-software-package
ArcGIS	https://www.esri.com/en-us/arcgis/products/arcgis-desktop/overview
R	https://www.r-project.org/

Table 2: Source of softwares used.

CHAPTER – 3

RESULTS AND DISCUSSIONS

This chapter presents the analysis carried out for the study and the findings from the results. The chapter is divided into three sub-sections based on the objectives of the study. Sub-section 3.1 discusses the observed mean seasonal rainfall and temperatures over the NER for the historical period (1970-2005), along with those from the CORDEX-SA historical simulations. Secondly, my last millennium analysis and the future projections study have been presented in sub-section 3.2 and the impact of climate change on the vegetation pattern during the current period in sub-section 3.3.

3.1 The climate variability during the historical period based on observations and corresponding climate models

3.1.1 Climatology for JJAS historical simulation from 1970 to 2005

Figure 3.1.1 is an effort to validate the simulated JJAS climatology of precipitation (RF-JJAS) from 1970 to 2005 with the IMD observations and the Aphrodite data. We find from the spatial distribution of the observed climatological RF-JJAS that it varies from 9 to 22 mm, Aphrodite data ranges from 3 to

13 mm, and model data range from 3 to 18 mm. However, the corresponding Aphrodite distribution and those from all models except the LMDZ show rainfall increasing from north to southwest. In LMDZ climatology, the RF-JJAS increases towards the southeast. Notwithstanding such discrepancy in the gradients, the range of climatological RF-JJAS across the observational datasets and models is not much different.

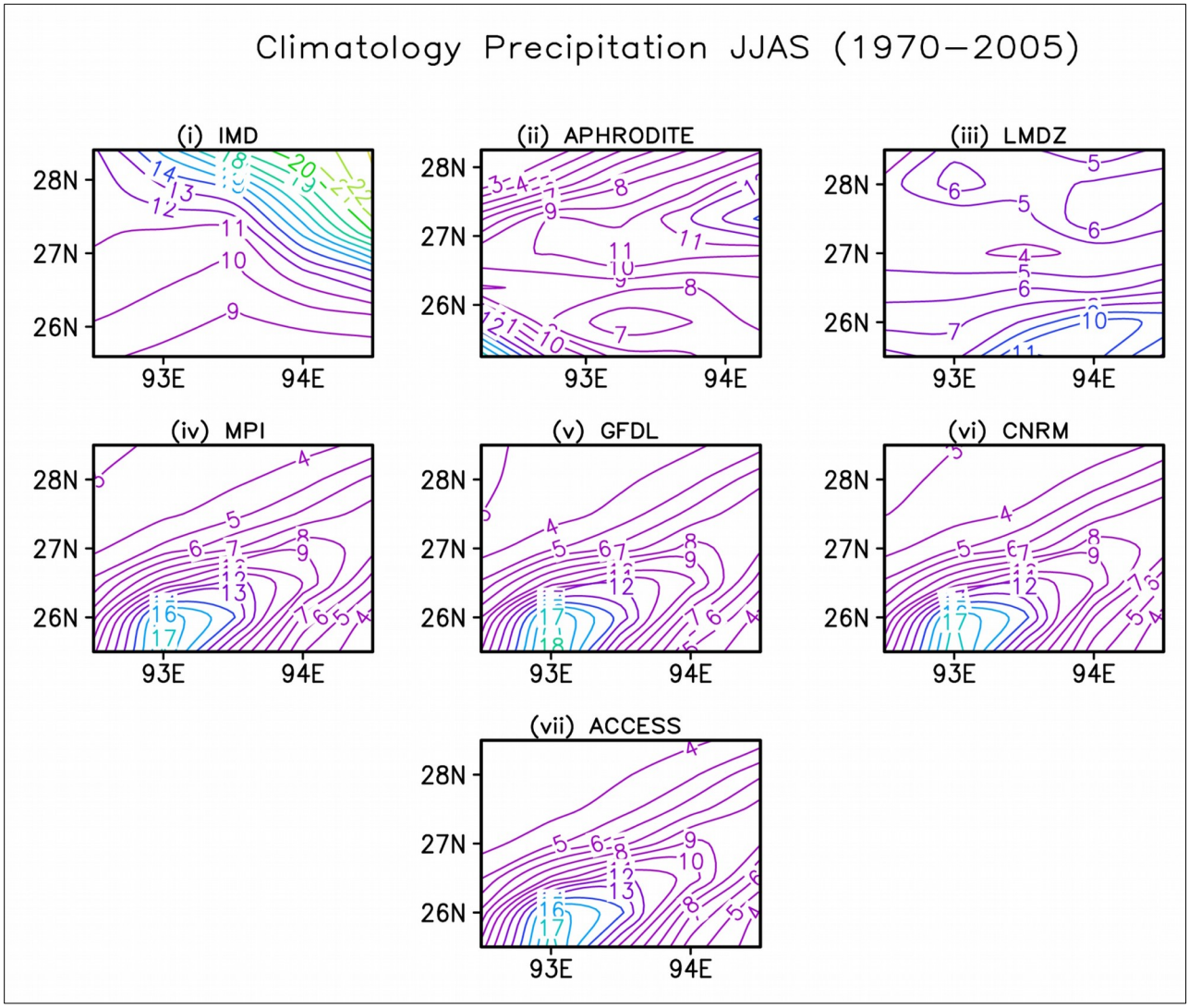

Figure 3.1.1: Spatial distributions of JJAS climatology of precipitation (mm) during 1970–2005 (historical) for (i) IMD, (ii) APHRODITE data, and climate model data from Cordex South Asia: (iii) LMDZ, (iv) MPI, (v) GFDL, (vi) CNRM and (vii) ACCESS over North East Region.

The observed climatological TMax-JJAS varies from 30.6 °C to 32 °C in figure 3.1.2. Its maximum occurs approximately in the central north-east and increases from west to east. The climatological TMax-JJAS across the NER from the CRU reanalysis ranges from 19 °C to 20.5 °C and decreases in the center. The CRU data and each model exhibit a relatively broad range of climatologies across the NER compared to the observed data. The simulated climatology of the (TMax-JJAS) by various models is lower with different spatial distribution than the observations. The simulated climatological values vary from 12 °C to 29 °C across the region in models. The LMDZ model shows an increasing TMax-JJAS from the northwest towards the south, with the maximum values occur in the center. The rest of the models show a rising TMax-JJAS from the northwest towards the southeast.

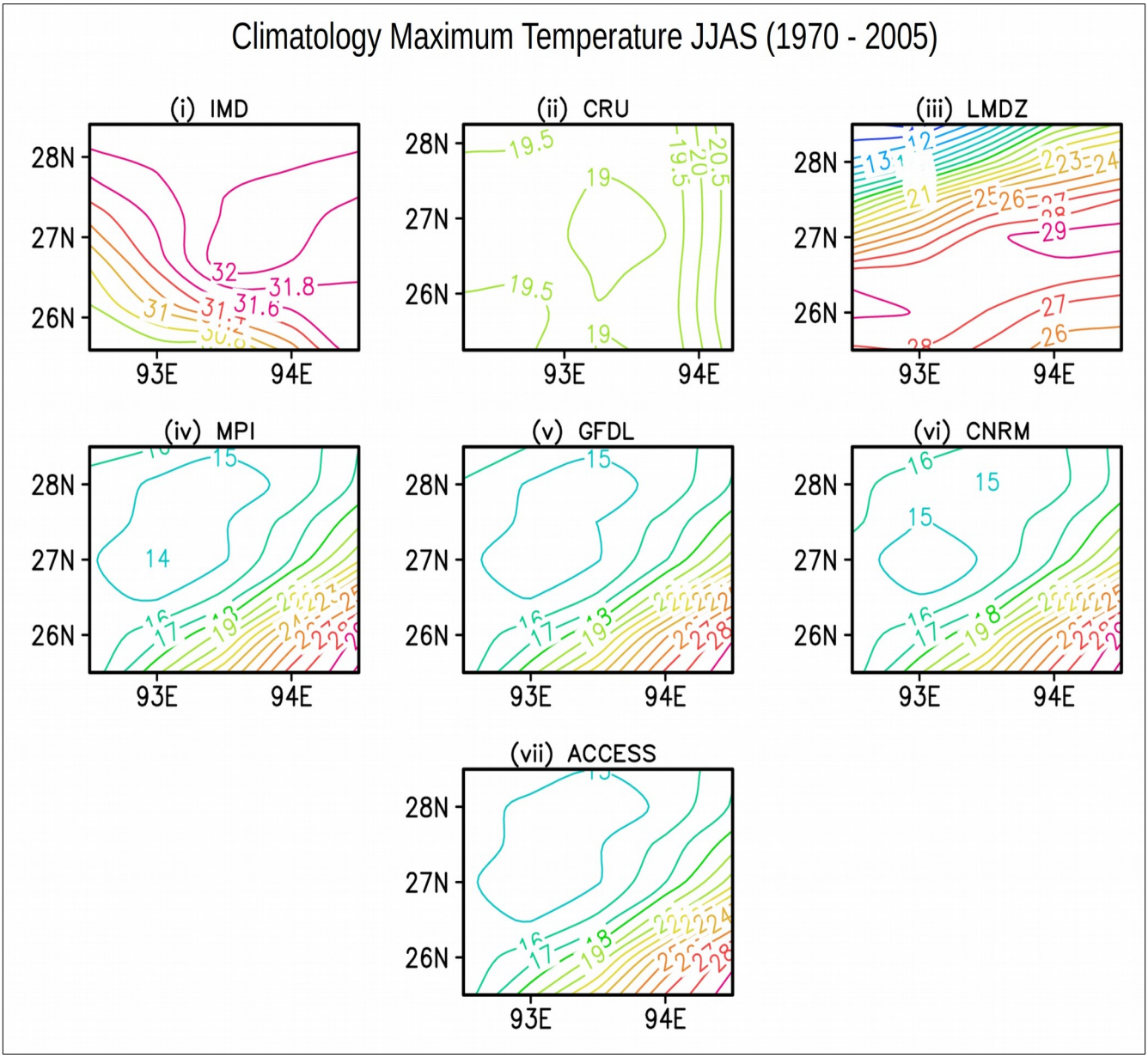

Figure 3.1.2: Spatial distributions of JJAS climatology of maximum temperature (°C) during 1970–2005 (historical) for (i) IMD, (ii) CRU data, and climate model data from Cordex South Asia: (iii) LMDZ, (iv) MPI, (v) GFDL, (vi) CNRM and (vii) ACCESS over North East Region.

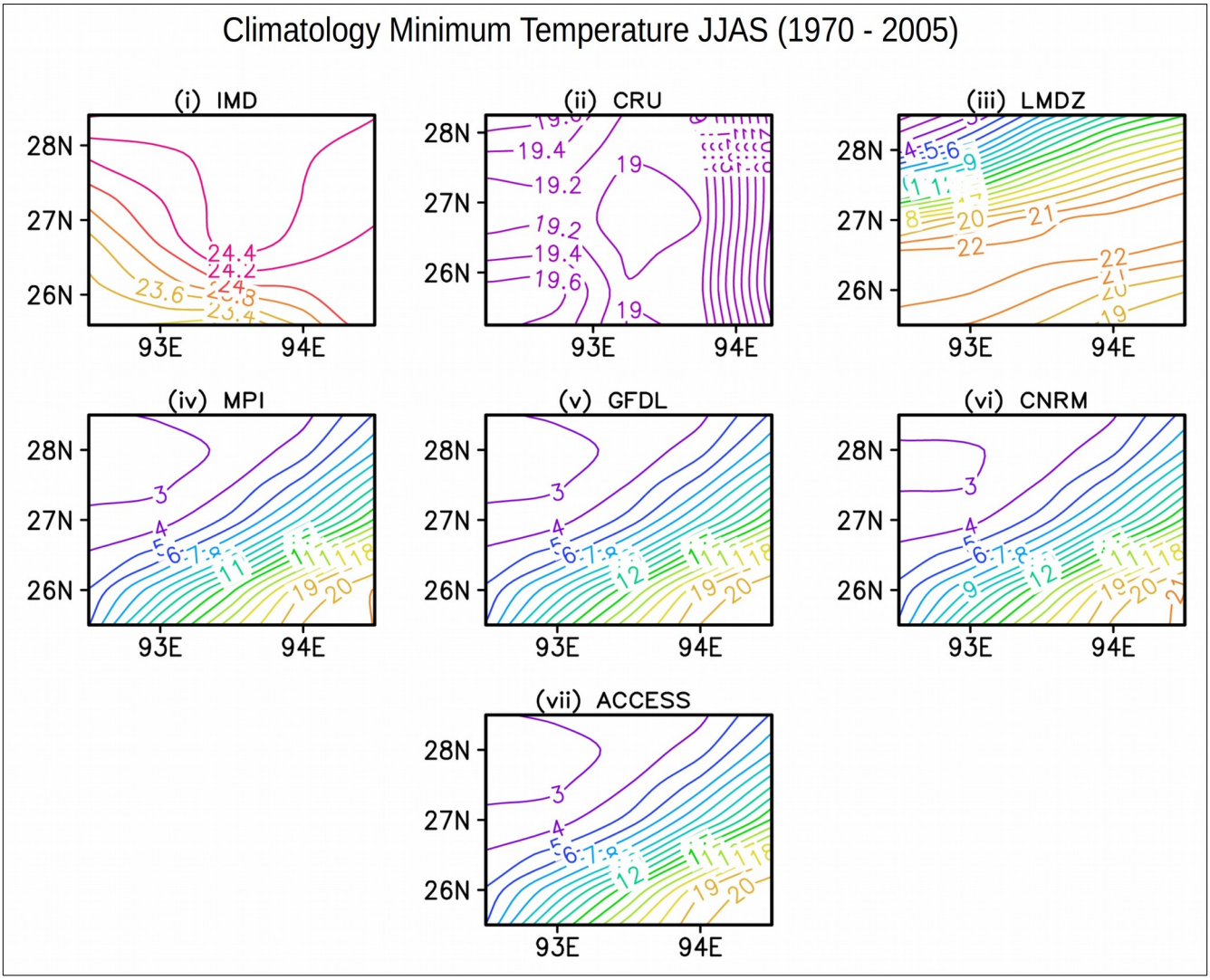

Figure 3.1.3: Spatial distributions of JJAS climatology of minimum temperature (°C) during 1970–2005 (historical) for (i) IMD, (ii) CRU data, for climate model data from Cordex South Asia: (iii) LMDZ, (iv) MPI, (v) GFDL, (vi) CNRM and (vii) ACCESS over North East Region.

The models also underestimate simulated climatological minimum temperature in JJAS (TMin-JJAS) relative to the CRU reanalysis (Figure 3.1.3). The simulated range is 3 °C~22 °C vis-a-vis the observed range of 28°C~32 °C in observed data varies from 19 °C to 20.2 °C from the CRU reanalysis datasets.

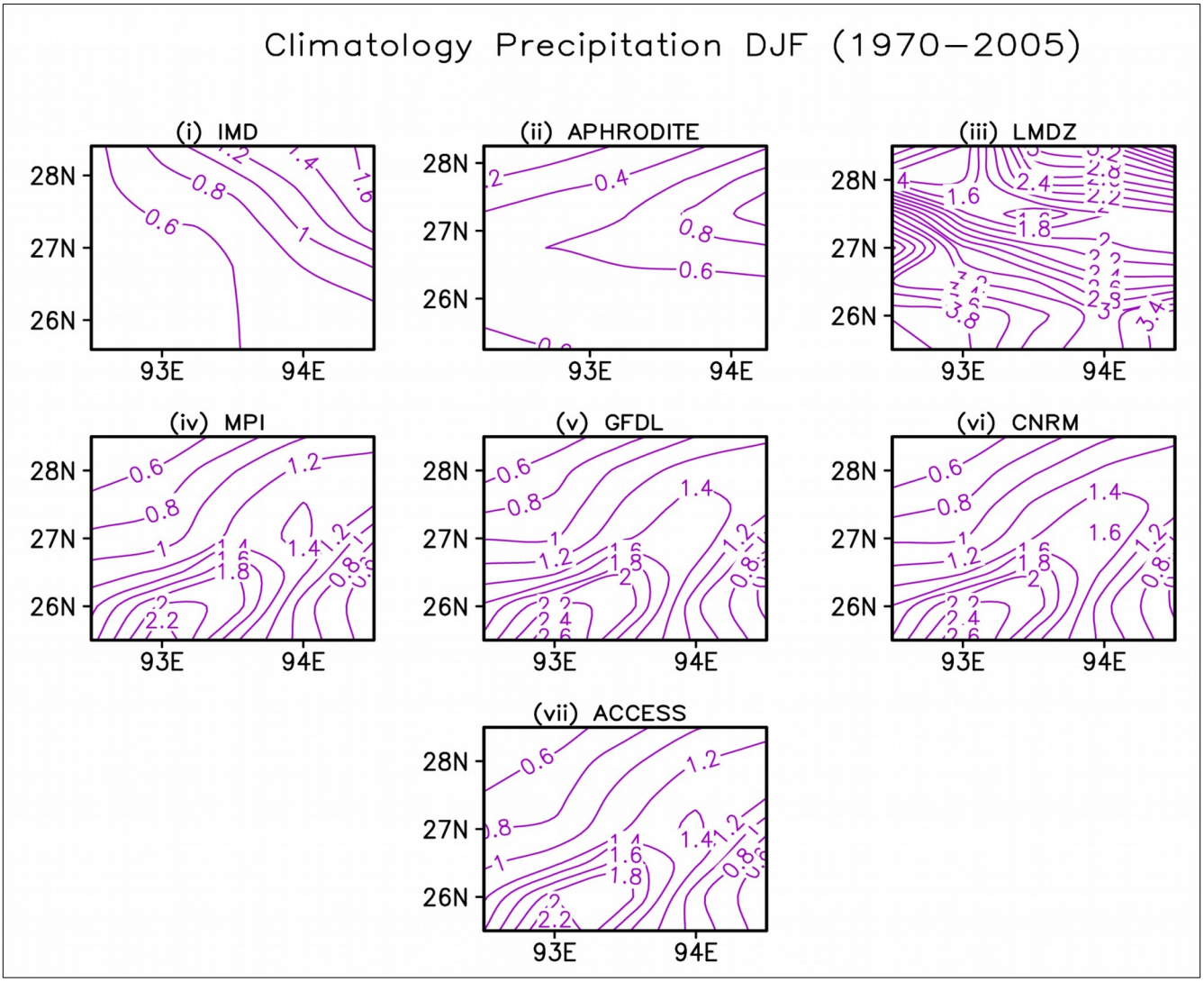

Figure 3.1.4: Spatial distributions of DJF climatology of precipitation (mm) during 1970–2005 (historical) for (i) IMD, (ii) APHRODITE data, and climate model data from Cordex South Asia: (iii) LMDZ, (iv) MPI, (v) GFDL, (vi) CNRM and (vii) ACCESS over North East Region.

Figure 3.1.4 shows the DJF climatology of precipitation (RF-DJF) for the period 1970–2005, derived from the IMD, Aphrodite, and model datasets. The magnitude of the RF-DJF across the NER ranges between 0.6 and 1.6 mm, with Aphrodite datasets ranging from 0.2 to 0.8 mm and the models, ranging from 0.5 to 3.8 mm, also capturing the relatively low seasonal climatological rainfall during the DJF season (Figure 3.1.4) as compared to the JJAS season (Figure 3.1.1).

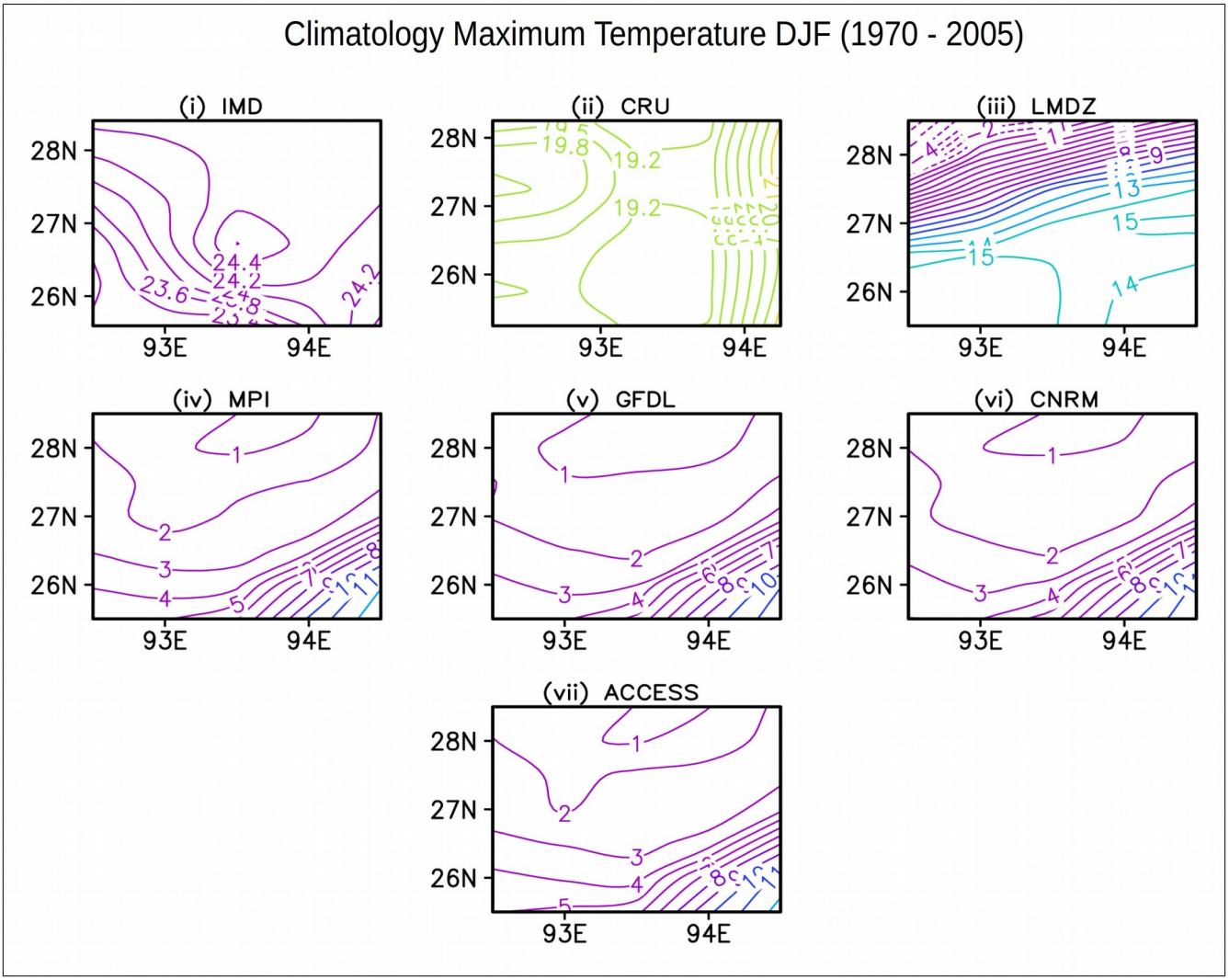

Figure 3.1.5: Spatial distributions of DJF climatology of maximum temperature (°C) during 1970–2005 (historical) for (i) IMD, (ii) CRU data, and climate model data from Cordex South Asia: (iii) LMDZ, (iv) MPI, (v) GFDL, (vi) CNRM and (vii) ACCESS over North East Region.

The DJF climatology of maximum temperature (TMax-DJF) in IMD observations varies from 23.4 °C to 24.4 °C (Figure 3.1.5) and increases from the south to north of the NER. The CRU data ranges from 19 °C to 21.2 °C, with a decrease in TMax-DJF in the center. The models underestimate the climatological TMax-DJF in the NER, with the simulated TMax-DJF ranging from 1 °C to 15 °C.

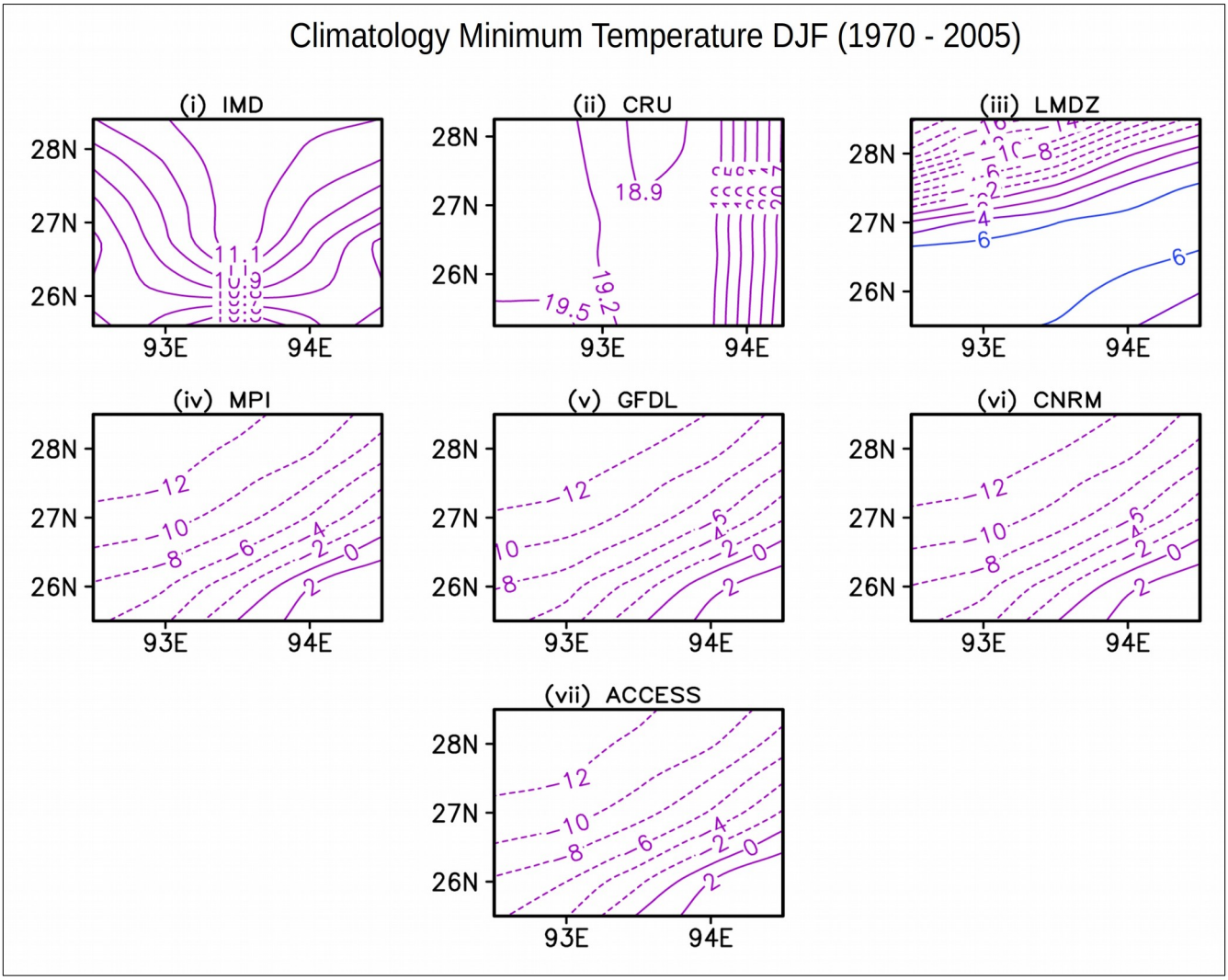

Figure 3.1.6: Spatial distributions of DJF climatology of minimum temperature (°C) during 1970–2005 (historical) for (i) IMD, (ii) CRU data, and climate model data from Cordex South Asia: (iii) LMDZ, (iv) MPI, (v) GFDL, (vi) CNRM and (vii) ACCESS over North East Region.

The simulated winter climatological minimum temperatures (TMin-DJF) in Figure 3.1.6 exhibit a range of values from 10.4 °C to 11 °C, which are relatively nearer to that from the IMD datasets, with CRU data having higher (TMin-DJF).

Mean climatology (mm)							
	Precipitation			Maximum Temperature		Minimum Temperature	
	JJAS	DJF		JJAS	DJF	JJAS	DJF
IMD	12.5	0.8	IMD	31.6	24.0	24.1	10.9
APHRODITE	8.7	0.6	CRU	19.6	19.7	19.6	19.7
LMDZ	6.1	2.7	LMDZ	24.6	10.5	17.7	1.6
MPI	7.1	1.2	MPI	17.5	3.2	8.1	-7.1
GFDL	7.0	1.3	GFDL	17.5	2.6	8.2	-7.5
CNRM	6.9	1.3	CNRM	17.7	2.9	8.4	-7.4
ACCESS	7.2	1.1	ACCESS	17.4	3.3	8.1	-6.9

Table 3: Mean climatological value for precipitation (mm), maximum and minimum temperature (°C) for observations (IMD & Aphrodite), and climate model data (LMDZ, MPI, GFDL, CNRM & ACCESS for the period 1970–2005.

Table 3 shows differences in the climatological means between observed data sets and simulated rainfall and maximum and minimum temperature from 1970 to 2005. In support of the above spatial climatological analysis, the models show a lower means than the observations datasets.

3.1.7 Seasonal mean cycle for historical simulation from 1970 to 2005

Figure 3.1.7(a) shows the mean seasonal cycle of precipitation for 1970 to 2005 from the two observed datasets and each model. All the datasets show a seasonal evolution similar to observations, with the simulated precipitation from most of the models peaking in July. However, the simulated precipitation from the LMDZ peaks in August and is much less than that from the IMD or Aphrodite datasets. To sum up, the models seem to capture the observed seasonal cycle of mean precipitation qualitatively for the study region.

The simulated mean seasonal cycles of the maximum and minimum temperatures in the NER are qualitatively similar to observations (Figure 3.7.1 b and c), though the simulated magnitudes are much lower than those from the observations.

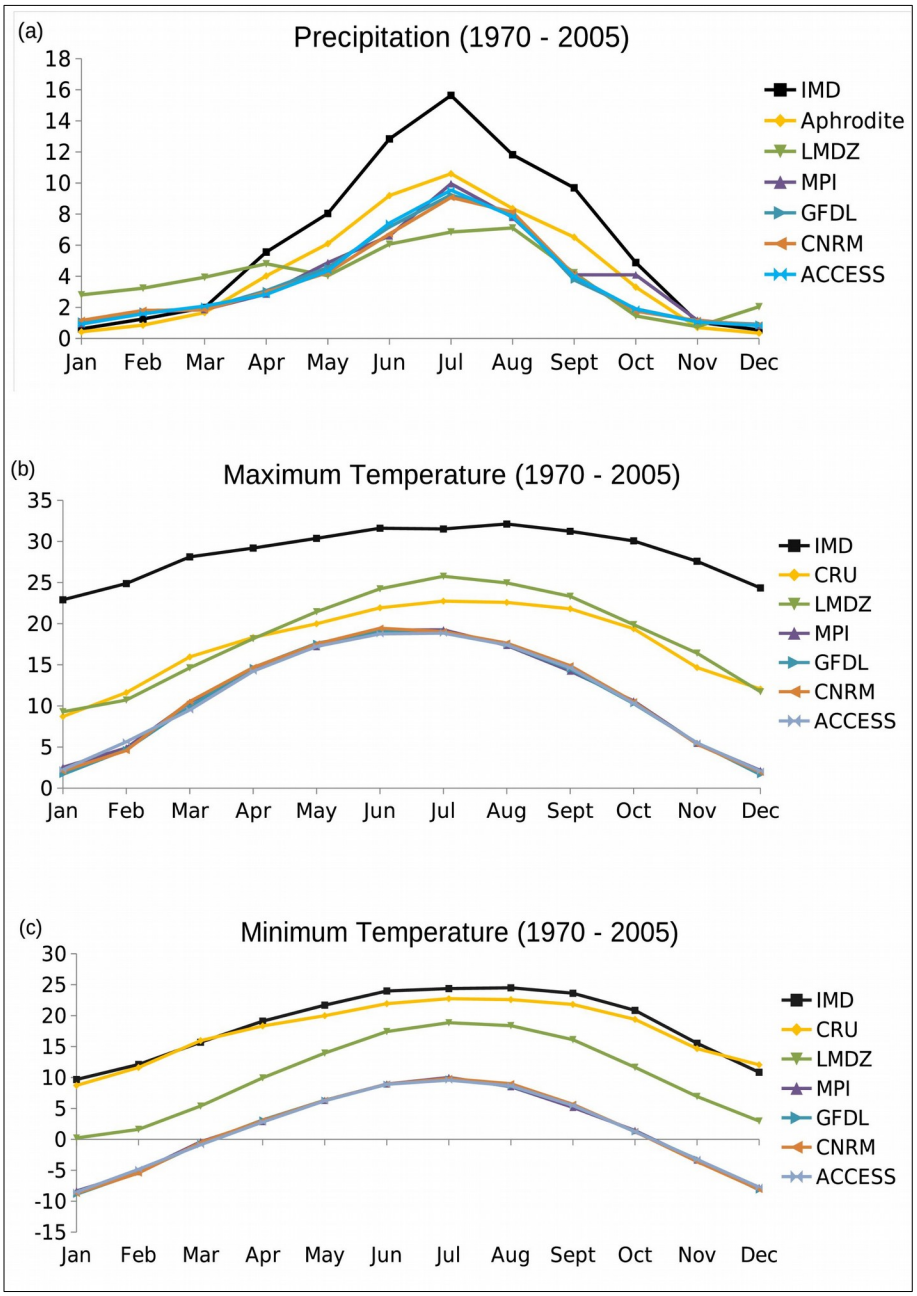

Figure 3.1.7: (a) Seasonal cycle (mean) of precipitation (mm) from IMD, Aphrodite, and Cordex-SA model (LMDZ, MPI, GFDL, CNRM, and ACCESS) for the period 1970 to 2005. (b) same as in (a) except for CRU Reanalysis and maximum temperature data (°C). (c) same as (b) but for minimum temperature.

3.1.8. Spatial plot of trend analysis JJAS for historical data from 1970 to 2005

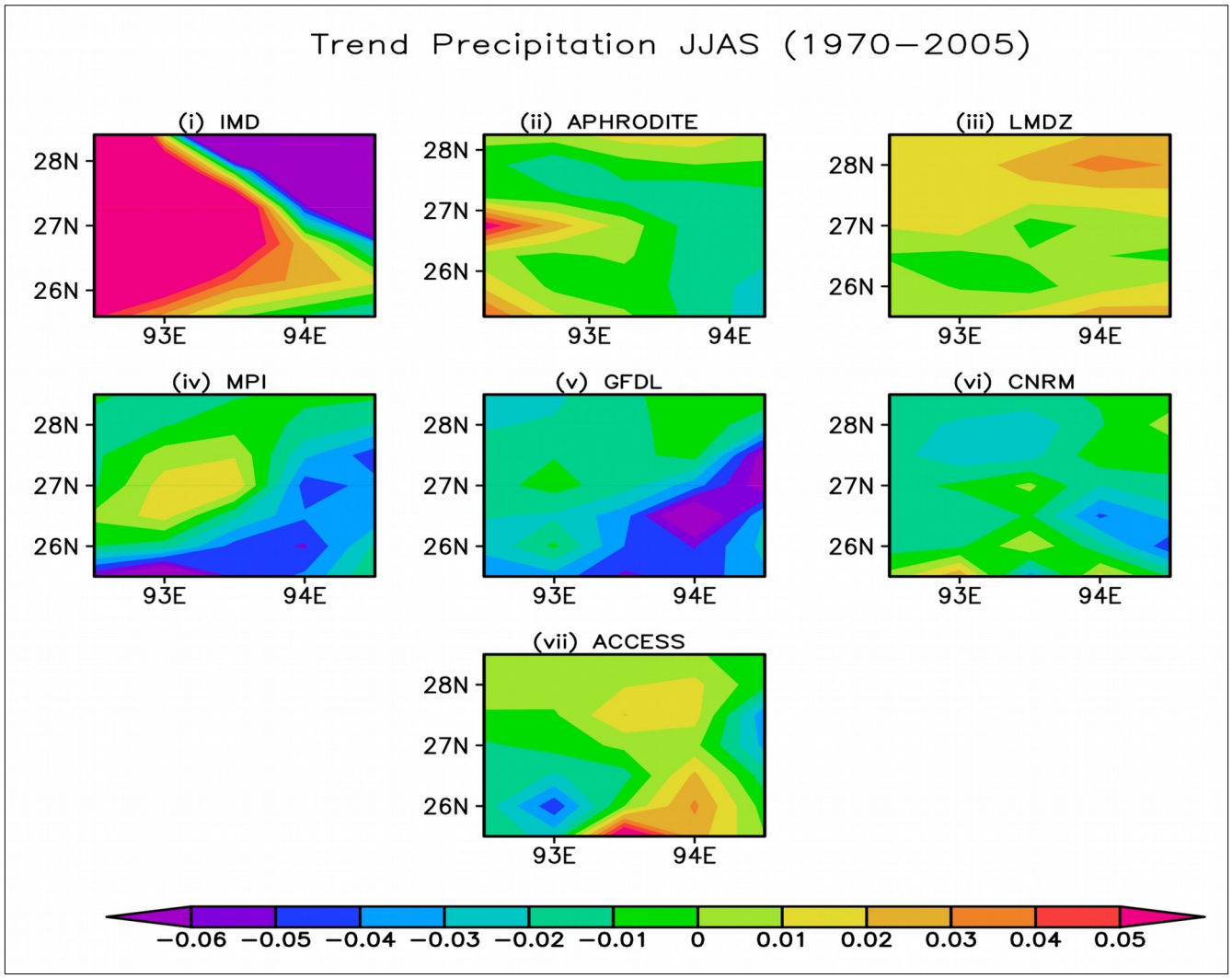

Figure 3.1.8: Spatial distribution of trends of precipitation for JJAS season for observations (i) IMD and (ii) Aphrodite and, for models (iii) LMDZ, (iv) MPI, (v) GFDL, (vi) CNRM, and (vii) ACCESS for the period 1970 to 2005 over the NER.

In Figure 3.1.8, the RF-JJAS season trends for the period 1970 to 2005 from each precipitation dataset are plotted. The IMD data shows a rising trend from the rest of the datasets. While the RF-JJAS from the IMD exhibits an increasing trend of about 0.5 mm/year in the western NER and a decreasing trend

of about 0.6 mm/year in the eastern portion of the NER, the APHRODITE datasets indicate a weaker but increasing trend in a larger portion of the NER. All models qualitatively reproduce the increasing trend in the rainfall over western NER, though with weaker magnitudes. The MPI and GFDL models and the ACCESS model somewhat weakly simulate a negative trend in pockets, not seen in observations.

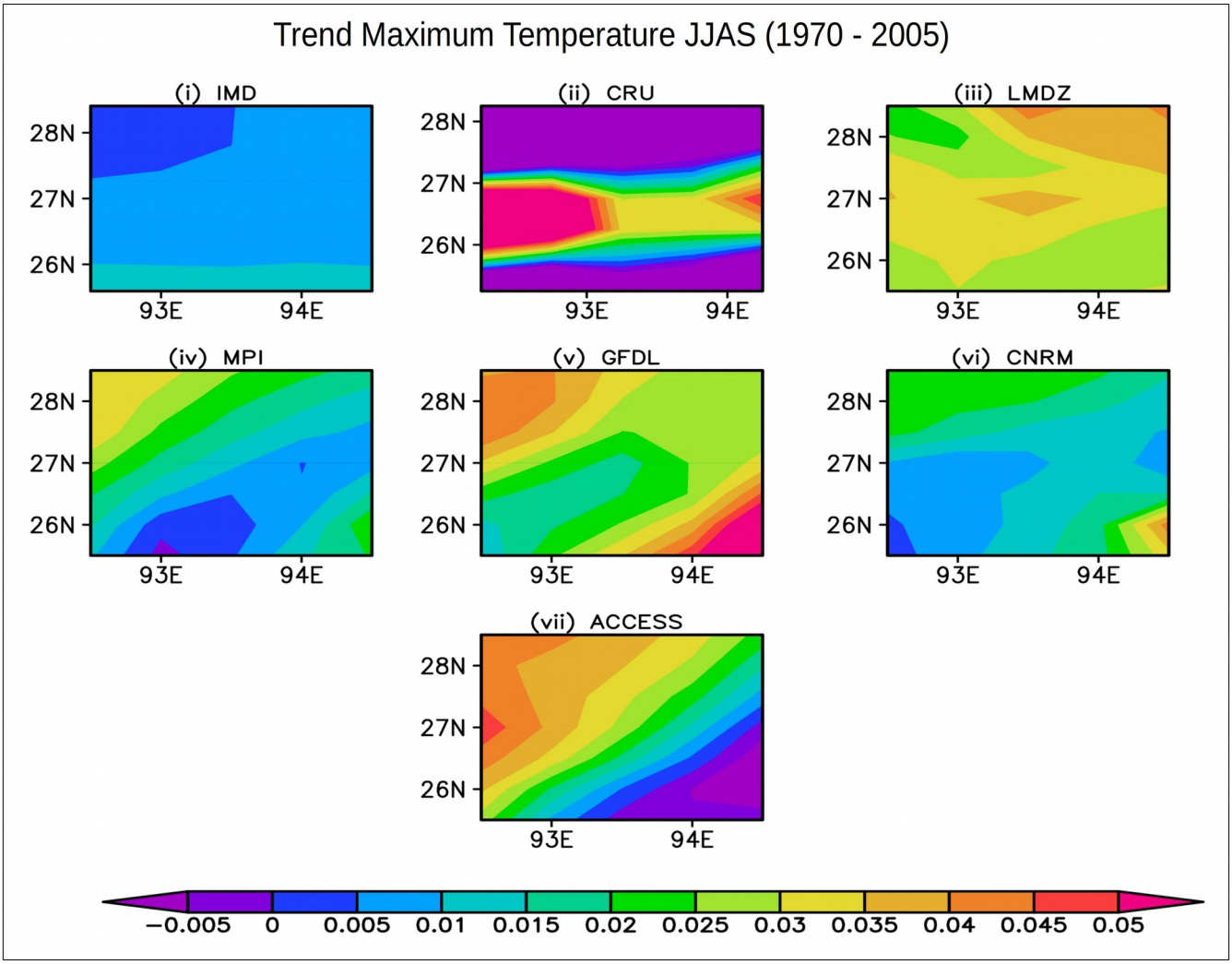

Figure 3.1.9: Spatial distribution of trends of maximum temperature (°C) for JJAS season for observations (i) IMD and (ii) CRU and, for models (iii) LMDZ, (iv) MPI, (v) GFDL, (vi) CNRM and (vii) ACCESS for the period 1970 to 2005 over the NER.

A trend analysis of TMax-JJAS maximum temperature from 1970 to 2005 is plotted in Figure 3.1.9 where the IMD data shows a positive trend 0.015 °C/year increasing towards the south. The CRU data, on the other hand, shows a higher magnitude of the trend than the IMD and an increasing trend towards the center. Models other than the MPI and ACCESS models show a positive trend.

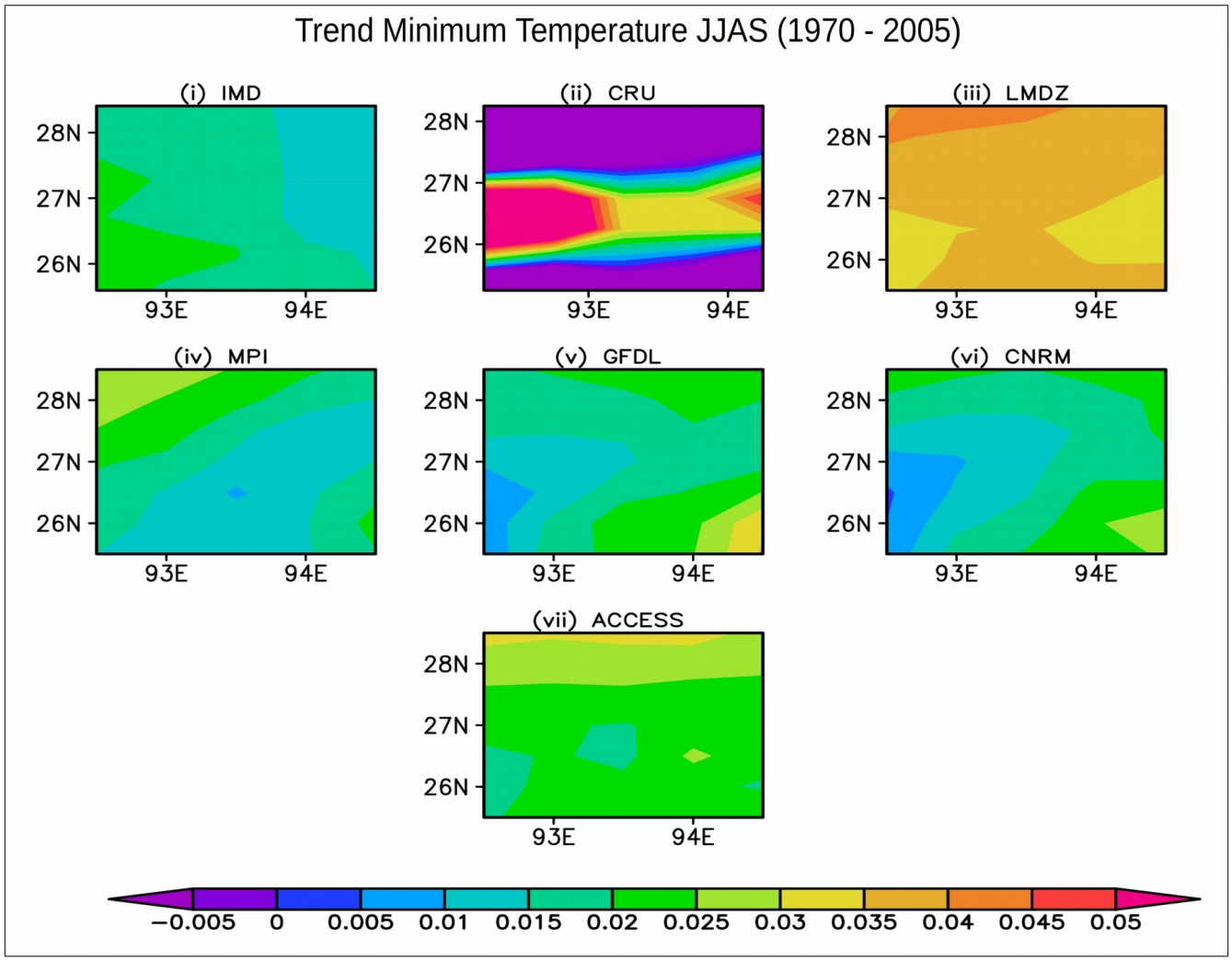

Figure 3.1.10: Spatial distribution of trends of minimum temperature (°C) for JJAS season for observations (i) IMD and (ii) CRU and, for models (iii) LMDZ, (iv) MPI, (v) GFDL, (vi) CNRM and (vii) ACCESS for the period 1970 to 2005 over the NER.

A trend of 0.02 °C/year in the TMin-JJAS is shown from the IMD datasets (Figure 3.1.10), increasing towards the west from the east. On the contrary, the CRU datasets show an increasing trend towards the center. The LMDZ model shows a higher magnitude of the trend than the rest of the datasets, with an increasing trend of 0.05 °C/year. The MPI, GFDL, and CNRM models are more or less similar to a lower positive trend in the central portion. The ACCESS model shows an increasing trend towards the north.

3.1.11. Spatial plot of trend analysis DJF for historical data from 1970 to 2005

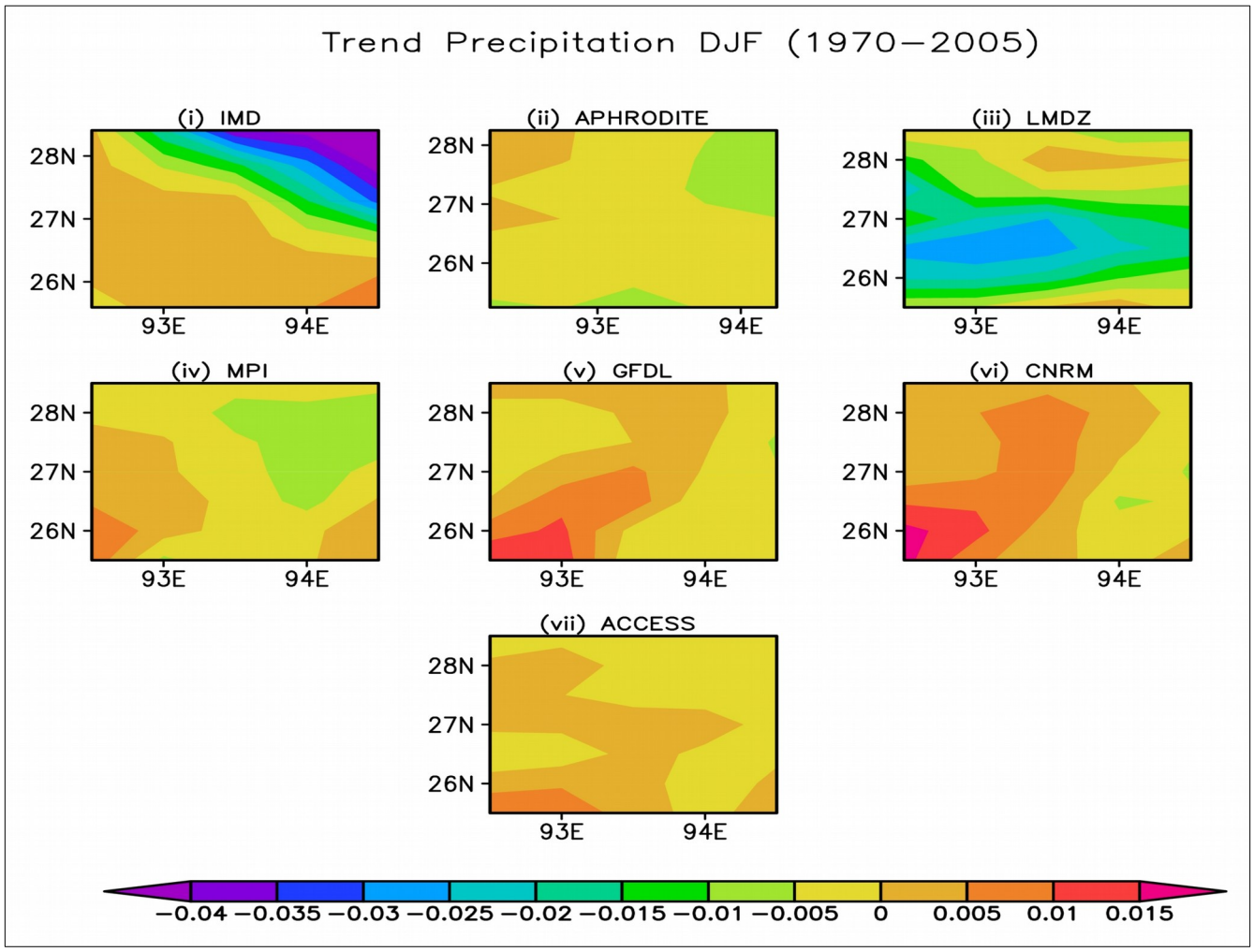

Figure 3.1.11: Spatial distribution of trends of precipitation (mm) for DJF season for observations (i) IMD and (ii) Aphrodite and, for models (iii) LMDZ, (iv) MPI, (v) GFDL, (vi) CNRM and (vii) ACCESS for the period 1970 to 2005 over the NER.

Figure 3.1.11 shows the trends in the observed and simulated RF-DJF in the NER for the period 1970 to 2005. All the datasets show a similar increasing trend in most of the region. The IMD data shows an increasing trend of 0.01 mm/year towards the southwest of the area and a decreasing trend of 0.4 mm/year towards the northeastern. The Aphrodite data shows a positive trend in most of the regions. The rest of the models, except for the LMDZ, shows a similar positive trend.

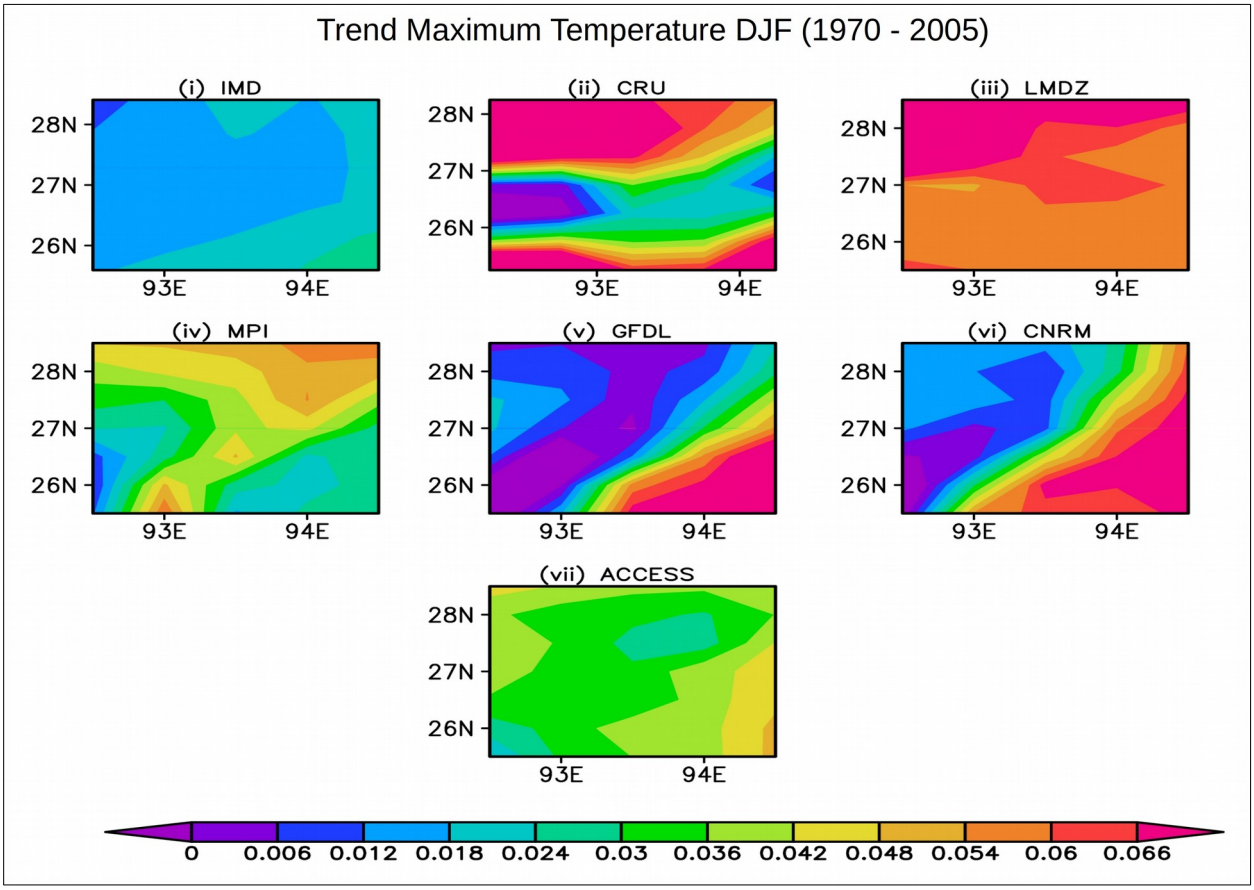

Figure 3.1.12: Spatial distribution of trends of maximum temperature (°C) for DJF season for observations (i) IMD and (ii) CRU and, for models (iii) LMDZ, (iv) MPI, (v) GFDL, (vi) CNRM and (vii) ACCESS for the period 1970 to 2005 over the NER.

The IMD datasets show an increasing trend in the TMax-DJF from the northwest towards the southeast, with respective values of 0.03 °C/year and 0.06 °C/year (Figure 3.1.12). CRU datasets show a higher trend than the IMD datasets. Only the LMDZ model shows a very high positive trend of 0.06 °C/year increasing towards the north. GFDL and CNRM models show an increasing trend towards the east while decreasing at the central east. The MPI model shows an increasing trend in the central portion while the ACCESS model shows a decreasing trend in the central portion. All the datasets show a positive trend.

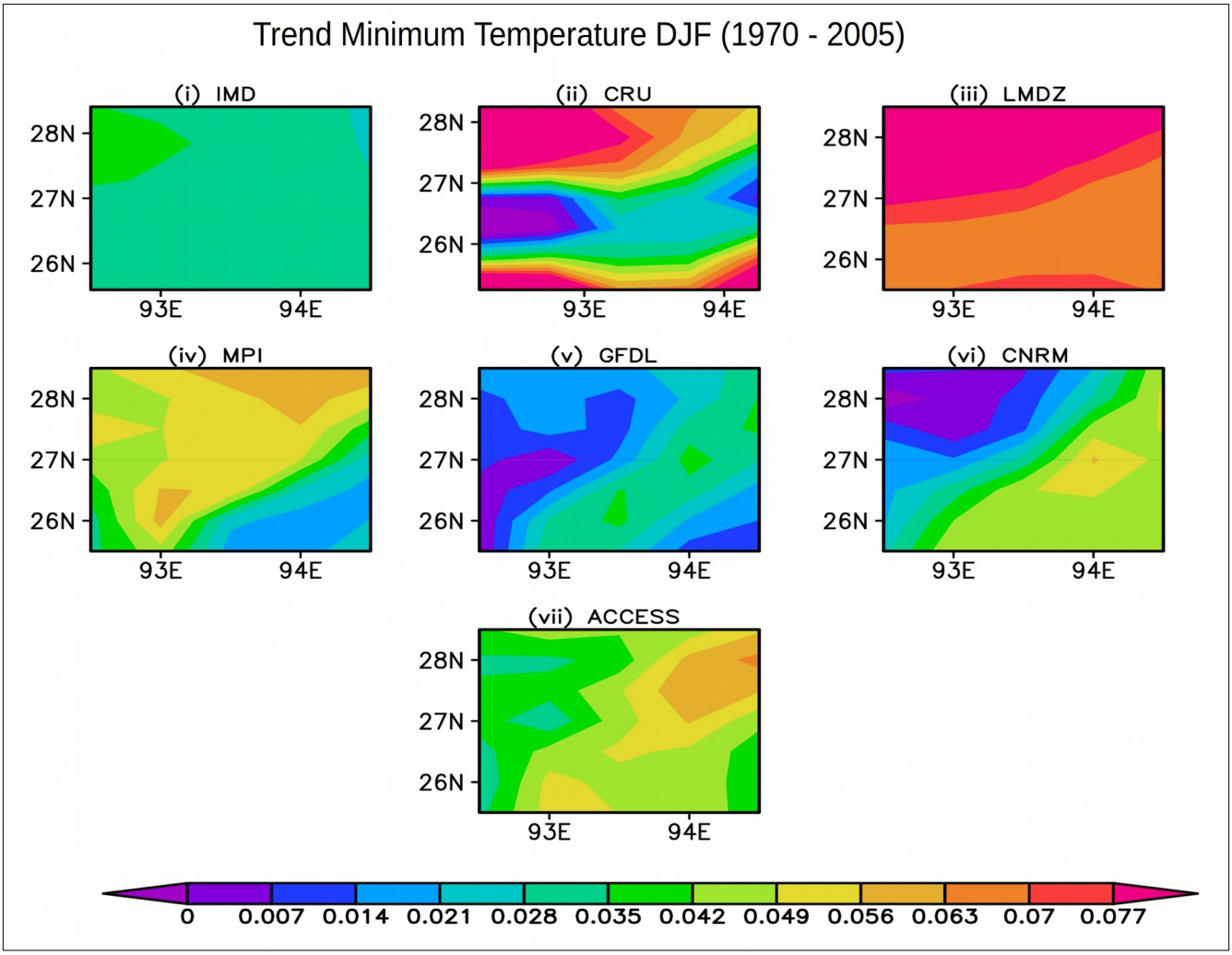

Figure 3.1.13: Spatial distribution of trends of minimum temperature (°C) for JJAS season for observations (i) IMD and (ii) CRU and, for models (iii) LMDZ, (iv) MPI, (v) GFDL, (vi) CNRM and (vii) ACCESS for the period 1970 to 2005 over the NER.

Figure 3.1.13 shows the trend analysis of TMin-DJF minimum temperature, from which it is clear that the IMD datasets show an increasing trend of 0.04 °C/year towards the west while CRU data shows a higher trend as compared to the IMD data. The LMDZ model also shows a higher trend of 0.07 °C/year, which increases towards the north and south but decreases in the center. The CNRM and ACCESS models show an increasing trend towards the central east and a decreasing trend at the west,

opposite to that in the MPI model. The ACCESS model shows an increasing trend in the central-east and decreases in the west.

From the above discussion, it's clear that the IMD and Aphrodite datasets agree as far as the location of highest and lowest trends in the rainfall, particularly during the summer monsoon, is concerned. However, the same cannot be said about the agreement between the IMD datasets and CRU datasets about the spatial distribution of temperature trends. This is not so surprising, given that the CRU datasets are not observational datasets but model forecasts constrained by the observations. We also note that the models are not up to simulate the spatial distribution of the trends well. The NER region is well known for its high convective rainfall associated with complex orography, which is challenging to simulate. The interpolation and calibration algorithms potentially contribute to uncertainty. However, suppose the historical simulations from various models can at least replicate the area-averaged trends in the NER climate parameters. In that case, we can then have qualitative confidence in their future projections. In the next section, we precisely explore this aspect.

3.1.14. Area-averaged trend analysis from the observations and models for the 1970 to 2005 period

This section discusses results from the analysis of the area-averaged trends in rainfall and temperature in the NER region. The significance of these tests was evaluated using both Mann-Kendall and Student's t-test. We find that the IMD and Aphrodite datasets show increasing and decreasing trends, which are not statistically significant (not shown as all the results show insignificant). Insignificant decreasing or no trend in the summer monsoon precipitation of NER, as seen from some stations observations in the NER has been also reported by Jain et al., 2013; Laskar et al., 2014 and Dash et al., 2015. All the model simulations also simulate only insignificant trends.

Further, both IMD and Aphrodite datasets only show a decreasing but statistically insignificant trend in the area-averaged rainfall during the DJF (RF- DJF) season in the NER. The area-averaged trends in the corresponding RF-DJF from various CORDEX models are also seen to be insignificant, though the GFDL and CNRM models show an increasing trend.

Though the nature of trends in the rainfall is insignificant in all the data sets, it indicates a decline in the rainfall over NER, in tandem with such a signal in the summer monsoon rainfall in the rest of India (Krishnan et al., 2016). On longer time scales, the warmer tropical ocean, especially the central-eastern Pacific and the western Indian Ocean, are suggested to play a role in weakening the monsoon (Roxy et al., 2015)

Data used	Mann-Kendall test		Student t-test			Nature of the trend
	Z value & α value	Statistic value (S)	p-Value	t-Value	Trend value	
JJAS						
LMDZ	4.19 > 1.96	308	0.00 < 0.05	5.53 > 2	1.14	Increasing trend & significant
GFDL	2.39 > 1.96	176	0.01 < 0.05	2.92 > 2	1.07	- do -
ACCESS	2.86 > 1.96	210	0.01 < 0.05	2.61 > 2	1.25	- do -
DJF						
LMDZ	3.79 > 1.96	290	0.01 < 0.05	4.52 > 2	2.35	- do -
CNRM	2.33 > 1.96	178	0.05 = 0.05	2.02 > 2	1.22	- do -
ACCESS	2.22 > 1.96	170	0.02 < 0.05	2.39 > 2	1.28	- do -

Table 4: Significance tests using Mann-Kendall and Student t-test for maximum temperature data from the IMD, NCEP, and climate model data for JJAS and DJF season for 1970–2005.

Only the significant results are shown in Table 4. The time series of the area-averaged JJAS maximum temperature and that for the DJF season, from the IMD datasets from 1970 to 2005 show increasing but statistically insignificant trends. Growing population accompanied by massive urbanization, changes in

land use, enormous highway development, increases in deforestation, biomass burning, fossil fuel consumption, and increasing atmospheric concentrations of greenhouse gases are suspected to be the cause of the temperature changes (Kothyari and Singh, 1996; Jhajhariaa and Singh, 2011). Notably, the CRU datasets for both the seasons show an insignificant increasing trend. Also, all the models successfully reproduce the observed increasing trends in the area-averaged seasonal maximum temperatures, through most of the simulated trends are statistically significant.

Data used	Mann-Kendall test		Student t-test			Nature of the trend
	Z value & α value	Statistic value (S)	p-Value	t-Value	Trend value	
JJAS						
IMD	3.26 > 1.96	240	0.00 < 0.05	4.48 > 2	0.63	Increasing trend & significant
LMDZ	4.79 > 1.96	352	0.00 < 0.05	7.92 > 2	1.32	- do -
MPI	2.48 > 1.96	182	0.03 < 0.05	2.92 > 2	0.61	- do -
GFDL	2.04 > 1.96	150	0.03 < 0.05	2.23 > 2	0.66	- do -
ACCESS	3.19 > 1.96	234	0.02 < 0.05	2.45 > 2	0.85	- do -
DJF						
IMD	3.92 > 1.96	300	0.00 < 0.05	4.59 > 2	1.19	- do -
LMDZ	4.15 > 1.96	318	0.00 < 0.05	5.42 > 2	2.97	- do -
MPI	3.22 > 1.96	246	0.00 < 0.05	3.24 > 2	1.59	- do -
GFDL	2.17 > 1.96	166	0.05 = 0.05	2.99 > 2	0.75	- do -
CNRM	2.30 > 1.96	176	0.03 < 0.05	2.33 > 2	1.11	- do -
ACCESS	3.16 > 1.96	242	0.00 < 0.05	3.70 > 2	1.62	- do -

Table 5: Significance tests using Mann-Kendall and Student t-test for minimum temperature data from the IMD and climate model data during JJAS and DJF seasons for the period 1970–2005.

Importantly, we find statistically significant increasing trends in the area-averaged minimum temperature over the NER during both summer and winter seasons over the period 1970 to 2005 (Table

5). It is intriguing that only the minimum temperature shows a statistically significant increasing trend, while the rainfall trends, though decreasing, are not significant.

From all these results, we can summarize that the downscaled CORDEX South-Asia datasets are successful in capturing the area-averaged seasonal cycles of rainfall and temperature observed during 1970–2005, and are also capable of capturing the corresponding trends, at least qualitatively. However, the climatological spatial distribution and the local long term trends are not well captured and are also subject to the uncertainties in the observations. Being an orographic region, the uncertainty between datasets is largest in North East India (Kulkarni et al., 2013 and Prakash et al., 2014).

3.1.15. Teleconnections of the historical data (1970–2005) with ENSO

Nino3.4	JJAS	DJF
Precipitation		
IMD	-0.08	-0.19
APHRODITE	-0.11	0.03
LMDZ	-0.09	-0.36
MPI	-0.21	-0.41
GFDL	0.13	0.13
CNRM	-0.04	-0.09
ACCESS	0.03	-0.12
Mean Temperature		
CRU	-0.08	0.2
Maximum Temperature		
IMD	0.04	-0.04
LMDZ	0.19	0.09
MPI	0.05	0.15
GFDL	-0.06	-0.04
CNRM	0.18	0.27
ACCESS	0.25	0.19
Minimum Temperature		
IMD	-0.04	-0.07
LMDZ	0.16	0.01
MPI	-0.01	0.12
GFDL	0.15	0.27
CNRM	0.05	0.28
ACCESS	0.13	0.33

Table 6: Teleconnections between ENSO index (Nino3.4) with precipitation, maximum temperature and minimum temperature for JJAS and DJF for the period 1970 to 2005.

Table 6 shows the teleconnections results ENSO, which is represented by the well-known NINO3.4 index, with precipitation, maximum and minimum temperature parameters from all relevant the datasets used in this study from the IMD, Aphrodite, CRU, and all the model's datasets for historical

period from 1970 to 2005. The results of this study suggest that the ENSOs do not have any statistically significant impacts on the NER precipitation and temperature, be it summer or winter, for the period. NINO3 (figure not shown) has also been analyzed where it also shows no significant impacts.

3.1.16. Extremes analysis for JJAS season for the period 1970 to 2005

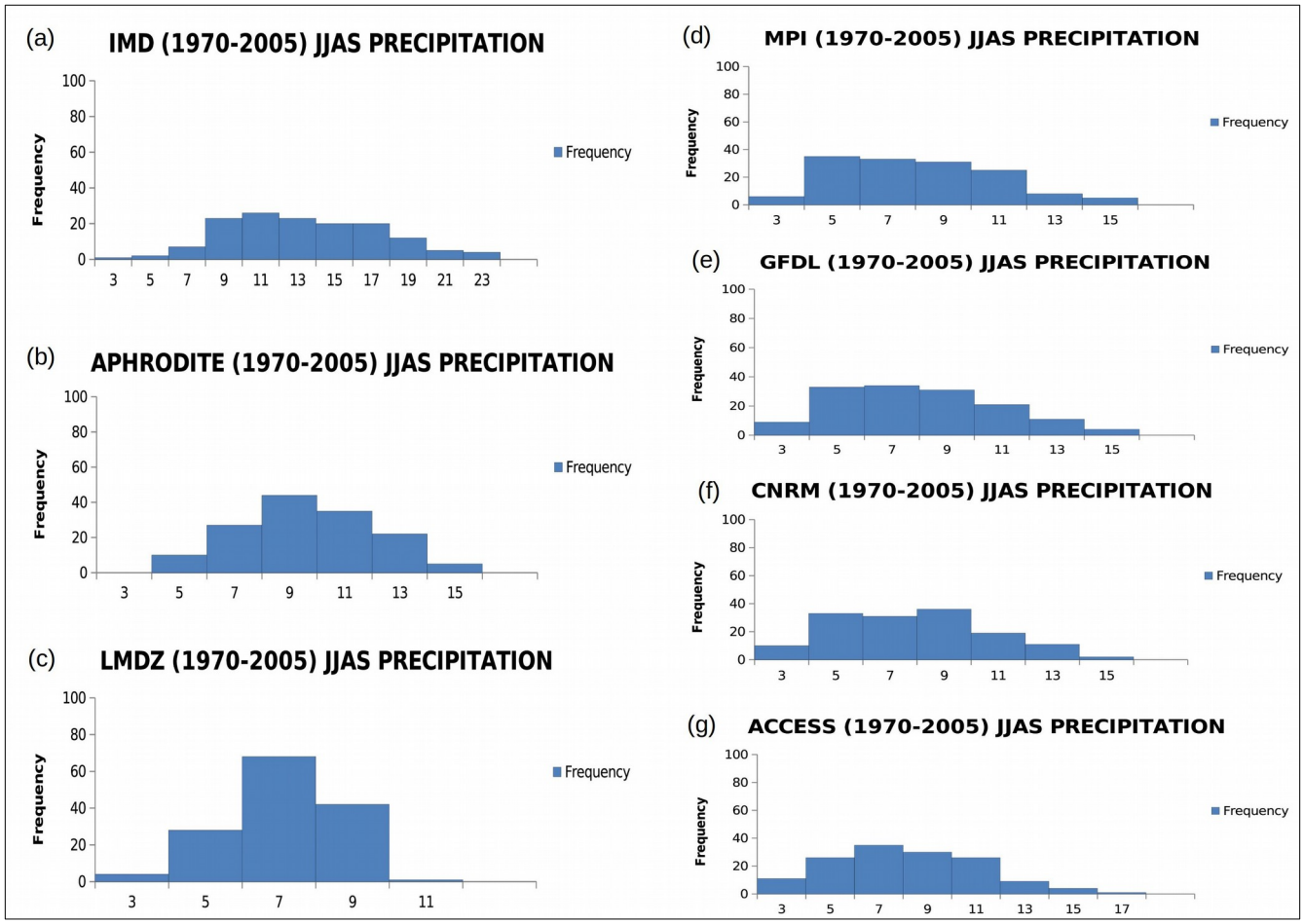

Figure 3.1.16: Histogram plots for JJAS precipitation (mm) of historical period (1970–2005): IMD, Aphrodite and CORDEX models ((LMDZ, MPI, GFDL, CNRM and ACCESS).

In Figure 3.1.16, histograms of observed and simulated JJAS monthly mean rainfall over the NER for the historical period from 1970 to 2005 are presented. While there are four heaviest rainfall monsoon seasons with rainfall of 23 mm/day in NER as per the IMD datasets, the APHRODITE datasets indicate

(Fig. 3.1.16) five heaviest rainfall months with rainfall amounting to 15 mm/day. Except for the LMDZ model, all other models simulate the heaviest seasonal rainfall of 15 mm/day. Only two models simulate at least four such extreme rainfall months (Fig. 3.1.16); The LMDZ model simulates only one heaviest rainfall month, with the magnitude of the rainfall amounting to 11 mm/day.

The extreme events of JJAS maximum temperature for the historical period from 1970 to 2005 are shown the Figures 3.1.17. The observation data from IMD recorded thirty-nine highest maximum temperature months with 34°C/day. The CRU and all the models record somewhat lower maximum temperature than the observation data, ranging from 22°C to 28 °C.

Figures 3.1.18 show the minimum temperature for JJAS season for the historical period (1970–2005). The observation data and CRU datasets record a minimum monthly temperature of 27 °C/day. The minimum temperature in all the models is underestimated, with a range of 12 °C to 21 °C across the models.

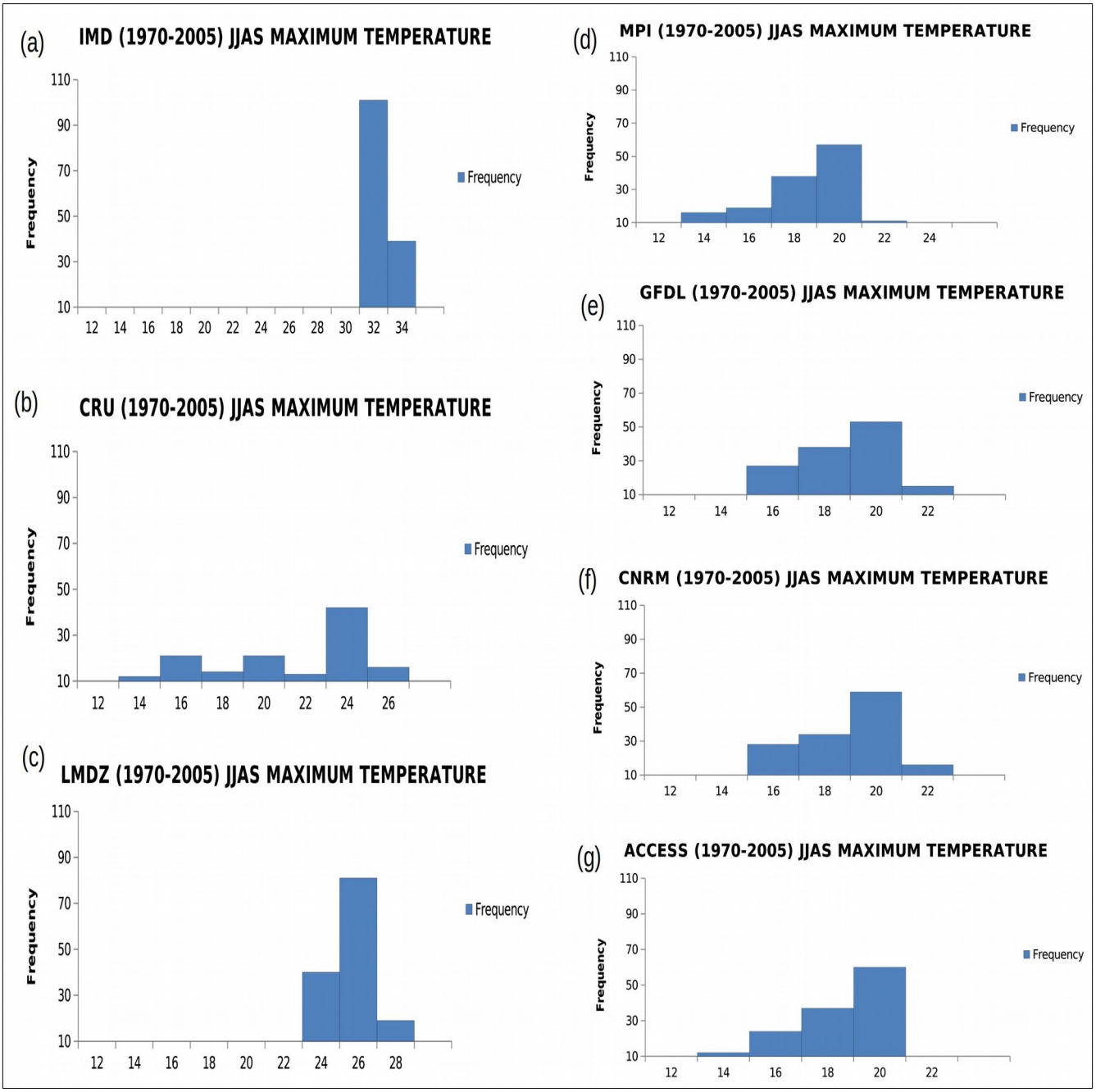

Figure 3.1.17: Histogram plots for JJAS maximum temperature (°C) of historical period (1970–2005): IMD, CRU and CORDEX models (LMDZ, MPI, GFDL, CNRM and ACCESS).

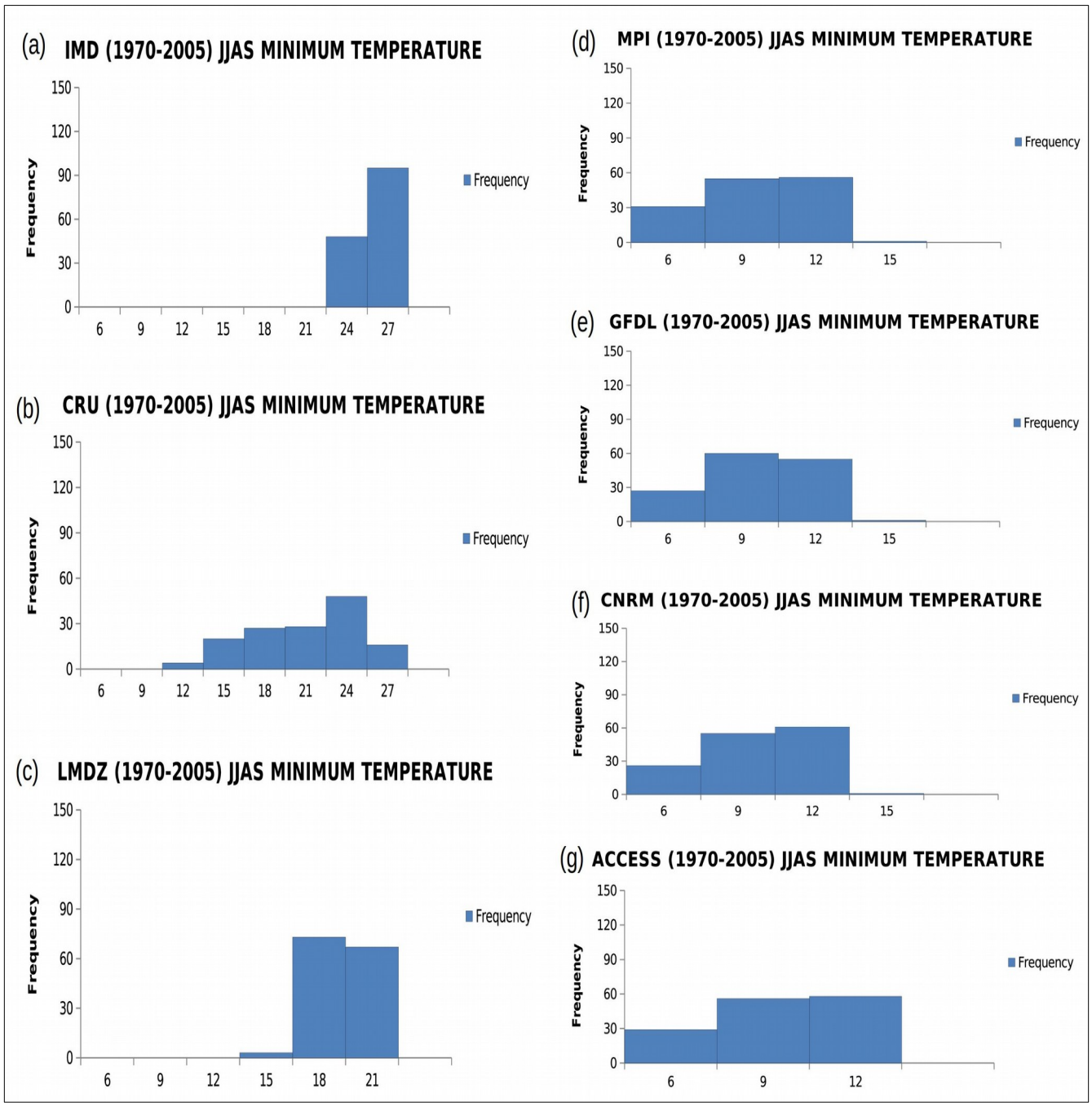

Figure 3.1.18: Histogram plots for JJAS minimum temperature (°C) of historical period (1970–2005): IMD, CRU and CORDEX models (LMDZ, MPI, GFDL, CNRM and ACCESS).

3.1.19. Extremes analysis for DJF season for the period 1970 to 2005

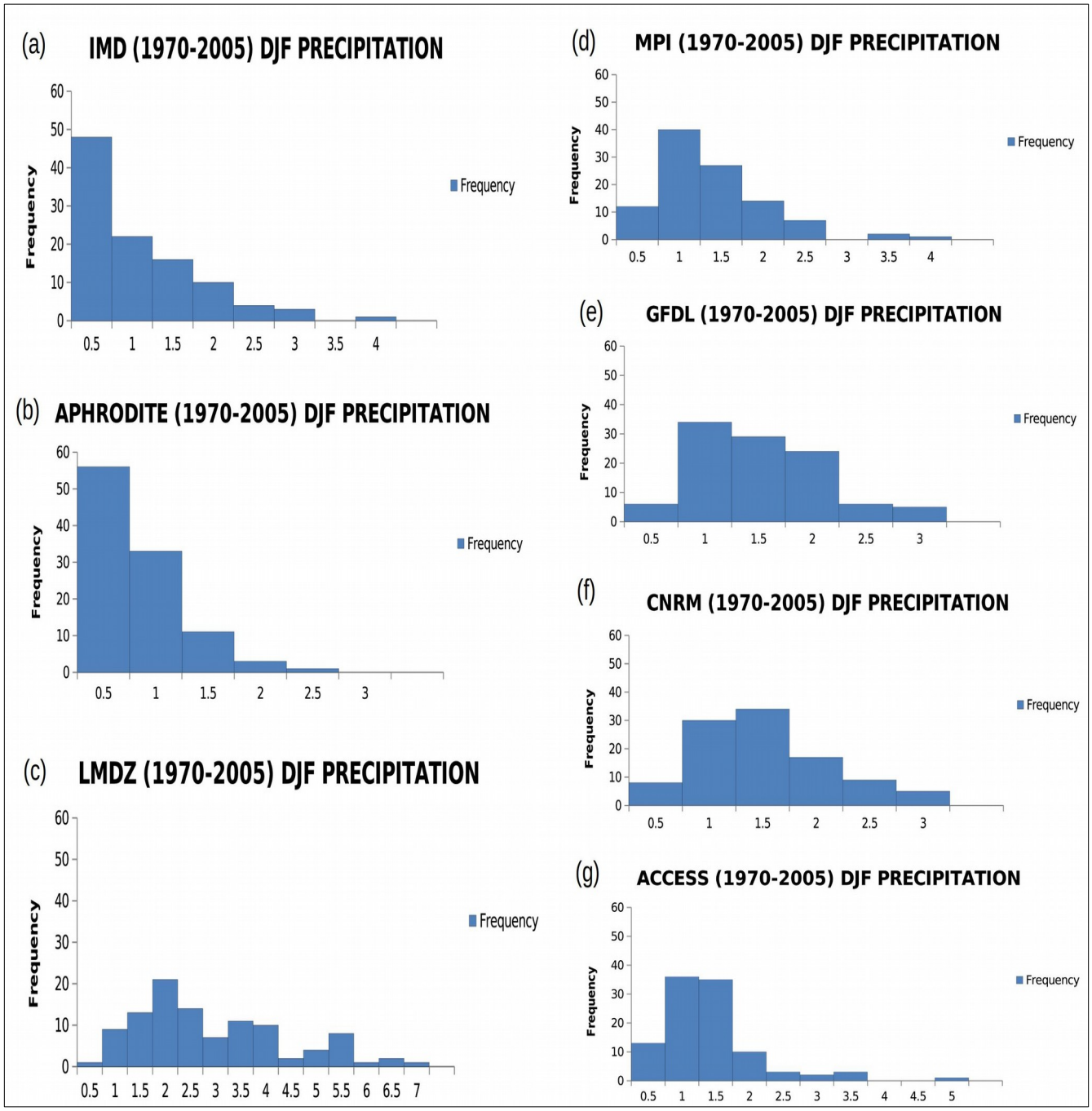

Figure 3.1.19: Histogram plots for DJF precipitation (mm) of historical period (1970–2005): IMD, CRU and CORDEX models (LMDZ, MPI, GFDL, CNRM and ACCESS).

Histograms of observed and simulated DJF monthly mean rainfall over the NER for the historical period from 1970 to 2005 are presented in Figure 3.1.19. The number of heaviest winter monsoon rainfall months is relatively low as corresponding to the summer monsoon season, as can be seen from both IMD and Aphrodite datasets. The models in general also qualitatively reproduce the difference. However, the heaviest rainfall simulated by the LMDZ model of 7 mm/day in the simulated historical period is noticeably high as compared to the 4.5 mm/day.

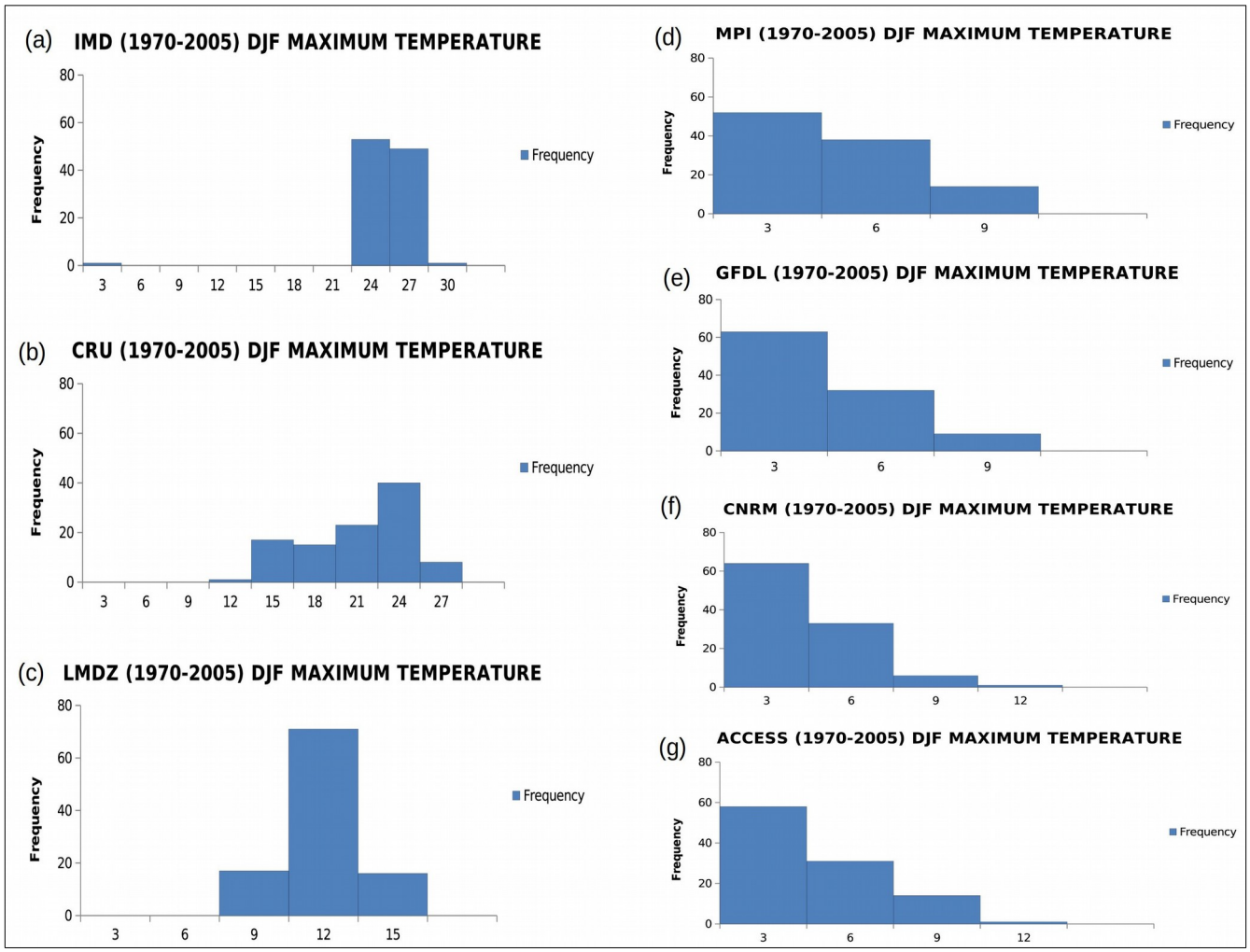

Figure 3.1.20: Histogram plots for DJF maximum temperature (°C) of the historical period (1970–2005): IMD, CRU, and CORDEX models (LMDZ, MPI, GFDL, CNRM, and ACCESS).

In Figure 3.1.20, the extreme months of maximum temperature for DJF season are shown for the historical period (1970–2005). IMD records show 30 months of the highest monthly maximum temperature of 30 °C/day during the historical period. The CRU records show the monthly mean highest temperature of 27 °C/day and all the models show a highly underestimated maximum temperature ranging from 9 °C to 15 °C.

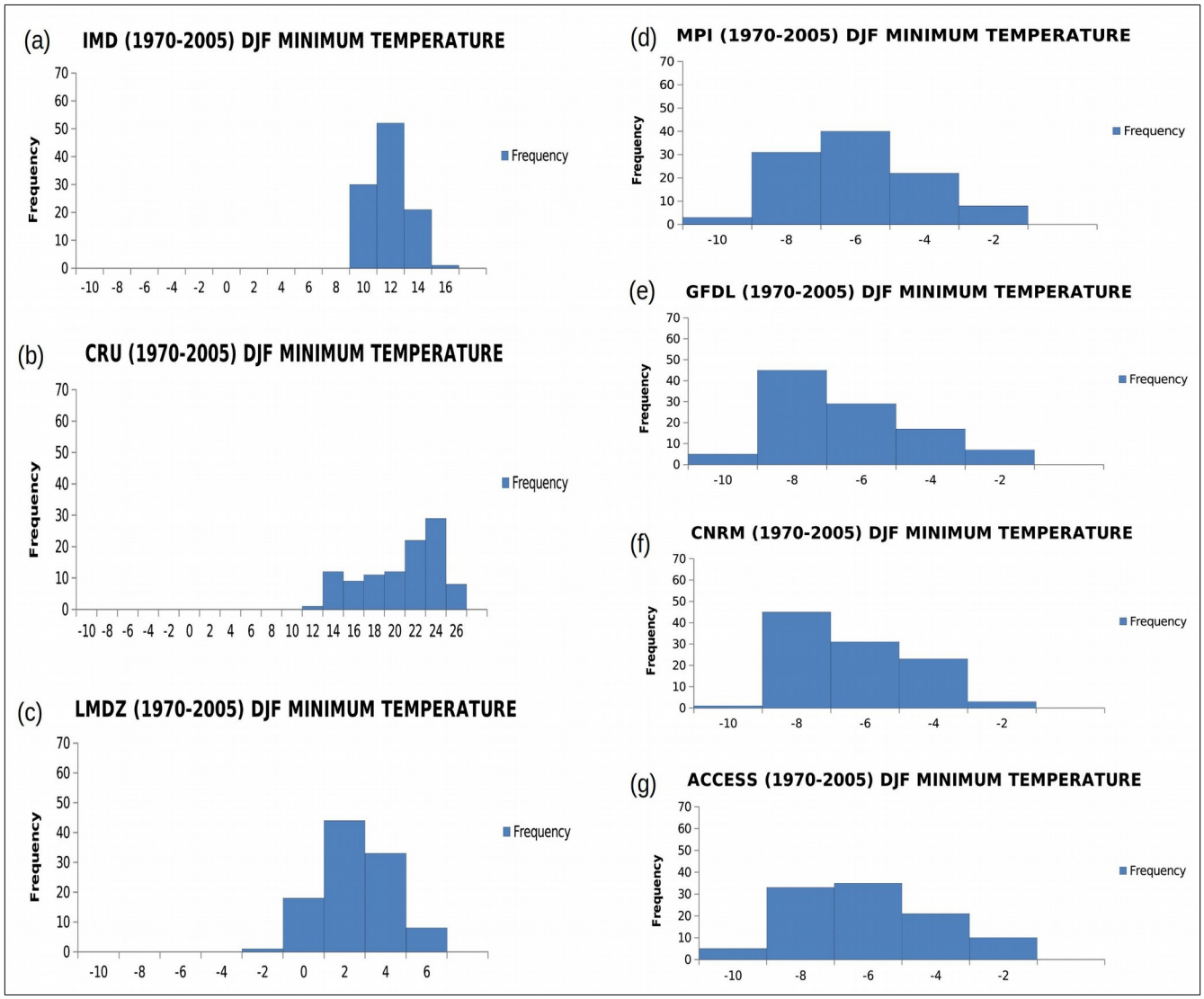

Figure 3.1.21: Histogram plots for DJF minimum temperature (°C) of the historical period (1970–2005): IMD, CRU, and CORDEX models (LMDZ, MPI, GFDL, CNRM, and ACCESS).

In the case of the DJF season, for the historical period (1970–2005), the observation data records minimum temperatures of 16 °C/day and CRU being 26 °C/day. However, all the models underestimate the minimum temperature, with a range from 6 °C to -2 °C.

3.2 The climate variability during the last millennium and future projections

Past-climate simulations provide valuable information in complementing findings from proxy observations, and hopefully reconcile with some of these paleo-observations, thereby leading to a more cohesive conclusion. They help in deciphering potential background dynamical mechanisms. With this aim, we analyze outputs from multiple coupled-model simulations under the PMIP3 protocol. In addition to this, the summer monsoon rainfall plays a major role in the region, and considering the importance of the NER, the study of the past climate during the summer monsoon season would be useful in projecting the future climate. Then we analyze the results from the five downscaled future scenarios, namely, the RCP4.5 simulations (LMDZ, MPI, GFDL, CNRM, and ACCESS) available from 2011 through 2060, to decipher the projected climate change in the northeast.

3.2.1. Simulated seasonal rainfall and circulation across NER during the MCA and LIA

The simulated area-averaged monthly mean rainfall over NER for the present-day period from the three CGCMs and the ECHAM AGCM (Figure 3.2.1) suggests that the evolution of the rainfall's simulated seasonal cycle conforms well to the observations. In general, the magnitude of the simulated monthly area-averaged rainfall is comparable to that from the observations, though the one simulated by the MRI model is smaller than in the observations, particularly for May and June. The magnitude of the

ECHAM5 simulation for the JJAS season is realistic, suggesting that tropical ocean-atmosphere coupling may not be a major driver of the NER climate. Notably, the summer monsoon rainfall from the ECHAM peaks later in the year relative to the observations and other models. The highest magnitude of area-averaged NEISMR is simulated by the ECHAM AGCM in both regimes, closely followed by the MPI model (Figure 3.2.1b). We should, however, be mindful of the relatively short span of the ECHAM5 simulations. All the further analysis will only involve the PMIP3 models.

The simulated normalized summer monsoon rainfall area-averaged over the central/core-monsoon region (74.5^{o}E to 86.5^{o}E and 16.5^{o}N to 26.5^{o}N, following Goswami et al., 2006; henceforth, CMR) from the MCA to LIA is presented in Figure 3.2.1c, with actual climatological values in Figure 3.2.2a. The simulated CMR decreases by 6% to 11%, from MCA to LIA (Figure 3.2.1c). The simulated rainfall difference between the MCA and LIA by the CCSM4 and MPI models (Figure 3.2.2a) is statistically significant at 90% confidence level, and for the MRI, significant at 85% confidence level. This conforms to the results from nine PMIP3 models by Tejavath et al., (2017, 2019), which show that the summer monsoon rainfall over India decreased from the MCA to LIA, in agreement with several proxy studies (e.g., Yadava et al., 2005; Sinha et al., 2007; Dixit and Tandon, 2016). The difference from the ECHAM model is not statistically significant.

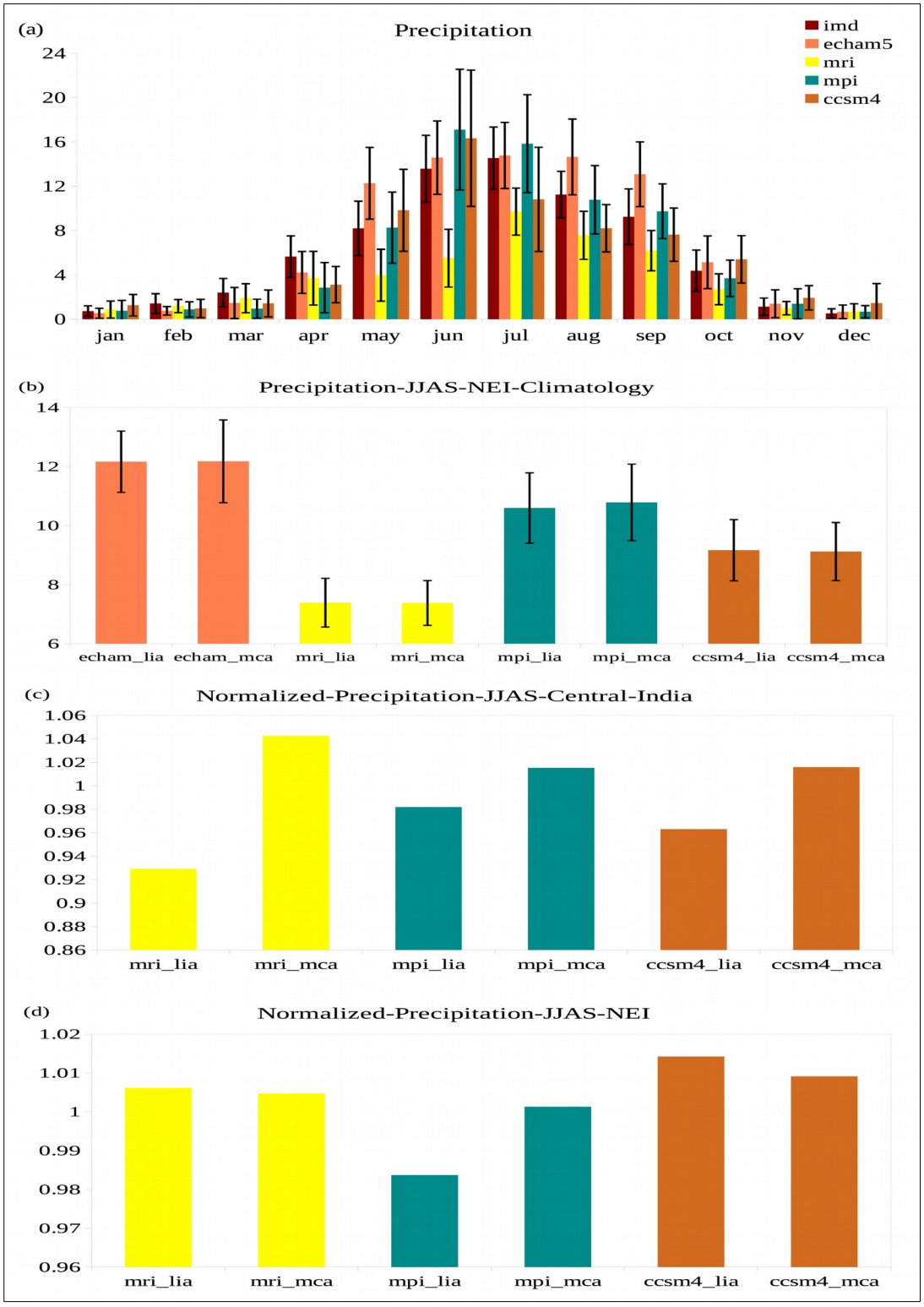

Figure 3.2.1: (a) Annual cycle of observed area-averaged NER rainfall (mm/day) for the period 1961 to 1990, and those from the historical simulations of three PMIP3 models of CCSM4, MRI, MPI, and that of ECHAM5 model (b) area-averaged climatological NER precipitation during JJAS season for MCA period (defined as 935 CE to 1034 CE for PMIP3 models, and 935 CE to 964 CE for ECHAM5) & LIA (1735 CE to 1834 CE for

PMIP3 models, and 1735 CE to 1764 CE for ECHAM5) (c) simulated normalized area-averaged JJAS precipitation over core monsoon region for the aforementioned 100 years of MCA by the PMIP3 models, and those from 100 years of LIA, and (d) same as Figure 1c but for northeastern India. The normalization of the rainfall has been done by dividing the simulated climatological rainfall of MCA or LIA by the average of the 100 years of MCA & 100 years of LIA.

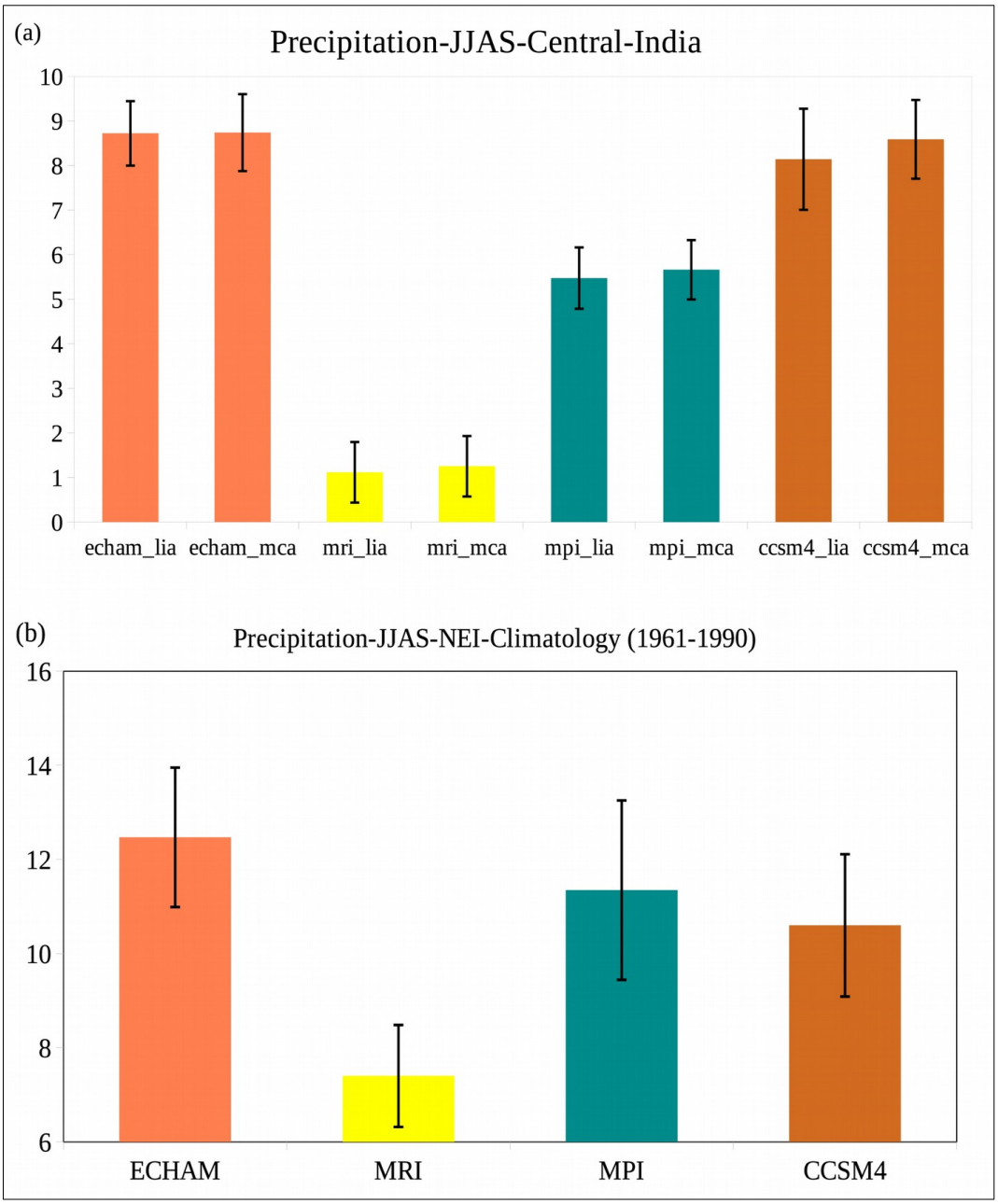

Figure 3.2.2 (a) Area-averaged climatological JJAS precipitation over Central India for 100 years of MCA and LIA simulated by the PMIP3 models. (b) Area-averaged climatological JJAS precipitation over northeastern India for the 1961-1990 period simulated by the ECHAM model and three PMIP3 models. Error bars are also shown.

The corresponding normalized area-averaged NEISMR for the MCA and LIA from each PMIP3 model is presented in Figure 3.2.1d. Contrary to the CMR, a difference (to be sure, only about 2%) between the simulated summer NEISMR between the MCA and LIA across all models is statistically insignificant. It is also to be noted that the simulated area-averaged mean seasonal rainfall over NER for the present-day period from each model is not significantly different from the rainfall during the MCA or the LIA (Figure 3.2.2b), indicating that NER-region has been insensitive to centennial changes in the forcing. The response of the models is unequivocal.

The interannual standard deviation of the NEISMR for the present day, as seen from the IMD rainfall datasets, is higher than that for the CMR (Table 7). This is also well-simulated, though the simulated standard deviations are weaker than the observations. Interestingly, unlike the mean rainfall, the standard deviations of the NEISMR show relatively higher inter-epochal variations as compared to those for the CMR.

Standard Deviation ($mm.day^{-1}$)						
NEISMR				ISMR		
	1961 to 1990	LIA	MCA	1961 to 1990	LIA	MCA
IMD	1.87			0.96		
ECHAM5	1.48	1.04	1.4	0.84	0.72	0.86
MRI	1.08	0.82	0.76	0.78	0.68	0.68
MPI	1.91	1.19	1.29	0.86	0.69	0.67
CCSM4	1.51	1.04	0.99	0.83	1.13	0.88

Table 7: A comparison of standard deviation values (mm/day) between Northeastern India summer monsoon rainfall (NEISMR) and Indian summer monsoon rainfall (ISMR) for the present day period

(1961 to 1990), Little Ice Age (LIA) and Medieval Climate Anomaly (MCA) for observation data (India Meteorological Department, IMD), and model data sets (ECHAM5, MRI, MPI & CCSM4).

3.2.3. TEJ changes and impacts on the ISMR

All the three models simulate the tropical easterly Jet stream (TEJ) over Peninsular India, associated with the Tibetan High (Figures 3.2.3 c, f & i), qualitatively similar to is present-day observations (Figure not shown). The simulations point to a stronger TEJ during the MCA relative to the LIA (Figures 3.2.3 c, f & i), which is normally associated with a high summer monsoon rainfall over the central-Indian region.

The analysis of the PMIP3 simulations by T19 suggests that a centennial westward shift of the overturning Walker Circulation in the tropical Indo-pacific could be a potential reason for the relatively high ISMR during the MCA. This, however, does not preclude any other large scale circulation changes, which may manifest an increase in the ISMR during the MCA.

Tropical dynamics suggest that the presence of the entrance of TEJ over the BoB facilitates strong convection over BoB and neighboring coastal regions of India. Briefly, the TEJ originates over the Western Pacific and BoB. Quasi-geostrophic dynamics (Hoskins and Wang (2006, section 9.5.2) suggest that the westward intensification of easterlies in the TEJ over the BoB and adjoining Indian region results in an ageostrophic convergence and upward motion at the mid-troposphere, and consequently, enhanced rainfall. We find an increase in the simulated 500 hPa relative vorticity (Figures 3.2.4a-3.2.4h) on the central east coast of India, particularly near to the Head BoB and/or over the neighboring Indian region. There, we see a higher summer monsoon rainfall during MCA (Figures 3.2.3 c, f & i). The difference in relative vorticity over NER looks high in Figure 3.2.4c. But it is just

due to its high climatological magnitude (e.g., Figures 3.2.4a & 3.2.4b). The differences in the area-averaged 500 hPa vorticity (Figure 3.2.5) confirm that the simulated circulation changes are relatively weak over the NER relative to CMR in all models, considerably so in two. This suggests that the strengthened TEJ during the MCA is important for the enhanced rainfall over the CMR during the MCA.

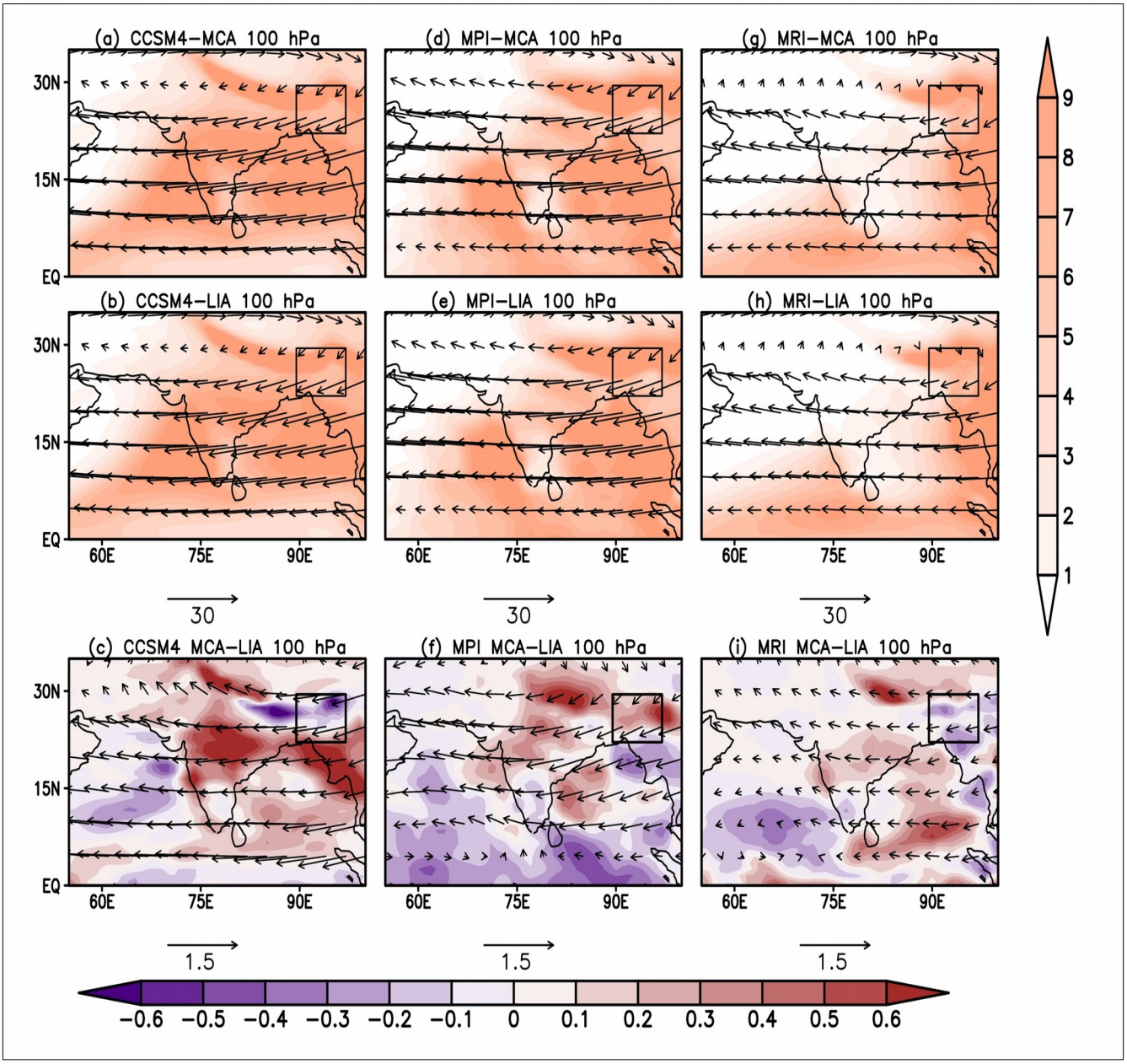

Figure 3.2.3: Panels a, d, & g show climatological precipitation (mm.day^{-1}) and 100 hPa wind circulation (m.s^{-1}) during JJAS season during MCA as simulated by three PMIP3 climate models. Panels b, e & h: same as panels a, d & g but for the LIA period (1735 CE to 1834 CE). Panels c, f & i show the climatological differences between MCA & LIA for the models. Northeastern Indian region is marked by a black box.

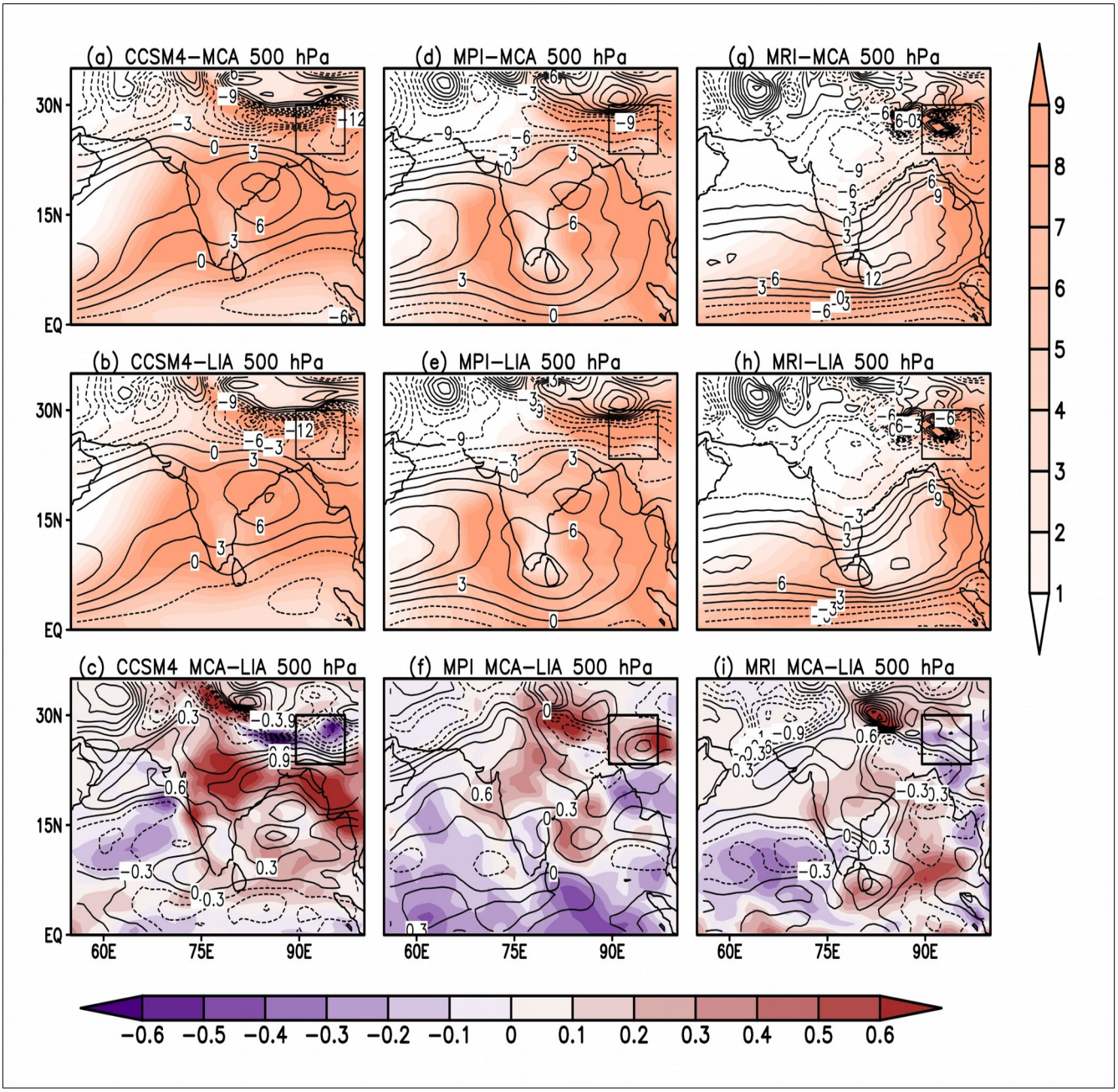

Figure 3.2.4: Same as Figure 3.2.3, but with simulated climatological 500 hPa relative vorticity (X 10^{-5} S^{-1}) instead of 100 hPa circulation. Note that rainfall (a, b, d, e, g & h), and rainfall differences in panels c, f & i is repeated from Figure 3.2.3, for convenience in interpreting relative vorticity changes.

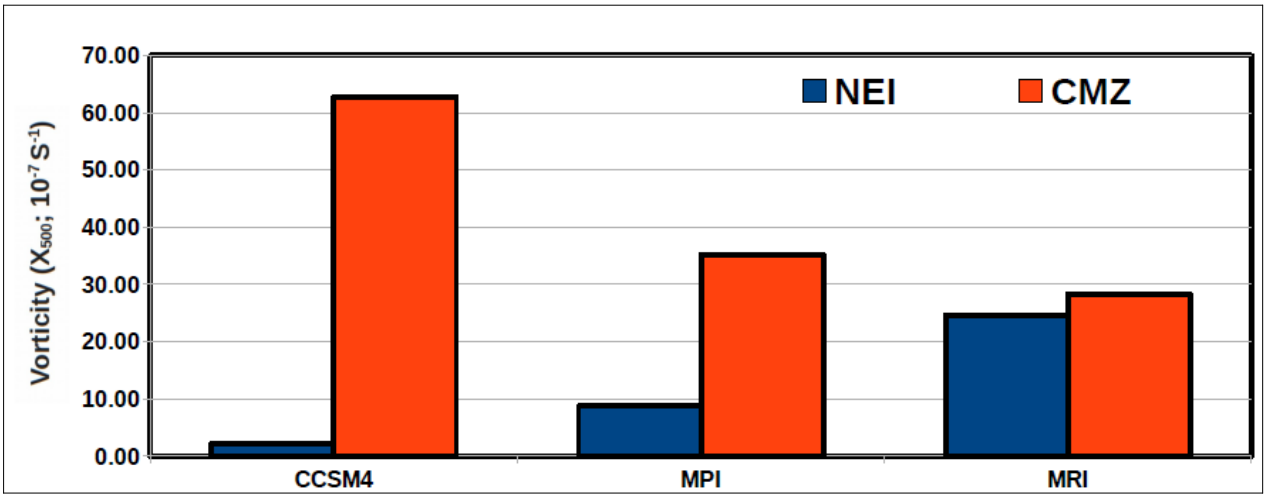

Figure 3.2.5: Area-averaged differences in simulated mean JJAS 500 hPa vorticity (MCA and LIA) for the three PMIP3 models.

This change in simulated TEJ during the MCA, however, does not affect NEISMR. This may be because the NER is farther from a moisture source such as the Head BoB region, relative to, say, the east coast peninsular India. Indeed, the simulated mid-level moisture flux convergence change into NER between MCA and LIA (not shown), unlike that in the east coastal Indian region and/or around the Head BoB, is small.

3.2.6 Association between the ENSO and NEISMR

Just as the present-day observations (Soraisam et al., 2018), the simulated rainfall over NEISMR during both MCA and LIA is insignificantly correlated at 95% confidence level with the NINO3.4 index (area-averaged sea surface anomalies over 5^{o} N to 5^{o} S and 170^{o} W to 120^{o} W; Figure 3.2.6). We have also ascertained that the correlations do not turn significant even if we use the NINO3 index

(area-averaged sea surface anomalies over 5^{o} S to 5^{o} N and 150^{o} W to 90^{o} W), which reflects the activities of both canonical and Modoki ENSOs (Ashok et al., 2007; Weng et al., 2007).

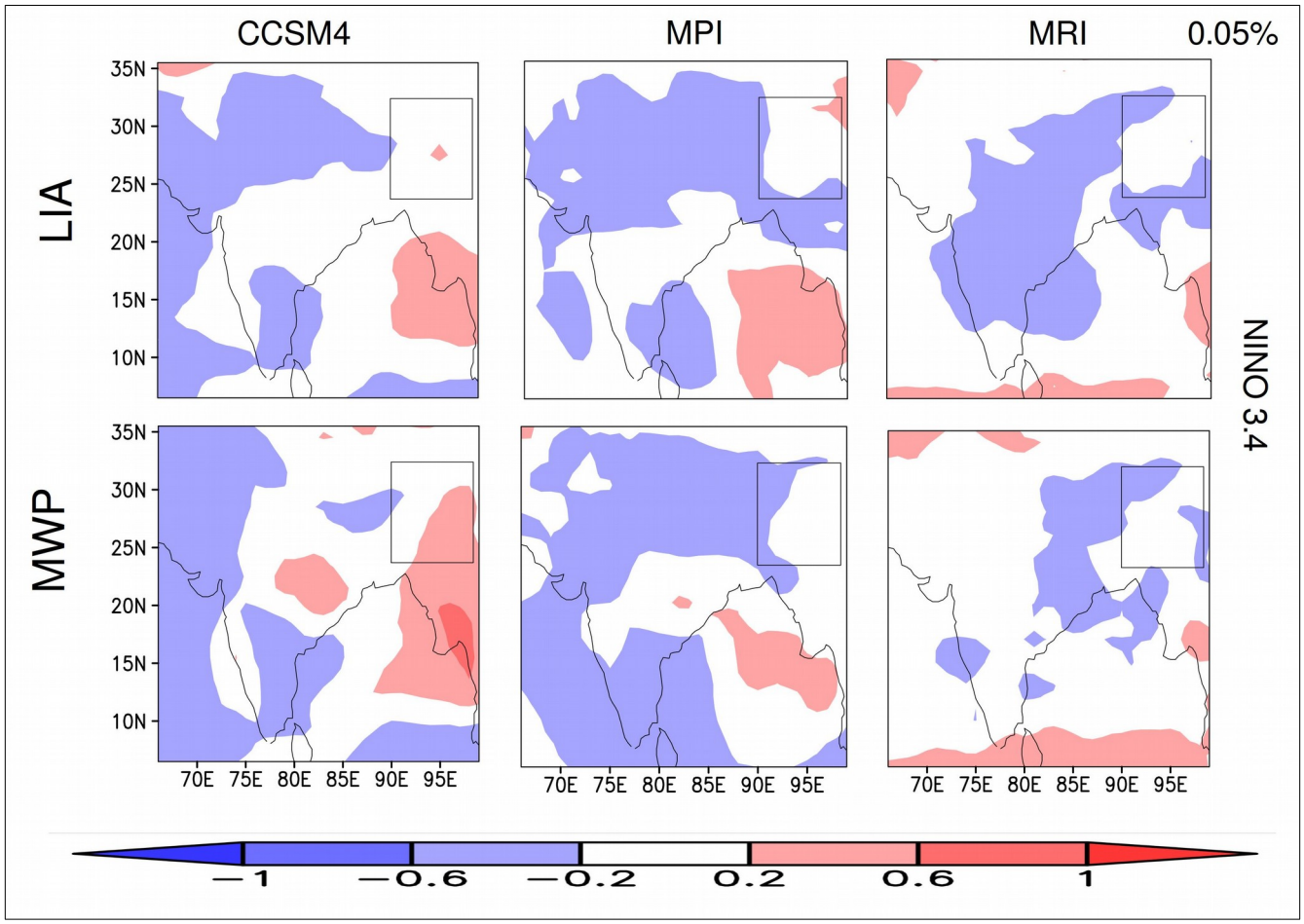

Figure 3.2.6: Spatial distribution of anomaly correlations between the NINO3.4 index and local precipitation during JJAS season for the LIA (top panels) and MWA (bottom panels) simulated by the three PMIP3 models.

3.2.7. Seasonal mean cycle for simulated future precipitation, maximum and minimum temperature data for the period 2011 to 2060

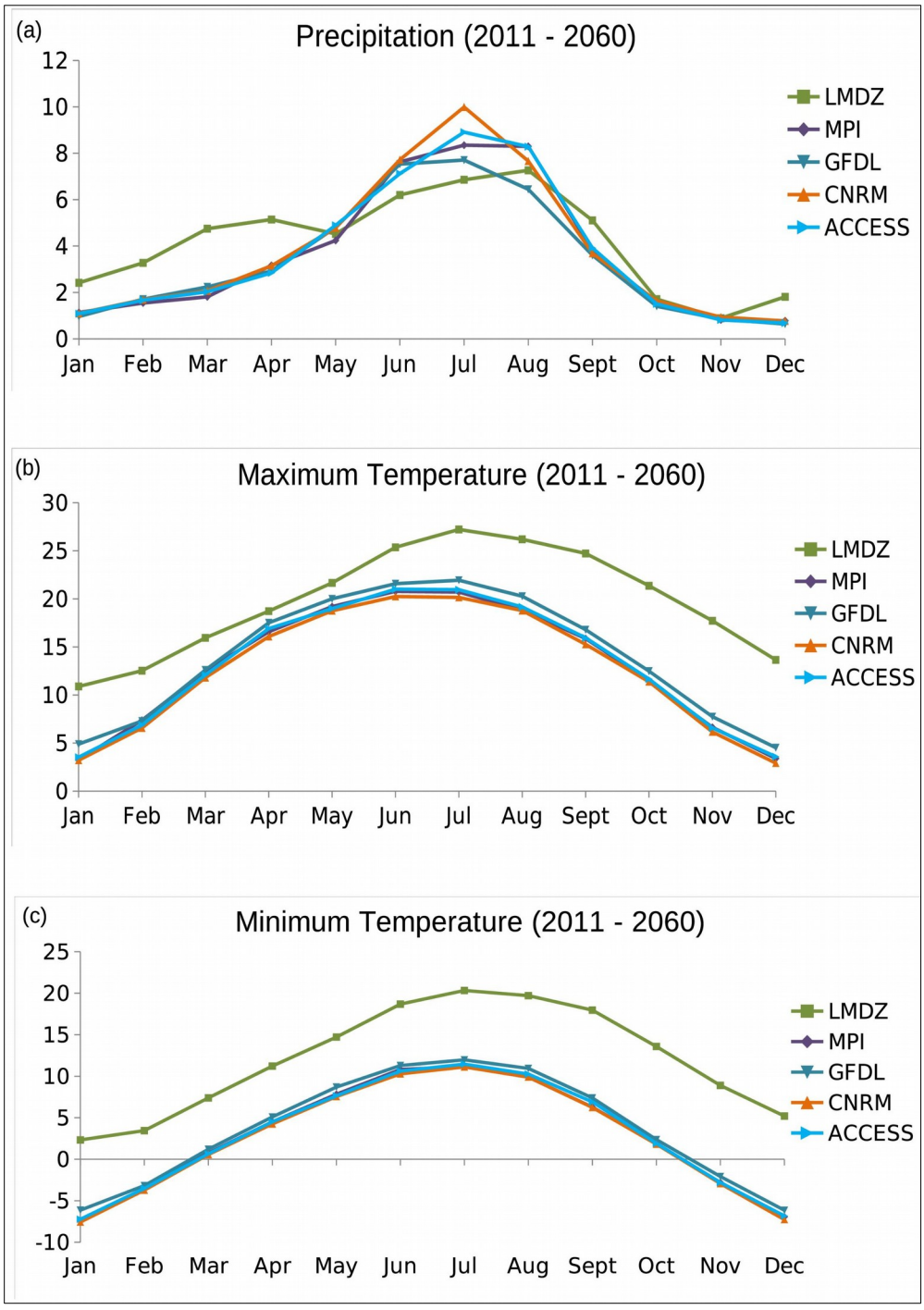

Figure 3.2.7: (a). Seasonal mean cycle of precipitation data (mm) from Cordex South Asia model data (LMDZ, MPI, GFDL, CNRM and ACCESS) for the period 2011 to 2060. (b) & (c) same but for maximum and minimum temperature (°C).

The individual model RCP4.5 projections of the seasonal cycle of precipitation for 2011 to 2060 (Figure 3.2.7a) indicate an evolution similar to the corresponding historical cycle. However, a majority of models indicate a slight decrease or no change in the magnitude of the summer monsoon rainfall, except the projection from the CNRM showing a moderate increase in July precipitation. Based on these results and an analysis of the spatial distribution of the simulated precipitation (to be discussed in the next paragraph), we can sum up that the models project a slight or no decrease in the rainfall over the NER in the future.

The simulated seasonal cycles of maximum and minimum temperature from the RCP4.5 shows an unchanged evolution. Still, models also project a substantial increase in the maximum and minimum temperatures (Fig. 3.2.7b & c) relative to the corresponding historical simulations, indicating a rise in the temperature in the future over the NER.

3.2.8. Simulated JJAS future climatology (RCP4.5) from 2011 to 2060

The simulated JJAS climatology of precipitation (RF-JJAS) from the RCP4.5 projections for the 2011–2060 period is presented in Figure 3.2.8, and the excess or deficit as compared to the corresponding historical simulations is shown in Fig. 1a. We find from Figs. 3.2.8 and 3.2.9 that the future projection of RF-JJAS from each CORDEX South-Asia model is not significantly different from the corresponding historical simulations (Figure 3.1.1), except for a weak decrease seen in simulations of a model or two. The RF-JJAS of the LMDZ model spatially ranges between 5~11 mm while in the rest of the models,3~19 mm.

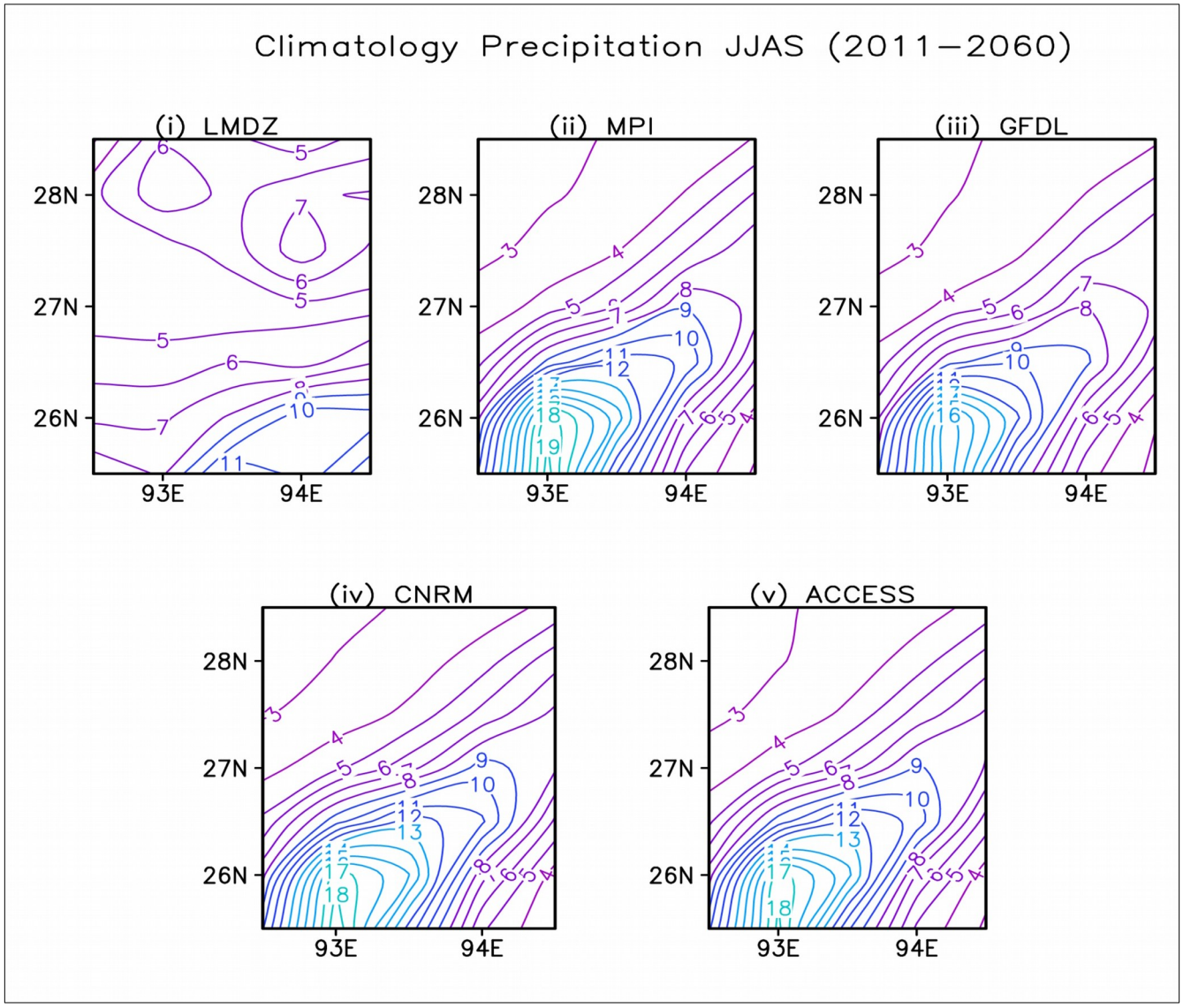

Figure 3.2.8: Spatial distributions of JJAS climatology of precipitation (mm) during 2011 to 2060 (future projections) for the climate model data from Cordex South Asia: (i) LMDZ, (ii) MPI, (iii) GFDL, (iv) CNRM and (v) ACCESS over North East Region.

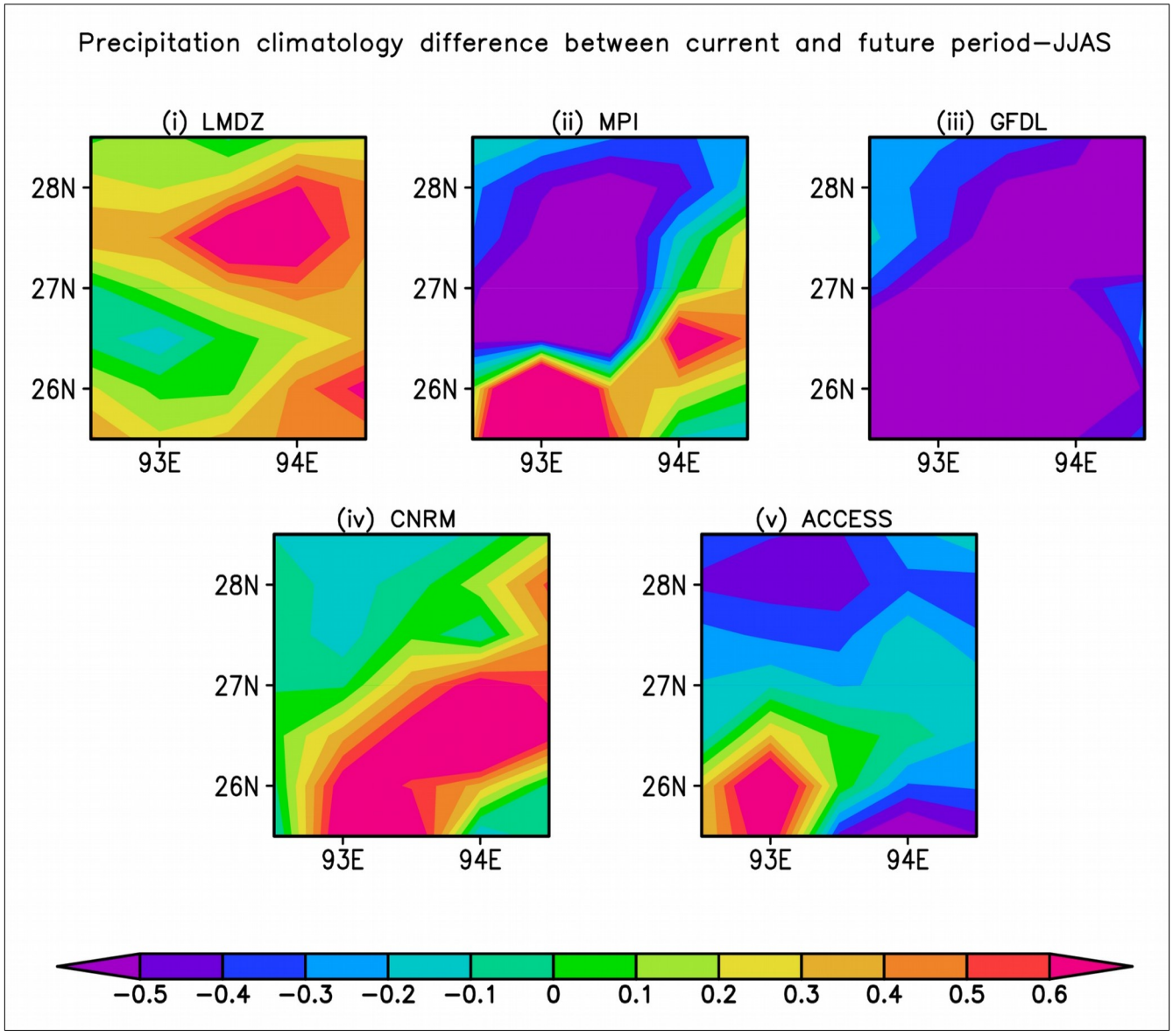

Figure 3.2.9: Climatology difference for precipitation (mm) between current and future period for JJAS for model data, namely, (i) LMDZ, (ii) MPI, (iii) GFDL, (iv) CNRM and (v) ACCESS.

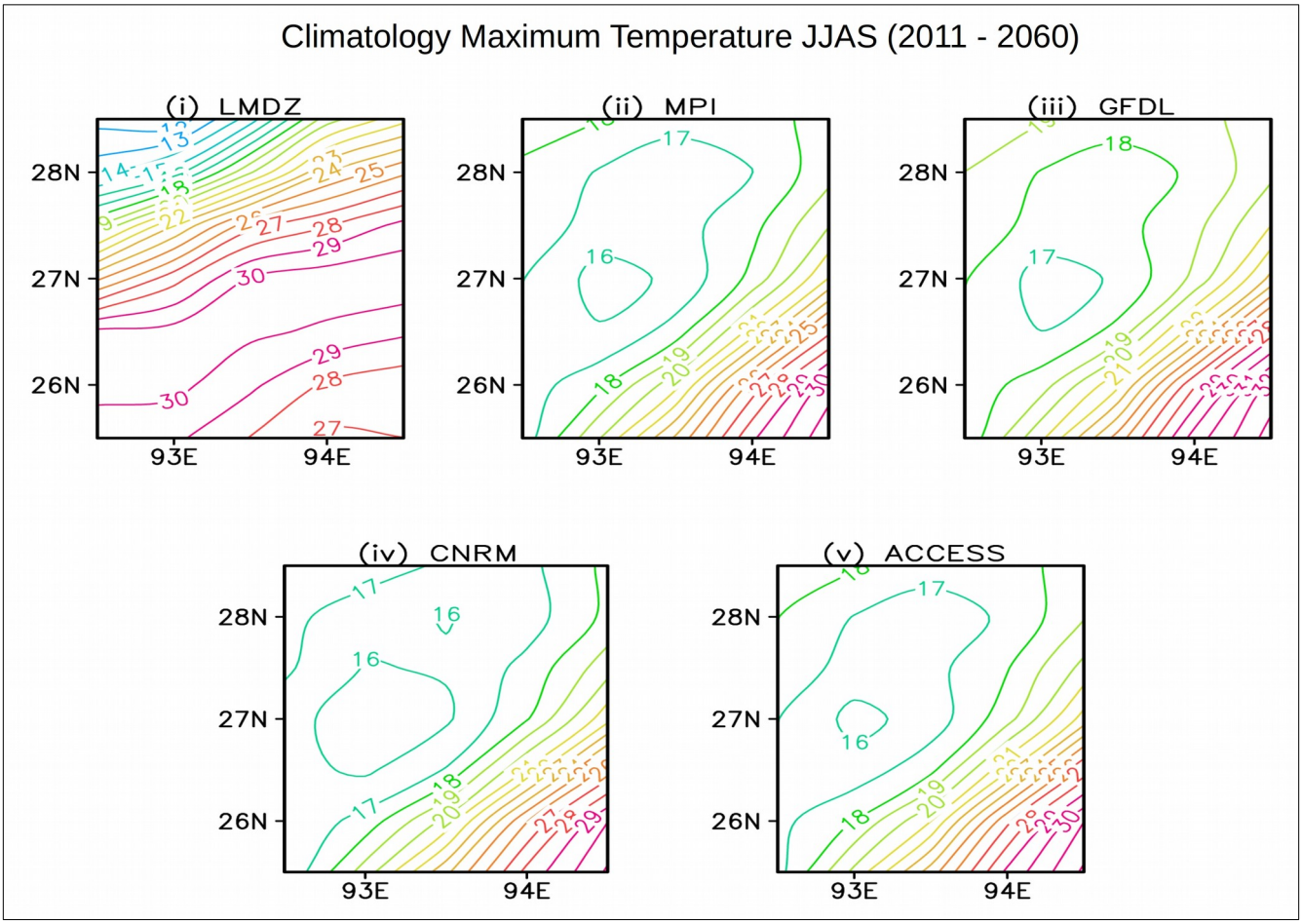

Figure 3.2.10: Spatial distributions of JJAS climatology of maximum temperature (°C) during 2011 - 2060 (future projections) for climate model data from Cordex South Asia: (i) LMDZ, (ii) MPI, (iii) GFDL, (iv) CNRM and (v) ACCESS over North East Region.

Notably, (the spatial distribution of TMax-JJAS and TMin-JJAS) in all the models in Figs. 3.2.10 and 3.2.12 show an increasing magnitude and are also warmer than the corresponding historical simulations (also match with Fig. 3.2.11 and 3.2.13) across the NER. The respective minimum temperature ranges are, 13 °C~30 °C and 5 °C~23 °C.

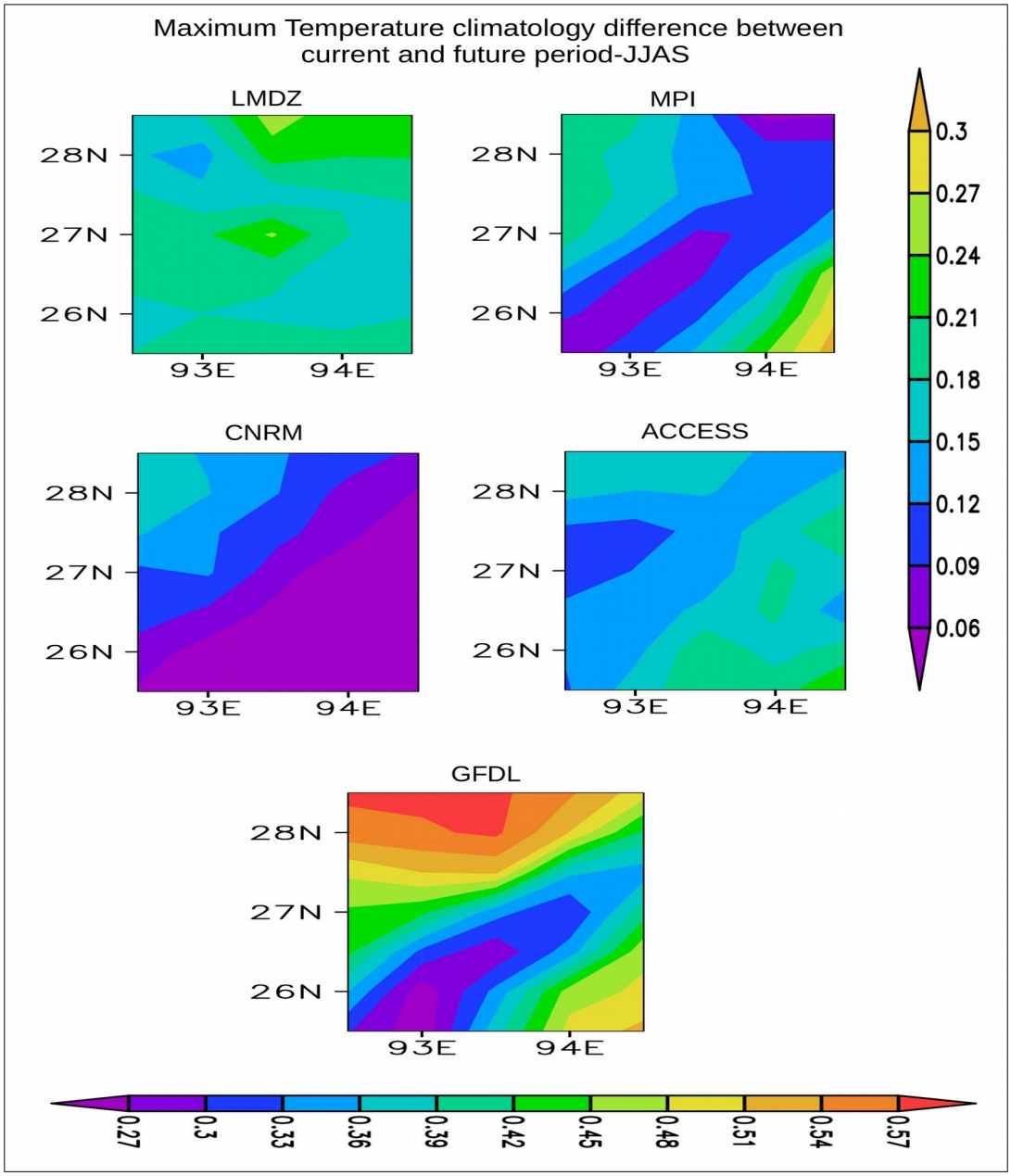

Figure 3.2.11: Climatology difference for maximum temperature (°C) between current and future period for JJAS for model data, namely, (i) LMDZ, (ii) MPI, (iii) GFDL, (iv) CNRM, and (v) ACCESS.

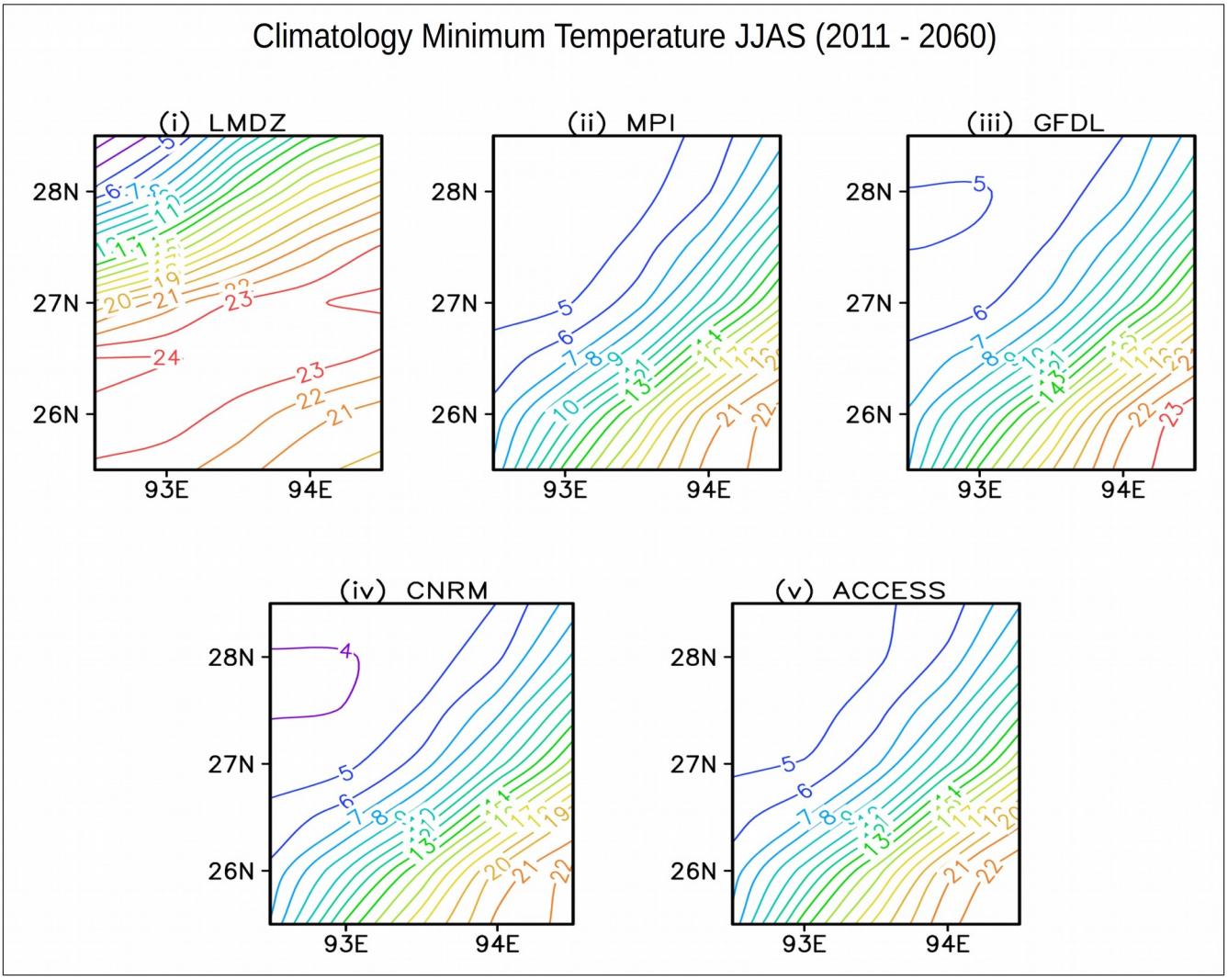

Figure 3.2.12: Spatial distributions of JJAS climatology of minimum temperature (°C) during 2011 - 2060 (future projections) for climate model data from Cordex South Asia: (i) LMDZ, (ii) MPI, (iii) GFDL, (iv) CNRM and (v) ACCESS over North East Region.

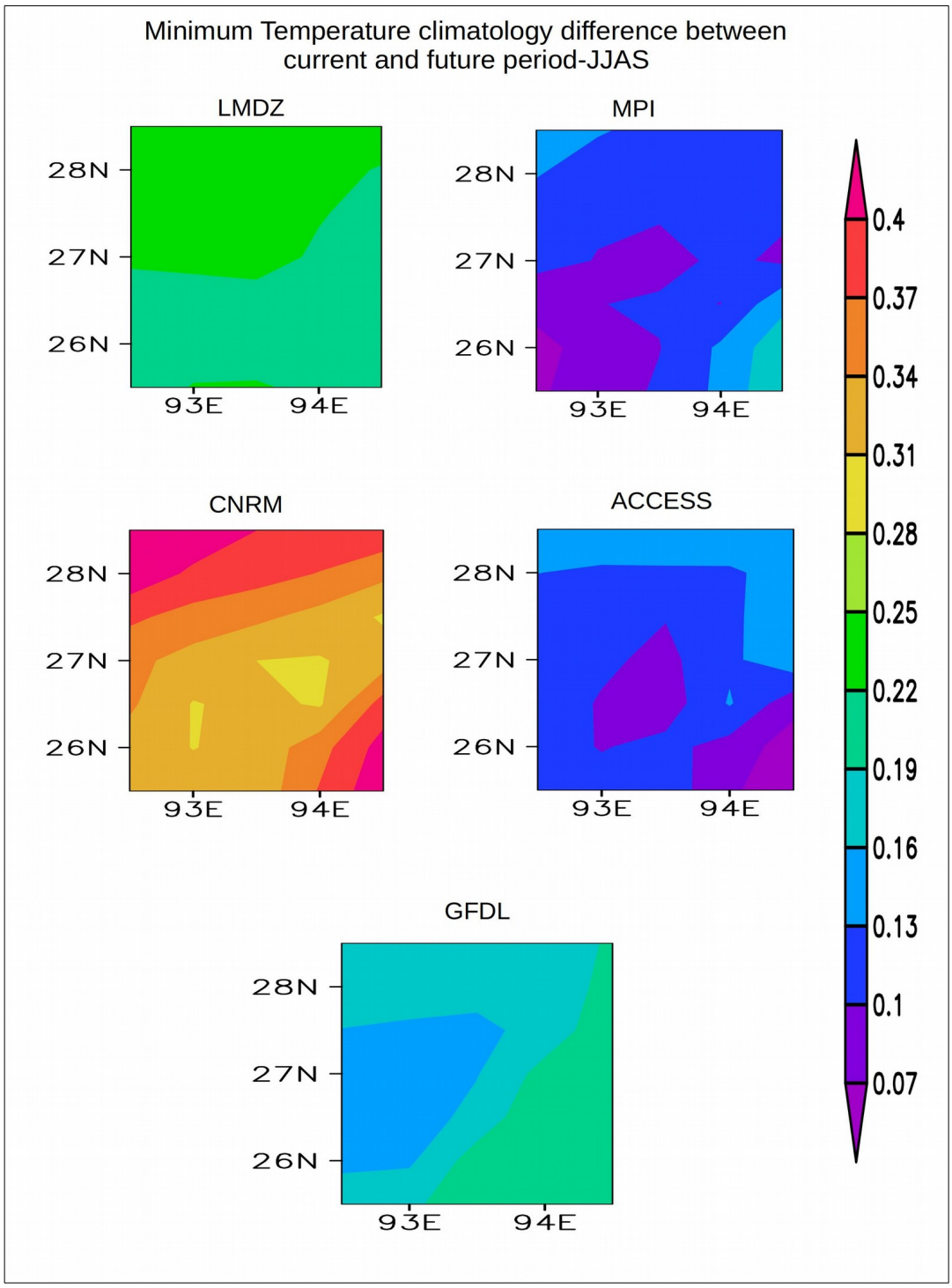

Figure 3.2.13: Climatology difference for minimum temperature (°C) between current and future period for JJAS for model data, namely, (i) LMDZ, (ii) MPI, (iii) GFDL, (iv) CNRM and (v) ACCESS.

3.2.14: Simulated DJF future climatology (RCP4.5) from 2011 to 2060

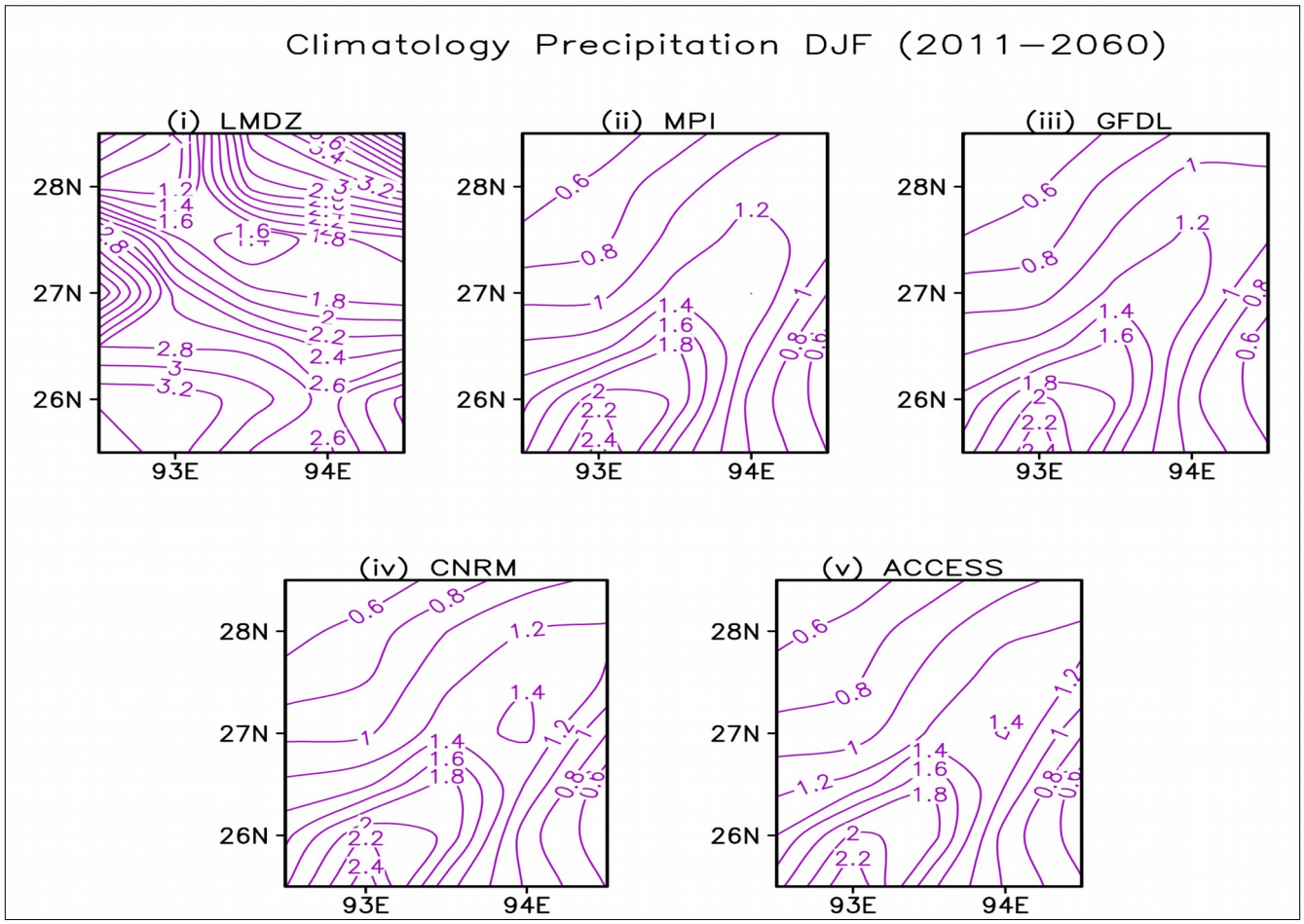

Figure 3.2.14: Spatial distributions of DJF climatology of precipitation (mm) during 2011 - 2060 (future projections) for climate model data from Cordex South Asia: (i) LMDZ, (ii) MPI, (iii) GFDL, (iv) CNRM and (v) ACCESS over North East Region.

The simulated climatological DJF precipitation (RF-DJF) does not show much change in the future projection (Figure 3.2.14), with values ranging from 0.6 to 3.2 mm. This is also seen in Fig. 3.2.15, though all the models are not simulating the same result. The range of RF-DJF is seen declining in the future projection.

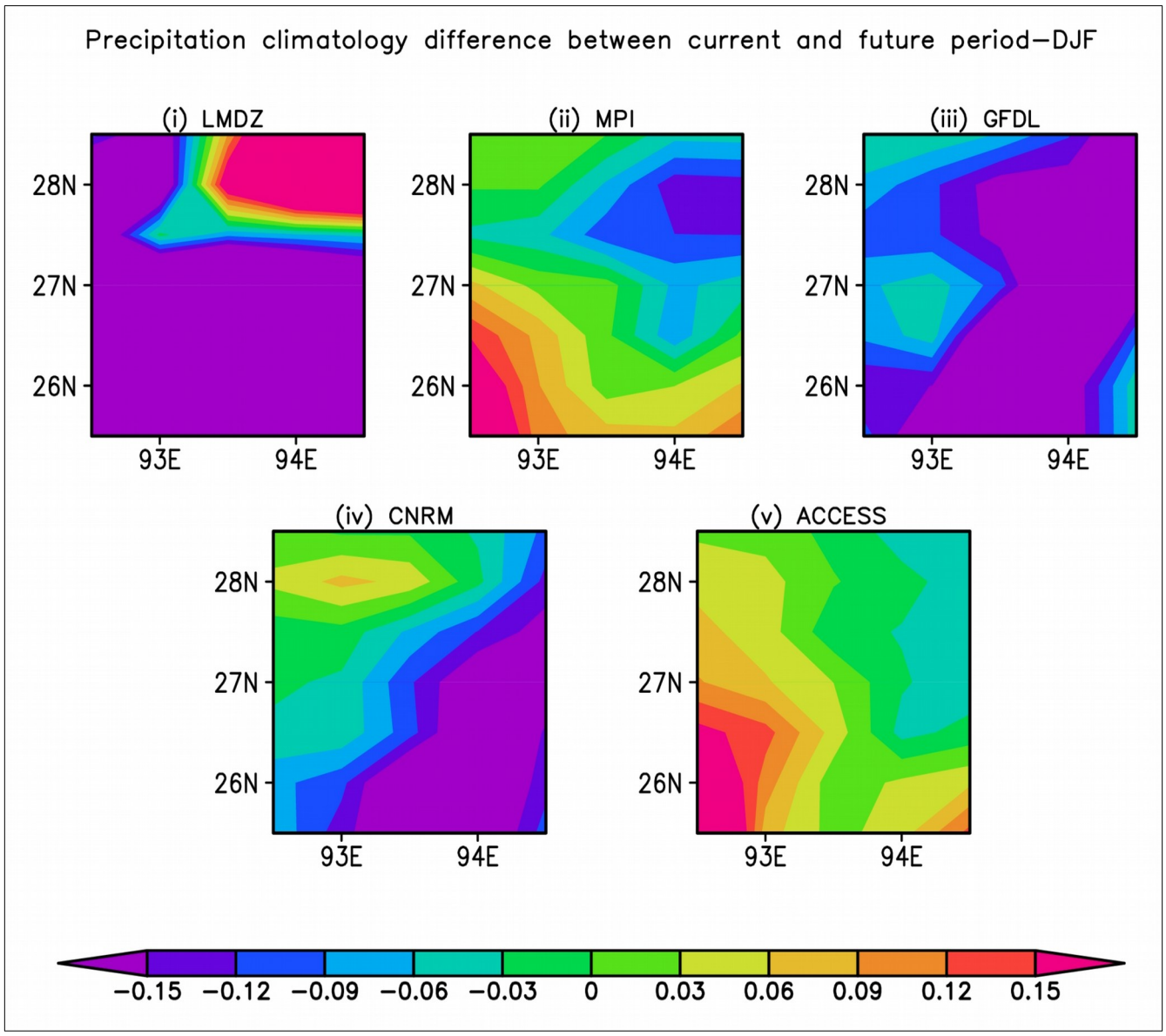

Figure 3.2.15: Climatology difference for precipitation (mm) between current and future period for DJF for model data, namely, (i) LMDZ, (ii) MPI, (iii) GFDL, (iv) CNRM and (v) ACCESS.

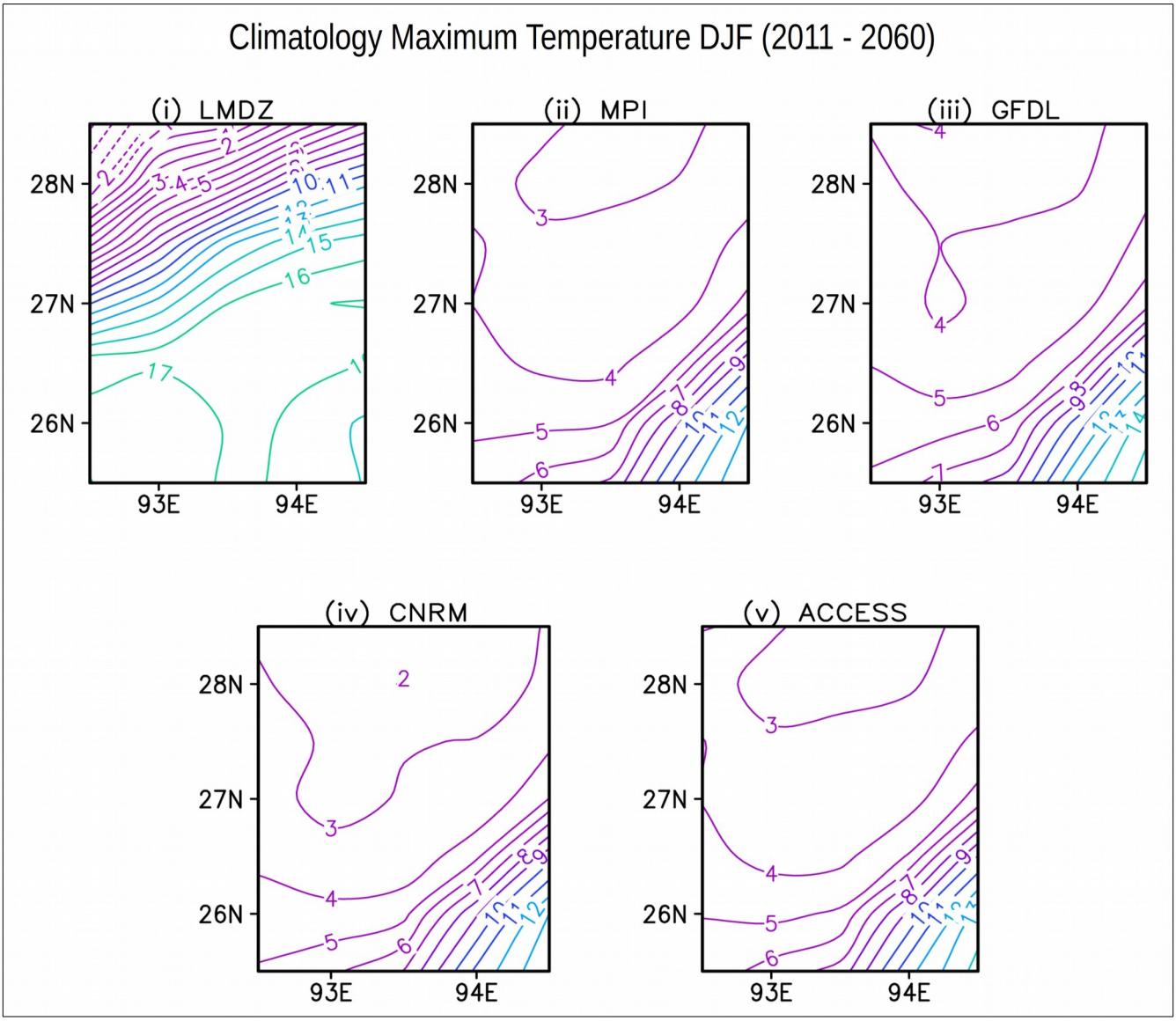

Figure 3.2.16: Spatial distributions of DJF climatology of maximum temperature (°C) during 2011 - 2060 (future projections) for climate model data from Cordex South Asia: (i) LMDZ, (ii) MPI, (iii) GFDL, (iv) CNRM and (v) ACCESS over North East Region.

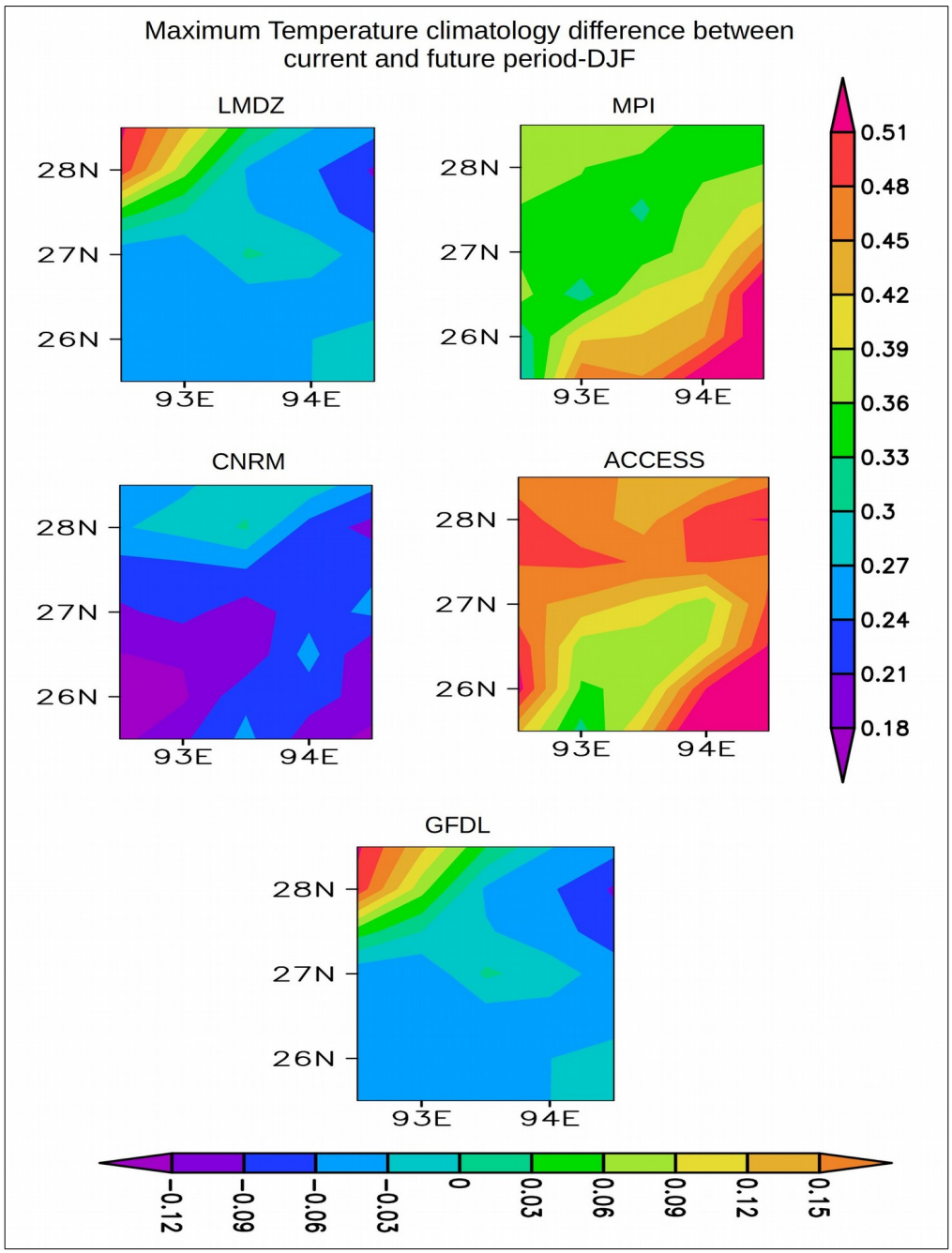

Figure 3.2.17: Climatology difference for maximum temperature (°C) between current and future period for DJF for model data, namely, (i) LMDZ, (ii) MPI, (iii) GFDL, (iv) CNRM and (v) ACCESS.

All the models also project an increased TMax-DJF (Figs. 3.2.16 and 3.2.17), with the values varying from 2 °C to 17 °C. Spatial distributions of TMax-DJF from the analyzed in all CORDEX South-Asia projections, the models are similar to those from the historical simulations.

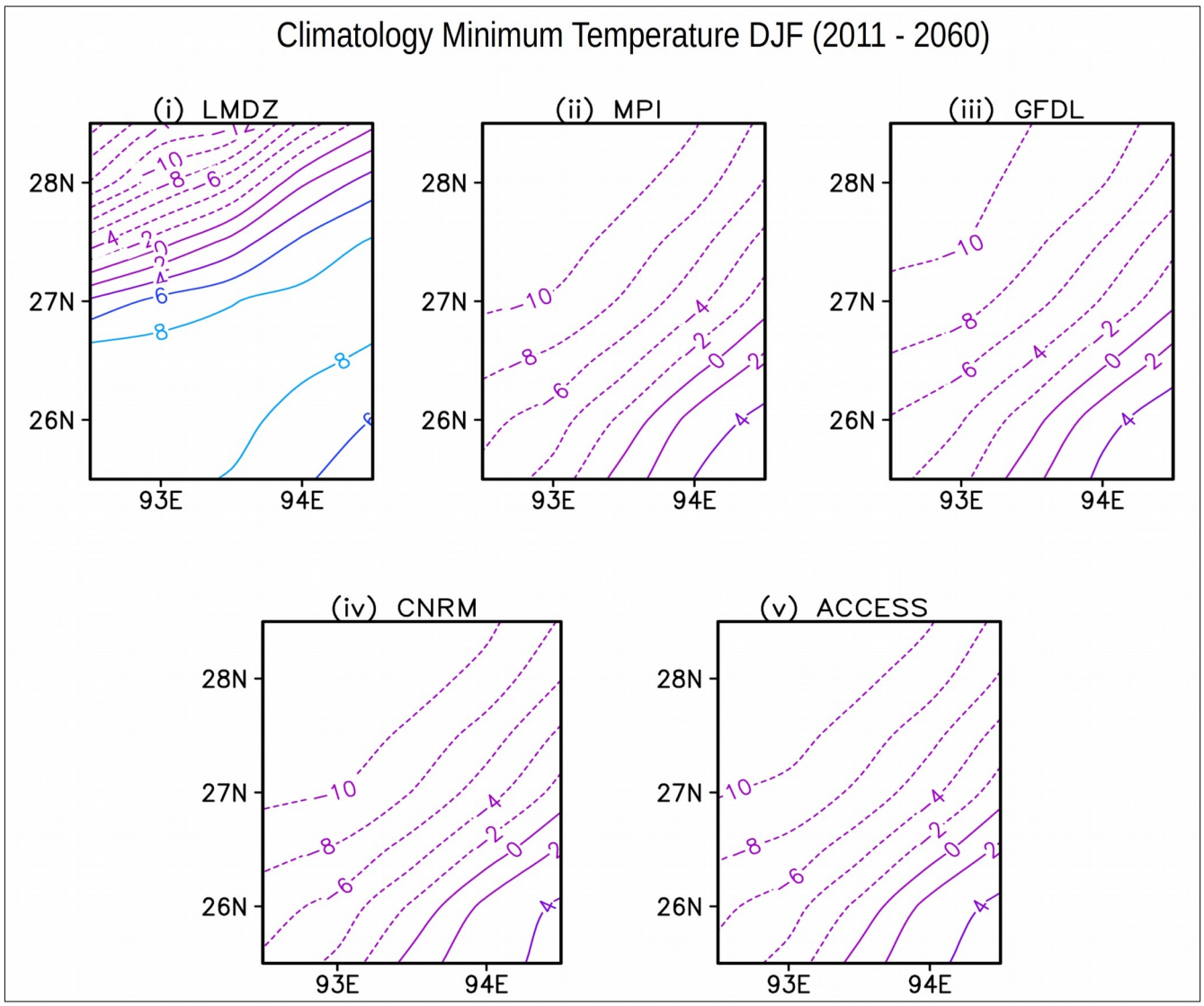

Figure 3.2.18: Spatial distributions of DJF climatology of minimum temperature (°C) during 2011 - 2060 (future projections) for climate model data from Cordex South Asia: (i) LMDZ, (ii) MPI, (iii) GFDL, (iv) CNRM and (v) ACCESS over North East Region.

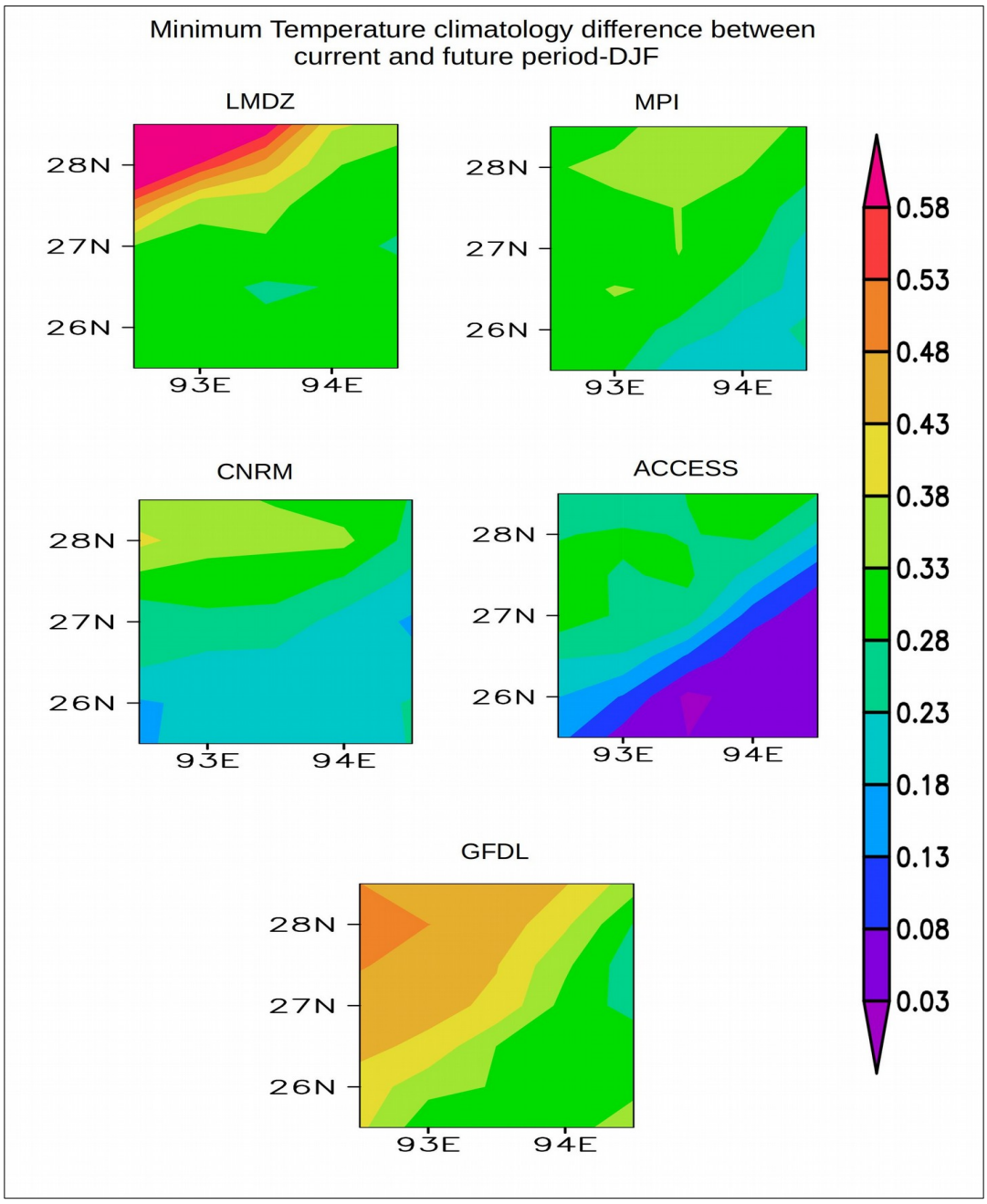

Figure 3.2.19:Climatology difference for minimum temperature (°C) between current and future period for DJF for model data, namely, (i) LMDZ, (ii) MPI, (iii) GFDL, (iv) CNRM and (v) ACCESS.

The projected minimum temperatures for DJF season (Figs. 3.2.18 and 3.2.19) also increases than the corresponding historical simulations. The future projected DJF climatology in the NER range from -10 °C to 8 °C.

3.2.20. Area-averaged Trends in projected climate in the NER for the period of 2011 to 2060

Data used	Mann-Kendall test		Student t-test			Nature of the trend
	Z value & α value	Statistic value (S)	p-Value	t-Value	Trend value	
JJAS						
LMDZ	3.17 > 1.96	379	0.00 < 0.05	3.10 > 2	0.67	Increasing trend & significant
CNRM	1.97 > 1.96	235	0.04 < 0.05	2.07 > 2	1.08	- do -

Table 8: Significance tests using Mann-Kendall and Student t-test for precipitation data for JJAS season from the climate model data for the period 2011–2060.

Table 8 shows that the JJAS precipitation signals for the 2011 to 2060 period as simulated in the LMDZ and CNRM models show a significantly increasing trend. The ACCESS model projects an increasing but statistically insignificant trend in summer precipitation during the above period. On the other hand, the MPI and GFDL models show an insignificant decreasing trend. The projected DJF precipitation in all the models except the ACCESS model shows an insignificantly decreasing trend. The ACCESS model simulates a weak increasing trend. Only the significant results are shown in the table.

Data used	Mann-Kendall test		Student t-test			Nature of the trend
	Z value & α value	Statistic value (S)	p-Value	t-Value	Trend value	
JJAS						
LMDZ	5.73 > 1.96	685	0.00 < 0.05	7.01 > 2	1.4	Increasing trend & significant
MPI	3.29 > 1.96	393	0.00 < 0.05	4.24 > 2	1.13	- do -
GFDL	6.25 > 1.96	747	0.00 < 0.05	8.84 > 2	2.86	- do -
ACCESS	3.81 > 1.96	455	0.00 < 0.05	4.07 > 2	1.07	- do -
DJF						
LMDZ	4.47 > 1.96	551	0.00 < 0.05	5.24 > 2	1.96	- do -
MPI	3.63 > 1.96	447	0.00 < 0.05	4.27 > 2	2.71	- do -
GFDL	4.41 > 1.96	543	0.00 < 0.05	4.84 > 2	3.01	- do -
CNRM	3.27 > 1.96	403	0.00 < 0.05	7.19 > 2	1.89	- do -

Table 9: Significance tests using Mann-Kendall and Student t-test for maximum temperature data from the climate model data for the period 2011–2060.

Data used	Mann-Kendall test		Student t-test			Nature of the trend
	Z value & α value	Statistic value (S)	p-Value	t-Value	Trend value	
JJAS						
LMDZ	7.25 > 1.96	867	0.00 < 0.05	11.78 > 2	1.66	Increasing trend & significant
MPI	3.89 > 1.96	465	0.00 < 0.05	4.27 > 2	0.95	- do -
GFDL	6.92 > 1.96	827	0.00 < 0.05	10.44 > 2	2.6	- do -
CNRM	2.68 > 1.96	321	0.01 < 0.05	2.87 > 2	0.71	- do -
ACCESS	5.08 > 1.96	607	0.00 < 0.05	6.20 > 2	1.45	- do -
DJF						
LMDZ	5.03 > 1.96	619	0.00 < 0.05	6.47 > 2	2.61	- do -
MPI	4.96 > 1.96	611	0.00 < 0.05	5.23 > 2	1.94	- do -
GFDL	4.64 > 1.96	571	0.00 < 0.05	6.07 > 2	2.38	- do -
CNRM	5.71 > 1.96	703	0.00 < 0.05	7.19 > 2	1.89	- do -
ACCESS	2.89 > 1.96	357	0.00 < 0.05	3.08 > 2	1.15	- do -

Table 10: Significance tests using Mann-Kendall and Student t-test for minimum temperature data from the climate model data for the period 2011–2060.

Interestingly, four out of five future simulations project a statistically significant increasing trend in summer maximum temperature (Table 9), while all of the projects a statistically significant increasing trend in minimum temperatures (Table 10). The significant increasing trend in the maximum and minimum trend is also projected for the DJF season (Tables 9 & 10). Thus, is clear although the projected models do not show quantitatively similar results, qualitatively there is a good agreement, particularly for the temperature. That is, as per the RCP4.5 simulations, the DJF precipitation is expected to further decline while both maximum and minimum temperatures are likely to increase further rapidly. However, there is considerable inter-model uncertainty in the future summer monsoon rainfall in the NER.

3.2.21. Extremes analysis for JJAS season for 2011 to 2060

In Figure 3.2.21, histograms of simulated JJAS monthly mean rainfall over the NER for the simulated future projections from 2011 to 2060 are presented. The frequency of the heaviest monthly-mean rainfall months in general increases in the simulated future projections for 2011–60, except in those from the GFDL which fall from 15 to 13. Further, it is also to be noted that the magnitude of the heaviest monthly rainfall decreases (increases) in two (one) models by about 2 mm/day (4 mm/day). Importantly, it shows that the total number of ‘low rainfall’ months (arbitrarily defined as rainfall < 7 mm/day) have increased quite substantially, with the range of increase being 34%–42%.

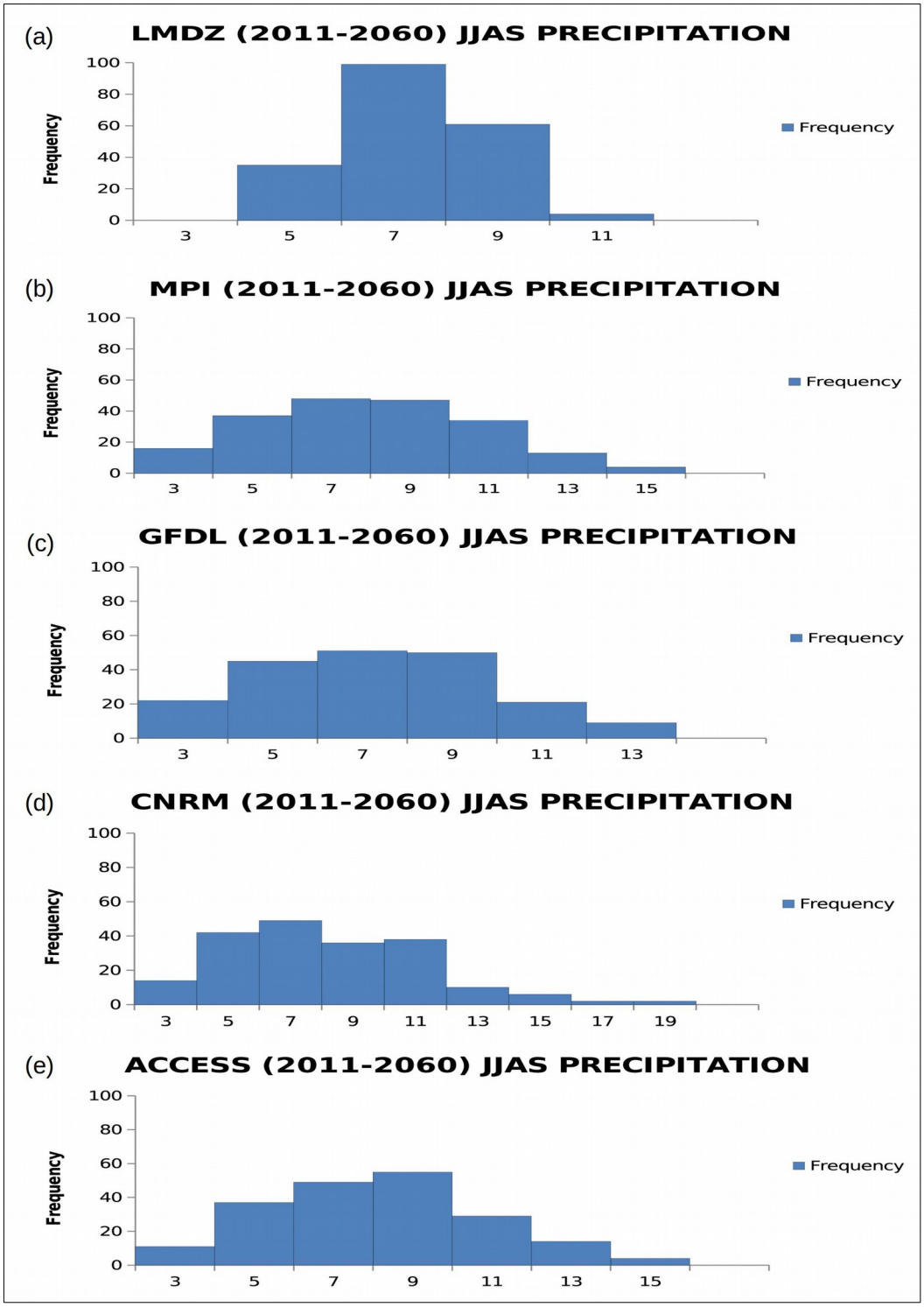

Figure 3.2.21: Histogram plots for JJAS precipitation (mm) of future period (2011 to 2060): CORDEX models ((LMDZ, MPI, GFDL, CNRM and ACCESS).

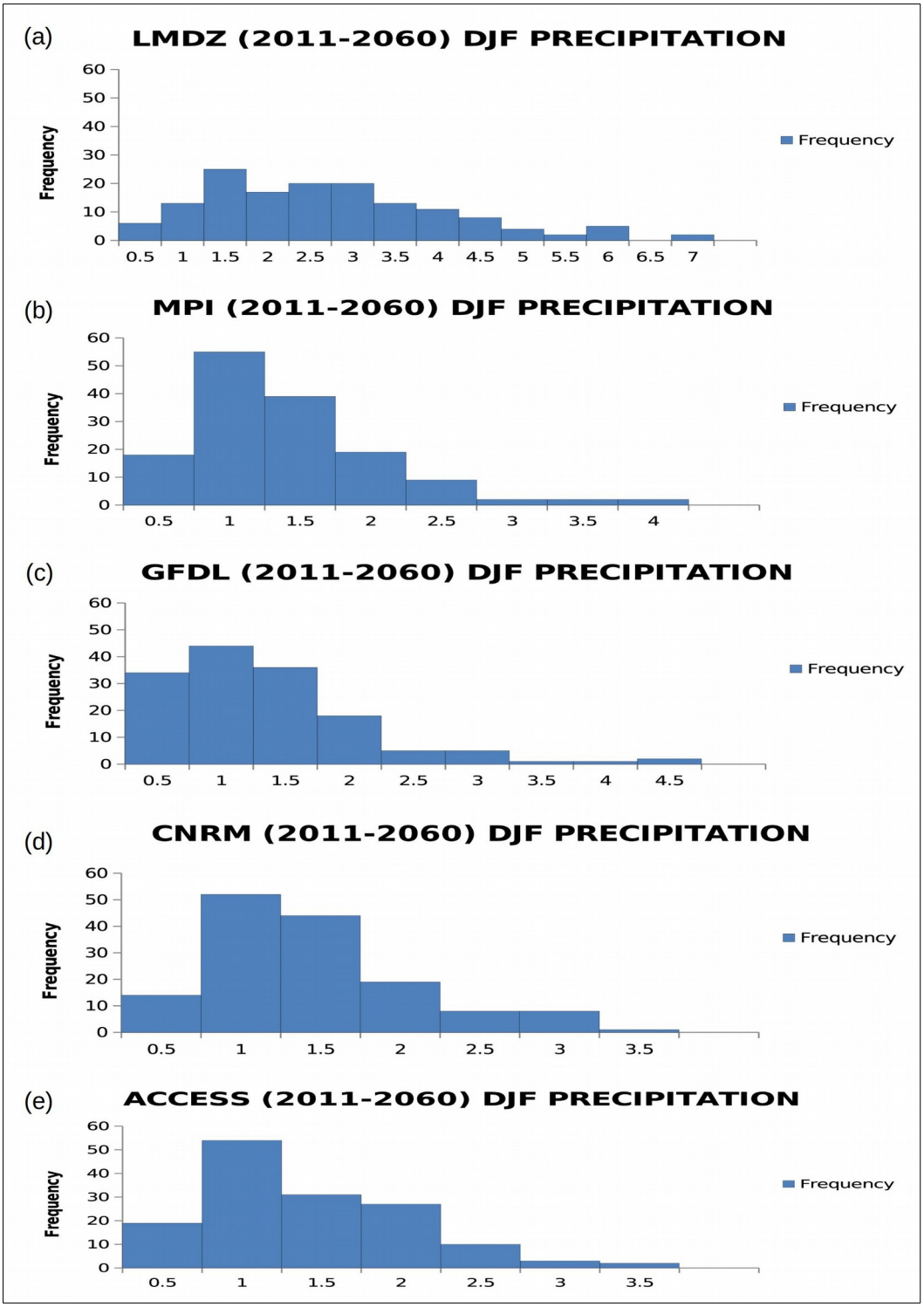

Figure 3.2.22: Histogram plots for DJF precipitation (mm) of future period (2011 to 2060): CORDEX models ((LMDZ, MPI, GFDL, CNRM and ACCESS).

Histograms of simulated DJF monthly mean rainfall over the NER for the simulated future projections from 2011 to 2060 are presented in Figure 3.2.22. In future projections, the frequency of simulated heavy rainfall months increases in all the model projections except GFDL and CNRM.

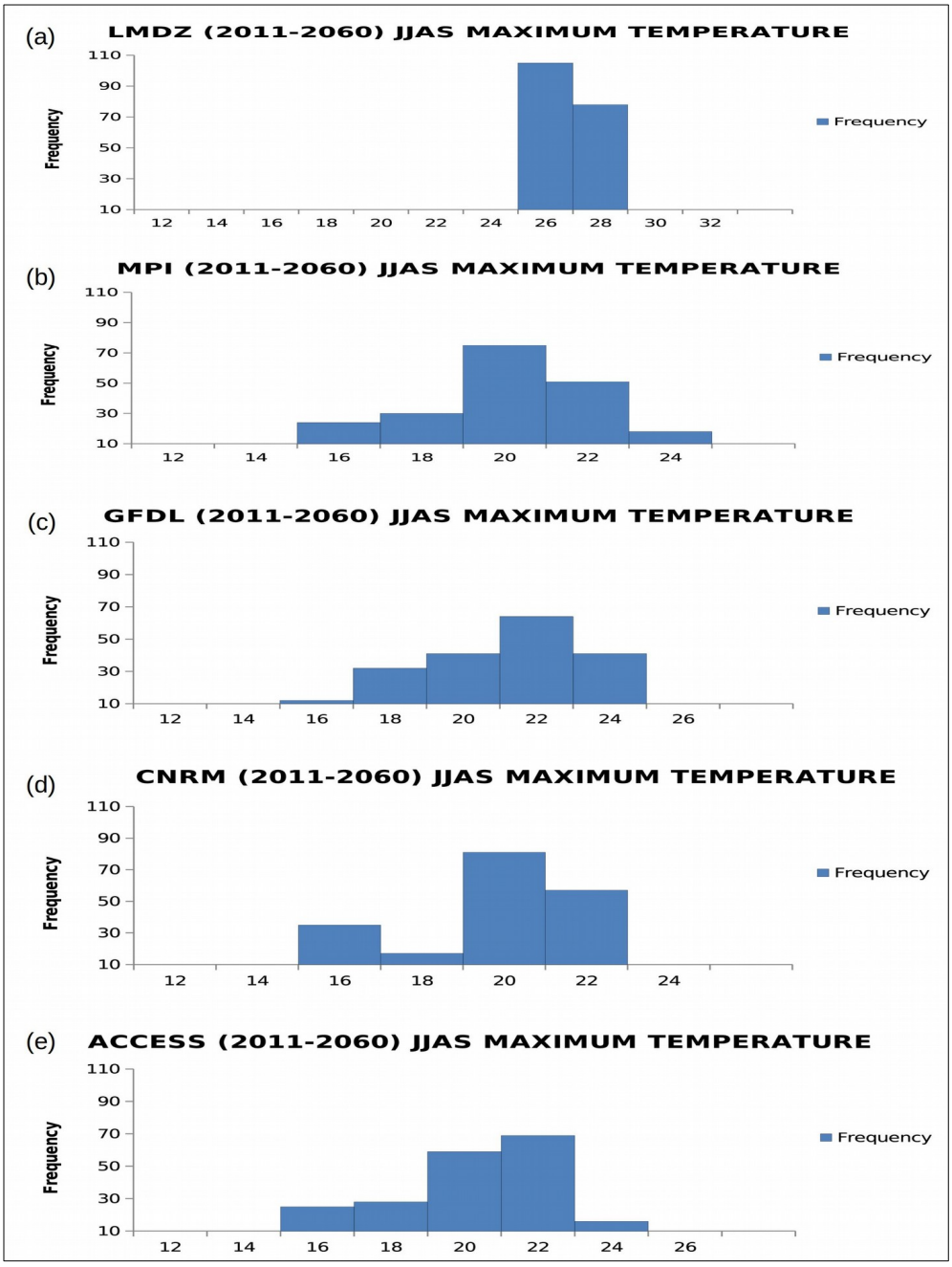

Figure 3.2.23: Histogram plots for JJAS maximum temperature (°C) of future period (2011 to 2060): CORDEX models (LMDZ, MPI, GFDL, CNRM and ACCESS).

The extreme events of JJAS maximum temperature for future projections from 2011 to 2060 are shown the Figure 3.2.23. The simulated highest maximum monthly temperature in the future projections relatively increases and ranges between 24 °C to 32 °C with LMDZ.

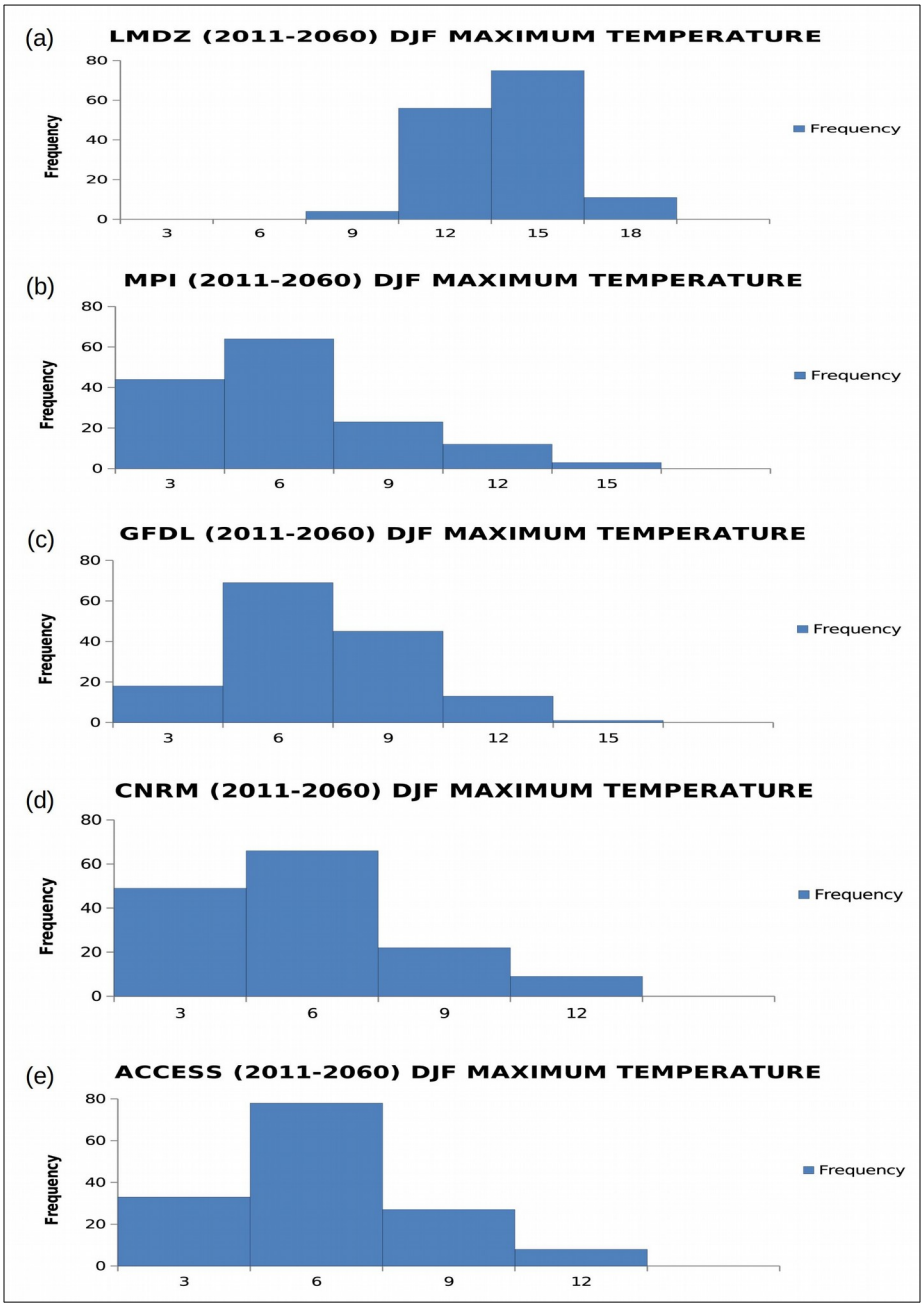

Figure 3.2.24: Histogram plots for DJF maximum temperature (°C) of future period (2011 to 2060): CORDEX models (LMDZ, MPI, GFDL, CNRM and ACCESS).

In Figure 3.2.24, the extreme months of maximum temperature for DJF season are shown for future projections (2011–2060). Even though the highest maximum temperature increases in the future projections, the maximum number of events with the highest frequency decreases.

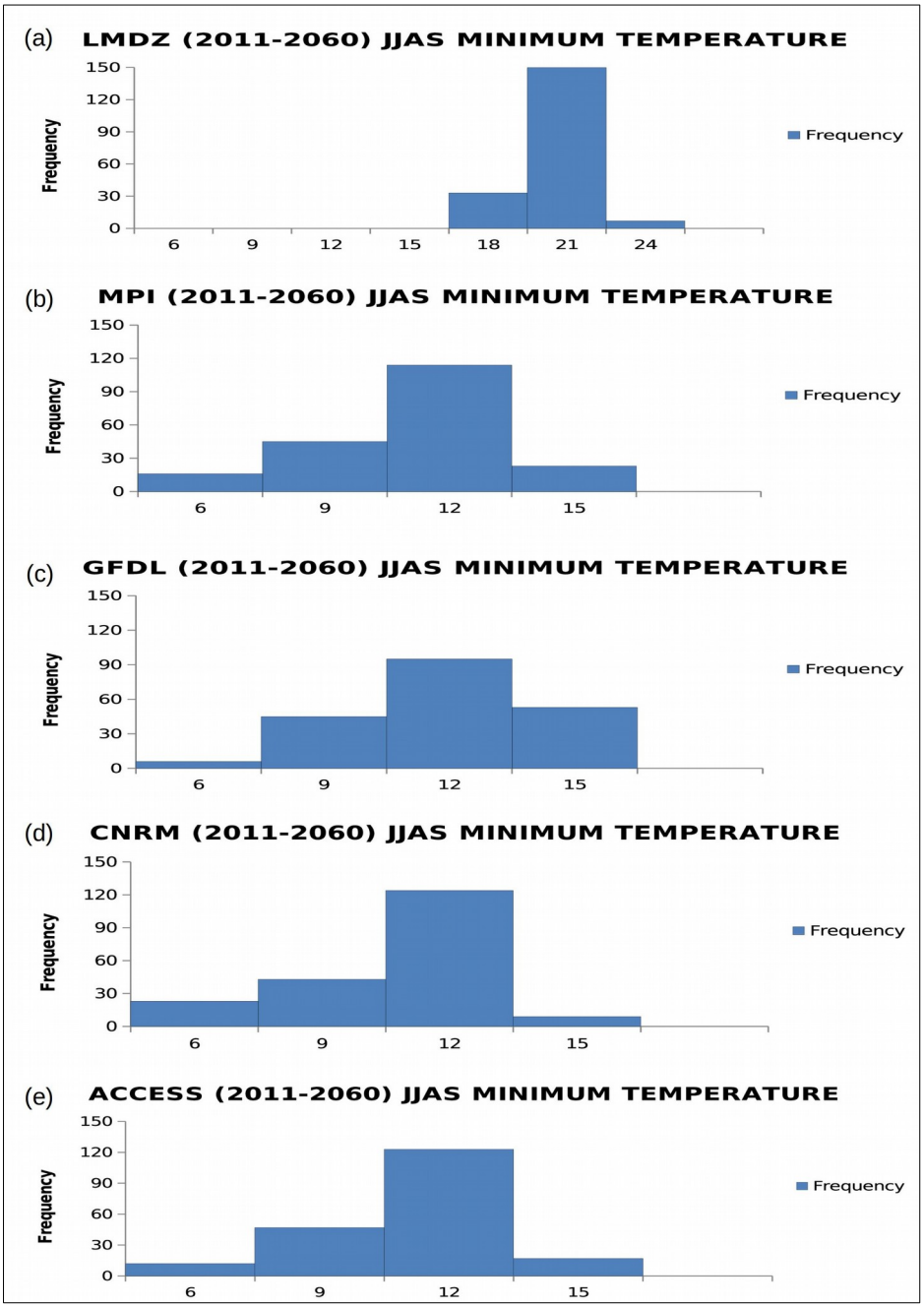

Figure 3.2.25: Histogram plots for JJAS minimum temperature (°C) of the future period (2011 to 2060): CORDEX models (LMDZ, MPI, GFDL, CNRM, and ACCESS).

Figure 3.2.25 shows the histogram of minimum temperature for JJAS season for future projections (2011–2060). The simulated frequency of highest minimum temperature in the three future projections increases, only models (LMDZ and GFDL) project a decreasing number of highest minimum temperature events.

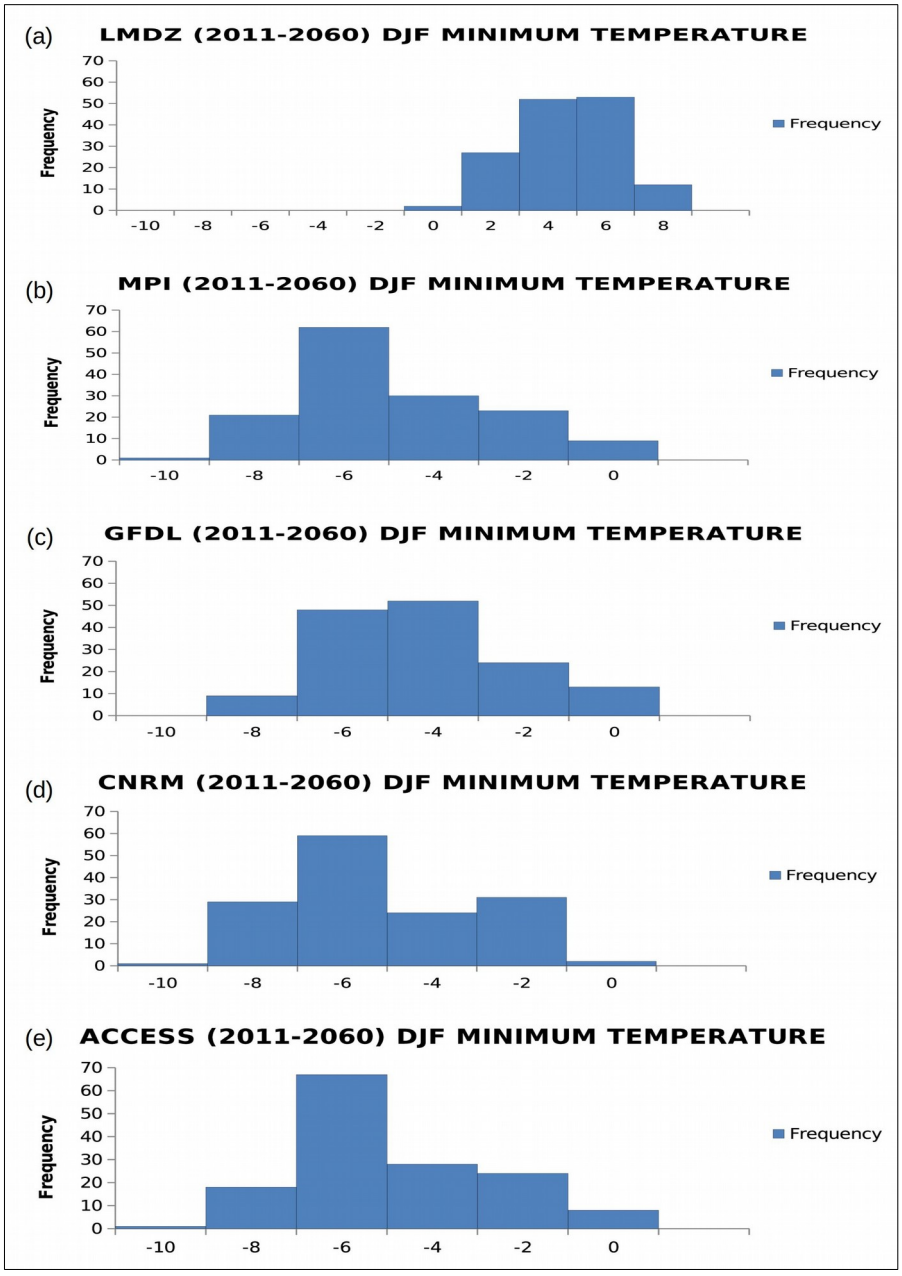

Figure 3.2.26: Histogram plots for DJF minimum temperature (°C) of future period (2011 to 2060): CORDEX models (LMDZ, MPI, GFDL, CNRM and ACCESS).

In the case of the DJF season for minimum temperature (2011 to 2060), the highest minimum temperature in the future projections increases as compared to the corresponding historical simulations.

3.3 Climate change impact on vegetation profile in the NER India

The vegetation profile of the NER is particularly important in terms of its ecology and biodiversity. In this context, understanding the relevance of factors such as rainfall, NDWI, aridity, maximum and minimum temperature over the NER to the local NDVI, which provides a good representation of the vegetation profile, is important. The sub-section examines if there is any covariation in the local climate and vegetation in the recent 17 years in the background of anthropogenic climate change. Accordingly, trends of the anomalies derived for the wet, winter, and dry three seasons in the NER are explained below. Also, the maximum NDVI values both temporally and spatially have been assessed to figure out the dependency of the NDVI on the climatic parameters for the region.

3.3.1 Area-averaged trends of anomalies based on vegetation types

In the following few paragraphs, the trends of extracted field sample points of Deciduous Broad Leaf Forest (DBF), Evergreen Broad Leaf Forest (EBF), Evergreen Needle Leaf Forest (ENF), Mixed Forest (MF), Shrubland (SL), and Grassland (GL) for the NER have been assessed. For this, the extracted field sample point's area-averaged anomalies of NDVI, rainfall, aridity, NDWI, maximum and minimum temperature for wet (June to October), winter (November to February), and dry (March to May) seasons for the period 2000 to 2017 for the NER have been evaluated and presented.

DECIDUOUS BROAD LEAF FOREST

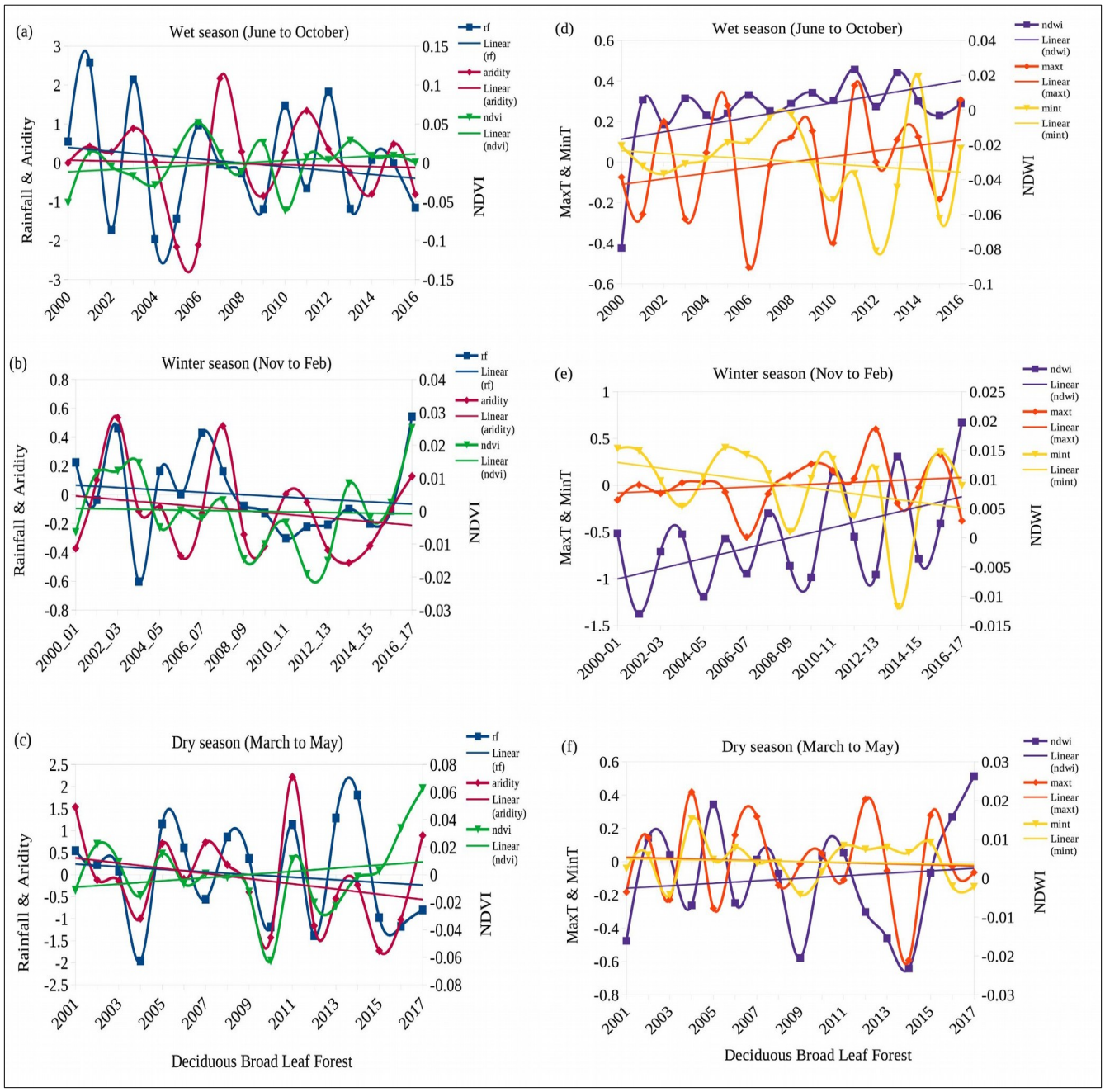

Figure 3.3.1.1: Anomalies of area-averaged trends of NDVI, rainfall & aridity for (a) wet season, (b) winter season & (c) dry season; maximum temperature, minimum temperature & NDWI for (d) wet season, (e) winter season & (f) dry season for Deciduous Broad Leaf Forest for the period 2000 to 2017 in the NER.

During the summer monsoon (wet) season (Figs. 3.3.1.1a and 3.3.1.1d), the area-averaged anomaly of DBF shows affected by the distribution of rainfall, aridity, NDWI, maximum, and minimum temperature depending on their intensity. Interestingly, depending on how the rainfall and moisture evolve over 2-3 years, we also see the signature of strong abundance as well as a deficit in rainfall and moisture reflected in the NDVI up to 2-3 years. However, a straight dependence of the NDVI on rainfall and moisture of previous years is not seen every year. This is natural because of the interannual variability as well as the impact of the previous season's rainfall and moisture because of interannual fluctuations of maximum and minimum temperature (figure 3.3.1.1d) with time lag which eventually influence the NDVI. For instance, the sharp decline of NDVI anomalies towards 2004 is likely because of the cumulative effect of a sharp decline in rainfall in 2002 (figure 3.3.1.1a) and a slight reduction in NDWI (Figure 3.3.1.1d) in 2004, thereby reducing the moisture needed for the growth. In addition to this, a decrease in rainfall and aridity (Figure 3.3.1.1c) along with the reduction in NDWI (Figure 3.3.1.1f) due to higher temperature in 2004 during the pre-monsoon (dry) season may have also reduced the available soil moisture, thereby moving the NDVI in the monsoon (wet) season towards negative anomalies in 2004. This is followed by higher NDVI in 2006 of monsoon (wet) season due to the contribution of high rainfall and aridity of 2006 during pre-monsoon (dry) season (Figure 3.3.1.1c). Then the moisture stress because of the reduction of aridity and rainfall seen in 2009 due to the extremely high maximum and minimum temperature in 2008 and 2009 (figure 3.3.1.1d) exacerbate the NDVI reduction in 2010. From 2010 onwards, the NDVI follows the pattern of rainfall and NDWI till the end of the period.

During the winter season (figure 3.3.1.1b); the NDVI, rainfall, and aridity anomalies show a sharp decline towards the end of the period compared to the other two seasons (monsoon and pre-monsoon). The sharp decline in the magnitude of the NDVI during this winter season indicates the cumulative

effects of decreasing summer monsoon rainfall (wet) as well as the winter monsoon rainfall. To corroborate this, we can see that the summer monsoon rainfall is decreasing towards the end of the period in figure 3.3.1.1a. Also, the sharp decline in the summer monsoon rainfall in 2009, 2011, and 2013 are seen affecting the decrease of NDVI of the same year of winter monsoon season while the increasing peak summer monsoon rainfall in 2003, 2006, and 2010 are seen contributing to the increasing NDVI of the same year of the winter monsoon season. In previous years rainfall and aridity dependency on the NDVI can be seen in some of the years too during this season. The fluctuations of NDWI (figure 3.3.1.1e) throughout the year are found to have reflected on the decreasing and increasing anomalies of NDVI of the corresponding years. To a great extent maximum, and minimum temperature fluctuations during this season have affected the NDWI variations which are reflected in the NDVI variations.

The pre-monsoon (dry) season in figure 3.3.1.1c indicates that the rainfall and aridity of the same year affect more to the NDVI than the previous year's rainfall and aridity. The maximum and minimum temperature fluctuations are seen clearly during this season in figure 3.3.1.1f affecting the moisture availability shown by the interannual variations of NDWI (Figure 3.3.1.1c) thereby ultimately affecting the NDVI. Apart from the winter monsoon season, the pre-monsoon (dry) and summer monsoon (wet) season depicts that the variation in NDVI is more related to the changing temperature which leads to moisture alteration thereby changing the NDVI.

EVERGREEN BROAD LEAF FOREST

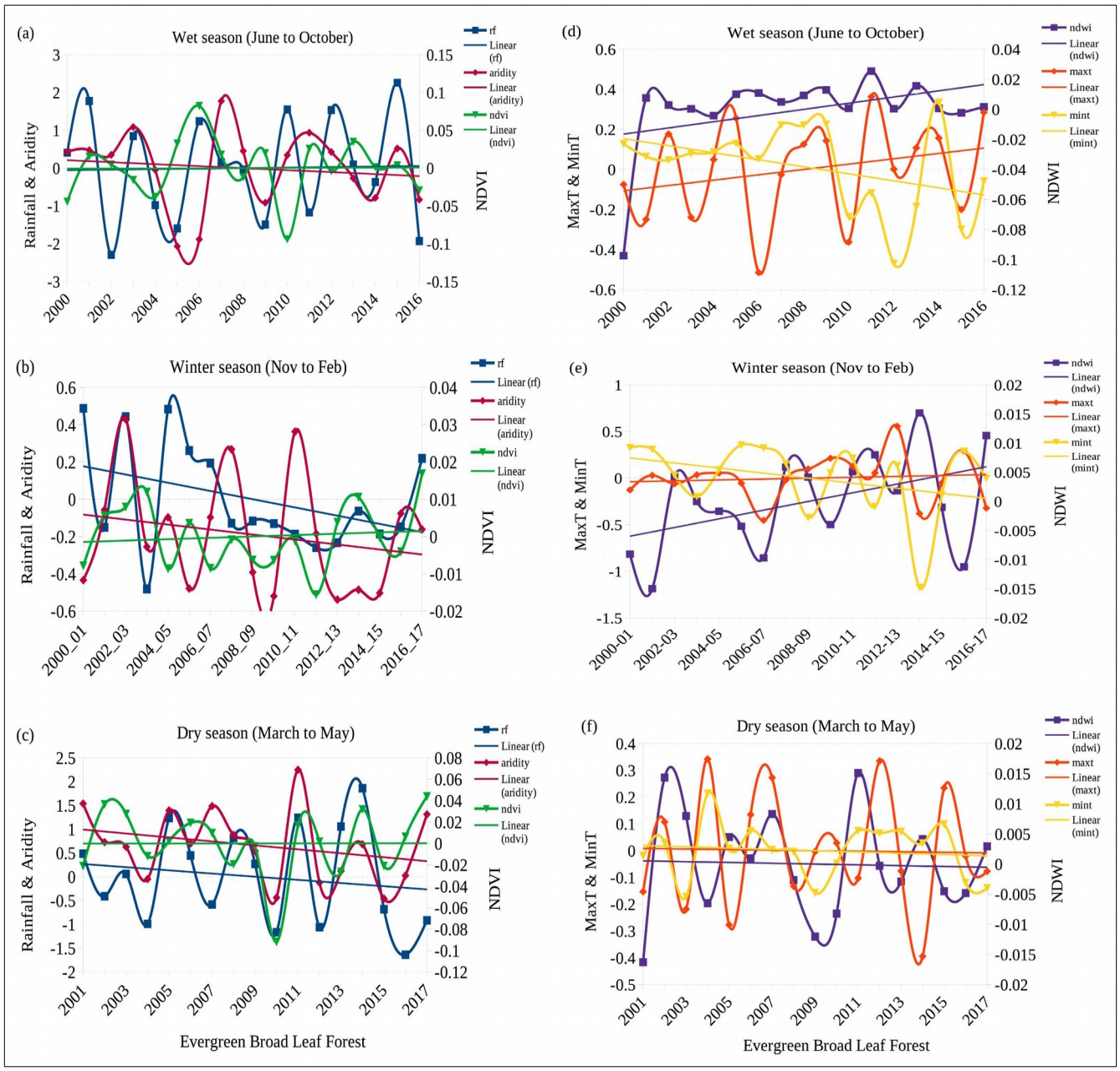

Figure 3.3.1.2: Anomalies of area-averaged trends of NDVI, rainfall & aridity for (a) wet season, (b) winter season & (c) dry season; maximum temperature, minimum temperature & NDWI for (d) wet season, (e) winter season & (f) dry season for Evergreen Broad Leaf Forest for the period 2000 to 2017 in the NER.

The dependence of the evolution of EBF on the climatic parameters in various seasons seen in figure 3.3.1.2 is like that of DBF shown in previous figure 3.3.1.1 for all the seasons. The summer monsoon (wet) season shows the time-lagged dependency of NDVI on rainfall and aridity (figure 3.3.1.2a) while NDWI shows the dependency of NDVI within the same years due to the changes in temperature in figure 3.3.1.2d. The previous years' maximum and minimum temperature are seen affecting the rainfall of the next year impacting the NDVI in this season. The winter monsoon season (figure 3.3.1.2b) of this vegetation type shows a similar drastic variation in the NDVI. Some of the years depict that the rainfall in previous years affects the NDVI of the following years. In the case of aridity, a similar year-to-year dependency is found but also depicts a two to three years lagged association with the NDVI. The NDWI (figure 3.3.1.2e) during this winter season indicates the same evolution seen in the summer monsoon season probably due to the fluctuations seen in temperature. Even in the pre-monsoon (dry) season, the EBF shows variations up to great extent. The aridity and rainfall in figure 3.3.1.2c and NDWI in figure 3.3.1.2f during this season show that the NDVI is affected by these parameters within the same years. The maximum and minimum temperature during this pre-monsoon (dry) season also shows a great impact on the NDWI (figure 3.3.1.2f) and aridity (figure 3.3.1.2c). Rather than the rainfall from the previous winter monsoon season, the moisture seems to play an important role during this pre-monsoon (dry) season which can be found from the aridity and NDWI variations due to the fluctuations in temperature.

EVERGREEN NEEDLE LEAF FOREST

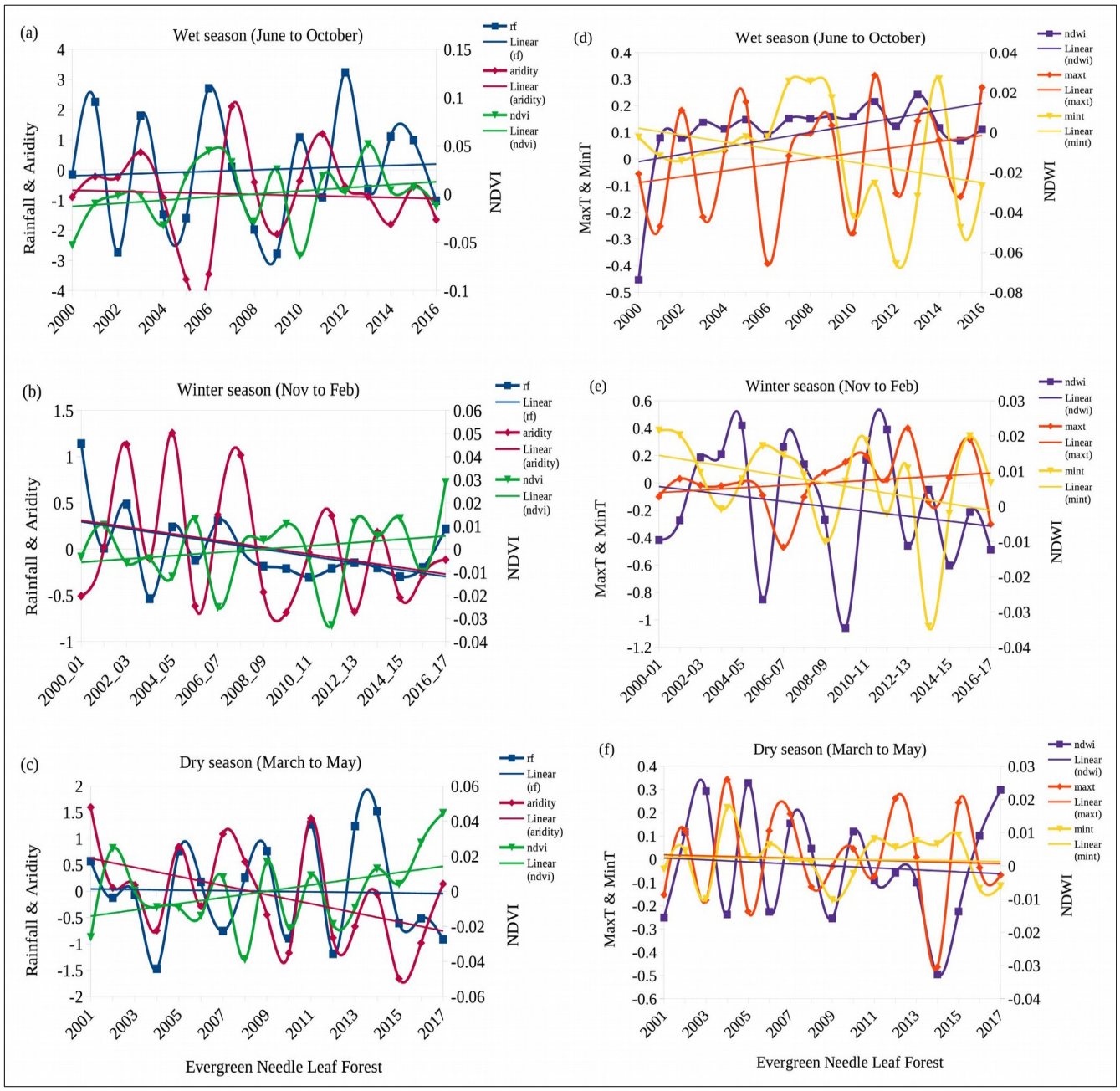

Figure 3.3.1.3: Anomalies of area-averaged trends of NDVI, rainfall & aridity for (a) wet season, (b) winter season & (c) dry season; maximum temperature, minimum temperature & NDWI for (d) wet season, (e) winter season & (f) dry season for Evergreen Needle Leaf Forest for the period 2000 to 2017 in the NER.

The ENF that does not get affected much by the changing climatic variations is found to be drastically affected in all three seasons (Figure 3.3.1.3) over the region. During summer monsoon (wet), winter monsoon, and pre-monsoon (dry) seasons, the moisture fluctuations were seen in aridity and NDWI due to extreme variations in maximum and minimum temperature are seen. This eventually affects the NDVI due to the variations in moisture needed for the growth of the vegetation. The impact of temperature variations on the rainfall is also found to a great extent thereby impacting the NDVI. Previous seasons as well as the interannual dependency of NDVI on these climatic parameters are reflected for this vegetation too in all the seasons.

MIXED FOREST

The MF during all the seasons in figure 3.3.1.4 shows that the NDVI exhibits variations though the forest is of mixed forests. During summer monsoon (wet) and pre-monsoon (dry) seasons, maximum and minimum temperature greatly affects the moisture seen in aridity and NDWI thereby affecting the NDVI. The similar dependency of the evolution found in the previous vegetations on the climatic parameters is also seen here. Seasonal, as well as interannual dependency, are also found in this vegetation. As for the winter monsoon season (figure 3.3.1.4b), the NDVI exhibits a decreasing trend towards the end of the period. Rainfall seems to affect more on the NDVI during this winter monsoon season throughout the period except for few years where the moisture from aridity and NDWI are seen impacting more on the NDVI.

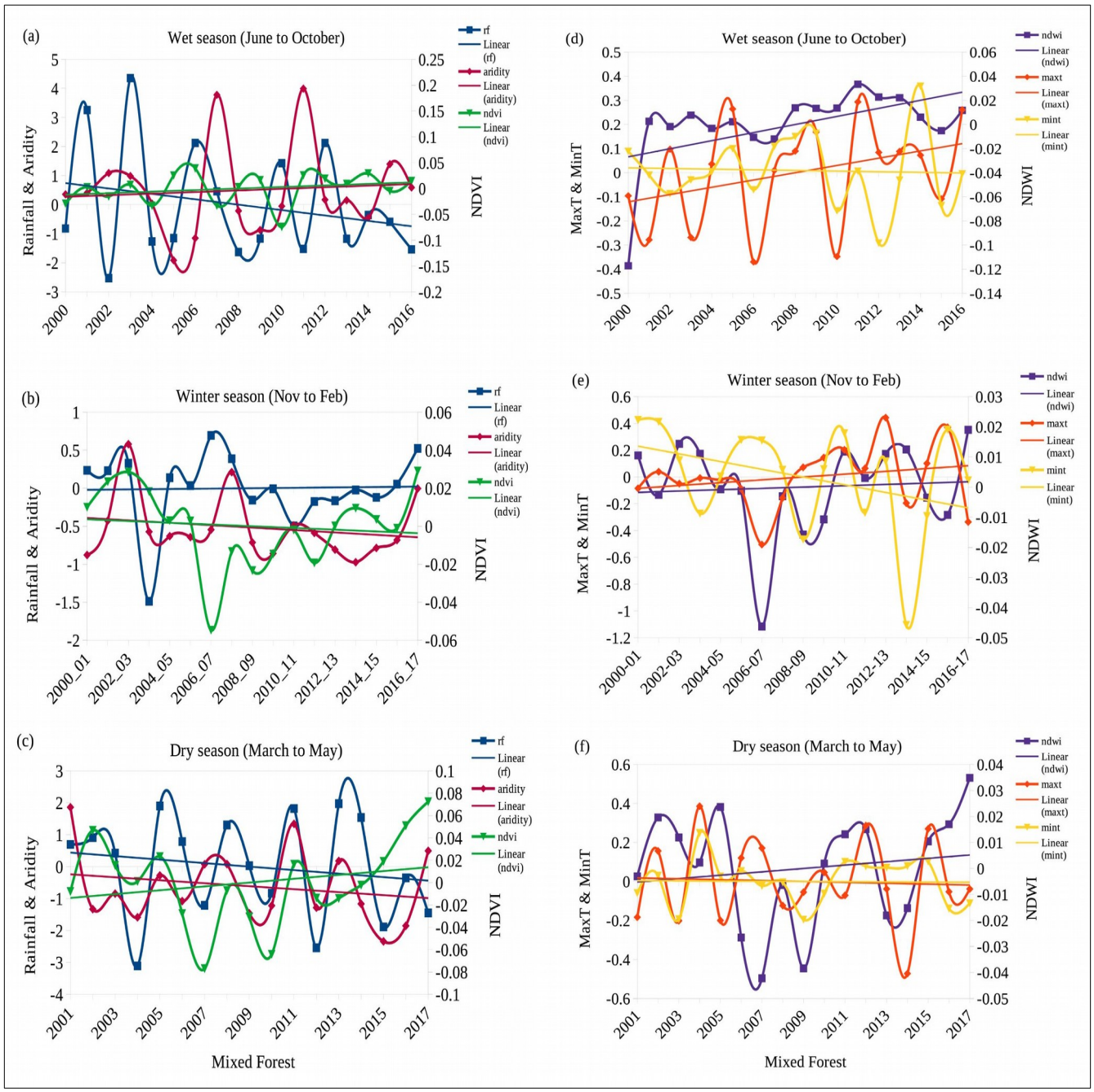

Figure 3.3.1.4: Anomalies of area-averaged trends of NDVI, rainfall & aridity for (a) wet season, (b) winter season & (c) dry season; maximum temperature, minimum temperature & NDWI for (d) wet season, (e) winter season & (f) dry season for Mixed Forest for the period 2000 to 2017 in the NER.

SHRUB LANDS

In figure 3.3.1.5 (a & c), similar patterns of NDVI dependency seen above are also observed on this vegetation type. In previous years, as well as two to three years, the lagged dependency of these parameters on the NDVI is also seen here. Effects of maximum and minimum temperature on the aridity and NDWI which ultimately affects the NDVI are seen more prominently during the summer monsoon (wet) and pre-monsoon (dry) seasons. While during the winter monsoon season (figure 3.3.1.5b), NDVI seems to be more affected due to rainfall variations. However, in addition to rainfall, in few years, aridity (figure 3.3.1.5b) and NDWI (figure 3.3.1.5e) show time-lagged dependency on the NDVI during the winter monsoon season.

GRASSLAND

During the summer monsoon (wet) season in figure 3.3.1.6 (a & d), the maximum and minimum temperature in previous years is seen affecting the NDWI, aridity, and rainfall in the next year. This eventually reflects on the NDVI of this season with time lag dependency. The NDVI during the winter monsoon season (figure 3.3.1.6b & e) seems to be affected by rainfall of previous years at the beginning of the period while the rest shows more dependency on the aridity and NDWI which could be due to the fluctuations of the temperature seen in figure 3.3.1.6e. The effect of summer monsoon rainfall is also seen on the NDVI of the winter monsoon season in some of the years. During the pre-monsoon (dry) season (figure 3.3.1.6c & f), impacts of the previous season and interannual variations of the climatic parameters are seen on the NDVI of this season. The maximum and minimum temperature during this season fluctuates more clearly which leads to the variations in the moisture seen in aridity and NDWI, also to rainfall affecting the NDVI.

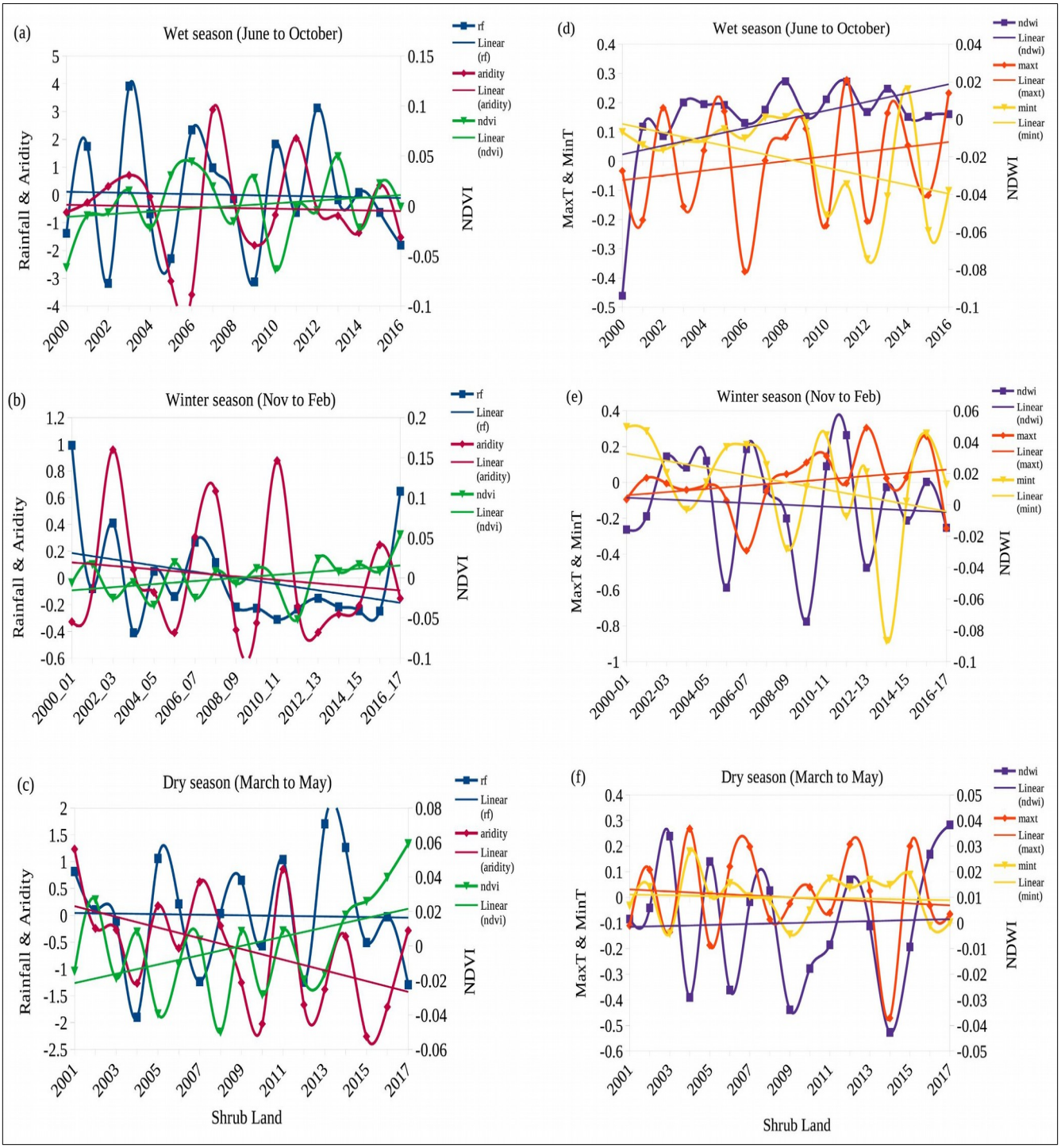

Figure 3.3.1.5: Anomalies of area-averaged trends of NDVI, rainfall & aridity for (a) wet season, (b) winter season & (c) dry season; maximum temperature, minimum temperature & NDWI for (d) wet season, (e) winter season & (f) dry season for Shrub Land for the period 2000 to 2017 in the NER.

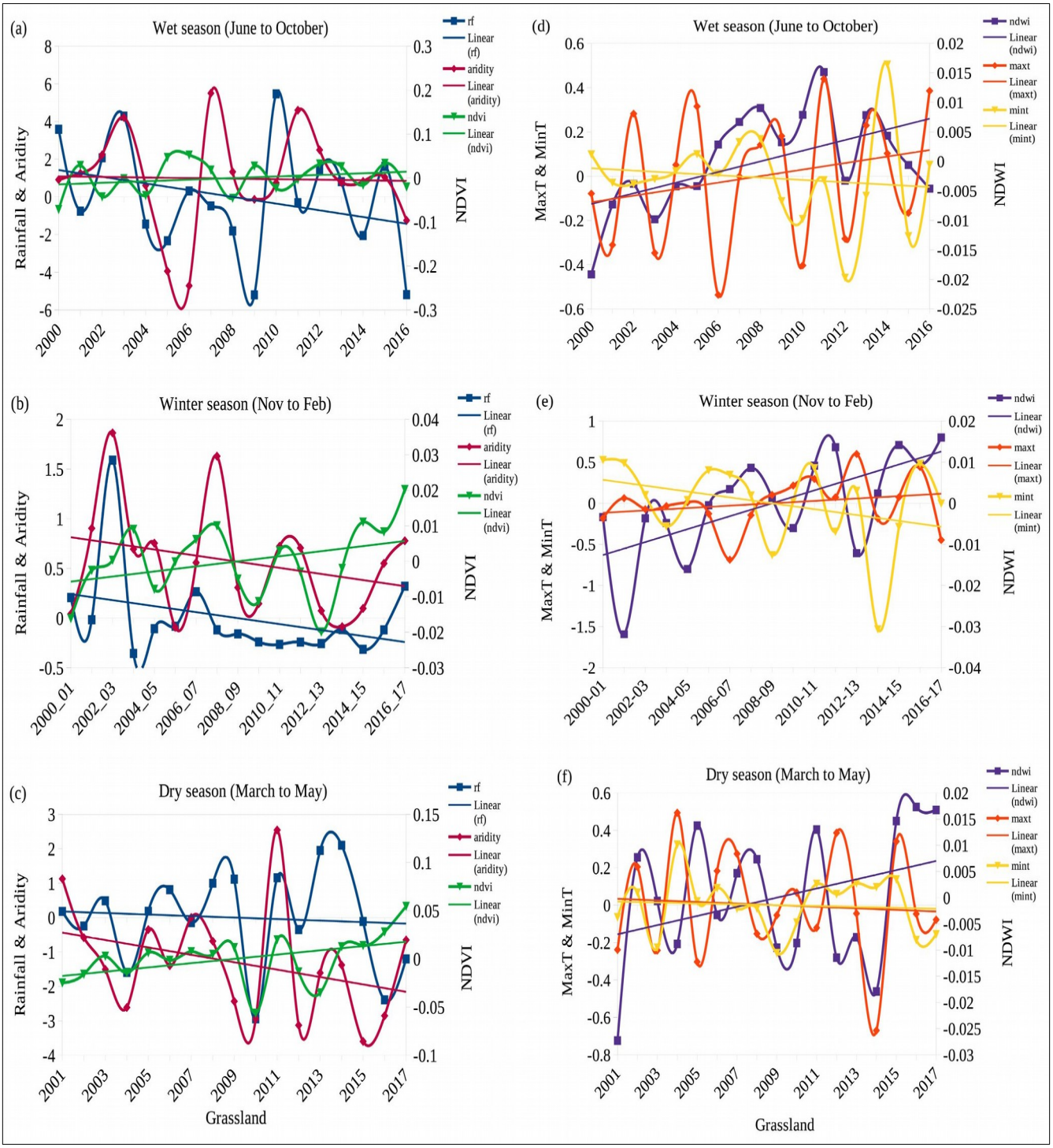

Figure 3.3.1.6: Anomalies of area-averaged trends of NDVI, rainfall & aridity for (a) wet season, (b) winter season & (c) dry season; maximum temperature, minimum temperature & NDWI for (d) wet season, (e) winter season & (f) dry season for Grassland for the period 2000 to 2017 in the NER.

From the above analysis, we can see that the six vegetation types studied exhibit interannual and inter-seasonal anomalies fluctuations, though the magnitudes saw are different in all three seasons. The winter season shows the greatest magnitude of the decreasing values of NDVI and other parameters than those of summer monsoon (wet) and pre-monsoon (dry) seasons. The weakening of NDVI in the winter season indicates the importance of summer monsoon rainfall as the decrease in summer monsoon rainfall leads to a decrease in the density of the vegetation cover in the NER. This is probably due to lower rainfall received during the summer monsoon season which supplies moisture water to winter season NDVI (Revadekar et al., 2012). Dry season shows the lowest magnitude comparatively than the other two seasons. Maximum and minimum temperature fluctuations are seen affecting the moisture availability seen in aridity and NDWI which ultimately affects NDVI during the summer monsoon and pre-monsoon seasons while rainfall affects more during the winter monsoon season. Both rainfall and temperature together seem to play roles in the NDVI variation over the NER. The positive and negative anomalies of NDVI correspond well with the negative and positive anomalies of rainfall which is also seen in another region studied by Wang et al., 2001 and Revadekar et al., 2012. The fluctuations of NDVI seen in all the three seasons of course reflect the seasonal variation of the growing season (Yu, Zhuang, & Hou, 2005). One important aspect of this study is that the Evergreen Needle Leaf forest which does not get affected much by rainfall also shows interannual and inter-seasonal fluctuations. Different vegetation types respond differently depending upon the nature of the rainfall, moisture, and temperature. A sustained negative and positive trend in the anomalies of NDVI in the NER along with the decrease and increase in the rainfall anomalies along with other necessary parameters have not been discussed so far. This study is the first of its kind to deliver the message of this prevailing situation in NER.

Any changes in summer monsoon rainfall led to water stress, changes in phenology, and decreased biomass, with a subsequent reduction in the NDVI (Zeppel, Wilks, & Lewis, 2014) not only concurrently, but also in the next season through 2-3 years. The fluctuations seen in the NDVI anomaly in all types of vegetation types indicate increasing stress in the vegetation which is a matter of serious concern. The negative trends in the NDVI agree with the analysis done by Chakraborty, Seshasai, Reddy, & Dadhwal (2018) which shows a significant negative trend in the wet and semi-evergreen forest, deciduous, subtropical broad-leaved forest in Arunachal Pradesh, Meghalaya, Sikkim, Manipur, Nagaland, and Mizoram. In addition to this, the forests in the lower ranges of Eastern Himalayas are vulnerable due to shifting cultivation and forest fires (Chakraborty, Seshasai, Sudhakar Reddy, & Dadhwal, 2018), which can be said to have added to the severity of the negative impact on vegetation over the region. The evergreen forest and deciduous forest are said to be facing a higher rate of transformation over the NER due to shifting cultivation, land use, and land cover, and deforestation (Chakraborty, 2009). These two forests are also seen as drastically affected in the study due to the variation in the rainfall and temperature patterns. In a study by Lele, Joshi, & Agarwal (2005), the vegetation cover of a coniferous broadleaf, sub-tropical evergreen forest, semi-evergreen forest, and moist mixed deciduous forest were found degraded. Jeyaseelan, Roy, & Young (2007) also showed that the decline in NDVI is related to lower rainfall received over India. In the study done by Parida et al., (2008), different vegetation types showed different responses to the temperature which is also found in my study. All these indicate that rainfall and temperature as the limiting factor for the growth of the vegetation types over broad regions covering India and China. Besides these parameters analyzed, moisture stress during droughts period occurred during 2005-06, 2009, 2010-11, 2013 (Assam, Manipur, Mizoram, Tripura, and Arunachal Pradesh) appear to be an additional factor responsible for the increase of negative anomalies of NDVI which are observed. Negative anomalies in NDVI during drought years are more prominently seen. This is because during the drought periods, the soil water

supply dries out, and foliage begins to shed, affecting the ability to mobilize (Feldpausch et al., 2016), and hence NDVI is reduced.

3.3.2 Trends of long-term rainfall anomalies for all the seasons

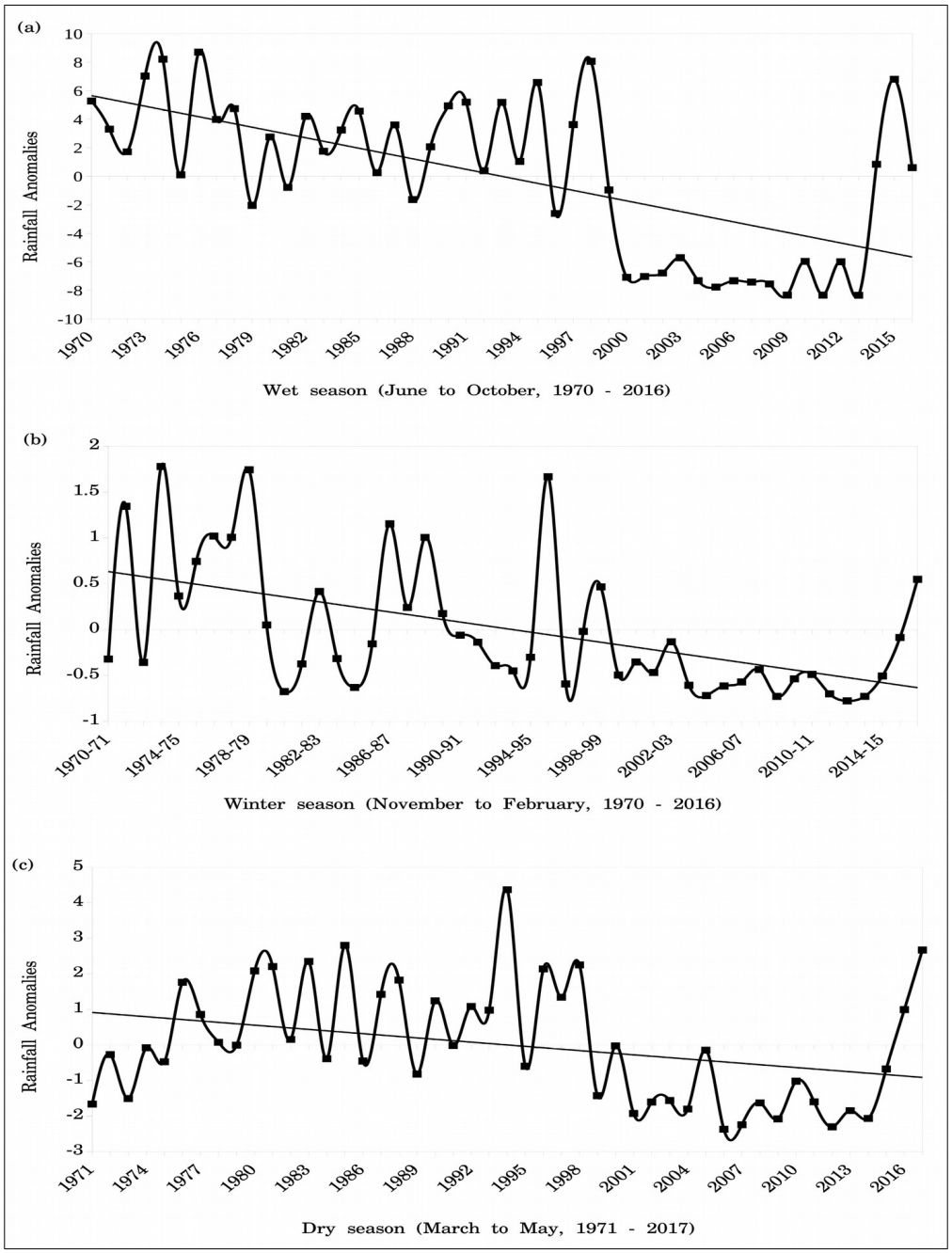

Figure 3.3.2: Trends of area-averaged anomalies of rainfall for (a) wet, (b) winter and (c) dry seasons for the period 1971 to 2017 ver Northeast India.

In figure 3.3.2, long-term rainfall anomalies for all three seasons have been analyzed for the period 1970 to 2017 over NER. Regardless of the seasons, the rainfall trend has been decreasing significantly at a 95% confidence level from 1970 till 2017. It indicates the recent decreasing tendency in the rainfall over NER, which could be a major factor for the decline in the NDVI values. Reduction in rainfall since the year 2000 is also seen in the Amazon forest region, which resulted in the significant diminishing of vegetation greenness including tropical evergreen forest and subtropical grasslands across large parts of the region (Hilkera et al., 2014). The weakening tendency in the rainfall in the NER has a potentially serious and unfavorable implication for the local vegetation. This will be subject to long-term cumulative water stress and leading to disastrous on the vegetation of the region.

3.3.3 Evaluation of NDVI and rainfall for the entire region of Northeast India

The entire region for Northeast India has also been evaluated using the NDVI and rainfall data from 2000 to 2017. Unlike the previous assessment, which was based on field sample points, this section evaluates the entire grid points of the region. The area-averaged anomalies for entire grid points, maximum NDVI values both temporal and spatial have been assessed. This would give some hints whether only the selected locations or the entire region have changed or not.

In figure 3.3.3.1, the entire region of NER from 2000 to 2017 period shows that the trends of the NDVI and rainfall anomalies increases in all three seasons indicating higher greenery. The discrepancy from the earlier field sample point analysis can be explained by the fact that the current analysis of averaging over the whole region leads to consideration of plantations outside recorded forest areas, regeneration of the forest, conservation measures, expansion of croplands, intensive irrigation, urban greening, agricultural practices, etc (e.g. Liu et al 2015 and Chen at al., 2019). Thus, human interventions seem to

alleviate the vegetation stress over a broad region. This is important information for policymakers as well. The relative contributions of each of these factors need to be ascertained through some dynamical modeling experiments.

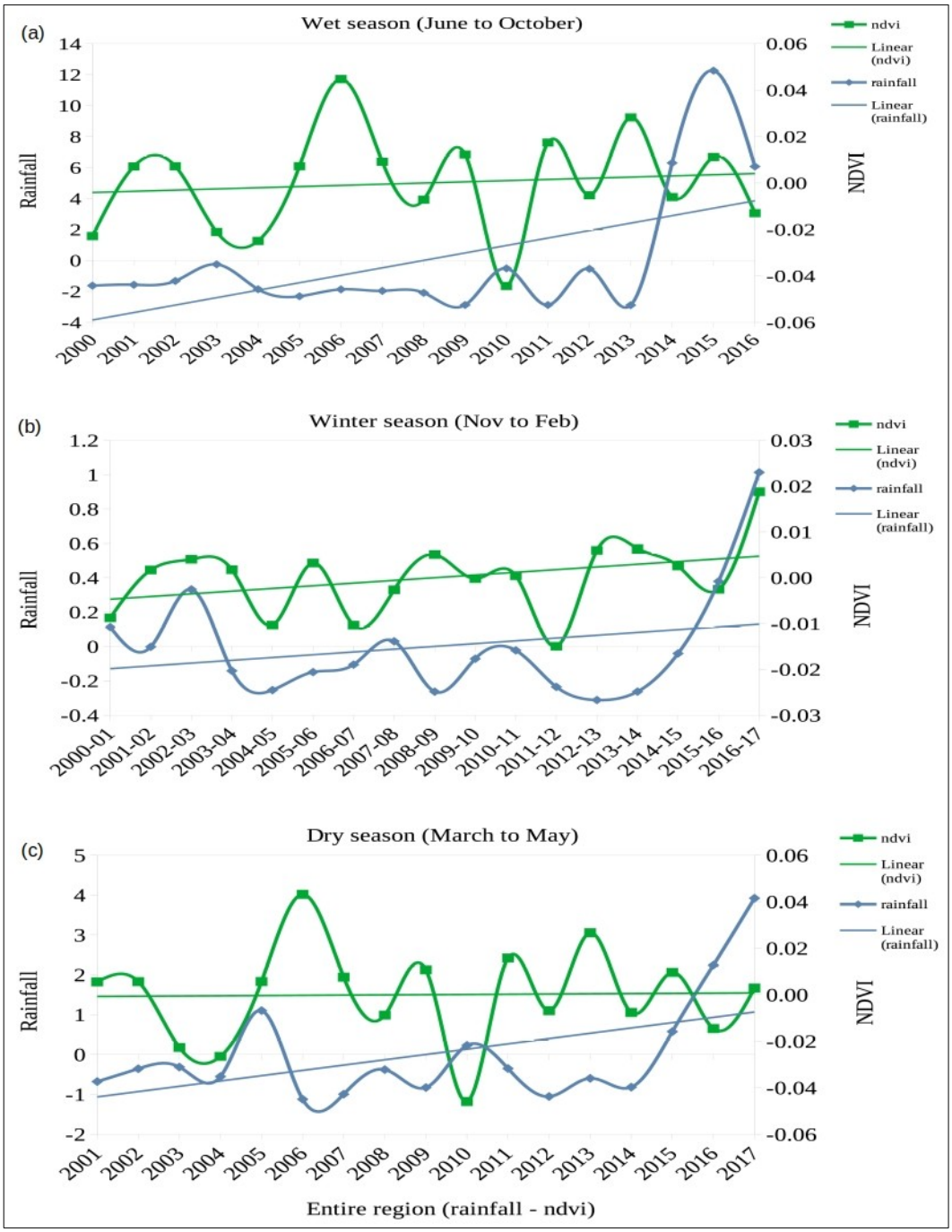

Figure 3.3.3.1:Anomalies of area-averaged NDVI and rainfall for entire Northeast region for wet season (June to October), winter season (November to February) and dry season (March to May) from 2000 to 2017.

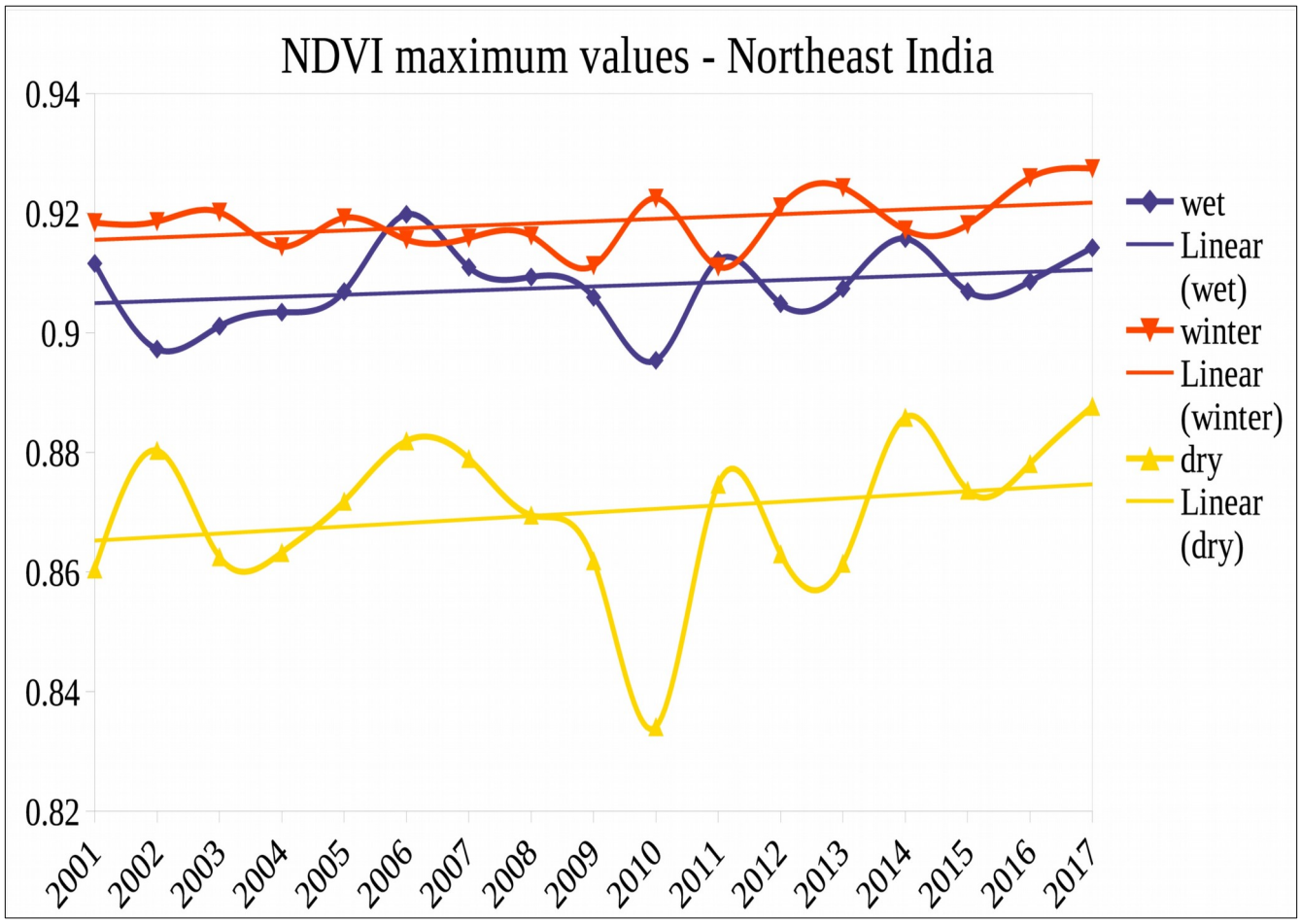

Figure 3.3.3.2: Maximum NDVI values collected from MODIS-Terra for wet season (June to October), winter season (November to February) and dry season (March to May) from 2001 to 2017 over Northeast India.

In figure 3.3.3.2, the time series of maximum NDVI values for summer monsoon (wet), winter monsoon, and pre-monsoon (dry) seasons from 2001 to 2017 have been analyzed. The winter season shows the highest maximum NDVI values followed by the wet season and dry season. This figure supports the previous analysis based on the area-averaged anomalies where winter monsoon season depicts the greatest magnitude comparatively to the other two seasons. The winter monsoon season

shows the highest NDVI value due to the cumulative contribution of summer monsoon rainfall and winter monsoon rainfall. The greenness reaches its maximum during the winter monsoon season because of adequate sunlight, the sky remains clear as the cloud disappears once the summer monsoon receded, which is needed for photosynthesis supported by water and nutrient charged soils (Nischitha et al., 2014). These are followed by wet season and dry season with the latter showing the least NDVI value. The maximum NDVI values for Deciduous Broad Leaf, Evergreen Broad Leaf, and Evergreen Needle Leaf forests are also analyzed (figure not shown) where the maximum values of NDVI for these three vegetation types show decreasing trends from 2001 towards 2018.

More clarity is also seen in the spatial distribution of NDVI (figure 3.3.3.3) of the entire region where the winter season shows the greenest (highest NDVI value) of all while during the summer monsoon (wet) and pre-monsoon (dry) season. The NDVI is a bit scattered and declines with dry season being the least NDVI value. The moisture deficit due to increased evapotranspiration during the dry season is associated with vegetation growth (Liu et al., 2015). The maximum values of NDVI in this figure also indicate that the winter season depicts a distinct interannual change as compared to the other two seasons. The year 2018 (figure not shown) also shows the variation of NDVI in the entire region indicating changes in the latest current period. However, in all three seasons, the changes seen are not static, as year-to-year variation in the same region shows fluctuations in NDVI throughout the period. This fluctuation of NDVI indicates that the increase and decrease of rainfall plays an important role in controlling the vegetation growth over the region.

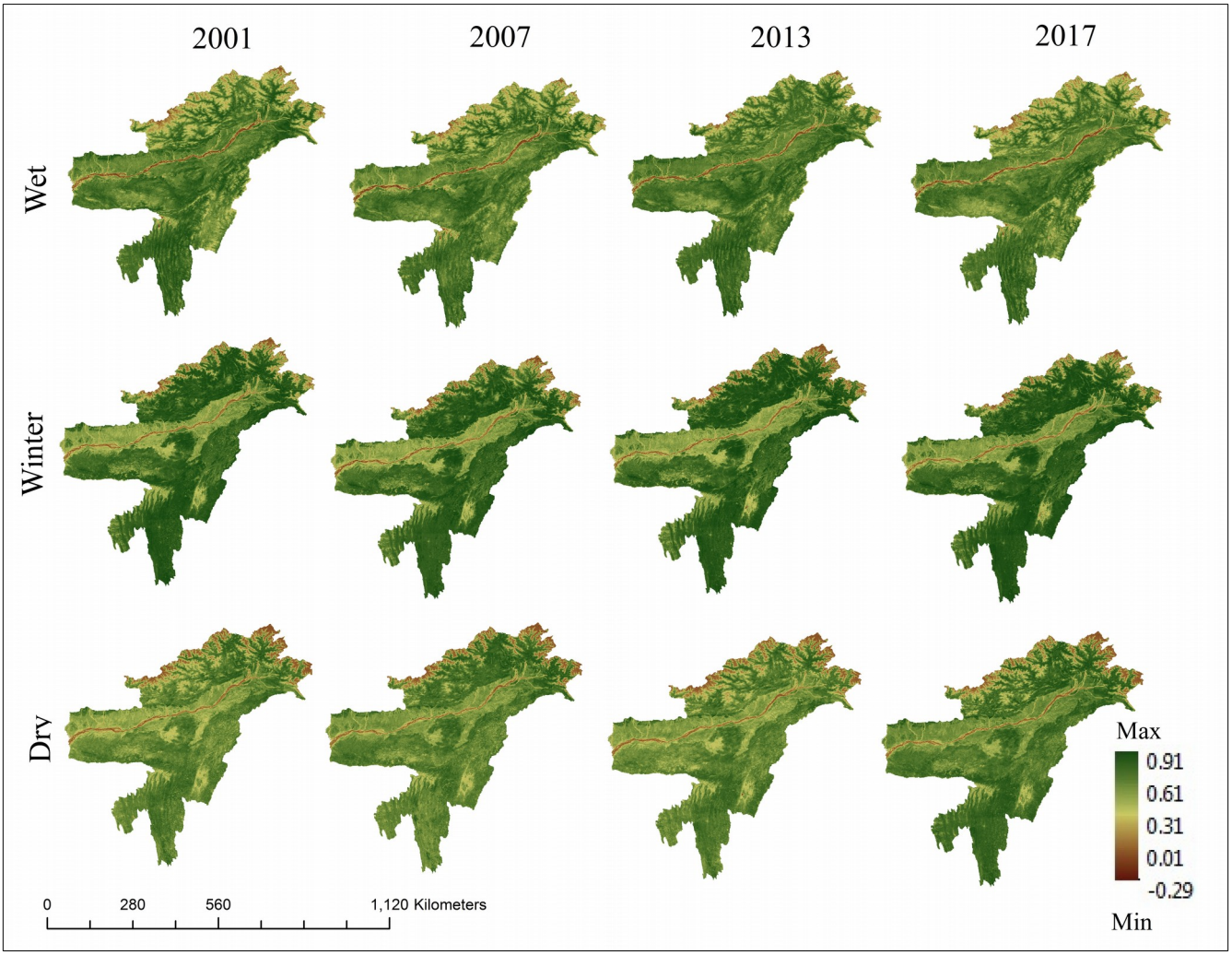

Figure 3.3.3.3: Spatial distribution of maximum NDVI values for wet, winter and dry seasons from 2001 to 2017 for Northeast India.

Nevertheless, my analysis-be selected field sample points or entire region-shows that the association of these climatic parameters such as rainfall, moisture availability from the aridity and NDWI, maximum and minimum temperature affects the distribution of NDVI. Summer monsoon and pre-monsoon season indicate that the temperature directly affects the moisture and rainfall leading to the variation in all the vegetation types studied. While the winter monsoon season shows dependency more on rainfall. Both rainfall and temperature's combine effect are seen in all the vegetation. All the vegetation types

are found sensitive more or less equally to all the changing climatic parameters given its time-lag effect, interannual and seasonal effect. However, rainfall indicates control on the vegetation as the moisture retains from it and the surrounding atmosphere due to temperature fluctuations eventually affects the vegetation over the region.

3.3.4 Means and standard deviations for NDVI and rainfall over the NER

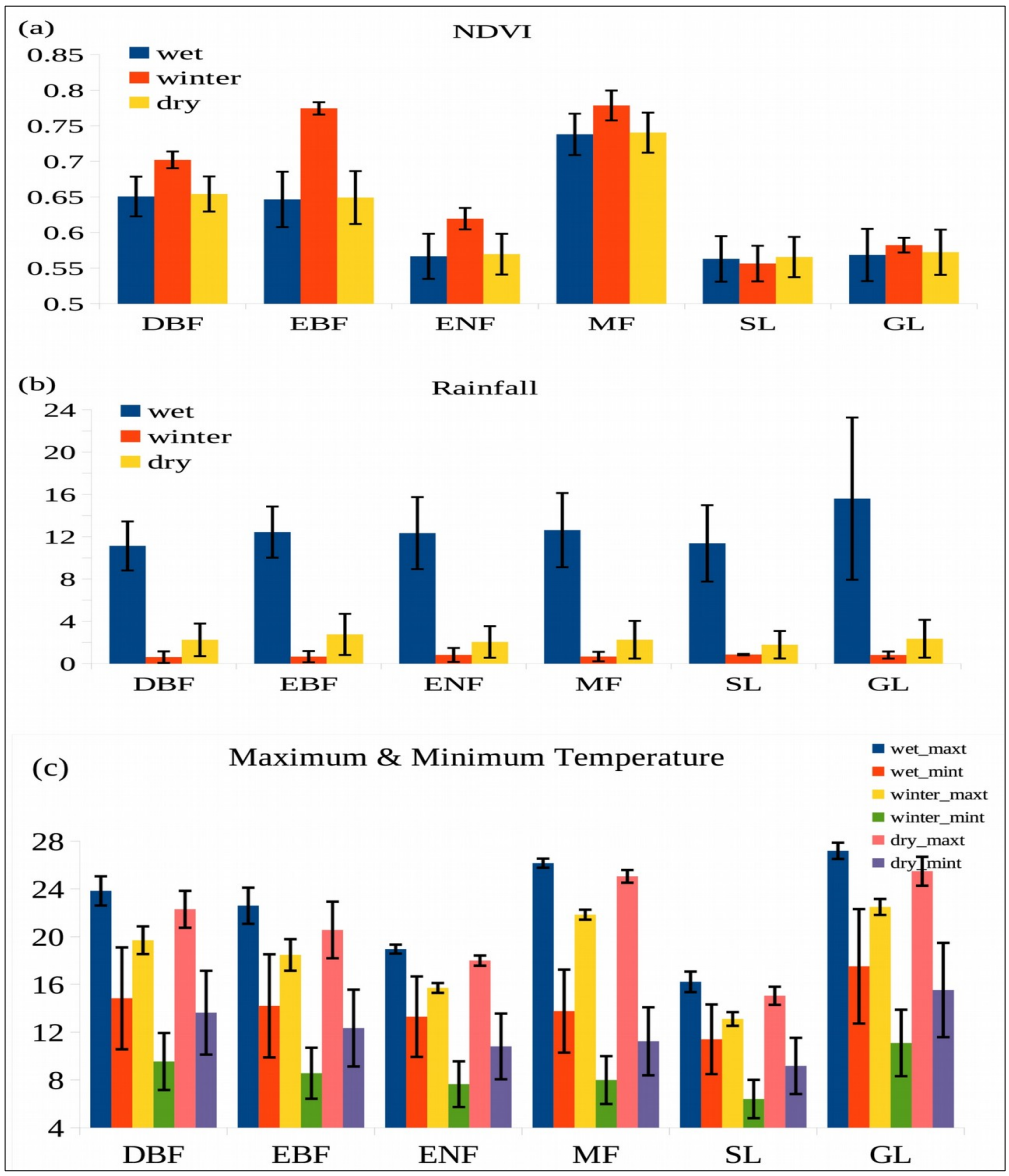

Figure 3.3.4: Means and standard deviations of NDVI and rainfall for wet, winter and dry seasons for the period of 2000 to 2017 over Northeast India.

In figure 3.3.4, the means and standard deviations of NDVI, rainfall, the maximum and minimum temperature for the period 2000 to 2017 have been computed. Statistically, at a 95% confidence level, the winter season mean NDVI is significantly different from the summer monsoon (wet) season mean NDVI for DBF, EBF, and ENF while the rest of the vegetation types are found insignificant. The winter season mean NDVI is also significantly different from the pre-monsoon (dry) season mean NDVI for DBF and EBF only. Summer monsoon (wet) and pre-monsoon (dry) season mean NDVI are statistically insignificant.

The summer monsoon (wet) season mean rainfall is significantly different from the mean rainfall of the winter monsoon and pre-monsoon (dry) season for all the vegetation types while the winter monsoon means rainfall and pre-monsoon (dry) season mean rainfall is statistically insignificant at 95% confidence level.

The mean maximum temperature of summer monsoon (wet) season is significantly different from the mean maximum temperature of winter monsoon season for all the vegetation types at a 95% confidence level. It also shows significantly different from pre-monsoon (dry) season mean maximum temperature for ENF, MF, and GL. The mean maximum temperature of the winter monsoon season is significantly different from the mean maximum temperature of the pre-monsoon (dry) season for MF and SL. As for the mean minimum temperature of summer monsoon (wet) season, it is significantly different from the mean minimum temperature of winter monsoon season for all the other vegetation types except for DBF. The rest of the seasons (minimum temperature) show insignificant at 95% confidence level.

In figure 3.3.4, though the rainfall is high during the summer monsoon season, NDVI shows lower during this season because of the higher temperature seen during the same season that leads to low moisture needed for the growth of the vegetation. The NDVI is high during the winter monsoon season though the rainfall is low as the temperature during this season is lower, also the summer monsoon season rainfall, as mentioned in the above analysis, contributes to the increasing NDVI of the winter monsoon season. This analysis indicates that DBF, EBF, and ENF are affected drastically while the rest of the vegetation types have also shown variation due to changes in rainfall and temperature. This result also matches with the above analysis carried out for field sample area-averaged points. Lastly, the correlation, lag correlation, and regression analyses calculated between NDVI and the rest of the parameters are statistically weak and insignificant for all the vegetation studied.

CHAPTER – 4

SUMMARY AND CONCLUSIONS

This chapter provides a summary, conclusions of the important findings and addresses the important recommendations of the future work.

4.1 Summary

As per the special report of the policymakers, IPCC 2018 reported that the impacts of warming due to anthropogenic emissions from the pre-industrial period (from 1870s) to the present period, which exacerbated in the last 4-5 decades are stated to persist for centuries to millennia thereby causing a long-term change in the climate system. Due to rising climate change, a developing country like India where agriculture is still rainfed is the main source of income and could be severely affected (Kumar et al., 2006). The Indian summer monsoon rainfall (ISMR) plays a vital role in the Indian sub-continent, home to more than 1 billion people, as the region receives 70% to 80% of its annual rainfall with mean area-averaged ISMR about 890 mm over the last 100 years. In India, the characteristics of the summer monsoon rainfall and its variability differ from region to region within the nation. The spatial pattern of its dominant mode of variability shows a dipolar structure (Parthsarathy et al., 1996); the signal in Northeast India (NER) is found in an out-of-phase relation with the rest of India (Fig. 6.5, Pant and Kumar, 1997). The NER (≈ 89.50 E to 98.50 E and 21.50 N to 29.50 N) is one of India's highest raining

regions, with an area-averaged seasonal rainfall of 152 cm (Parthasarathy et al., 1995). Moreover, the NER is endemic to many flora and fauna, making it one of the world's richest in terms of biological values (Chakraborty et al., 2012).

Nevertheless, uncertainties across various observational datasets and in high-resolution projections arise due to limited field samples of future climate projections for NER. The NER, being a complex orographic region in Himalayan mountain ranges, experiences changes in rainfall over short distances, and therefore complicated to model (Prakash et al., 2014). Due to being a neglected region in terms of climate observations and model studies, there is a need to address these issues properly. The high-resolution CORDEX South-Asia (LMDZ, MPI, ACCESS, GFDL & CNRM) models of 0.5° x 0.5° horizontal resolution, which are downscaled versions of the CMIP5 projections allow us to study the future climate change in the NER at higher resolution, taking into account uncertainty associated with inter-model variability and those in observations. Along with these, several observation-based and reanalyzed datasets are also used in the study. It will also be useful to ascertain at least qualitatively, using available model simulations, whether the climate in the NER has changed in tandem with that elsewhere in India in the last millennium when many regions in the world experience as warm as in the first half of the twentieth century (IPCC, 2013).

Further, any change in local climate is a potentially critical factor in assessing the responses of the ecosystem to climate change at the regional scale. The regional and local patterns of climate control the growth of the vegetation, due to the seasonal and annual dynamics of the climatic variables of the respective region (Revadekar et al., 2012). The inconsistency in the precipitation and temperature influences the water balance, causing changes in the soil moisture, which affects the growth and distribution of plants (Revadekar et al., 2012 & Nischitha et al., 2014). The NER, one of the global

biodiversity hotspots, is under the threats of deforestation (Saikia, 2009) and traditional shifting cultivation (Roy & Joshi, 2002), the population explosion, encroachments, illicit felling, lopping for fuelwood and fodder, removal of forest cover for litter, forest fires, land use and land cover change from agriculture, etc. (Lele & Joshi, 2009; Ravindranath et al., 2011 & Roy et al., 2015b). Therefore, an analysis of Normalized Difference Vegetation Index (NDVI) fortnightly data of 500 m resolution derived from Moderate Resolution Imaging Spectroradiometer (MODIS) instruments onboard the Terra (EOS AM) satellite (Didan, 2015) can provide information on Spatio-temporal patterns in linkages among phenological and climate cycles of vegetation and trends in vegetative cover. There is a need to improve our understanding of the climatic variability implications for the seasonal vegetation dynamics in this region.

4.2 Conclusions

4.2.1 Conclusions in the context of current climate variability in the NER.

The climate variability studied during the current period from 1970 to 2005 reveals the following findings:

1. The area-averaged monthly means of rainfall and temperature observations during the 1970 to 2005 period have been well-captured by historical simulations of CORDEX South Asia models.

2. The area-averaged summer monsoon rainfall and winter monsoon rainfall show a weak and statistically insignificant decreasing trend as seen from both the observations and model data sets.

3. Importantly, there is uncertainty across various observational and model datasets as differences are noted in the locations of highest and lowest climatological rainfall & temperatures across the observation and models in climatological spatial distribution, pointing at uncertainties.

4. The ENSO events do not have any significant impact on the climate of the NER, during both summer monsoon and winter monsoon season.

5. As for extreme events over the NER, the heaviest seasonal rainfall of 15 mm/day captured by the models is underestimated compared to the observed value of 23 mm/day.

4.2.2 Conclusions in the context of last millennium climate variability in the NER

The climate variability studied during the Last Millennium (Medieval Climate Anomaly period: 935 CE to 1034 CE & Little Ice Age: 1735 CE to 1834 CE) reveals the following findings:

1. Unlike the rest of India, the NEISMR differences over NEI from the MCA to LIA are as low as 2% and also small compared to present-day conditions. The model simulations show that the NER summer monsoon rainfall is insensitive towards changes in the forcing during the last millennium, and on centennial timescale, decoupled from the response of the rest of India.

2. All the simulations indicate a strengthening of the tropical easterly jet (TEJ) at 100 hPa during the MCA relative to the LIA. This results in anomalous convergence over the North BoB, and an enhancement of monsoonal rainfall along with the CMR.

3. The analysis also shows that ENSO, in all periods, hardly has an impact on the NEISMR. Also, the mechanisms that potentially play a role in the warm and wet MCA, and cold and dry LIA over the

major Indian regions -the multi-centennial tropical Indo-pacific Walker circulation that affects the ENSO impacts on India (T19), and changes associated with the TEJ- do not seem to influence the NEISMR, at least in our PMIP3 results. That is why it's almost constant magnitude from MCA through the LIA.

4.2.3 Conclusions in the context of future climate projections in the NER

The climate variability studied during the future period 2011 to 2060 from the CORDEX South Asia models reveals the following findings:

1. The RCP4.5 projections for the 2011 to 2060 period future indicate a possible insignificant decline in summer monsoon and winter monsoon rainfall in the NER.

2. The future projections simulate a significant increasing trend in the maximum & minimum temperatures for the same period.

3. Considerable inter-model uncertainty is seen in future projections of summer monsoon rainfall over the NER.

4.2.4 Conclusions in the context of climate change impact on vegetation profile for the current period in the NER

The responses of vegetation patterns (Deciduous Broad Leaf forest, Evergreen Broad Leaf forest, Evergreen Needle Leaf forest, Mixed Forest, Shrubland, and Grassland) to the current day climate observations from 2000 to 2017 over the NER reveals the following findings:

1. Interannual and inter-seasonal variations in the anomalies of the area-averaged gridded NDVI field sample points (LULC points) in all the vegetation types are observed which can be attributed to

variation in rainfall, aridity, NDWI, maximum and minimum temperature distribution during wet, winter, and dry season.

2. There are two/three years lagged dependency, or even a one year lag of the NDVI anomaly to the rainfall anomaly within each season. The rainfall anomaly in the previous year seems to affect the NDVI anomaly in the following years i.e. an increase or decrease in rainfall anomaly in the previous year is well-matched with a similar increase or decrease in NDVI anomaly in the following years.

3. The NDVI anomalies of winter season show a greater magnitude in declining towards negative anomalies than the other two seasons (wet and dry season). The weakening of NDVI anomaly during the winter season indicates the importance of summer monsoon rainfall, whose reduction reduces the density of vegetation over the NER. A decline in the summer monsoon rainfall leads to water stress, phenology changes, and a decreased biomass response with a subsequent reduction in the NDVI.

4. The NDVI anomaly responses are seen to be more strongly associated with rainfall in all seasons. However, during the summer monsoon and pre-monsoon season, the moisture availability from the NDWI, aridity due to the fluctuations of maximum and minimum temperature are also seen.

5. Evergreen Broad Leaf forest and Deciduous Broad Leaf forests are particularly seen to be affected drastically by rainfall fluctuations, indicating a major control of rainfall in the tropical forest.

6. Evergreen Needle Leaf forest, which does not get affected much by negative rainfall anomaly, is seen to be affected by interannual and inter-seasonal rainfall fluctuations, making this study a first of its kind in delivering the message of the prevailing situation in NER.

7. The NDVI and rainfall anomalies for entire Northeast India show an increasing trend in all three seasons indicating higher greenery which could be due to plantations outside recorded forest areas, regeneration of the forest, conservation measures, expansion of croplands, intensive irrigation, urban greening, agricultural practices, etc (Liu et al 2015 and Chen at al., 2019).

8. The time series of maximum NDVI values reaches its maximum during the winter monsoon season than the other two seasons because of adequate sunlight, the sky remains clear as the cloud disappears once the summer monsoon receded, which is needed for photosynthesis supported by water and nutrient charged soils (Nischitha et al., 2014).

9. The spatial distribution of maximum NDVI value for the entire region shows the greenest (highest NDVI value) during the winter season while during the wet and dry season, the NDVI is a bit scattered and decline with dry season being the least NDVI value. Year-to-year variations over the same region are seen throughout the period. This fluctuation of NDVI throughout the period indicates that the increase and decrease of rainfall plays an important role in controlling the vegetation growth over the region.

4.3 Scope for further research

This research provides useful insights into climate change and its impacts in Northeast India, a region known for its complexity and ecological importance. The present study opens the scope for further research in the area mention below:

1. A higher density of observations and higher resolution climate models are suggested for better estimation and understanding of climate change in NER.

2. An intense and more comprehensive study is suggested to examine in more detail to determine if the changes are due to climate change, or can be due to direct human interventions.

3. As can be understood from the present study, setting up a denser network of meteorological observations will be also critical.

List of References

Abatzoglou, J., S. Dobrowski, S. Parks, et al., 2018: TerraClimate, a high-resolution global dataset of monthly climate and climatic water balance from 1958–2015. *Sci Data 5,* 170191, https://doi.org/10.1038/sdata.2017.191.

Agrawal, et al., 2012: Stable (δ13C and δ15N) Isotopes and Magnetic Susceptibility Record of Late Holocene Climate Change from a Lake Profile of the Northeast Himalaya. *Journal Geological Society of India*, 86, 696-705.

Ashok, K., F. Feba, and C. T. Tejavath, 2019: The Indian summer monsoon rainfall and ENSO. *Mausam*, 70 (3), 443-452.

Basumatary, S. K., and S. K. Bera, 2010: Development of vegetation and climatic change in West Garo hills since Late Holocene: pollen sequence and anthropogenic impact. *The Journal of the Indian Botanical Society*, 89, 143-148.

Bhandari, A. K., A. Kumar, and G. K. Singh, 2012: Feature Extraction using Normalized Difference Vegetation Index (NDVI): a Case Study of Jabalpur City. *Procedia Technology,* 6, 612 – 621.

Bhattacharyya, A., J. Sharma, S. K. Shah, and V. Chaudhury, 2007: Climatic changes last 1800 years BP from Paradise lake, Sela pass, Arunachal Pradesh, Northeast Himalaya. *Current Science,* 93 (7), 983-987.

Breitenbach, S. F. M., J. F. Adkins, H. Meyer, N. Marwan, K. K. Kumar, and G. H. Haug, 2010: Strong influence of water vapor source dynamics on stable isotopes in precipitation observed in Southern Meghalaya, NE India. *Earth and Planetary Science Letters*, 292 (1–2), 212–220.

Braconnot, P., S. P. Harrison, M. Kageyama, P. J. Bartlein, V. Masson-Delmotte, A. Abe-Ouchi, B. Otto-Bliesner, and Y. Zhao, 2012: Evaluation of climate models using palaeoclimatic data. *Nature Climate Change*, 2, 417–424. (doi:10.1038/nclimate1456).

Ceccato, P., S. Flasse, S. Tarantola, S. Jacquemond, and J. M. Gregoire, 2001: Detecting vegetation water content using reflectance in the optical domain. *Remote Sensing of Environment*, 77, 22–33.

Chakraborty, K. 2009: Vegetation change detection in Barak Basin Kasturi Chakraborty. *Current Science*, *96*(9), 1236-1242. http://www.jstor.org/stable/24105415.

Chakraborty, R., B. De, N. Devanna, and S. Sen, 2012: North-East India an Ethnic Storehouse of Unexplored Medicinal Plants. *Journal of Natural Product and Plant Resources*, 2 (1), 143-152, ISSN : 2231 – 3184, CODEN (USA): JNPPB7, http://scholarsresearchlibrary.com/archive.html.

Chakraborty, A., M. V. R. Seshasai, C. Sudhakar Reddy, and V. K. Dadhwal, 2018: Persistent negative changes in seasonal greenness over different forest types of India using MODIS time series NDVI data (2001–2014). *Ecological Indicators*, 85, 887–903. https://doi.org/10.1016/j.ecolind.2017.11.032.

Chakravarty, S., C. P. Suresh, A. Puri, and G. Shukla, 2012: North-east India, the geographical gateway of India's phytodiversity. *Indian Forester*, 138 (8), 702–709.

Chaturvedi, R.K., N. H. Ravindranth, J. Mathangi, J. Jaideep, and G. Bala, 2012: Multi-model climate change projections for India under representative concentration pathways. *Current Science*, 103 (7), 791-802.

Chandola, V., D. Hui, L. Gu, B. Bhaduri, and R. R. Vatsavai, 2010: Using time series segmentation for deriving vegetation phenology indices from MODIS NDVI data. IEEE *International Conference on Data Mining Workshops*. INSPEC, Accession Number: 11771639. https://doi.org/10.1109/ICDMW.2010.143.

Chang, C. T., S. F. Wang, A. V. Matthew, and T. C. Lin, 2014: Relating vegetation dynamics to temperature and precipitation at monthly and annual timescales in Taiwan using MODIS vegetation indices. *International Journal of Remote Sensing, 35*(2), 598–620. https://doi.org/10.1080/01431161.2013.871593.

Chauhan, M. S., and B. D. Mandaokar, 2006: Pollen proxy records of vegetation and climate change during recent past in southern Mizoram, India. *Gondwana Geological Magazine*, 21 (2), 115-119.

Chen et al., 2019: China and India lead in greening of the world through land-use management. *Nature Sustainability*, 2 (122), 122–129, https://doi.org/10.1038/s41893-019-0220-7.

Chinchorkar, S. S., F. G. Sayad, V. B. Vaidya, and V. Pandye, 2015: Trend detection in annual maximum temperature and precipitation using the Mann Kendal test – a case study to assess climate change on Anand of central Gujarat. Mausam 66 (1), 1–6.

Collins, M., K. A. Rao, K. Ashok, S. Bhandari, K. Ashis, M. S. Prakash, R. Srivastava, and A. Turner, 2013: Observational challenges in evaluating climate models. *Nature Climate Change*, 3, 940–941.

Dash, S.K., N. Sharma, K. C. Pattnayak, X. J. Gao, and Y. Shi, 2012: Temperature and precipitation changes in the north-east India and their future projections. *Global and Planetary Change*, 98-99, 31–44.

Dash, et al., 2015: Projected seasonal mean summer monsoon over India and adjoining regions for the twenty-first century. *Theoretical and Applied Climatology*, 122, 581–593.

Dixit, S., and S. K. Bera, 2012: Pollen-inferred vegetation vis-á-vis climate dynamics since Late Quaternary from western Assam, Northeast India: signal of global climatic events. *Quaternary International*, 286, 56-68.

Dixit, Y., and S. K. Tandon, 2016: Earth-science reviews hydroclimatic variability on the Indian subcontinent in the past millennium? Review and assessment. *Earth-Science Reviews,* 161, 1–15. https://doi.org/10.1016/j.earsc irev.2016.08.001.

Dubey, D. P., and G. Krishnakumar, 2014: Trends in precipitation extremes over Central India. *Mausam,* 65 (1), 103–108.

Dufresne, J. L. et al., 2013: Climate change projections using the IPSL-CM5 Earth System Model: from CMIP3 to CMIP5. *Climate Dynamics,* 40, 2123–2165. http://dx.doi.org/10.1007/s00382-012-1636-1.

Forest Survey of India., 2017: India State of Forest Report (Ministry of Environment, Forests and Climate Change).

Forest Survey of India, 2019: India State of Forest Report (Ministry of Environment, Forests and Climate Change). ISBN 978-81-941018-0-2.

Gao, B. C, 1996: NDWI - A normalized difference water index for remote sensing of vegetation liquid water from space. *Remote Sensing of Environment,* 58, 257-266.

Goswami, B. N., V. Venugopal, D. Sengupta, M. S. Madhusoodanan, and P. K. Xavier, 2006: "Increasing trend of extreme rain events over India in a warming environment", *Science*, 314, 1442-1445.

Goswami, B. B., P. Mukhopadhyay, R. Mahanta, and B. N. Goswami, 2010: Multiscale interaction with topography and extreme rainfall events in the northeast Indian region. *Journal of Geophysical Research*, 115, D12114. doi:10.1029/2009JD012275.

Guhathakurta, P., and M. Rajeevan, 2008: Trends in the rainfall pattern over India. *International Journal of Climatology,* 1453–1469, DOI: 10.1002/joc.1640.

Gupta, A. K., S. Dutt, H. Cheng, and R. K. Singh, 2019: Abrupt changes in Indian summer monsoon strength during the last ~900 years and their linkages to socio-economic conditions in the Indian subcontinent. *Palaeogeography, Palaeoclimatology, Palaeoecology*, 536:109347, DOI: 10.1016/j.palaeo.2019.109347.

Harris, P. D., T. J. Jones, and D. H. L. Osborna, 2014: Updated high-resolution grids of monthly climatic observations – the CRU TS3.10 Dataset. *International Journal of Climatology*, 34, 623–642.

Hasan, K. F., Md. A. Shahjahan, and Md. S. Rahman, 2011: A digital approach of satellite image processing for retrieving surface parameters. *International Journal of Engineering Research and Applications*, 1(3), 1242–1246.

Hilkera, T., I. L et al., 2014: Vegetation dynamics and rainfall sensitivity of the Amazon. *PNAS, 111*(45), 16041–16046. https://doi.org/10.1073/pnas.1404870111.

Hoskins, B., and B. Wang, 2006: Large Scale Atmospheric Dynamics, Asian Monsoon, Ed. Bin Wang, Springer-Praxis Publishing, (Chapter 9, Sec. 9.5.2, pp 377-378).

Huete, A., K. Didan, T. Miura, E. P. Rodriguez, X. Gao, and L. Gferreira, 2002: Overview of the radiometric and biophysical performance of the MODIS vegetation indices. *Remote sensing of Environment*, 83 (1-2), 195-213.

IPCC, 2013: Climate change 2013: the physical science basis. In: Stocker, T.F., Qin, D., Plattner, G.-K., Tignor, M., Allen, S.K., Boschung, J., Nauels, A., Xia, Y., Bex, V., Midgley, P.M. (Eds.), Contribution of Working Group I to the Fifth Assessment Report of the Intergovernmental Panel on Climate Change. Cambridge University Press, Cambridge, United Kingdom and New York, NY, USA (1535 pp).

IPCC, 2018: Summary for Policymakers. In: Global Warming of 1.5°C. An IPCC Special Report on the impacts of global warming of 1.5°C above pre-industrial levels and related global greenhouse gas emission pathways, in the context of strengthening the global response to the threat of climate change, sustainable development, and efforts to eradicate poverty [Masson-Delmotte, V., P. Zhai, H.-O. Pörtner, D. Roberts, J. Skea, P.R. Shukla, A. Pirani, W. Moufouma-Okia, C. Péan, R. Pidcock, S. Connors, J.B.R. Matthews, Y. Chen, X. Zhou, M.I. Gomis, E. Lonnoy, T. Maycock, M. Tignor, and T. Waterfield (eds.)]. In Press.

IPCC, 2019: Summary for Policymakers. In: Climate Change and Land: an IPCC special report on climate change, desertification, land degradation, sustainable land management, food security, and greenhouse gas fluxes in terrestrial ecosystems [P.R. Shukla, J. Skea, E. Calvo Buendia, V. Masson-Delmotte, H.- O. Pörtner, D. C. Roberts, P. Zhai, R. Slade, S. Connors, R. van Diemen, M. Ferrat, E. Haughey, S. Luz, S. Neogi, M. Pathak, J. Petzold, J. Portugal Pereira, P. Vyas, E. Huntley, K. Kissick, M. Belkacemi, J. Malley, (eds.)]. In press.

Jain, S.K., and V. Kumar, 2012: Trend analysis of rainfall and temperature data for India. *Current Science*, 102 (1), 37–49.

Jain, S. K., V. Kumar, and M. Saharia, 2013: Analysis of rainfall and temperature trends in northeast India. *International Journal of Climatolology*, 33, 968–978, DOI: 10.1002/joc.3483.

Jeyaseelan, A. T., P. S. Roy, and S. S. Young, 2007: Persistent changes in NDVI between 1982 and 2003 over India using AVHRR GIMMS (Global Inventory Modeling and Mapping Studies) data. *International Journal of Remote Sensing*, 28 (21), 4927–4946. https://doi.org/10.1080/01431160701253279.

Jhajhariaa, D., and V. P. Singh, 2011: Trends in temperature, diurnal temperature range and sunshine duration in Northeast India. *International Journal of Climatology*, 31, 1353–1367.

Jong, R, D., J. Verbesselt, M. E. Schaepman, and S. D. Bruin, 2012: Trend changes in global greening and browning: contribution of short-term trends to longer-term change. *Global Change Biology*, 18, 642–655, doi: 10.1111/j.1365-2486.2011.02578.x.

Jourdain, N. C., A. S. Gupta, A. S. Taschetto, C. C. Ummenhofer, A. F. Moise, and K. Ashok, 2013: The Indo-Australian monsoon and its relationship to ENSO and IOD in reanalysis data and the CMIP3/CMIP5 simulations. *Climate Dynamics*, 41, 3073–3102. http://dx.doi.org/10.1007/s00382-013-1676-1.

Keshavamurty, R. N., 1982: Response of the atmosphere to sea surface temperature anomalies over the equatorial pacific and the teleconnections of the southern oscillation. *Journal of the Atmospheric Sciences*, 39 (6), 1241-1259.

Kothawale, D. R., K. K. Kumar, and G. Srinivasan, 2012: Spatial asymmetry of temperature trends over India and possible role of aerosols. *Theoretical and Applied Climatology*, 110, 263–280. http://dx.doi.org/10.1007/s00704-012-0628-8.

Kothyari, U.C., and V. P. Singh, 1996: Rainfall and temperature trends in India. *Hydrological Processes*, 10, 357–372.

Krishnan, R., T. P. Sabin, R. Vellore, M. Mujumdar, J. Sanjay, B. N. Goswami, F. Hourdin, J. L. Dufresne, and P. Terray, 2016: Deciphering the desiccation trend of the South Asian monsoon hydroclimate in a warming world. *Climate Dynamics*, http://dx.doi.org/10.1007/s00382-015-2886-5.

Krishnan, R., J. Sanjay, C. Gnanaseelan, M. Mujumdar, A. Kulkarni, and S. Chakrborty, 2020: Assessment of Climate Change over the Indian Region. A Report of the Ministry of Earth Sciences (MoES), Government of India. ISBN 978-981-15-4326-5, ISBN 978-981-15-4327-2, https://doi.org/10.1007/978-981-15-4327-2.

Kulkarni, et al., 2013: Projected climate change in the Hindu Kush–Himalayan region by using the high-resolution regional climate model PRECIS. *Mountain Research* and *Development,* 33 (2), 142–151.

Kumar, V., S. K. Jain, and Y. Singh, 2010: Analysis of long-term rainfall trends in India. *Hydrological Sciences Journal,* 55 (4), 484–496.

Laskar, S. I., S. D. Kotal, and S. K. B. Roy, 2014: Analysis of rainfall and temperature trends of selected stations over Northeast India during last century. *Mausam,* 65 (4), 497–508.

Lele, N. V., P. K. Joshi, and S. P. Agarwal, 2005: Fractional Vegetation Cover Analysis for Understanding Vegetation Cover Dynamics in Northeast India. *International Journal of Geoinformatics,* 1(3), 63-70.

Lele, N. V., P. K. Joshi, and S. P. Agarwal, 2008: Assessing forest fragmentation in northeastern region (NER) of India using landscape matrices. *Ecological Indicators, 8,* 657-663. https://doi.org/10.1016/j.ecolind.2007.10.002.

Li, H., J. Jiang, B. Chen, Y. Li, Y. Xu, and W. Shen, 2016: Pattern of NDVI-based vegetation greening along an altitudinal gradient in the eastern Himalayas and its response to global warming. *Environmental Monitoring and Assessment,* 188-186, DOI 10.1007/s10661-016-5196-4.

Liu, Y., Y. Li, S. Li, and S. Motesharrei, 2015: Spatial and Temporal Patterns of Global NDVI Trends: Correlations with Climate and Human Factors. *Remote Sensing,* 7, 13233-13250; doi:10.3390/rs71013233.

Mehrotra, N., K. S. Santosh, and A. Bhattacharyya, 2014: Review of palaeoclimate records from Northeast India based on pollen proxy data of Late Pleistocenee Holocene. *Quaternary International,* 325, 41–54.

Milesi, C et al., 2010: Decadal variations in NDVI and food production in India. *Remote Sensing,* 2, 758-776. http://dx.doi.org/10.3390/rs2030758.

Mohanty, U.C., M. Mohapatra, K. Ashok, R. Krishnan, J. S. Chowdary, and P. Mukhopadhyay, 2020: Indian Monsoons Variability and Extreme Weather Events: Recent Improvements in Observations and Modelling, *Proceedings of the Indian National Science Academy,* 86, DOI: 10.16943/ptinsa/2020/49817.

Mohapatra, M., H. R. Biswas, and G. K. Sawaisarje, 2011: Spatial variability of daily rainfall over Northeast India during summer monsoon season. *Mausam,* 62 (2), 215-228.

Mondal, A., D. Khare, and S. Kundu, 2014: Spatial and temporal analysis of rainfall and temperature trend of India. *Theoretical and Applied Climatology*, 122 (1-2), 143-158. http://dx.doi.org/10.1007/s00704-014-1283-z.

Nautiyal, C. M., and M. S. Chauhan, 2009: Late Holocene vegetation and climate change in Loktak Lake region, Manipur, based on pollen and chemical evidence. *The Palaeobotanis,* 58, 21-28.

Nischitha, V., S. A. Ahmed, H. Varikoden, and J. V. Revadekar, 2014: The impact of seasonal rainfall variability on NDVI in the Tunga and Bhadra river basins, Karnataka, India. *International Journal of Remote Sensing*, 35 (23), 8025–8043. https://doi.org/10.1080/01431161.2014.979301.

Pai, D. S., L. Sridhar, M. Rajeevan, O. P. Sreejith, N. S. Satbhai, and B. Mukhopadhyay, 2014: Development of a new high spatial resolution (0.25° × 0.25°) long period (1901-2010) daily gridded rainfall data set over India and its comparison with existing data sets over the region. *Mausam*, 65, 1, 1-18.

Parida, B. R., B, Oinam, N. R. Patel, N. Sharma, R. Kandwal, and M. K. Hazarika, 2008: Land surface temperature variation in relation to vegetation type using MODIS satellite data in Gujarat state of India. *International Journal of Remote Sensing, 29* (14), 4219–4235. https://doi.org/10.1080/01431160701871096.

Parthasarathy, B., 1984: Interannual and long-term variability of Indian summer monsoon rainfall; *Journal of Earth System Science*, 93, 371-385.

Parthasarathy, B., A. A. Munot, and D. R. Kothawale, 1995: Monthly and seasonal time series for all India, homogeneous regions and meteorological subdivisions: 1871–1994, Res. Rep. RR-065, 113 pp., Indian Institute of Tropical Meteorology, Pune, India.

Pattanaik, D. R., 2012: Indian monsoon variability. Monsoon Monograph 2012, (Chapter 2, Vol. 2, pp.35-77), Ed. A. Tyagi et al.

Pattnayak, K. C., S. C. Kar, D. Mamta, and R. K. Pattnayak, 2017: Projections of annual rainfall and surface temperature from CMIP5 models over the BIMSTEC countries. *Global and Planetary Change,* Vol. 152, 152-166.

Pant, G.B., and R. K. Kumar, 1997: Climates of South Asia. (ISBN: 978-0-471-94948-0).

Pant, G.B., 2003: Long-Term Climate variability and change over monsoon Asia. *Journal of Indian Geophysical Union*, 7 (3), 125-134.

Prakash, S., A. K. Mitra, I. M. Momin, E. N. Rajagopal, S. Basu, M. Collins, A. G. Turner, K. Achuta, Rao, and K. Ashok, 2014: Seasonal intercomparison of observational rainfall datasets over India during the southwest monsoon season. *International Journal of Climatology,* 35 (9), 2326–2338. http://dx.doi.org/10.1002/joc.4129.

Rajeevan, M., J. Bhate, J. D. Kale, and B. Lal, 2005: Development of a high resolution daily gridded rainfall data for the Indian region. Met. Monograph Climatology No. 22/2005. National Climate Centre India Meteorological Department.

Rajendran, K., S. Sajani, C. B. Jayasankar, and A. Kitoh, 2013: How dependent is climate change projection of Indian summer monsoon rainfall and extreme events on model resolution? *Current Science*, 104 (10), 1409–1418.

Rao, Y. P., 1976: Southwest Monsoon. Met. Monograph, India Meteorological Department, 367, 1/76, India Meteorological Department, Delhi, India. 140 pp.

Reed, B. C., J. F. Brown, D. Vanderzee, T. R. Loveland, J. W. Merchant, and D. O. Ohlen, 1994: Measuring phenological variability from satellite imagery. *Journal of Vegetation Science*, 5 (5), 703–714. https://doi.org/10.2307/3235884.

Revadekar, J. V., D. R. Kothawale, S. K. Patwardhan, G. B. Pant, and R. K. Kumar, 2012: About the observed and future changes in temperature extremes over India. *Natural Hazards*, 60, 1133–1155. http://dx.doi.org/10.1007/s11069-011-9895-4.

Revadekar, J. V., Y. K. Tiwari, and K. Ravi Kumar, 2012: Impact of climate variability on NDVI over the Indian region during 1981–2010. *International Journal of Remote Sensing*, 33 (22), 7132-7150. https://doi.org/10.1080/01431161.2012.697642.

Rouse, J. W. Jr., R. H. Haas, J. A. Schell, and D. W. Deering, 1973: Monitoring vegetation systems in the Great Plains with ERTS. In Proceedings of the 3rd ERT S Symposium, NASA SP-351 1:48–62.

Roxy, M., R. Kapoor, T. Pascal, R. Murtugudde, K. Ashok, and B. N. Goswami, 2015: Drying of Indian subcontinent by rapid Indian Ocean warming and a weakening land-sea thermal gradient. *Nature Communition*, 6, Article number: 7423. http://dx.doi.org/10.1038/ncomms8423.

Roy, P. S. et al., 2015a: Development of decadal (1985–1995–2005) land use and land cover database for India. *Remote Sensing*, 7, 2401–2430. https://doi.org/10.3390/rs70302401.

Roy, P.S. et al., 2015b: New vegetation type map of India prepared using satellite remote sensing: Comparison with global vegetation maps and utilities. *International Journal of Applied Earth Observation and Geoinformation*, 39, 142-159. https://doi.org/10.1016/j.jag.2015.03.003.

Ravindranath, et al., 2011: Climate change vulnerability profiles for North East India. *Current Science*, 101 (3), 384–394.

Roeckner, et al., 2003: The Atmospheric General Circulation Model Echam5, Part I: Model Description, internal report 349:144.

Sabin, T. P., R. Krishnan, J. Ghattas, S. Denvil, J. L. Dufresne, F. Hourdin, and T. Pascal, 2013: High resolution simulation of the South Asian monsoon using a variable resolution global climate model. *Climate Dynamics*, 41, 173–194, http://dx.doi.org/10.1007/s00382-012-1658-8.

Saikia, A., 2009: NDVI variability in North-east India. *Scottish Geographical Journal*, 125 (2), 195–213. https://doi.org/10.1080/14702540903071113.

Sarmah, S., G. Jia, and A. Zhang, 2018: Satellite view of seasonal greenness trends and controls in South Asia. *Environmental Research Letters*, 13 034026.

Sharma, C., and M. S. Chauhan, 1999: Palaeoclimatic inferences from quaternary palynostratigraphy of the Himalayas. In: Dash, S.K., Bahadur, J. (Eds.), *The Himalayan Environment*. New Age International, New Delhi, 193-207.

Sharma, C., and M. S. Chauhan, 2001: Late Holocene vegetation climate Kupup (Sikkim), Eastern Himalaya, India. *Journal of the Palaeontological Society of India*, 46, 51-58.

Shepard, D. A, 1968: Two-dimensional interpolation function for irregularly spaced data. *In Proceedings ACM National Conference*, 517–524.

Sikka, D. R., 1980. Some aspects of the large scale fluctuations of summer monsoon rainfall over India in relation to fluctuations in the planetary and regional scale circulation parameters. *Proceedings of the Indian Academy of Sciences - Earth & Planetary Sciences*, 89, 179–195, https://doi.org/10.1007/BF02913749.

Sinha, et al., 2007: A 900-year (600 to 1500 AD) record of the Indian summer monsoon precipitation from the core monsoon zone of India. *Geophysical Research Letters*, 34.

Singhvi A. K., and R. Krishnan, 2014: Past and the Present Climate of India. In: Kale V. (eds) *Landscapes and Landforms of India,* 15-23, World Geomorphological Landscapes. Springer, Dordrecht. https://doi.org/10.1007/978-94-017-8029-2_2.

Soraisam, B., K. Ashok, and D. S. Pai, 2018: Uncertainties in observations and climate projections for the North East India. *Global and Planetary Change,* 160, 96–108. https://doi.org/10.1016/j.gloplacha.2017.11.010.

Srivastava, A. K., M. Rajeevan, and S. R. Kshirsagar, 2009: Development of a high resolution daily gridded temperature data set (1969–2005) for the Indian region. *Atmospheric Science Letters,* 10 (4), 249 – 254.

Taylor, K. E., R. J. Stouffer, and G. A. Meehl, 2012: An overview of CMIP5 and the experiment design. *American Meteorological Society*, 485–498, http://dx.doi.org/10.1175/BAMS-D-11-00094.1.

Tejavath, C. T., K. Ashok, S. Chakraborty, and R. Ramesh, 2017: The Indian summer monsoon climate during the Last Millennium, as simulated by the PMIP3. *Climate of the Past,* doi:10.5194/cp-2017-24.

Tejavath, C. T., K. Ashok, S. Chakraborty, and R. Ramesh, 2019: A PMIP3 narrative of modulation of ENSO teleconnections to the Indian summer monsoon by background changes in the Last Millennium. *Climate Dynamics,* 53, 3445–3461.

Tripathi, S. K., A. Roy, D. Kushwaha, F. Lalnunmawia, H. Lalraminghlova, C. Lalnunzira, and P. S. Roy, 2016: Perspectives of forest biodiversity conservation in North-east India. *Journal of Biodiversity, Bioprospecting and Development,* 3 (2), 157. http://dx.doi.org/10.4172/2376-0214.1000157.

Tripathi, S., Y. R. Singh, C. M. Nautiyal, and B. Thakur, 2017: Vegetation history, monsoonal fluctuations and anthropogenic impact during the last 2330 years from Loktak Lake (Ramsar site), Manipur, north-east India: a pollen based study. *Palynology,* DOI: 10.1080/01916122.2017.1375441.

Vermote, E. 2015: MYD09A1 MODIS/Aqua Surface Reflectance 8-Day L3 Global 500m SIN Grid V006 [Data set]. NASA EOSDIS Land Processes DAAC. Accessed 2020-12-28 from https://doi.org/10.5067/MODIS/MYD09A1.006.

Wang, J., P. M. Rich, and K. P. Price, 2001: Spatial patterns of NDVI in response to precipitation and temperature in the central great plains. *International Journal of Remote Sensing, 22* (18), 3827-3844. https://doi.org/10.1080/01431160010007033.

Yadava, M. G., and R. R. Ramesh, 2005: Monsoon reconstruction from radiocarbon dated tropical speleothems. *The Holocene,* 15:48–59.

Yatagai, A. et al., 2012: APHRODITE: constructing a long-term daily gridded precipitation dataset for Asia based on a dense network of rain gauges. *American Meteorological Society,* 1401–1415. http://dx.doi.org/10.1175/BAMS-D-11-00122.1.

Yu, X., D. Zhuang, D and X. Hou, 2005: Forest phenological pattern of Northeast China inferred from MODIS data. *Journal of Geographical Sciences, 15* (2), 239-246. https://doi.org/10.1007/BF02872689.

Zeppel, M. J. B., J. V. Wilks, and J. D. Lewis, 2014: Impacts of extreme precipitation and seasonal changes in precipitation on plants. *Biogeosciences,* 11: 3083–3093. https://doi.org/10.5194/bg-11-3083-2014.

List of Publications

1. Soraisam, B., Ashok, K., & Pai, D. S. (2018). Uncertainties in observations and climate projections for the North East India. Global and Planetary Change, 160, 96–108. https://doi.org/10.1016/j.gloplacha.2017.11.010 (Publised).

2. Karumuri Ashok, Soraisam Bidyabati, Charan Teja Tejavath and Ulrich Cubash. Summer monsoon over northeastern India during the last millennium. (Under revision on International Journal of Climatology).

3. Soraisam, B., P. S. Roy, Ashok, K and Pinjarla, B. Different vegetation pattern responses to climate change in Northeast India (tentative title). (To be submitted).

Global and Planetary Change 160 (2018) 96–108

Contents lists available at ScienceDirect

Global and Planetary Change

journal homepage: www.elsevier.com/locate/gloplacha

Uncertainties in observations and climate projections for the North East India

Bidyabati Soraisam[a,*], Ashok Karumuri[a], Pai D.S.[b]

[a] University Centre for Earth, Ocean and Atmospheric Sciences, University of Hyderabad, Gachibowli, Hyderabad, Telangana 500046, India
[b] India Meteorological Department, Pune 411 005, India

ARTICLE INFO

Editor: Dr. Sierd Cloetingh

Keywords:
Climate change
AR5/CORDEX-South-Asia
Historical-simulations
Future-projections
Northeast-India

ABSTRACT

The Northeast-India has undergone many changes in climatic-vegetation related issues in the last few decades due to increased human activities. However, lack of observations makes it difficult to ascertain the climate change. The study involves the mean, seasonal cycle, trend and extreme-month analysis for summer-monsoon and winter seasons of observed climate data from Indian Meteorological Department (1° × 1°) and Aphrodite & CRU-reanalysis (both 0.5° × 0.5°), and five regional-climate-model simulations (LMDZ, MPI, GFDL, CNRM and ACCESS) data from AR5/CORDEX-South-Asia (0.5° × 0.5°). Long-term (1970–2005) observed, minimum and maximum monthly temperature and precipitation, and the corresponding CORDEX-South-Asia data for historical (1970–2005) and future-projections of RCP4.5 (2011–2060) have been analyzed for long-term trends. A large spread is found across the models in spatial distributions of various mean maximum/minimum climate statistics, though models capture a similar trend in the corresponding area-averaged seasonal cycles qualitatively. Our observational analysis broadly suggests that there is no significant trend in rainfall. Significant trends are observed in the area-averaged minimum temperature during winter. All the CORDEX-South-Asia simulations for the future project either a decreasing insignificant trend in seasonal precipitation, but increasing trend for both seasonal maximum and minimum temperature over the northeast India. The frequency of extreme monthly maximum and minimum temperature are projected to increase. It is not clear from future projections how the extreme rainfall months during JJAS may change. The results show the uncertainty exists in the CORDEX-South-Asia model projections over the region in spite of the relatively high resolution.

1. Introduction

The WG1 (Working Group I) report of the IPCC (2013) states that global warming occurring since 1950's is unequivocal and unprecedented over decades to millennia, and that human influence has been detected in the warming of the atmosphere and oceans. CMIP5 (Coupled model intercomparison project phase 5) models simulation have also projected an increase in global mean surface temperature over a range from 1.1 °C to 2.6 °C (IPCC, 2013), which seems to be qualitatively realistic as seen from the consistently increasing global temperatures.

Anthropogenic climate change manifested in changing temperature and precipitation, and is likely to pose serious risk to human society, economy and ecosystems, such as loss of agriculture, water shortages and widespread health impacts as well as increased in heat-induced mortality to extreme events, etc. (Kumar et al., 2006; Kumar et al., 2011; Ravindranath et al., 2011; Jain et al., 2012; Choudhury et al., 2012 and Sharmila et al., 2015). The effects of climate change are expected to be greatest in the developing countries which rely on primary production as a major source of income (Kumar et al., 2006). According to the Fourth and Fifth Assessment Reports of the Intergovernmental Panel on Climate Change (IPCC, 2007 and 2013), the Indian subcontinent will be adversely affected by enhanced variability of climate, rising temperature and substantial changes summer rainfall in some parts and thereby water stress by the 2020s.

Several studies from the CMIP3 and CMIP5 simulations (Kumar et al., 2006; Chaturvedi et al., 2012; Kumar et al., 2013; Dufresne et al., 2013 and Jourdain et al., 2013, etc.) and several studies based on the downscaled projections (Kumar et al., 2011; Dash et al., 2012; Kumar et al., 2013 and Krishnan et al., 2016) project an increasing trend in the atmospheric temperature over India associated with increased anthropogenic activities. This conjecture also matches with the results from observational studies such as those by Kothawale et al. (2012) and Kothawale and Kumar (2005) and Revadekar et al. (2012) which show an increase of surface temperatures across various regions of India during the recent 3–4 decades as compared to the earlier period.

* Corresponding author.
E-mail address: sorai1989@uohyd.ac.in (B. Soraisam).

https://doi.org/10.1016/j.gloplacha.2017.11.010
Received 26 December 2016; Received in revised form 9 November 2017; Accepted 10 November 2017
Available online 11 November 2017
0921-8181/

Notwithstanding this, the CMIP3 models as well as those from the CMIP5 (Collins et al., 2013; Dufresne et al., 2013; Jourdain et al., 2013; Saha et al., 2014 and Sharmila et al., 2015) have challenges in simulating the teleconnections and trends of the Indian summer monsoon rainfall, which is seasonally phaselocked to the June–September months (henceforth JJAS), correctly. Though the CMIP5 models show better skills in reproducing the mean Indian summer monsoon rainfall (Jourdain et al., 2013 and Shashikanth et al., 2013), the amplitude of interannual variability and seasonal cycle reasonably close to the observations data as compared to the best CMIP3 models (Jourdain et al., 2013). The decreasing Indian summer monsoon rainfall trend during the past decades (Guhathakurta and Rajeevan, 2008; Rajendran et al., 2013 and Krishnan et al., 2016, etc.) is not reproduced by the CMIP5 models, which is a serious limitation of the GCMs at coarse resolution in capturing the south Asian climate change in the recent decades (Krishnan et al., 2016 and Roxy et al., 2015).

Fortunately, dynamical downscaling of the historical simulations by various regional climate models (Dash and Hunt, 2007; Dash et al., 2012, Dash et al., 2015) or using high resolution GCMs in the Indian region (Krishnan et al., 2016) have been successful in capturing the decreasing Indian Summer Monsoon Rainfall trend (ISMR), which is essentially area-averaged June–September rainfall over a major homogeneous rainfall region of India (northeast India not included). Therefore, the corresponding future projection of a weakening ISMR trend by the high resolution models (e.g. Dash et al., 2015; Krishnan et al., 2016) may have some reliability in a qualitative sense. Some of these studies are sort of a first but sure step in understanding the relative contribution of various climate change drivers such as greenhouse gases, aerosols, and land surface processes (Kothawale et al., 2012; Krishnan et al., 2016 and Roxy et al., 2015). Having said that, if sub-regional level in India is concerned, uncertainties exist in some climate statistics across various observational datasets, and high resolution projections as well (Kumar et al., 2013).

The northeast India (NEI) is a prominent portion of India, covering a geographic area of 26.2 mha, and home to a population of about 45 million (Ministry of Home Affairs, Government of India). In India, the characteristics of the summer monsoon rainfall and its variability differ from region to region within the nation (Mooley and Parthasarathy, 1983a, 1983b). An empirical orthogonal analysis by Parthasarathy et al. (1996) of long term summer monsoon rainfall records for the 1871–1990 from 306 stations widely-distributed stations in India shows a dipolar structure of the gravest mode, wherein the signal in the northeast India is seen in an out of phase relation with the rest of India (see Fig. 6.5, Pant and Kumar, 1997). The NEI is also endemic to many flora and fauna making it one of the richest in the world in terms of biological values (Chakraborty et al., 2012). It has a subtropical climate with wide variation in weather and climate, and is characterized by large rural population (82%), low population density, large percentage of indigenous tribal communities (34–91%) and large area under forests (60%) (Ravindranath et al., 2011). The NEI is highly dependent on the south west monsoon and over 60% of the crop area is under rain-fed agriculture (Ravindranath et al., 2011). However, the climate statistics vary from study to study owing to the rather sparse observations and computational methods that depend on the area over which the rainfall is averaged, and the method of averaging. For example, Parthasarathy et al. (1996) compute the summer monsoon rainfall over the homogeneous Northeast Indian region to be 142 cm. Nonetheless, it is clear that the region receives a high seasonal rainfall during JJAS.

Dash et al. (2015) analyzed temporal trends in rainfall from nine stations in the NEI on monthly, seasonal and annual scales for 1961–2010. Several other studies that analyze station data from about 7 sub-divisions (Jain et al., 2012), 9 stations (Laskar et al., 2014) and 2 sub-divisions (Mondal et al., 2014) in NEI over the period of 1913–2012, or part of this period, also support this finding of Dash et al. (2015).

On the temperature front, (Jain et al., 2012; Laskar et al., 2014; Mondal et al., 2014, and Wagholikar et al., 2014) have analyzed either the temperature recorded at a few station in the NEI or the homogenized regional temperature records for the 1871–2008, or a portion of that period. These studies suggest an increasing trend in the maximum and/or minimum temperature in some portions of the NEI. Mondal et al. (2014) states that the NEI region is clearly seen affecting by climate change which may lead to droughts in the future due to decrease in rainfall and increase in temperature. Arora et al. (2005) evaluated the temperature trends based on 125 stations in NEI which showed a falling trend in annual mean minimum temperature as most of the stations are located in the foothills of the Himalayas. Climate change vulnerability profiles have been developed at the district level in NEI for agriculture, water and forest sectors for the current and projected future climates where the majority of the districts are subjected to climate induced vulnerability currently and in the near future (Ravindranath et al., 2011). These studies, in general hint, show a significant rise in the observed temperature, and a decreasing tendency in rainfall in various places in the northeast India.

As far as the model studies are concerned, so far, only Dash et al. (2012) have studied the recent and projected future changes in precipitation and temperature of the NEI by downscaling CMIP3 datasets using RegCM3, for the periods 1971 to 2005, and 2011 to 2100. Dash et al. (2012) also record an overestimation of simulated rainfall by the CMIP3 for 1971–2005, and project an increase in the annual mean temperature by about 0.64 °C from 2011 to 2040, and also an increase in annual mean precipitation by about 0.09 mm/day in the near future and by 0.48 mm/day at the end of the century in NEI. Having said this, it indicates the very limited sample of future climate projections for the northeast Indian climate, which means that there would be a significant uncertainty. The differences in datasets add to the uncertainty associated with the inter-model differences when one tries to validate a climate model simulation, particularly the climate change projections (Jourdain et al., 2013 and Collins et al., 2013). This applies acutely for the NEI (Prakash et al., 2014), where the impact of climate change on NEI is explored lesser both in terms of observational analysis as well as from the modeling perspective (Laskar et al., 2014).

Fortunately, of late, several climate centers have dynamically downscaled various CORDEX South-Asia based on CMIP5 projections for the Indian region. The downscaled simulations-four regional climate models, namely MPI, GFDL, CNRM, ACCESS and a high resolution suite of future climate projections by the LMDZ model (Sabin et al., 2013) are available from the cccr.tropmet.res.in under the aegis of the Coordinated Regional Downscaling Experiment, SOUTH ASIA (CORDEX). This gives us an opportunity to address the future climate change in the NEI at a higher resolution, while also taking into account any uncertainty associated with inter-model variability. In addition, we have high resolution gridded rainfall and temperature datasets, derived from the observed IMD datasets among other things, which will be useful to validate the CORDEX South-Asia outputs.

The rest of the current paper is organized as follows. In the next section, we present the study area, various model datasets, and observed and Aphrodite, and reanalyzed climate datasets used, along with a description of our methodology. In the Section 3, we present the results from our analysis, and in the Section 4, our concluding summary and remarks.

2. Datasets and methodology

No study has been done using CORDEX South-Asia output on future scenarios on NEI. Thus the assessment of rainfall and temperature change in the last few decades, and its future projection are very important. These will provide an insight for the present and possible future condition to the planners for climate change adaptation. Taking this note into account, with the help of these five regional climate model data a proper assessment of future trends would help in setting up uncertainties of future for risk management and vulnerability

assessment. Knowledge of spatial and temporal variability of climate parameters is very much useful for overall development of the region and for future planning, which can be attained from this work.

2.1. Model datasets & observational datasets used

In this study, we use the gridded datasets of rainfall (Rajeevan et al., 2005) and temperature (Rajeevan et al., 2008, 2008) derived from the observations the India Meteorological Department (IMD) for the period 1970 to 2005, available at 1° × 1° resolution for temperature and also for precipitation at 1° × 1° resolution. We also use the Asian Precipitation Highly-Resolved Observational Data Integration Towards Evaluation of water resource (Aphrodite) precipitation data with 0.5° × 0.5° resolution from 1970 to 2005 for comparison (Yatagai et al., 2012). For convenience, we refer to these interpolated datasets as 'observations'. Further, as the observations in the NEI are sparse, we also analyze the reanalyzed mean temperature data collected from CRU TS v. 4.00 (0.5° × 0.5° resolution) from 1970 to 2005 (Harris et al., 2014), in addition to the observed temperature datasets from the IMD, in order to have a sense of uncertainty across these two datasets.

In order to estimate the future climate change in the NEI, we also use the high resolution climate model simulation outputs from AR5/CORDEX SOUTH ASIA (See A.1 for details) for the period 1970 to 2005 and 2011 to 2060 at 0.5° × 0.5° resolution. Model-simulated data including maximum and minimum temperature, and precipitation were obtained from the five RCMs[1] that participated in the CORDEX SOUTH ASIA: LMDZ, MPI, GFDL, CNRM and ACCESS. Details on these five model data can be procured from the CCCR, IITM and from the given links, http://cccr.tropmet.res.in/workshop/oct2012/presentations/R%20Krishnan_CCCR_CORDEXSA.pdf http://cccr.tropmet.res.in/workshop/oct2012/presentations/JSanjay_CORDEX-SAsia_RCM_data.pdf http://cordex.dmi.dk/joomla/images/CORDEX/cordex_archive_specifications_120126.pdf Gridded data sets for SST from 1970 to 2005 is collected from HadSST, Met office to see the teleconnections between the precipitation and maximum and minimum temperature datasets with Nino 3.4.

As known, the CORDEX South Asia based on CMIP5 historical runs, forced by observed natural and anthropogenic atmospheric composition, cover the period from 1950 to 2005, whereas the projections from 2011 to 2060 used in the study are forced by Representative Concentration Pathways (RCP) i.e. RCP4.5. As mentioned earlier, we use the downscaled historical simulations of the CORDEX South Asia models for the period 1970–2005 for the NEI, and regional simulations obtained by downscaling RCP4.5 future scenario of the CORDEX South Asia, are used. The CMIP5 historical simulations covers few hundred centuries long pre-industrial and industrial period (from the mid-nineteenth century to near present) control simulations (Taylor et al., 2012 and Dufresne et al., 2013). The CMIP5 RCP4.5 simulations have both natural and anthropogenic forcing, where in the representative concentration pathways have been and were designed to have a top of the atmosphere radiation at 4.5 Wm-2 at the end of 2100 and CO_2 concentration stabilizes at 543 ppmv in 2150. Global CO_2 concentration is directly prescribed in the simulations from 1886 to 2095 for computing radiative budget (Krishnan et al., 2016).

2.2. Model validation

In this paper, the region bounded by the latitudes from 25.5° N through 28.5° N, and longitudes from 92.5° E through 94.5° E is referred to as the northeast India (NEI) for the purpose of statistical analysis such as the area-averaging, etc. The downscaled historical simulations are validated by comparing the mean model climatology with observed precipitation and temperature patterns. To facilitate this, the observed datasets are resampled into 0.5° resolutions using a bilinear interpolation method. We explore the interannual variability and climate change of the seasonal rainfall and temperature during the two important seasons in the NEI, namely, the monsoon season (JJAS) and the winter season (DJF).

To have an estimate of the future climate change in any climatic parameter C, we subtract the simulated (LMDZ, MPI, GFDL, CNRM and ACCESS) historical climatology of the parameter (precipitation and maximum and minimum temperature), say 'C_{hist}', from the corresponding climatology from the RCP4.5 simulations, say 'C_{RCP}' i.e., $\Delta C = C_{RCP} - C_{hist}$.

In this study, we apply a linear trend analysis, by the method of Least square linear fit (Jhajhariaa and Singh, 2011; Jain and Kumar, 2012 and Dubey and Krishnakumar, 2014), on the simulated and observed data of temperature and precipitation, as necessary. The statistical significance of the identified trend is evaluated using the Mann Kendall (M-K) trend test and Student *t*-test. The M-K test is a non-parametric test for identifying trend in time series data, and extensively used in climate studies in checking spatial variation and temporal deviation of any climatic series (Kumar et al., 2010; Jain and Kumar, 2012; Jain et al., 2012; Laskar et al., 2014 and Chinchorkar et al., 2015). This statistics is used to test the null hypothesis such that no trend exists. The presence of a statistically significant trend is evaluated using the Z value. If the computed value of $|Z| > Z_{\alpha/2}$, the null hypothesis (H_0) is rejected at α level of significance in a two-sided test. A very high positive value of S indicates increasing trend and a very low negative value of S indicates decreasing trend (Laskar et al., 2014). In this study, the M-K test is run at 5% level of significance on time series data. Further details of the M-K test are available in the A.2. Further, the observed and simulated teleconnections with the ENSO have been estimated by using the well-known Nino3.4 index to represent the ENSO activity. The Nino 3.4 index is obtained by area-averaging, the SST anomalies over the 5° N–5° S and 120° W–170° W. We use linear correlation analysis to establish any association of the ENSO events with the NEI climate. Last but not the least, extremes of precipitation and, maximum and minimum temperature of both historical and future projections have been estimated with the help of histogram.

3. Results and discussion

In this section, we study the observed seasonal rainfall and temperature climatologies in the NEI for the 1970–2005 period and the respective long term linear trends therein. We also evaluate the fidelity of the downscaled historical simulations using the observational results. Then we analyze the results from the five downscaled future scenarios, namely, the RCP4.5 simulations (LMDZ, MPI, GFDL, CNRM and ACCESS) available for the period of 2011–2060, in order to decipher the projected climate change in the northeast. The teleconnections of precipitation and, maximum and minimum temperature with the ENSO index known as Nino 3.4 are also studied. And extremes of JJAS and DJF for precipitation, maximum and minimum temperature for both historical and future projections are analyzed in the last part.

3.1. Climatology for JJAS historical simulation from 1970 to 2005

Fig. 1(a) is an effort to validate the simulated, JJAS climatology of precipitation ($RF\text{-}_{JJAS}$) for the period of 1970–2005 with that from the IMD observations and the Aphrodite data. We find from spatial distribution of the observed climatological $RF\text{-}_{JJAS}$ that it varies from 9 to 22 mm, Aphrodite data ranges from 3 to 13 mm and model data range from 3 to 18 mm. However, as it can be seen that the corresponding climatological $RF\text{-}_{JJAS}$ distribution from the Aphrodite datasets as well as those from all models except the LMDZ model show the magnitude of the climatological rainfall increasing from the north towards the south west, and in LMDZ climatology, the $RF\text{-}_{JJAS}$ increases towards the south

[1] Note that the LMDZ is an atmospheric general circulation model, but with a 0.5° resolution in the Indian region. However, for simplicity, we refer to that as a regional model.

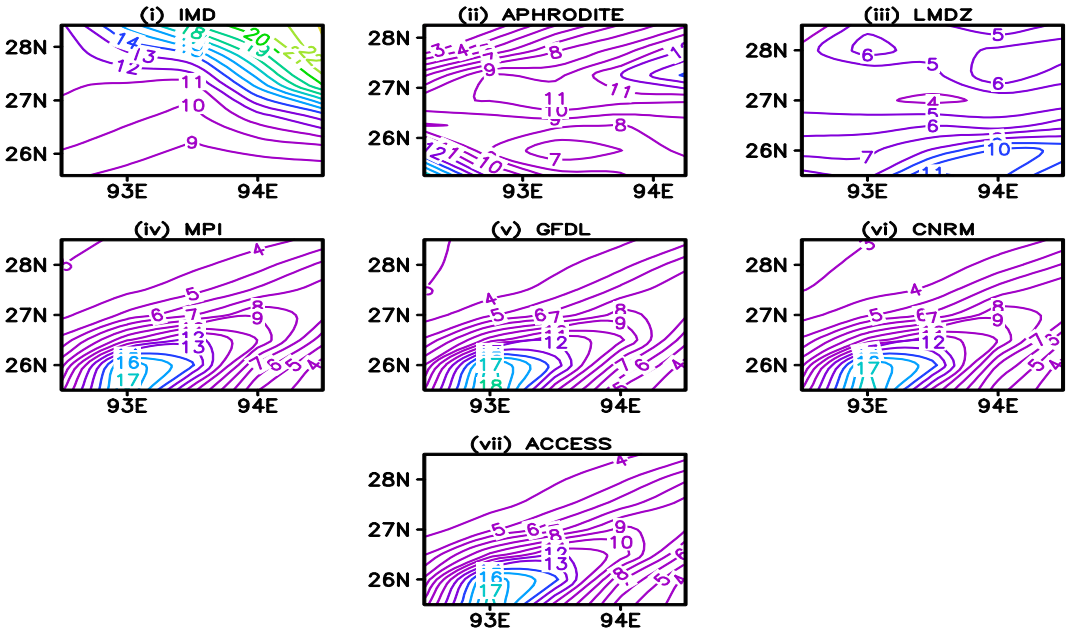

Fig. 1. (a) Spatial distributions of JJAS climatology of precipitation (mm) during 1970–2005 (historical) for (i) IMD, (ii) APHRODITE data, and climate model data from Cordex South Asia: (iii) LMDZ, (iv) MPI, (v) GFDL, (vi) CNRM and (vii) ACCESS over North East Region.

east. Notwithstanding such discrepancy in the gradients, the range of climatological RF-$_{JJAS}$ across the observational datasets as well as models is not much different.

The observed climatological $T_{Max\text{-}JJAS}$ varies from 30.6 °C to 32 °C (Fig. S1, it can be found in supplementary figures and please note that all the figures with S denote the supplementary figures); the maximum $T_{Max\text{-}JJAS}$ occurs approximately in the central north-east, and increases from the west to the east. The spatial distribution of the climatological $T_{Max\text{-}JJAS}$ across the NEI from the CRU reanalysis, ranging from 19 °C to 20.5 °C, decreases in the centre. The CRU data and each model exhibit a relatively broad range of climatologies ($T_{Max\text{-}JJAS}$) across the NEI as compared to the observed data, so the ranges are shown made differently as appropriate. The simulated climatology of the ($T_{Max\text{-}JJAS}$) by various models is lower with different spatial distribution than the observations, with the simulated climatological values varying from 12 °C to 29 °C across the region in models. The LMDZ model shows an increasing $T_{Max\text{-}JJAS}$ from northwest towards the south with the maximum values occur in the centre. The rest of the models show an increasing $T_{Max\text{-}JJAS}$ from northwest towards the south east.

The models also underestimate the climatology of minimum temperature in JJAS (TMin-JJAS) as compared to the CRU reanalysis (Fig. S2), with a simulated range of 3 °C to 22 °C as against the corresponding values of 28 °C to 32 °C in observed data varies from 19 °C to 20.2 °C from the CRU reanalysis datasets.

3.2. Climatology for DJF historical simulation from 1970 to 2005

Fig. S3 shows the DJF climatology of precipitation (RF-$_{DJF}$) for the period 1970–2005, derived from the IMD, Aphrodite and model datasets. The magnitude of the RF-$_{DJF}$ across the NEI ranges between 0.6 and 1.6 mm, with Aphrodite datasets ranging from 0.2 to 0.8 mm and the models, ranging from 0.5 to 3.8 mm, also capturing the relatively low seasonal climatological rainfall during the DJF season (Fig. S3) as compared to the JJAS season (Fig. 1a).

The DJF climatology of maximum temperature ($T_{Max\text{-}DJF}$) in IMD observations varies from 23.4 °C to 24.4 °C (Fig. S4), and increases from the south to north of the NEI. The CRU data ranges from 19 °C to 21.2 °C, with a decrease $T_{Max\text{-}DJF}$ in the centre. The models underestimate the climatological $T_{Max\text{-}DJF}$ in the NEI with the simulated $T_{Max\text{-}DJF}$ ranging from 1 °C to 15 °C.

The simulated winter climatological minimum temperatures ($T_{Min\text{-}DJF}$) in Fig. S5 exhibit a range of values from 10.4 °C to 11 °C, which are relatively nearer to that from the IMD datasets, with CRU data having higher ($T_{Min\text{-}DJF}$).

Table 1 shows the difference in the climatological means of observed data sets from those of the simulated rainfall and, maximum and minimum temperature from 1970 to 2005. In support to the above spatial climatological analysis, the models show a lower means than the observations datasets.

3.3. Seasonal mean cycle for historical simulation from 1970 to 2005

In Fig. 2(a), mean seasonal cycle of precipitation for the 1970 to 2005 from the two observed datasets are shown, along with those from each model. All the datasets show a seasonal evolution similar to observations, with the simulated precipitation from most of the models peaking in July. However, the simulated precipitation from the LMDZ, peaks in the month of August, and the simulated magnitude is in general much less than that from the IMD or Aphrodite datasets. To sum up, the models seem to capture the observed seasonal cycle of mean of precipitation qualitatively for the study region.

The simulated mean seasonal cycles of the maximum and minimum temperatures in the NEI are also qualitatively similar to observations

Table 1
Mean climatological value for observation and model data (1970–2005).

Mean climatology							
	Precipitation		Maximum temperature			Minimum temperature	
	JJAS	DJF		JJAS	DJF	JJAS	DJF
IMD	12.5	0.8	IMD	31.6	24.0	24.1	10.9
APHRODITE	8.7	0.6	CRU	19.6	19.7	19.6	19.7
LMDZ	6.1	2.7	LMDZ	24.6	10.5	17.7	1.6
MPI	7.1	1.2	MPI	17.5	3.2	8.1	−7.1
GFDL	7.0	1.3	GFDL	17.5	2.6	8.2	−7.5
CNRM	6.9	1.3	CNRM	17.7	2.9	8.4	−7.4
ACCESS	7.2	1.1	ACCESS	17.4	3.3	8.1	−6.9

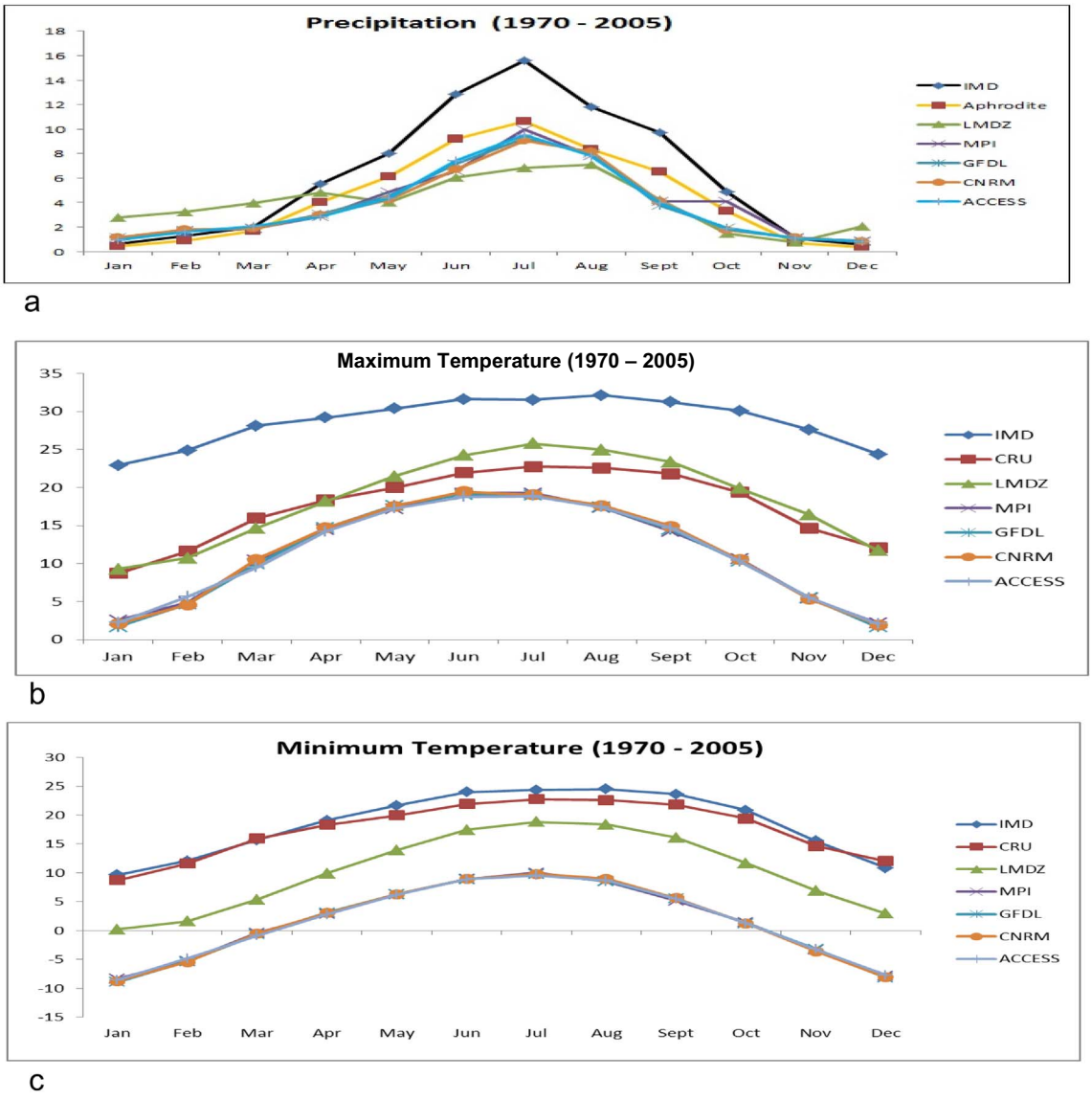

Fig. 2. (a). Seasonal mean cycle of precipitation data (mm) from IMD (observed data), Aphrodite, and Cordex South Asia model data (LMDZ, MPI, GFDL, CNRM and ACCESS) for the period 1970 to 2005.
(b). Seasonal mean cycle of maximum temperature data (°C) from IMD (observed data), CRU Reanalysis and Cordex South Asia model data (LMDZ, MPI, GFDL, CNRM and ACCESS) for the period 1970 to 2005.
(c). Seasonal mean cycle of minimum temperature data (°C) from IMD (observed data), CRU reanalysis and Cordex South Asia model data (LMDZ, MPI, GFDL, CNRM and ACCESS) for the period 1970 to 2005.

(Fig. 2b and c); though the simulated magnitudes are much lower than those from the observations.

3.4. Spatial plot of trend analysis JJAS for historical data from 1970 to 2005

In Fig. S6, the trend in the RF-$_{JJAS}$ season for the period 1970 to 2005 from each precipitation dataset used is plotted. The IMD data shows a rising trend from the rest of the datasets. While the RF-$_{JJAS}$ from the IMD exhibits an increasing trend of about 0.5 mm/year in the western NEI and decreasing trend of about 0.6 mm/year in the eastern portion of the NEI, the APHRODITE datasets indicate a weaker but increasing trend in a larger portion of the NEI. All models, in general, qualitatively reproduce the increasing trend in the western NEI, through with weaker magnitudes. The MPI and GFDL models and the ACCESS model somewhat weakly, simulate a negative trend in pockets, which is not seen in observations.

A trend analysis of $T_{Max\text{-}JJAS}$ maximum temperature from 1970 to 2005 is plotted in Fig. (S7) where the IMD data shows a positive trend 0.015 °C/year increasing towards the south. The CRU data, on the other hand, shows higher magnitude of trend than the IMD and an increasing trend towards the centre. Models other than the MPI and ACCESS models show a positive trend.

A trend of 0.02 °C/year in the $T_{Min\text{-}JJAS}$ is shown from the IMD datasets (Fig. S8), increasing towards the west from the east. On the contrary, the CRU datasets show an increasing trend towards the centre. The LMDZ model shows a higher magnitude of trend than the rest of the datasets, with an increasing trend of 0.05 °C/year. The MPI, GFDL and CNRM models are more or less similar with a lower positive trend in the central portion. The ACCESS model shows an increasing trend towards the north.

3.5. Spatial plot of trend analysis DJF for historical data from 1970 to 2005

Fig. (S9) shows the trends in the observed and simulated RF-$_{DJF}$ in

Table 2
Significance tests using Mann-Kendall and Student *t*-test for maximum temperature data from the IMD, NCEP and climate model data for the period 1970–2005.

Data used	Mann-Kendall test		Student *t*-test			Nature of the trend
	Z value & α value	Statistic value (S)	*p*-Value	t-Value	Trend value	
JJAS						
LMDZ	4.19 > 1.96	308	0.00 < 0.05	5.53 > 2	1.14	Increasing trend & **significant**
GFDL	2.39 > 1.96	176	0.01 < 0.05	2.92 > 2	1.07	Increasing trend & **significant**
ACCESS	2.86 > 1.96	210	0.01 < 0.05	2.61 > 2	1.25	Increasing trend & **significant**
DJF						
LMDZ	3.79 > 1.96	290	0.00 < 0.05	4.52 > 2	2.35	Increasing trend & **significant**
CNRM	2.33 > 1.96	178	0.05 = 0.05	2.02 > 2	1.22	Increasing trend & **significant**
ACCESS	2.22 > 1.96	170	0.02 < 0.05	2.39 > 2	1.28	Increasing trend & **significant**

the NEI for the period 1970 to 2005 where all the datasets show a similar increasing trend in most of the region. The IMD data shows an increasing trend of 0.01 mm/year towards the southwest of the region, and a decreasing trend of 0.4 mm/year towards the north eastern. The Aphrodite data shows a positive trend in most of the regions. Rest of the models except for the LMDZ shows a similar positive trend.

The IMD datasets show an increasing trend in the $T_{Max\text{-}DJF}$ from northwest towards the south east; with respective values of 0.03 °C/year and 0.06 °C/year (Fig. S10). CRU datasets shows a higher trend than the IMD datasets. Only the LMDZ model shows a very high positive trend of 0.06 °C/year increasing towards the north. GFDL and CNRM models show an increasing positive trend towards the east while decreasing at central east. MPI model shows an increasing trend in the central portion while the ACCESS model shows a decreasing trend in the central portion. All the datasets show a positive trend.

Fig. (S11) shows the trend analysis of $T_{Min\text{-}DJF}$ minimum temperature, from which it is clear that the IMD datasets show an increasing trend of 0.04 °C/year towards the west while CRU data shows a higher trend as compare to the IMD data. Here also, the LMDZ model shows a higher magnitude of trend of 0.07 °C/year increasing towards the north and south while decreasing in the centre. The CNRM and ACCESS models show an increasing trend towards the central east and decreasing trend at the west, opposite to that in the MPI model. The ACCESS model shows an increasing trend in the central east and decreases at the west.

From the above discussion, is it clear that there is some agreement between the IMD and Aphrodite datasets as far as the location of highest and lowest trends in the rainfall, particularly during summer monsoon is concerned. However, the same cannot be told about the agreement between the IMD datasets and CRU datasets in relation to the spatial distribution of the trends in temperature. This is not so surprising given that the CRU datasets are not observational datasets, but model forecasts constrained by the observations. We also note that the models are not up to simulating the spatial distribution of the trends well. As the region is well known for its high convective rainfall associated with complex orography along with relatively high mountains and rainfall processes of the monsoon system, the interpolation and calibration algorithms could contribute to the uncertainty. However, if the historical simulations from various models can at least replicate the area-averaged trends in the climate parameters over the NEI, we can have a qualitative confidence in their future projections. In the next section, we precisely explore this aspect.

3.6. Area-averaged trend analysis from the observations and models for the 1970 to 2005 period

In this section, we report results from the analysis of the area-averaged trends in rainfall and temperature in the NEI region. The significance of these tests was evaluated using both Mann-Kendall and Student's *t*-test. We find that the IMD and Aphrodite datasets show, respectively, increasing and decreasing trends, which are however, not statistically significant (not shown as all the results show insignificant). Insignificant decreasing or no trend in the summer monsoon precipitation of NEI, as seen from some stations observations in the NEI has been also reported by Jain et al., 2012; Laskar et al., 2014 and Dash et al., 2015. All the model simulations also simulate only insignificant trends.

Further, both IMD and Aphrodite datasets only show a decreasing but statistically insignificant trend in the area averaged rainfall during the DJF ($RF\text{-}_{DJF}$) season in the NEI. The area-averaged trends in the corresponding $RF\text{-}_{DJF}$ from various CORDEX models are also seen to be insignificant, though the GFDL and CNRM models show an increasing trend.

Though the nature of trends in the rainfall is insignificant in all the data sets, it indicates a decline in the rainfall over NEI, in tandem with such a signal in the summer monsoon rainfall in rest of India (Krishnan et al., 2016). On longer time scales, the warmer tropical ocean, especially the central eastern Pacific and the western Indian Ocean are suggested to play a role in weakening the monsoon (Roxy et al., 2015).

Only the significant results are shown in the Table 2. The time series of the area-averaged JJAS maximum temperature and that for the DJF season, from the IMD datasets for the period of 1970 to 2005 show an increasing but statistically insignificant trends. Growing population accompanied by massive urbanization, changes in land use, enormous highway development, increases in deforestation, biomass burning, fossil fuel consumption and increasing atmospheric concentrations of greenhouse gases are suspected to be the cause of the changes in temperature (Kothyari and Singh, 1996; Jhajhariaa and Singh, 2011).

Notably, the CRU datasets for both the seasons show an insignificant increasing trend and also, all the models successfully reproduce the observed increasing trends in the area-averaged seasonal maximum temperatures, through most of the simulated trends are statistically significant.

Importantly, we find statistically significant increasing trends in the area-averaged minimum temperature over the NEI during both summer and winter seasons over the period 1970 to 2005 (Table 3). It is intriguing that only the minimum temperature shows a statistically significant increasing trend, while the rainfall trends, though decreasing, are not significant.

From all these results, we can summarize that the downscaled CORDEX South-Asia datasets are successful in capturing the area-averaged seasonal cycles of rainfall and temperature observed during 1970–2005, and are also capable of capturing the corresponding trends, at least qualitatively. However, the climatological spatial distribution and the local long term trends are not well captured, and are also subject to the uncertainties in the observations. Being an orographic region, uncertainty between datasets is largest in North East India (Kulkarni et al., 2013 and Prakash et al., 2014).

3.7. Teleconnections of the historical data (1970–2005) with Nino 3.4

Table S1 shows the teleconnections results ENSO, which is

Table 3
Significance tests using Mann-Kendall and Student *t*-test for minimum temperature data from the IMD and climate model data for the period 1970–2005.

Data used	Mann-Kendall test		Student *t*-test			Nature of the trend
	Z value & α value	Statistic value (S)	*p*-Value	t-Value	Trend value	
JJAS						
IMD	3.26 > 1.96	240	0.00 < 0.05	4.48 > 2	0.63	Increasing trend & **significant**
LMDZ	4.79 > 1.96	352	0.00 < 0.05	7.92 > 2	1.32	Increasing trend & **significant**
MPI	2.48 > 1.96	182	0.03 < 0.05	2.92 > 2	0.61	Increasing trend & **significant**
GFDL	2.04 > 1.96	150	0.03 < 0.05	2.23 > 2	0.66	Increasing trend & **significant**
ACCESS	3.19 > 1.96	234	0.02 < 0.05	2.45 > 2	0.85	Increasing trend & **significant**
DJF						
IMD	3.92 > 1.96	300	0.00 < 0.05	4.59 > 2	1.19	Increasing trend & **significant**
LMDZ	4.15 > 1.96	318	0.00 < 0.05	5.42 > 2	2.97	Increasing trend & **significant**
MPI	3.22 > 1.96	246	0.00 < 0.05	3.24 > 2	1.59	Increasing trend & **significant**
GFDL	2.17 > 1.96	166	0.05 = 0.05	2.99 < 2	0.75	Increasing trend & **significant**
CNRM	2.30 > 1.96	176	0.03 < 0.05	2.33 > 2	1.11	Increasing trend & **significant**
ACCESS	3.16 > 1.96	242	0.00 < 0.05	3.70 > 2	1.62	Increasing trend & **significant**

represented by the well-known NINO3.4 index, with precipitation, maximum and minimum temperature parameters from all relevant the datasets used in this study from the IMD, Aphrodite, CRU and all the models datasets for historical period from 1970 to 2005. The results of this study suggest that the ENSOs do not have any statistically significant impacts on the NEI precipitation and temperature, be it summer or winter, for the period.

3.8. Seasonal mean cycle for simulated future precipitation, maximum and minimum temperature data for the period 2011 to 2060

The individual model RCP4.5 projections of the seasonal cycle of precipitation for the 2011 to 2060 (Fig. 3a) indicate an evolution similar to the corresponding historical cycle. A majority of models, however, indicate a slight decrease or no change in the magnitude of the summer monsoon rainfall, except the projection from the CNRM showing a moderate increase in July precipitation. Based on these results as well as an analysis of the spatial distribution of the simulated precipitation (to be discussed in the next paragraph), we can sum up that the models project slight or no decrease in the rainfall over the NEI in future.

The simulated seasonal cycles of maximum and minimum temperature from the RCP4.5 shows an unchanged evolution, but models also project a substantially increased in the maximum and minimum temperatures (Fig. 3b & c) relative to the corresponding historical simulations which indicates a rise in the temperature in the future over the NEI.

3.9. Simulated JJAS future climatology (RCP4.5) from 2011 to 2060

The simulated JJAS climatology of precipitation ($RF\text{-}_{JJAS}$) from the RCP4.5 projections for the 2011–2060 is presented in Fig. (S12), and the excess or deficit as compared to the corresponding historical simulations of is shown in Fig. 1a. We find from Figs. S12 and 4a that the future projection of $RF\text{-}_{JJAS}$ from each CORDEX South-Asia model is not significantly different from the corresponding historical simulations (Fig. 1a), except for a weak decrease seen in simulations of a model or two. The $RF\text{-}_{JJAS}$ of LMDZ model spatially ranges from 5 to 11 mm while in the rest of the models varies from 3 to 19 mm.

Notably, (the spatial distribution of $T_{Max\text{-}JJAS}$ and $T_{Min\text{-}JJAS}$) in all the models in Fig. S13 and S14 show an increasing magnitude and are also warmer than the corresponding historical simulations (also match with Fig. 4b and c) across the NEI as compared to the respective historical simulation, with the temperature values ranging from 13 °C to 30 °C and 5 °C to 23 °C for minimum temperature.

3.10. Simulated DJF future climatology (RCP4.5) from 2011 to 2060

The DJF climatology of precipitation ($RF\text{-}_{DJF}$) in all the models does not show much change in the future projection (Fig. S15), with values ranging from 0.6 to 3.2 mm, which is also seen in Fig. 5a, though all the models are not simulating the same result, the range of $RF\text{-}_{DJF}$ is seen declining in the future projection.

All the models also project an increased $T_{Max\text{-}DJF}$ (Figs. S16 and 5b), with the values varying from 2 °C to 17 °C. Spatial distributions of $T_{Max\text{-}DJF}$ from the analyzed in all CORDEX South-Asia projections, the models are similar to those from the historical simulations (Fig. S4).

The projected minimum temperatures for DJF season (Figs. S17 and 5c) also increases than the corresponding historical simulations (Fig. S5). The future projected DJF climatology in the NEI range from −10 °C to 8 °C.

3.11. Area-averaged Trends in projected climate in the NEI for the period of 2011 to 2060

Table 4 shows that the JJAS precipitation signals for the 2011 to 2060 period as simulated in the LMDZ and CNRM models show a significantly increasing trend. The ACCESS model projects an increasing but statistically insignificant trend in summer precipitation during the above period. On the other hand, the MPI and GFDL models show an insignificant decreasing trend. The projected DJF precipitation in all the models except the ACCESS model shows an insignificantly decreasing trend. The ACCESS model simulates a weak increasing trend. Only the significant results are shown in the table.

Interestingly, four out of five future simulations project a statistically significant increasing trend in summer maximum temperature (Table 5), while all of them project a statistically significant increasing trend in minimum temperatures (Table 6).

The significant increasing trend in the maximum and minimum trend is also projected for the DJF season (Tables 5 & 6). Thus, is clearly despite the fact that, the projected models do not show quantitatively similar results, qualitatively there is a good agreement, particularly for the temperature. That is, as per the RCP4.5 simulations, the DJF precipitation is expected to further decline while both maximum and minimum temperature are likely to increasing further rapidly. However, there is considerable inter-model uncertainty in the future summer monsoon rainfall in the NEI.

3.12. Extremes analysis for JJAS and DJF seasons for historical and future projections for precipitation, maximum temperature and minimum temperature

In the Fig. 6a & b, histograms of observed and simulated JJAS

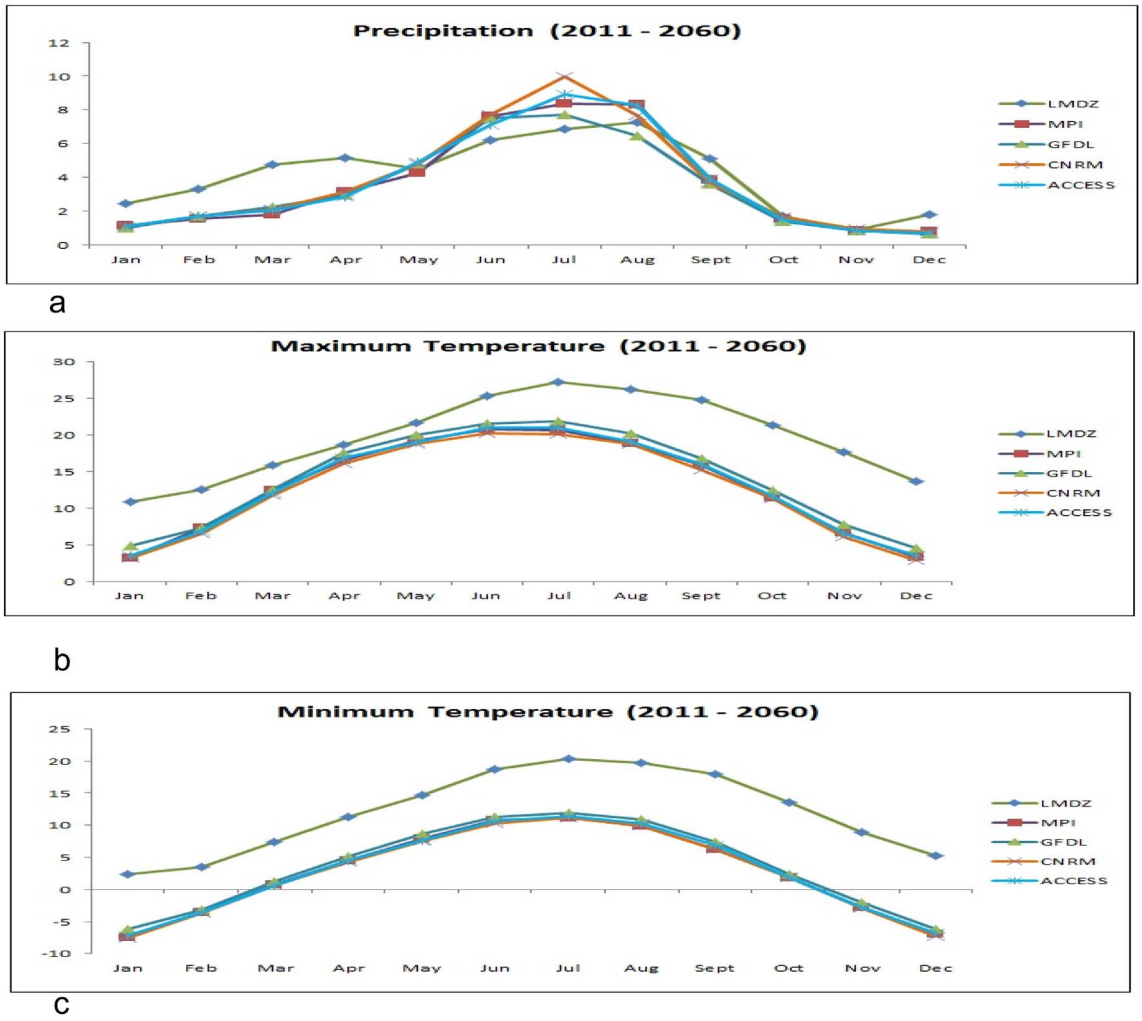

Fig. 3. (a). Seasonal mean cycle of precipitation data (mm) from Cordex South Asia model data (LMDZ, MPI, GFDL, CNRM and ACCESS) for the period 2011 to 2060. (b). Seasonal mean cycle of maximum temperature data (°C) from Cordex South Asia model data (LMDZ, MPI, GFDL, CNRM and ACCESS) for the period 2011 to 2060. (c). Seasonal mean cycle of minimum temperature data (°C) from Cordex South Asia model data (LMDZ, MPI, GFDL, CNRM and ACCESS) for the period 2011 to 2060.

monthly mean rainfall over the NEI for the historical period from 1970 to 2005, and simulated future projections from 2011 to 2060 are presented. While there are four heaviest rainfall monsoon seasons with rainfall of 23 mm/day in NEI as per the IMD datasets, the APHRODITE datasets indicate (Fig. 6a) five heaviest rainfall months with rainfall amounting to 15 mm/day. Except the LMDZ model, all other models simulate the heaviest seasonal rainfall of 15 mm/day, and only two models simulate at least four such extreme rainfall months (Fig. 6a); The LMDZ model simulates only one heaviest rainfall month, with the magnitude of the rainfall amounting to 11 mm/day.

The frequency of the heaviest monthly-mean rainfall months in general increases in the simulated future projections for 2011–60, except in those from the GFDL which fall from 15 to 13 (Fig. 6b). Further, it is also to be noted that the magnitude of the heaviest monthly rainfall decreases (increases) in two (one) models by about 2 mm/day (4 mm/day). Importantly, Fig. 6a and b show that the total number of 'low rainfall' months (arbitrarily defined as rainfall < 7 mm/day) have increased quite substantially, with the range of increase being 34%–42%. It is, however, to be noted that the frequencies of simulated low rainfall event months for the historical period are heavily overestimated as compared to those from the corresponding IMD frequency.

Histograms of observed and simulated DJF monthly mean rainfall over the NEI for the historical period from 1970 to 2005, and simulated future projections from 2011 to 2060 are presented in the Figs. S18 & S19. The number of heaviest winter monsoon rainfall months is relatively low as corresponding to the summer monsoon season, as can be seen from both IMD and Aphrodite datasets (Fig. 6a & 6b). The models in general also qualitatively reproduce the difference. However, the heaviest rainfall simulated by the in LMDZ model of 7 mm/day in simulated historical period is noticeably high as compared to the 4.5 mm/day. In future projections, the frequency of simulated heavy rainfall months increases in all the model projections except GFDL and CNRM.

The extreme events of JJAS maximum temperature for the historical period from 1970 to 2005 and for future projections from 2011 to 2060 are shown the Figs. S20 & S21. The observation data from IMD recorded 39 highest maximum temperature months with 34 °C/day. The CRU and all the models record somewhat lower maximum temperature than the observation data, ranging from 22 °C to 28 °C (Fig. S20). The simulated highest maximum monthly temperature in the future projections relatively increases, and ranges between 24 °C to 32 °C with LMDZ (Fig. S21).

In the Figs. S22 & S23, the extreme months of maximum temperature for DJF season are shown for historical period (1970–2005) and future projections (2011–2060). IMD records show 30 months of the highest monthly maximum temperature of 30 °C/day during the historical period. The CRU records show monthly mean highest temperature 27 °C/day and all the models show a highly underestimated maximum temperature ranging from 9 °C to 15 °C. Even though the highest maximum temperature increases in the future projections, the

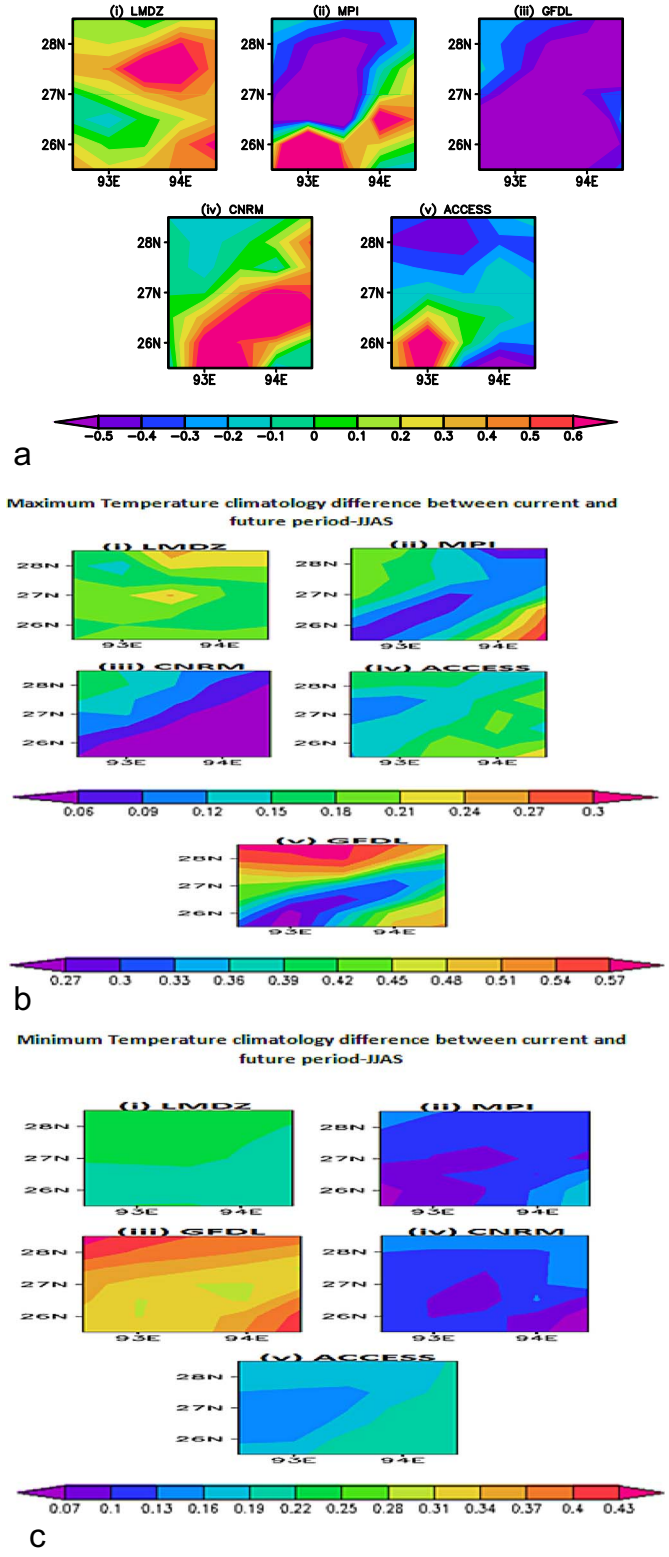

Fig. 4. (a). Climatology difference for precipitation (mm) between current and future period for JJAS for model data, namely, (i) LMDZ, (ii) MPI, (iii) GFDL, (iv) CNRM and (v) ACCESS.
(b). Climatology difference for maximum temperature (°C) between current and future period for JJAS for model data Cordex South Asia: (i) LMDZ, (ii) MPI, (iii) CNRM, (iv) ACCESS and (v) GFDL. Separate color bar has been plotted because of the large difference in the range of climatology in GFDL model.
(c). Climatology difference for minimum temperature (°C) between current and future period for JJAS for model data Cordex South Asia: (i) LMDZ, (ii) MPI, (iii) CNRM, (iv) GFDL and (v) ACCESS.

maximum number of events with highest frequency decreases.

Figs. S24 & S25 show the minimum temperature for JJAS season for historical period (1970–2005) and future projections (2011–2060). The observation data and CRU datasets record a minimum monthly temperature of 27 °C/day. The minimum temperature in all the models is underestimated, with a range of 12 °C to 21 °C across the models. While the simulated frequency of highest minimum temperature in the three future projections increases, only models (LMDZ and GFDL) project a decreasing number of highest minimum temperature events.

In the case of the DJF season, for the historical period (1970–2005), the observation data records minimum temperatures of 16 °C/day and CRU being 26 °C/day. However all the models underestimate the minimum temperature, with a range from 6 °C to −2 °C. The highest minimum temperature in the future projections increases as compared to the corresponding historical simulations.

4. Conclusions

This work studies the climate trends in the northeast India (NEI) using observations during 1970–2005, a period for which five high resolution (50 km) climate simulations, known as historical simulations, are available under the aegis of CORDEX South Asia. The observation datasets we use are gridded data of rainfall and, maximum and minimum temperature from IMD at 1° × 1° resolution (Rajeevan et al., 2005, 2008, 2008), and Aphrodite datasets at 0.5° × 0.5° resolution (Yatagai et al., 2012), along with mean temperature from CRU TS v. 4.00 (0.5° × 0.5° resolution) from 1970 to 2005. Further, using the historical and future climate change projections of the CORDEX South Asia, we estimate the possible future climate change under the RCP4.5 conditions, which is designed to reflect a scenario of moderate anthropogenic emissions from 2011 to 2060. These five regional climate model dataset are generated by the LMDZ, MPI, GFDL, CNRM and ACCESS models.

We find that the seasonal cycle of rainfall and temperature of the NEI are in conformation with that over the rest of the Indian region. There is a reasonable agreement in the area-averaged seasonal cycle and climatology of the rainfall in NEI between the IMD and Aphrodite datasets. However, we find that there are differences in the locations of highest and lowest climatological rainfall and temperatures, maximum trend region, etc. during the summer monsoon. Such a mismatch of location is also seen in the models. Such a discrepancy across the observations/reanalysis and model datasets is seen in the spatial distribution of the maximum and minimum temperatures also. Therefore, one needs to be mindful of this limitation while using these observations and model results in local climate change adaptation planning.

Interestingly, there is a reasonable synergy across the observations and models when the climate signals are area-averaged over the NEI. We find a weak and statistically insignificant decreasing trend in the area-averaged summer monsoon rainfall in the NEI. The IMD observations also show an increasing minimum temperature trend of 0.63 °C and 1.19 °C in 36 years that is statistically significant for both the summer and winter seasons respectively. While the maximum temperatures have also been increasing, the trend is not statistically significant. The area-averaged trends, particularly in the summer monsoon, are in general agreement with those reported in various earlier studies that are based on a few selected stations (Jain et al., 2012; Laskar et al., 2014 and Dash et al., 2015).

Importantly, the area-averaged rainfall and temperatures from the historical simulations also qualitatively reproduce the observed trends, though they overestimate the statistical significance in some instances. This tells us that we can have some confidence in the area-averaged trends in future climate change projections for the NEI. The future projections suggest that there will be a significant increasing trend in the minimum temperature (ranging from 0.71 °C/50 years to 2.6 °C/50 years for summer and 1.15 °C/50 years to 2.61 °C/50 years for winter season) and maximum temperature (0.33 °C/50 years to

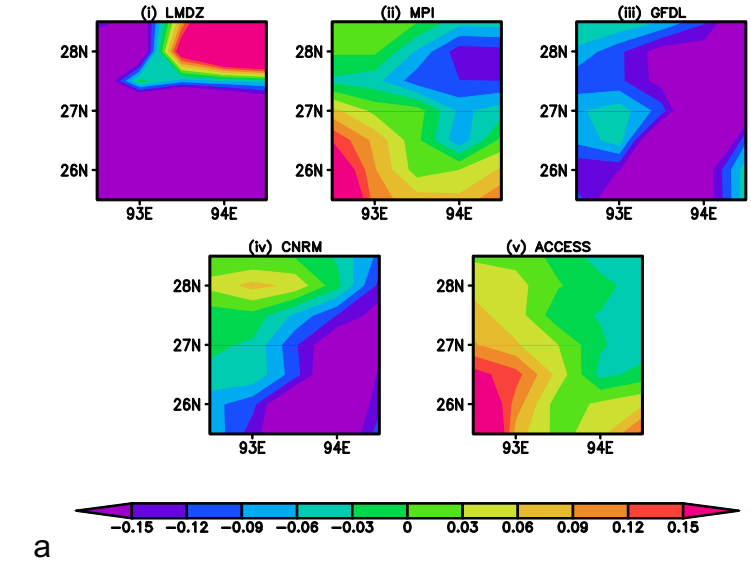

a

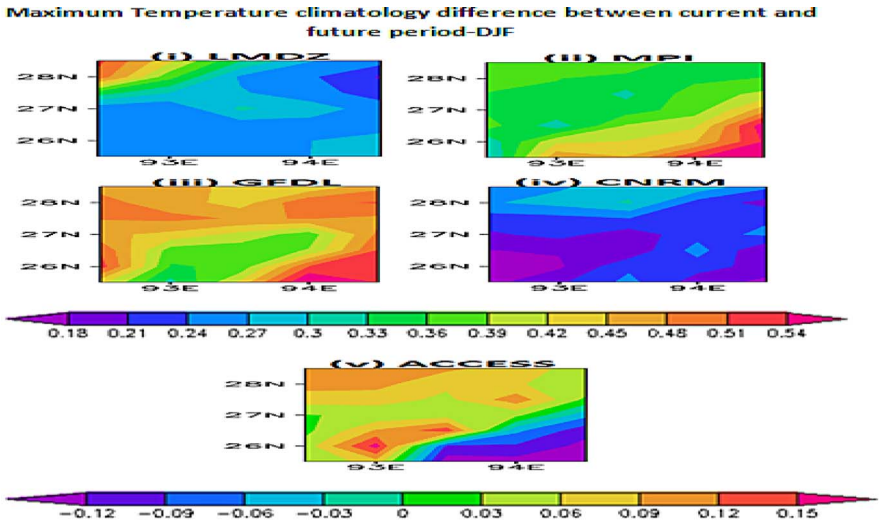

b

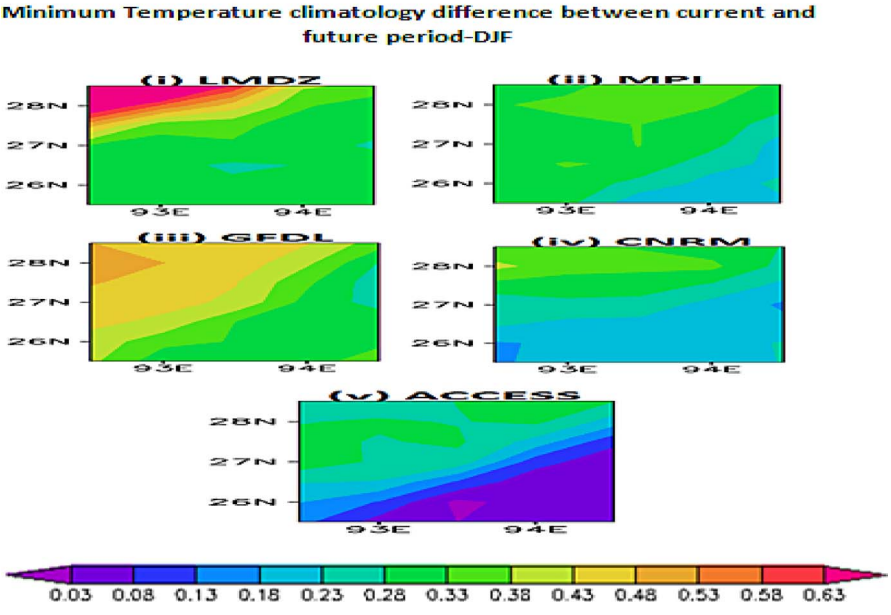

c

Fig. 5. (a). Climatology difference for precipitation (mm) between current and future period for JJAS for model data Cordex South Asia: (i) LMDZ, (ii) MPI, (iii) GFDL, (iv) CNRM and (v) ACCESS.
(b). Climatology difference for maximum temperature (°C) between current and future period for DJF for model data Cordex South Asia: (i) LMDZ, (ii) MPI, (iii) CNRM, (iv) GFDL and (v) ACCESS. Separate color bar has been plotted because of the large difference in the range of climatology in ACCESS model.
(c). Climatology difference for minimum temperature (°C) between current and future period for DJF for model data Cordex South Asia: (i) LMDZ, (ii) MPI, (iii) CNRM, (iv) GFDL and (v) ACCESS.

Table 4
Significance tests using Mann-Kendall and Student *t*-test for precipitation data from the climate model data for the period 2011–2060.

Mann-Kendall test			Student *t*-test			
Data used	Z value & α value	Statistic value (S)	*p*-Value	t-Value	Trend value	Nature of the trend
LMDZ	3.17 > 1.96	379	0.00 < 0.05	3.10 > 2	0.67	Increasing trend & **significant**
CNRM	1.97 > 1.96	235	0.04 < 0.05	2.07 > 2	1.08	Increasing trend & **significant**

Table 5
Significance tests using Mann-Kendall and Student *t*-test for maximum temperature data from the climate model data for the period 2011–2060.

Data used	Mann-Kendall test		Student *t*-test			Nature of the trend
	Z value & α value	Statistic value (S)	*p*-Value	t-Value	Trend value	
JJAS						
LMDZ	5.73 > 1.96	685	0.00 < 0.05	7.01 > 2	1.4	Increasing trend & **significant**
MPI	3.29 > 1.96	393	0.00 < 0.05	4.24 > 2	1.13	Increasing trend & **significant**
GFDL	6.25 > 1.96	747	0.00 < 0.05	8.84 > 2	2.86	Increasing trend & **significant**
ACCESS	3.81 > 1.96	455	0.00 < 0.05	4.07 > 2	1.07	Increasing trend & **significant**
DJF						
LMDZ	4.47 > 1.96	551	0.00 < 0.05	5.24 > 2	1.96	Increasing trend & **significant**
MPI	3.63 > 1.96	447	0.00 < 0.05	4.27 > 2	2.71	Increasing trend & **significant**
GFDL	4.41 > 1.96	543	0.00 < 0.05	4.84 > 2	3.01	Increasing trend & **significant**
CNRM	3.27 > 1.96	403	0.00 < 0.05	7.19 > 2	1.89	Increasing trend & **significant**

Table 6
Significance tests using Mann-Kendall and Student *t*-test for minimum temperature data from the climate model data for the period 2011–2060.

Data used	Mann-Kendall test		Student *t*-test			Nature of the trend
	Z value & α value	Statistic value (S)	*p*-Value	t-Value	Trend value	
JJAS						
LMDZ	7.25 > 1.96	867	0.00 < 0.05	11.78 > 2	1.66	Increasing trend & **significant**
MPI	3.89 > 1.96	465	0.00 < 0.05	4.27 > 2	0.95	Increasing trend & **significant**
GFDL	6.92 > 1.96	827	0.00 < 0.05	10.44 > 2	2.6	Increasing trend & **significant**
CNRM	2.68 > 1.96	321	0.01 > 0.05	2.87 > 2	0.71	Increasing trend & **significant**
ACCESS	5.08 > 1.96	607	0.00 < 0.05	6.20 > 2	1.45	Increasing trend & **significant**
DJF						
LMDZ	5.03 > 1.96	619	0.00 < 0.05	6.47 > 2	2.61	Increasing trend & **significant**
MPI	4.96 > 1.96	611	0.00 < 0.05	5.23 > 2	1.94	Increasing trend & **significant**
GFDL	4.64 > 1.96	571	0.00 < 0.05	6.07 > 2	2.38	Increasing trend & **significant**
CNRM	5.71 > 1.96	703	0.00 < 0.05	7.19 > 2	1.89	Increasing trend & **significant**
ACCESS	2.89 > 1.96	357	0.00 < 0.05	3.08 > 2	1.15	Increasing trend & **significant**

2.86 °C/50 years for summer & 0.87 °C/50 years to 3.01 °C/50 years for winter season), and a possible decreasing but statistically insignificant trend in summer and winter rainfall in the NEI for the 2011–2060 period. In summary, notwithstanding the uncertainties, when the NEI is taken as a whole, as the models qualitatively capture the historical trend, we can conjecture, that the future projections of decrease in rainfall and increase in temperature may be expected to be realized, though quantifying the same would be difficult. We also find that the ENSO events do not have any significant impact on the climate of the NEI, and, we may not expect any perceivable impact of ENSOs.

Extreme monthly means for precipitation and maximum and minimum temperature for historical and future projections have also been studied over NEI for both JJAS and DJF seasons. The simulated models underestimate the extreme mean monthly values. Overall the extreme monthly means of maximum and minimum temperature increase in the future projections. The frequency of simulated the heaviest rainfall months during JJAS increase in the simulated future projections for 2011–60 from four out of five models as compared to the historical period. Having said that, the magnitude of the heaviest monthly rainfall moderately decreases in future projections in two models. Importantly, total number of 'low rainfall' months (arbitrarily defined as rainfall < 7 mm/day) has increased quite substantially, with the range of increase being 34%–42%. All this suggest that the CORDEX models are not definitive about any increase of extreme rainfall months over northeast India during summer monsoon season.

As the region is well known for its high convective rainfall associated with complex orography along with relatively high mountains and rainfall processes of the monsoon system, the interpolation and calibration algorithms could contribute to the uncertainty. To improve the uncertainties in the climatological datasets pertaining to the in NEI, a higher density of observations would be critical to address various sub-regional climate change/variability issues with confidence.

Acknowledgements

The authors acknowledge the COLA, IMD, Aphrodite and NCEP for making the software and data available. We thank Dr. Milind Mujumdar (IITM) for his kind support in data acquisition on CORDEX South Asia and Mr. Malay Ganai (IITM) for his assistance in data analysis. This research did not receive any specific grant from funding agencies in the public, commercial, or not-for-profit sectors. The authors acknowledge useful comments from anonymous reviewers.

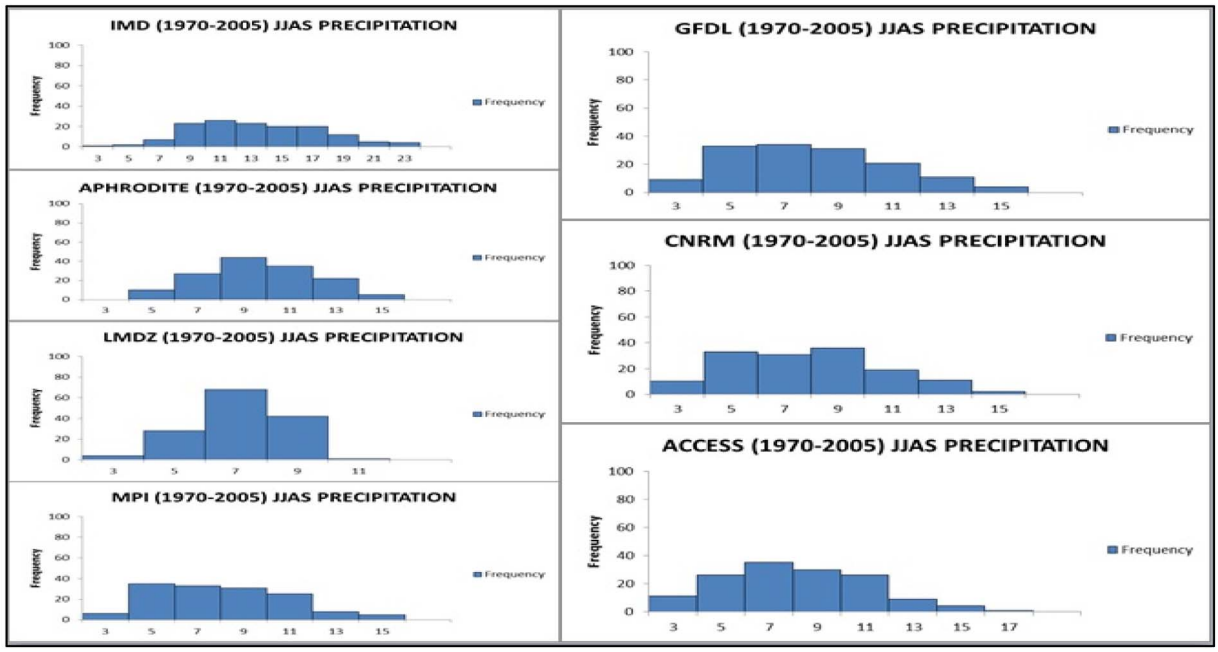

a

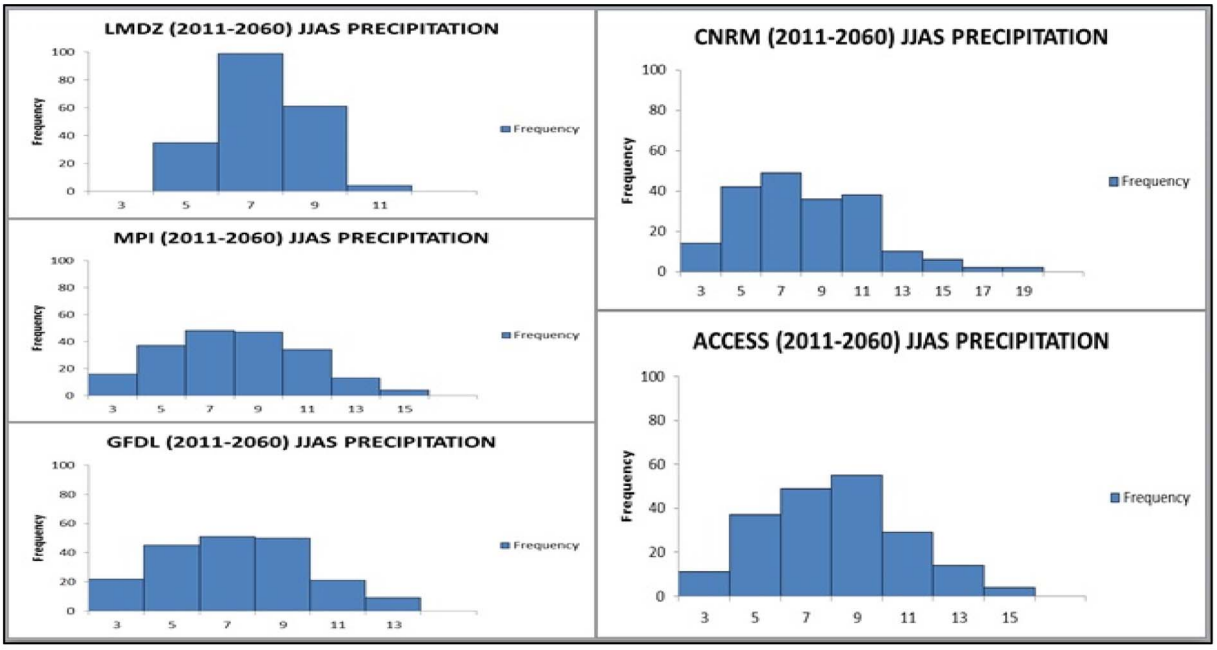

b

Fig. 6. (a). Histogram plots for JJAS precipitation (mm) of historical period (1970–2005): IMD, Aphrodite along with CORDEX models ((LMDZ, MPI, GFDL, CNRM and ACCESS). (b). Histogram plots for JJAS precipitation (mm) of future projections (2011–2060) of CORDEX models ((LMDZ, MPI, GFDL, CNRM and ACCESS).

Appendix 1

The driving simulations of the LMDZ, MPI, GFDL, CNRM and ACCESS are performed within the framework of CMIP5. To downscale the CMIP5 (Coupled Model Intercomparison Project Phase 5) scenarios, the World Climate Research Program (WCRP) initiated a coordinated effort known as CORDEX, which provides an ensemble of high resolution regional climate projections for all the major continental regions of the world. Currently CORDEX involves > 20 RCM groups around the world and provides a quality-controlled data set of downscaled information for historical past and 21st century projections (Taylor et al., 2012). The CORDEX outputs are used for input or adaptation work, and also for IPCC Fifth Assessment Report (Giorgi et al., 2009). CORDEX focus on the emission scenarios known as RCP4.5 and RCP8.5 which represent a mid and a high level emission scenario, also roughly corresponding to the IPCC SRES emission scenarios B1 and A1B, respectively (Giorgi et al., 2009). These high resolution regional climate models are selected because these models provide an opportunity to dynamically downscale global model simulations to superimpose the regional detail of specific regions and moreover global climate model suffers from errors due to inadequate representation as well as its expensiveness (Krishna Kumar et al., 2011 and Kumar et al., 2006).

Supplementary data

Supplementary data to this article can be found online at https://doi.org/10.1016/j.gloplacha.2017.11.010.

References

Arora, M., Goel, N.K., Singh, P., 2005. Evaluation of temperature trends over India. Hydrol. Sci. J. 50 (1), 81–93.

Chakraborty, R., Deb, B., Devannac, N., Sena, S., 2012. North-East India an ethnic storehouse of unexplored medicinal plants. J. Nat. Prod. Plant Resour. 2 (1), 143–152.

Chaturvedi, R.K., Ravindranth, N.H., Mathangi, J., Jaideep, J., Bala, G., 2012. Multi-model climate change projections for India under representative concentration pathways. Curr. Sci. 103 (7).

Chinchorkar, S.S., Sayad, F.G., Vaidya, V.B., Pandye, V., 2015. Trend detection in annual maximum temperature and precipitation using the Mann Kendal test – a case study to assess climate change on Anand of central Gujarat. Mausam 66 (1), 1–6.

Choudhury, B.U., Das, A., Ngachan, S.V., Slong, A., Bordoloi, L.J., Chowdhury, P., 2012. Trend analysis of long term weather variables in mid altitude Meghalaya, North-East India. J. Agr. Phys. 12 (1), 12–22.

Collins, M., Rao, K.A., Ashok, K., Bhandari, S., Ashis, K., Prakash, M.S., Srivastava, R., Turner, A., 2013. Observational challenges in evaluating climate models. Nat. Clim. Chang. 3, 940–941.

Dash, S.K., Hunt, J.C.R., 2007. Variability of climate change in India. Curr. Sci. 93 (6), 782–788.

Dash, S.K., Sharma, N., Pattnayak, K.C., Gao, X.J., Shi, Y., 2012. Temperature and precipitation changes in the north-east India and their future projections. Glob. Planet. Chang. 98-99, 31–44.

Dash, et al., 2015. Projected seasonal mean summer monsoon over India and adjoining regions for the twenty-first century. Theor. Appl. Climatol. 122, 581–593.

Dubey, D.P., Krishnakumar, G., 2014. Trends in precipitation extremes over Central India. Mausam 65 (1), 103–108.

Dufresne, J.L., Foujol, M.A., Denvil, S., et al., 2013. Climate change projections using the IPSL-CM5 Earth System Model: from CMIP3 to CMIP5. Clim. Dyn. 40, 2123–2165. http://dx.doi.org/10.1007/s00382-012-1636-1.

Giorgi, F., Jones, C., Asrar, G.R., 2009. Addressing climate information needs at the regional level: the CORDEX framework. WMO Bull. 58 (3), 175–183.

Guhathakurta, P., Rajeevan, M., 2008. Trends in the rainfall pattern over India. Int. J. Climatol. 28, 1453–1469. http://dx.doi.org/10.1002/joc.1640.

Harris, P.D., Jones, T.J., Osborna, Listera, D.H., 2014. Updated high-resolution grids of monthly climatic observations – the CRU TS3.10 Dataset. Int. J. Climatol. 34, 623–642.

IPCC, 2007. Climate change 2007: impacts, adaptation and vulnerability. In: Parry, M.L., Canziani, O.F., Palutikof, J.P., van der Linden, P.J., Hanson, C.E. (Eds.), Contribution of Working Group II to the Fourth Assessment Report of the Intergovernmental Panel on Climate Change. Cambridge University Press, Cambridge, UK, pp. 469–506.

IPCC, 2013. Climate change 2013: the physical science basis. In: Stocker, T.F., Qin, D., Plattner, G.-K., Tignor, M., Allen, S.K., Boschung, J., Nauels, A., Xia, Y., Bex, V., Midgley, P.M. (Eds.), Contribution of Working Group I to the Fifth Assessment Report of the Intergovernmental Panel on Climate Change. Cambridge University Press, Cambridge, United Kingdom and New York, NY, USA (1535 pp).

Jain, S.K., Kumar, V., 2012. Trend analysis of rainfall and temperature data for India. Curr. Sci. 102 (1), 37–49.

Jain, S.K., Kumar, V., Saharia, M., 2012. Analysis of rainfall and temperature trends in northeast India. Int. J. Climatol. http://dx.doi.org/10.1002/joc.3483.

Jhajhariaa, D., Singh, V.P., 2011. Trends in temperature, diurnal temperature range and sunshine duration in Northeast India. Int. J. Climatol. 31, 1353–1367.

Jourdain, N.C., et al., 2013. The Indo-Australian monsoon and its relationship to ENSO and IOD in reanalysis data and the CMIP3/CMIP5 simulations. Clim. Dyn. 41, 3073–3102. http://dx.doi.org/10.1007/s00382-013-1676-1.

Kothawale, D.R., Kumar, K.K., Srinivasan, G., 2012. Spatial asymmetry of temperature trends over India and possible role of aerosols. Theor. Appl. Climatol. 110, 263–280. http://dx.doi.org/10.1007/s00704-012-0628-8.

Kothawale, D.R., Kumar, R.K., 2005. On the recent changes in surface temperature trends over India. Geophys. Res. Lett. 32, L18714. http://dx.doi.org/10.1029/2005GL023528.

Kothyari, U.C., Singh, V.P., 1996. Rainfall and temperature trends in India. Hydrol. Process. 10, 357–372.

Krishnan, et al., 2016. Deciphering the desiccation trend of the South Asian monsoon hydroclimate in a warming world. Clim. Dyn. http://dx.doi.org/10.1007/s00382-015-2886-5.

Kulkarni, et al., 2013. Projected climate change in the Hindu Kush–Himalayan region by using the high-resolution regional climate model PRECIS. Mt. Res. Dev. 33 (2), 142–151.

Kumar, K.K., Patwardhan, S.K., Kulkarni, A., Kamala, K., Rao, K.K., Jones, R., 2011. Simulated projections for summer monsoon climate over India by a high-resolution regional climate model (PRECIS). Curr. Sci. 101 (3), 312–326.

Kumar, P., et al., 2013. Downscaled climate change projections with uncertainty assessment over India using a high resolution multi-model approach. Sci. Total Environ. http://dx.doi.org/10.1016/j.scitotenv.2013.01.051.

Kumar, R.K., et al., 2006. High-resolution climate change scenarios for India for the 21st century. Curr. Sci. 90 (3), 334–345.

Kumar, V., Jain, S.K., Singh, Y., 2010. Analysis of long-term rainfall trends in India. Hydrol. Sci. J. 55 (4), 484–496.

Laskar, S.I., Kotal, S.D., Roy, S.K.B., 2014. Analysis of rainfall and temperature trends of selected stations over Northeast India during last century. Mausam 65 (4), 497–508.

Mondal, A., Khare, D., Kundu, S., 2014. Spatial and temporal analysis of rainfall and temperature trend of India. Theor. Appl. Climatol. http://dx.doi.org/10.1007/s00704-014-1283-z.

Mooley, D.A., Parthasarathy, B., 1983a. Variability of the Indian Summer monsoon and tropical circulation features. Am. Meteorol. Soc. 111 (5), 967–978.

Mooley, D.A., Parthasarathy, B., 1983b. Indian Summer Monsoon and E1 Nino. Pure Appl. Geophys. 121 (2), 339–352.

Pant, G.B., Kumar, R.K., 1997. Climates of South Asia. (ISBN: 978-0-471-94948-0).

Parthasarathy, B., Rupakumar, K., Munot, A.A., 1996. Homogeneous regional summer monsoon rainfall over India: inter annual variability and teleconnections. Res. Rep (RR–070, ISSN, 0252–1075).

Prakash, S., et al., 2014. Seasonal intercomparison of observational rainfall datasets over India during the southwest monsoon season. Int. J. Climatol. http://dx.doi.org/10.1002/joc.4129.

Rajeevan, M., Bhate, J., Jaswal, A.K., 2008. Analysis of variability, and trends of extreme rainfall events over India using 104 years of gridded daily rainfall data. Geophys. Res. Lett. 35, L18707. http://dx.doi.org/10.1029/2008GL035143. (…..august).

Rajeevan, M., Bhate, J., Kale, J.D., Lal, B., 2005. Development of a high resolution daily gridded rainfall data for the Indian region. IMD Met Monograph No: Climatology 22/2005. pp. 27 (Available from National Climate Centre, IMD Pune. ncc@imdpune.gov.in).

Rajeevan, M., Srivastava, A.K., Kshirsagar, S.R., 2008. Development of a high resolution daily gridded temperature data set (1969–2005) for the Indian Region. In: NCC Research Report 8. National Climate Centre India Meteorological Department.

Rajendran, K., Sajani, S., Jayasankar, C.B., Kitoh, A., 2013. How dependent is climate change projection of Indian summer monsoon rainfall and extreme events on model resolution? Curr. Sci. 104 (10), 1409–1418.

Ravindranath, et al., 2011. Climate change vulnerability profiles for North East India. Curr. Sci. 101 (3), 384–394.

Revadekar, J.V., Kothawale, D.R., Patwardhan, S.K., Pant, G.B., Kumar, R.K., 2012. About the observed and future changes in temperature extremes over India. Nat. Hazards 60, 1133–1155. http://dx.doi.org/10.1007/s11069-011-9895-4.

Roxy, M., Kapoor, R., Pascal, T., Murtugudde, R., Ashok, K., Goswami, B.N., 2015. Drying of Indian subcontinent by rapid Indian Ocean warming and a weakening land-sea thermal gradient. Nat. Commun. http://dx.doi.org/10.1038/ncomms8423.

Sabin, T.P., Krishnan, R., Ghattas, J., Denvil, S., Dufresne, J.-L., Hourdin, F., Pascal, T., 2013. High resolution simulation of the South Asian monsoon using a variable resolution global climate model. Clim. Dyn. http://dx.doi.org/10.1007/s00382-012-1658-8.

Saha, A.S., Ghosh, A.S., Sahana, Rao, E.P., 2014. Failure of CMIP5 climate models in simulating post-1950 decreasing trend of Indian monsoon. Geophys. Res. Lett. 41, 7323–7330. http://dx.doi.org/10.1002/2014GL061573.

Sharmila, S., Joseph, S., Sahai, A.K., Abhilash, S., Chattopadhyay, R., 2015. Future projection of Indian summer monsoon variability under climate change scenario: an assessment from CMIP5 climate models. Glob. Planet. Chang. 124, 62–78.

Shashikanth, K., Salvi, K., Ghosh, S., Rajendran, K., 2013. Do CMIP5 simulations of Indian summer monsoon rainfall differ from those of CMIP3? Atmos. Sci. Lett. 15, 79–85. http://dx.doi.org/10.1002/asl2.466.

Taylor, K.E., Stouffer, R.J., Meehl, G.A., 2012. An overview of CMIP5 and the experiment design. Am. Meteorol. Soc. http://dx.doi.org/10.1175/BAMS-D-11-00094.1.

Wagholikar, N.K., Ray, S.K.C., Sen, P.N., Kumar, P.P., 2014. Trends in seasonal temperatures over the Indian Region. J. Earth Syst. Sci. 123 (4), 673–687.

Yatagai, A., et al., 2012. APHRODITE: constructing a long-term daily gridded precipitation dataset for Asia based on a dense network of rain gauges. Am. Meteorol. Soc. http://dx.doi.org/10.1175/BAMS-D-11-00122.1.

Sixth WMO International Workshop on Monsoons (IWM-VI)

13-17 November 2017, Singapore

CERTIFICATE OF PARTICIPATION AND ATTENDANCE

It is certified that SORAISAM BRIDYABATI of University of Hyderabad participated in the scientific sessions of the Sixth WMO International Workshop on Monsoons (IWM-VI) and presented a paper entitled, “Uncertainties in Observations and Climate Projections for the North East India”.

18 November 2017

Chih-Pei Chang

Chih-Pei Chang

Chair, IWM-VI International Organizing Committee

Chair, WMO/CAS/WGTMR Monsoon Panel

(Distinguished Professor Emeritus, Naval Postgraduate School, Monterey, California, USA)

NESAC

Shillong Chapter

ISG

Shillong Chapter

CERTIFICATE OF PARTICIPATION

THIS IS TO CERTIFY THAT

SORAISAM BIDYABATI

has attended the Seminar On "Advances In Remote Sensing & GIS Applications" as a Delegate and presented technical paper on *"North East forests are facing stress due to precipitation anomaly: an analysis based on MODIS normalized vegetation index, filed data and IMD precipitation data for the period of 2000-2014"* held on May 10 -11, 2018 at North Eastern Space Applications Centre, Umiam, Meghalaya India.

Dr. K.K. Sarma
Secretary, ISRS
Shillong Chapter

Prof. B. S. Mipun
President, ISG
Shillong Chapter

Dr. S. Hamilton
President, ISRS
Shillong Chapter

P.L.N. Raju
Secretary, ISG
Shillong Chapter

TROPMET 2016

National Symposium on Tropical Meteorology: Climate Change and Coastal Vulnerability

18 - 21 December, 2016 , Bhubaneswar, Odisha, India

Organised by

This Certificate of Participation is Awarded to

Soreisam Bidyabati

for his/ her Contribution for Invited talk/ Technical Presentation / Poster Presentation .
In TROPMET 2016, "National Symposium on Tropical Meteorology: Climate Change and Coastal Vulnerability"
Organized by Indian Meteorological Society, Bhubaneswar Chapter,
in colaboration with Government of Odisha and Siksha 'O' Anusandhan University, Bhubaneswar, India
Under the Auspices of Indian Meteorological Society, New Delhi

AVM Dr. Ajit Tyagi, Co-Chairman
National Organizing Committee
& President IMS, New Delihi

Prof. U. C. Mohanty
Chairman
Scientific Steering & Publication Committee

Dr. S. C. Sahu, Convener
National Organizing Committee
& President IMS-Bhubaneswar Ch.

National Seminar on

Tectonics of the Evolving Earth

Certificate of Participation

This is to certify that

Soraisam Bidyabati

Presented a poster in the National Seminar on

TECTONICS OF THE EVOLVING EARTH

held at CEOAS, University of Hyderabad during March 1 - 2, 2019

Prof. K.S. Krishna
(Convenor)

Organized by
Centre for Earth, Ocean and Atmospheric Sciences
University of Hyderabad

Prof. M. Jayananda
(Convenor)

A study on the recent climate variability and climate change in Northeast India, and its influence on vegetation pattern

by Bidyabati Soraisam

A study on the recent climate variability and climate change in Northeast India, and its influence on vegetation pattern

ORIGINALITY REPORT

32%	6%	31%	2%
SIMILARITY INDEX	INTERNET SOURCES	PUBLICATIONS	STUDENT PAPERS

PRIMARY SOURCES

1	Bidyabati Soraisam, Ashok Karumuri, Pai D.S., "Uncertainties in observations and climate projections for the North East India", Global and Planetary Change, 2018 Publication	24%
2	"Assessment of Climate Change over the Indian Region", Springer Science and Business Media LLC, 2020 Publication	<1%
3	High-Impact Weather Events over the SAARC Region, 2015. Publication	<1%
4	www.earthobservations.org Internet Source	<1%
5	rmets.onlinelibrary.wiley.com Internet Source	<1%
6	onlinelibrary.wiley.com Internet Source	<1%

Student's own paper

This paper is from the current thesis, and first-authored by the candidate. i.e. this is student's own paper.

28 Dec 20

Prof. KARUMURI ASHOK
Centre for Earth, Ocean & Atmospheric Sciences
University of Hyderabad
Hyderabad-500 046, INDIA.